Photophysics of a Few Bichromophoric Organic Molecules in Homogeneous and Microheterogeneous Environments

A dissertation
as partial fulfillment for the degree of
Doctor of Philosophy in Chemistry

by

Anasuya Mishra
Roll No. 08612203

Department of Chemistry
Indian Institute of Technology Guwahati
Guwahati 781039
Assam, India

October 2013

Statement

I hereby declare that the thesis entitled “Photophysics of a few organic bichromophoric molecules in homogeneous and microheterogeneous environments” is the outcome of my research work done under the supervision of Dr. G. Krishnamoorthy, Department of Chemistry, Indian Institute of Technology Guwahati, India.

In the present thesis the general practice of the scientific observations are reported and whenever needed, the work on the findings of other investigators are described and thus due acknowledgements have been made.

Anasuya Mishra

Anasuya Mishra
Department of Chemistry
Indian Institute of Technology Guwahati
Guwahati-781039
Assam, India
23rd October, 2013

INDIAN INSTITUTE OF TECHNOLOGY GUWAHATI
Guwahati 781 039, Assam, India
Tel: +91 – 361 – 258 2315, 258 3101
Fax: +91 – 0361 – 2582349
E-mail: gkrishna@iitg.ernet.in, gkrishna_2000@yahoo.com

Dr. G. Krishnamoorthy
Head, Central Instruments Facility
& Associate Professor of Chemistry

It is certified that the work reported in the thesis entitled "Photophysics of a few organic bichromophoric molecules in homogeneous and microheterogeneous environments" by Anasuya Mishra is an authentic record of the results obtained from the research work carried out under my supervision in the Department of Chemistry, Indian Institute of Technology Guwahati, India.

Guwahati
23rd October, 2013

Dr. G. Krishnamoorthy

Dedicated to my parents

Acknowledgements

I humbly express my deep sense of gratitude to my supervisor Dr. G. Krishnamoorthy, for his constant guidance and encouragement throughout the period of my research work. I truly appreciate the guidance and assistances that he has provided. I am indebt to him for inspiring me towards scientific research. His meticulous analyses of the results and patience motivated me to able to complete my thesis work. He is an excellent supervisor and taught me how to carry out research. I am very fortunate to get him as my guide. Special thanks to his family for making me feel at home.

I would like to express my sincere thanks to the doctorial committee members Prof. T. Punniyamurthy, Dr. R. Boomisankar, Dr. Lalmohan Kundu and Dr. Utpal Bora for spending their valuable time and suggestions which helped me to improve my thesis. I would like to thank Dr. M. Qureshi for allowing me to use microwave oven and fluorimeter in his laboratory. I would like to take the opportunity to thank all other faculties of our department for their kind cooperation whenever I needed. Further I would like to extend my thanks to all nonteaching staffs of our department for their constant support. I would like to thank Department of Chemistry, Indian Institute of Technology Guwahati for the infrastructure provided, which helped me to complete my research work smoothly. I would like to thank the Central Instrument facilities for allowing me to use NMR, fluorimeter, lifetime instrument, LCMS instrument. I am also thankful to Indian institute of Technology Guwahati for the financial support.

I am grateful to all my teachers from school, college and university, especially Srinibas sir, Rabi sir, Pati sir, Dr. Sanjukta mam, Dr. Usa mam, Dr. Dilip Das sir, Prof. S. Jena sir, Prof S. P. Rout sir, Prof. P. K. Sahoo sir for their blessing and delivering knowledge to go ahead. I would like to convey special thanks to my teacher Late Yudhisthir Dhal, who motivated me and my father for my higher studies and was always happy with my progress and success. One of his wish was to see me as very successful personnel for which he blessed me always.

I would like to thank all my PhD batchmates for a nice friendly environment for continuing my research work. I remain thankful to my former and present labmates Dr. Monali mam, Dr. A. Thangamani, Mrinmoy, Dr. Nihar, Dr. Francis, Somu bhaiya, Debpratim, Rameswar, Manoj, Sourav, Ankur, Timir, Ananda,

Sabyosachi, Sumit, Ashim, Santosh and Saugata for creating a friendly atmosphere inside the lab and their help and support whenever I needed. Especially I would like to thank Nihar and Francis for raising their helping hand for learing some of the scientific techniques. I would like to thank Himanshu for learning NMR and giving some idea for the syntheses of some molecules. I would also like to extend my thanks to Mohanlal for helping me to learn docking for the present work. I would like to acknowledge some other friends in department Babulal bhaiya, Jashmini di, Sadhu, Subhojit, Rama, Anushree, Palash, Dipankar, Tridip and Momina for creating a healthy atmosphere.

It is not possible to acknowledge each and everyone by name. Still I wish to thank my hostel friends Namita, Bharti, sumi, swati, Kuni, sunita, Raihana, Biju, Rojalin, Madhu di, Rik di, Tribedi, Madhu etc. for their cooperation and support. I would like to appreciate some of my friends Sanjida, Mustafa, Manju, Jhunu, Rinky, Sunita, Mami for their support throughout my life.

My heartiest thanks to my husband Dr. B. R. Panda for his constant encouragement, motivation and mental support without which it would not have been possible for me to devote my time to the present thesis work. Thanks to my in-laws family especially mother in law for her understanding and support.

Last, but not the least I would like to thank my family members, who mean the world to me. I am here today because of their sacrifices, blessings, love and affection. They encouraged me a lot in each and every step of my life. No matter how much I thank them it will be insufficient.

Grateful to God for being with me forever!

With Best Regards
Anasuya Mishra

Synopsis

Organic bichromophoric molecules having electron donor and acceptor moieties linked by a spacer, upon excitation undergo charge transfer from the donor to the acceptor. This charge transfer results in the formation of a highly dipolar state known as intramolecular charge transfer (ICT) state. ICT process has gained a substantial attention because of its wide application in various fields such as photoelectronic, nonlinear optics, chemical sensing etc. Several photochemical as well as photobiological processes involve ICT. Several models were proposed to explain the formation and the stabilization of the ICT state. Among them planar intramolecular charge transfer (PICT) and twisted intramolecular charge transfer (TICT) models are leading models prevailing to explain the structure of the molecule in the ICT state. In PICT model a planar structure is proposed for ICT emitting species, whereas in the TICT model the electron donor is twisted with respect to the rest of the molecule at an angle close to 90º. Thus in TICT model the donor moiety is orbitally decoupled with respect to the rest of the moiety. The ICT emission is highly sensitive to the local environment. The present thesis describes the photophysics of a few bichromophoric ICT molecules in various environments. The thesis is divided into eight chapters and the chapters are briefed below.

Chapter 1: Introduction

Chapter 1 gives an introduction to ICT process with factors affecting the process with a few examples from literatures. The photoisomerization process is also discussed in short with some examples from the literature. The chapter ends with the scope of the present work.

Chapter 2: Material, methods and instrumentations

Chapter 2 describes the details of the chemicals and the solvents used in the present work and the procedures followed for the syntheses of the fluorophores. This chapter also elaborates preparation of the samples, methods used for the analyses and the calculations. Methods used for the quantum mechanical calculations and a brief description of the instruments such as UV-visible absorption spectrophotometer, steady state and time resolved fluorescence spectrometers are also provided.

Chapter 3: Spectral characteristics of a few pyridazole analogous organic bichromophoric molecules: An understanding towards the mechanism of twisted intramolecular charge transfer emission of 2-(4'-*N*,*N*-dimethylaminophenyl) imidazo[4,5-b]pyridine

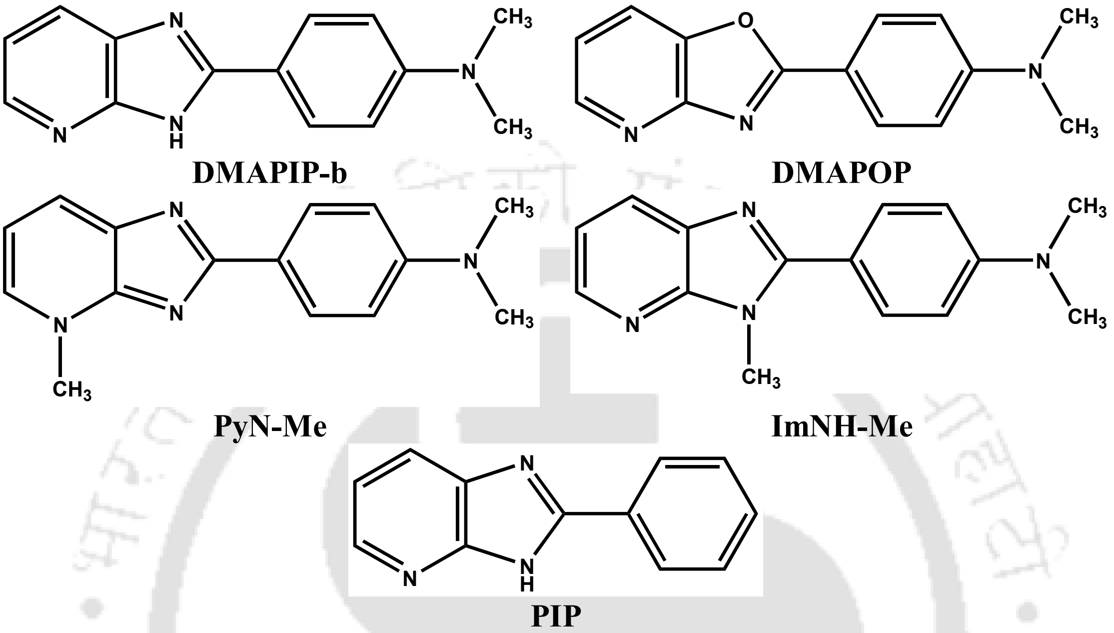

Chart 1. Structures of DMAPIP-b and related molecules.

2-(4'-*N*,*N*-Dimethylaminophenyl)imidazo[4,5-b]pyridine (DMAPIP-b, **Chart 1**) is reported to emit single emission in aprotic solvent and dual emission in protic solvents. To understand the mechanism of dual emission in DMAPIP-b, the photophysical characteristics of some analogues of DMAPIP-b are investigated in **Chapter 3**. This chapter is divided into two sections. In **Section 1**, the effect of oxazole ring substitution is illustrated. The oxazole ring substitution in DMAPIP-b results in 2-(4'-*N*,*N*-dimethylaminophenyl)oxazolo[4,5-b]pyridine (DMAPOP). The emission characteristics of DMAPOP are significantly different from those of its imidazole analogue DMAPIP-b in protic solvents (**Scheme 1**). Though DMAPOP emits single emission from the ICT state, no protic solvent induced dual emission is observed in DMAPOP. This indicates that imdazole >NH is also plays a vital role for the formation of TICT state in DMAPIP-b. DMAPOP also forms two kinds of monocations in the ground and the excited states. But the monocations are formed by protonation at pyridyl and dimethylamino nitrogens (**Scheme 1**).

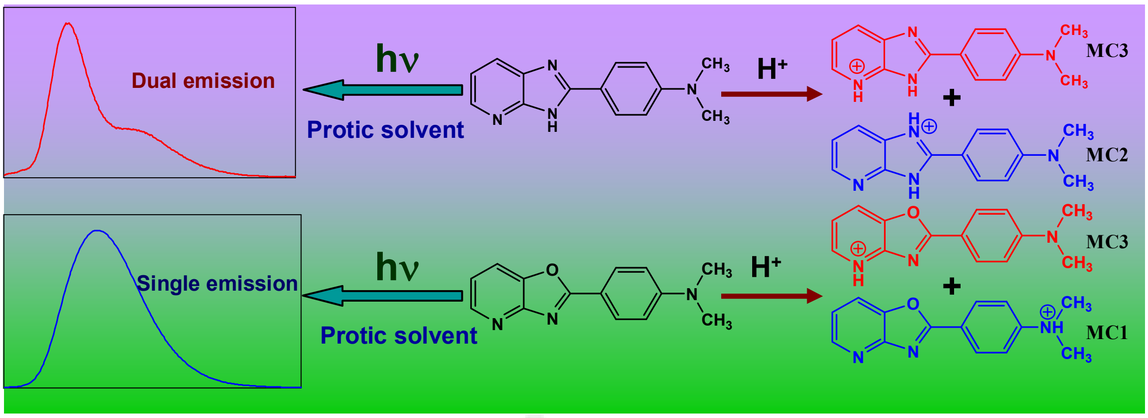

Scheme 1. Overall conclusion obtained from substitution effect of >NH by oxygen.

In **Section 2**, studies on DMAPIP-b and its related molecules (**Chart 1**), *N*,*N*-dimethyl-4-(4-methyl-4*H*-imidazo[4,5-b]pyridin-2-yl)benzenamine (PyN-Me), *N*,*N*-dimethyl-4-(3-methyl-3*H*-imidazo[4,5-b]pyridin-2-yl)benzenamine or 1-methyl-2-(4′-(*N*,*N*-dimethylaminophenyl)imidazo[4,5-b]pyridine (ImNH-Me) and 2-phenylimidazo [4,5-b]pyridine (PIP) are reported. Both PyN-Me and ImNH-Me exhibit single emissions not only in aprotic solvents, but also in protic solvents. The absence of dual emission in PyN-Me where pyridyl nitrogen is prevented from hydrogen bonding with protic solvents emphasizes that the hydrogen bonding with pyridyl nitrogen is crucial for the dual emission of DMAPIP-b in protic solvents. On the other hand, the absence of dual emission in ImNH-Me suggests that the hydrogen bonding with hydrogen of imidazole >NH group is also playing an important role in the process. One such possibility is transfer of proton from >NH group to pyridyl nitrogen to form the tautomer. To verify the proton transfer hypothesis the spectral characteristics of PIP is investigated (without charge donor dimethylamino group). The absence of dual emission in PIP indicates that the tautomer formation is not due to simple proton transfer process and electron donating group is absolutely necessary for the dual emission in DMAPIP-b. This substantiates the conclusion that the longer wavelength emitting state is an ICT state. The higher dipole moment indicates that the ICT emitting state is the TICT state. The enhancement of the longer wavelength emission at higher pH illustrates that the formation of charge transfer state involves the deprotonation of imidazole >NH hydrogen. Thus, the dual emission of DMAPIP-b in protic solvents is attributed due to the formation of the TICT state that is induced by double proton transfer followed by charge transfer assisted by protic solvent molecules which is an intermolecular process. The energy level diagram obtained by theoretical calculation (**Scheme 2**) also supports the hypothesis.

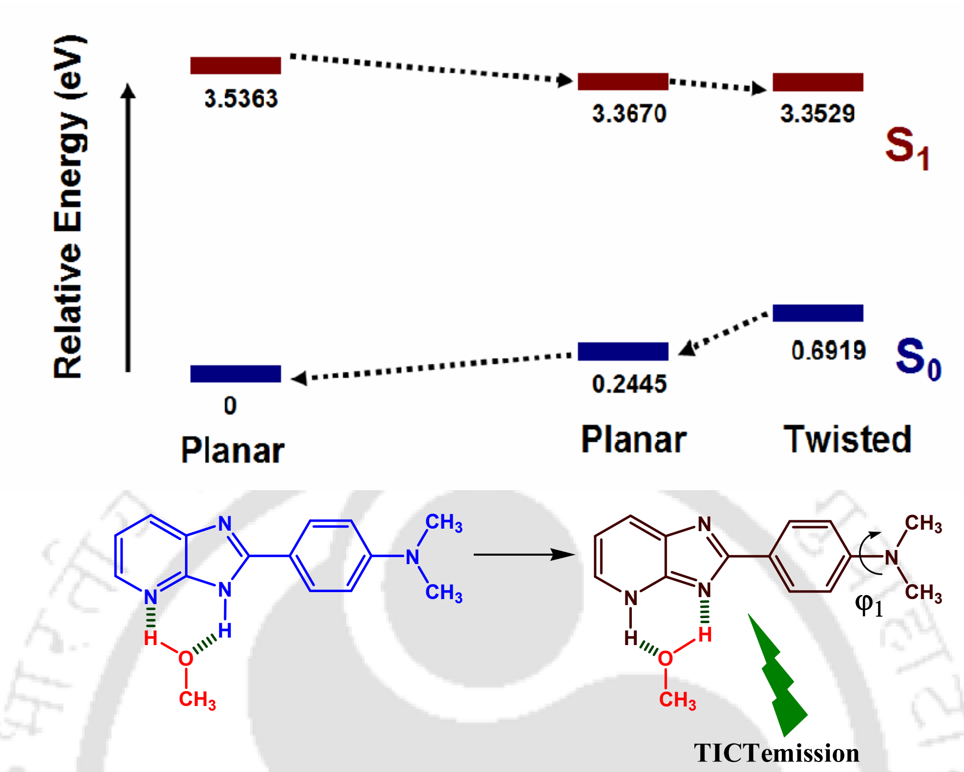

Scheme 2. Energy level diagram of DMAPIP-b and its tautomer.

Chapter 4: Photoinduced intramolecular charge transfer in *trans*-2-[4'-(dimethylamino)styryl]imidazo[4,5-b]pyridine

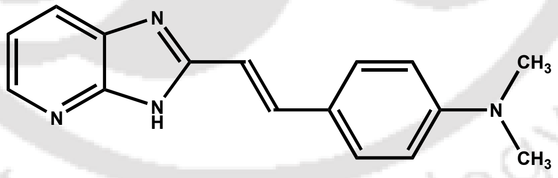

Chart 2. Structure of *t*-DMASIP-b

This chapter describes the effect of double bond introduction on the spectral characteristics of DMAPIP-b. Presence of carbon-carbon double bond in *trans*-2-[4'-(dimethylamino)styryl]imidazo[4,5-b]pyridine (*t*-DMASIP-b, **Chart 2**) strongly perturbs the photophysics of the molecule. In contrast to DMAPIP-b, *t*-DMASIP-b emits single emission in all the solvents including protic solvents. However, solvatochromic plot suggests the emitting states of *t*-DMASIP-b in nonpolar and polar solvents are different. The emitting state in polar solvents is a PICT state and not a TICT state. From the solvatochromic approach it is observed that the maximum contribution of stabilization arises from the dipolar interaction in the excited state. Theoretical calculations suggest that the TICT emission does not observed even in protic solvent as the energy of the TICT states are higher than planar states. The energy of the tautomer is also higher than that of normal form. Both experimental and theoretical results lead to the conclusion that introduction of the olefinic double bond not only hinders the stabilization of the TICT state, but also the solvent assisted proton transfer process. The *trans-cis* photoisomerization competes with the fluorescence process in both nonpolar and polar solvents. The fluorescence quantum yield is much higher in glycerol due to hindrance of isomerization by the restricted twisting motion of the olefinic double bond. The isomerization of *t*-DMASIP-b occurs via a nonadiabatic path. The irradiation experiments suggest that the photostationary state composition is solvent dependent. Temperature effect studies show that upon increase in temperature the quantum yield decreases due to increase in the competing nonradiative processes. The effect of introduction of olefinic double bond affects the prototropic equilibrium also. Unlike in DMAPIP-b, in *t*-DMASIP-b protonation takes place at imidazole nitrogen and pyridyl nitrogen to form monocations.

Chapter 5: Spectral characteristics of 2-(4′-*N*,*N*-dimethylaminophenyl)imidazo [4,5-b]pyridine in aerosol OT reverse micelle

In **Chapter 5** the photophysical characteristics of DMAPIP-b in aerosol OT (AOT, dioctyl sodium sulfosuccinate) reverse micelle are presented. In AOT/*n*-heptane/water reverse micelle, DMAPIP-b exists in both neutral and monocationic forms at lower w_0 values and the fluorophore is present in the micellar phase near the polar head group. The presence of two forms depends upon the size of the water pool. Upon addition of water the fluorophores shifts towards the core and at large pool size the neutral-monocation equilibrium shifts towards neutral form. At higher w_0, DMAPIP-b exists only in neutral form. This also suggests that the bound water of the AOT reverse micelle is more acidic than free water. Though, the polarity of the reverse micelle increases with increase in w_0, even at $w_0 = 36$, the polarity of the confined water in nano pool is less than that of bulk water and is same as that of methanol-water mixture. DMAPIP-b also emits dual emission in reverse micelle due to double proton transfer induced TICT emission. Both normal and TICT emission are quenched by increasing the water content.

Chapter 6: Interactions of a few dimethylaminophenyl substituted azoles with bovine serum albumin: role of heteroatoms

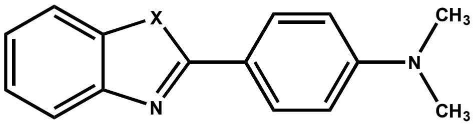

X = NH, DMAPBI

X = O, DMAPBO

Chart 3. Structures of DMAPBI and DMAPBO.

This chapter illustrates the interaction of BSA with 2-(4′-*N*,*N*-dimethyl aminophenyl)benzimidazole (DMAPBI, **Chart 3**), 2-(4′-*N,N*-dimethylaminophenyl) benzoxazole (DMAPBO, **Chart 3**) and DMAPOP (**Chart 1**). The interactions are also compared with DMAPIP-b reported in the literature. The docking studies are performed for all the four ligands. The hypsochromic shift in the fluorescence spectra of the ligands suggest that they bind in the hydrophobic pocket of BSA. The fluorescence intensity of DMAPBI decreases in BSA. On the other hand, enormous enhancements in fluorescence intensity are observed in those of DMAPBO and DMAPOP. This difference in fluorescence is due to differences in the binding location and the orientation of the ligands in the binding sites. From the study, it is inferred that the replacement of imidazole >NH by –O– increases the binding ability of the fluorophore with BSA. This is due to increase in hydrogen bond accepting ability of the oxygen in hydrogen bond accepting nature of the ligand. Thus the binding constants of these ligands increases in the order: DMAPBI < DMAPIP-b < DMAPBO < DMAPOP. Docking study also substantiates the experimental results. These results clearly indicate that the BSA is acting as hydrogen bond donor and the hydrogen bonding plays a crucial role in molecular binding.

Chapter 7: Sensing ability of a few dimethylaminophenyl substituted azoles toward metal ions: role of heteroatoms

In **Chapter 7**, the effect of heteroatom on the sensing abilities of DMAPBI, DMAPBO and DMAPOP towards a series of metal cations are depicted. Due to charge transfer from dimethylamino group to azole nitrogen, DMAPBI interacts with all the metal ions through azole nitrogen. It also has higher binding affinity than the oxazole derivatives. Since, the charge on the azole nitrogen is decreased in DMAPBO, depending on the metal ion, it coordinates through azole nitrogen and/or dimethylamino nitrogen. When pyridyl nitrogen was substituted in benzene ring the molecule interacts through dimethylamino nitrogen, azole nitrogen and/or pyridyl nitrogen. From the histogram plot it is found that the change in fluorescence intensity ratios of DMAPBI is highest in presence of Zn^{2+} followed by that of Cu^{2+} (**Figure 1**). However for both oxazole derivatives change in fluorescence intensity ratios are more in presence of Cu^{2+}.

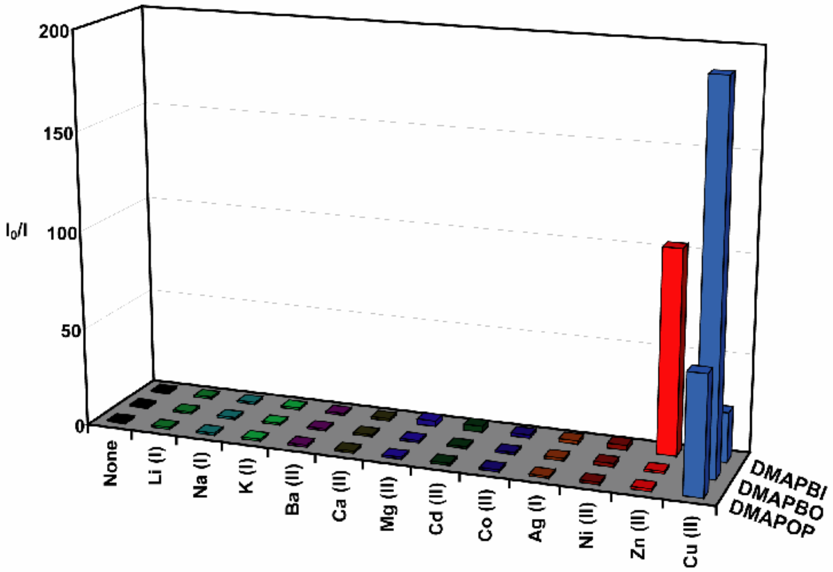

Figure 1. Histogram plot of the intensity ratio (I_0 / I) of the three fluorophores to different metal cations (metal ion concentrations fixed at 100 µM).

Chapter 8: Effect of micelles on the prototropic equilibriums of a few push-pull styryl azoles

The effect of micelles on the prototropic equilibriums of *trans*-2-[4′-(dimethylamino)styryl]benzothiazole (*t*-DMASBT) and *trans*-2-[4′-(dimethylamino) styryl]imidazo[4,5-c]pyridine (*t*-DMASIP-c) and *t*-DMASIP-b (**Scheme 3**) were presented in **Chapter 8**. In *t*-DMASBT, alike in aqueous medium, in micelle also dimethylamino nitrogen and azole nitrogen are protonated to form two kinds of monocations MC1 and MC2, respectively. Though, same as in water the relative population of MC1 is higher than MC2 in micelles, their relative ratio varies with nature of the micelle. The relative population of MC2 increases in anionic micelles compared to that in nonionic, cationic micelles and water. Same as in water, only the ring nitrogens of imidazopyridine derivatives are protonated to form the monocations in micelles except on *t*-DMASIP-b where the dimethylamino nitrogen is also protonated in anionic micelle. The relative populations of MC2 and MC3 depend on

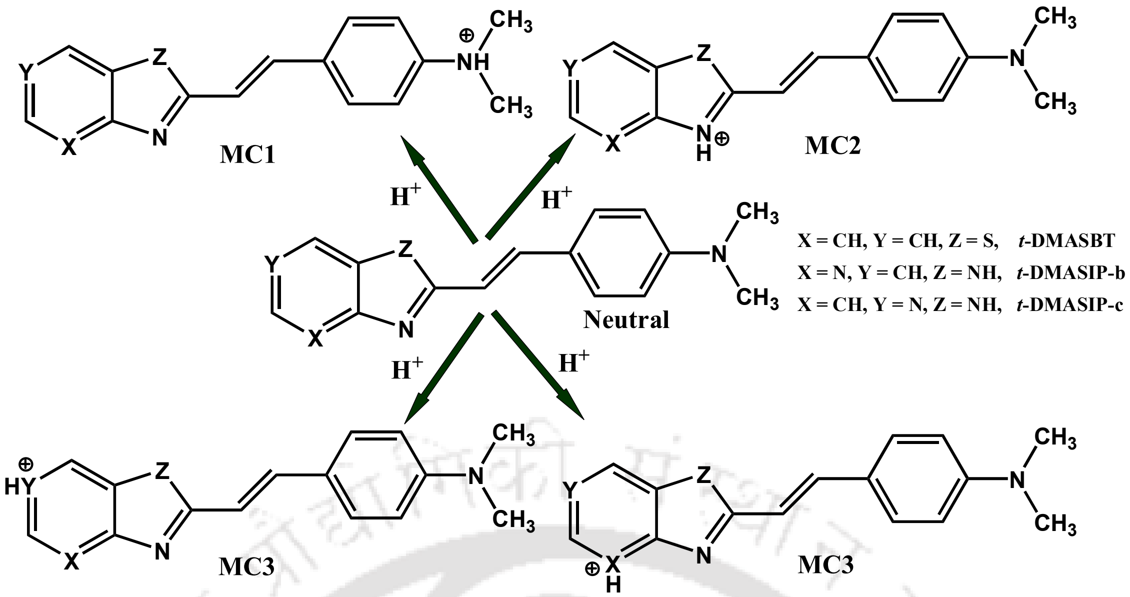

Scheme 3. Structures of possible monocations of benzazole and pyridazole derivatives of styryl compounds.

the position of the ring nitrogen and it increases in *t*-DMASIP-b than in *t*-DMASIP-c. The monocations formations of imidazopyridine derivatives are completed before further protonation (of monocation) in anionic and nonionic micelles, but not completed in cationic micelle due to repulsion of proton by the cationic head group. Therefore, the dimethylamino nitrogen is also protonated in *t*-DMASIP-b and *t*-DMASIP-c to form dications before the completion of monocation formation. All the three molecules remain in the micelle-water interface. The orientation of the fluorophores in all the micelles are same, where the dimethylamino group projects outside (towards the bulk water) and the benzazole/pyridazole moiety projects towards the micellar core (**Figure 2**).

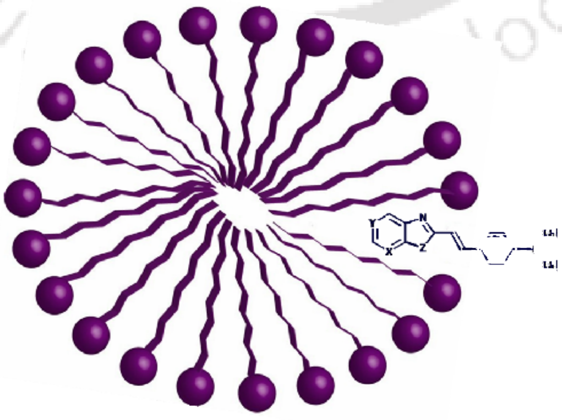

Figure 2. Orientation of the fluorophore inside the micelles.

Chapter 9: Summary and scope for future work

The thesis work is summarized in the last chapter and the scope for future work is also presented in the last chapter.

Contents

List of abbreviations

A	Acceptor
ADC	Analogue to digital converter
AOT	Aerosol orange T
AR	Analytical reagent
BSA	Bovine serum albumin
CASSCF	Complete active space self-consistent field
CIS	Configuration interaction singles
CD	Cyclodextrins
CMC	Critical micelle concentration
CT	Charge transfer
CTAB	Cetyltrimethylammonium bromide
D	Donor
DC	Dication
DFT	Density functional theory
DMAPIP-b	2-(4′-*N*,*N*-dimethylaminophenyl)imidazo[4,5-b]pyridine
DMAPIP–c	2-(4′-*N*,*N*-dimethylaminophenyl)imidazo[4,5-c]pyridine
DMAPOP	2-(4′-*N*,*N*-dimethylaminophenyl)oxazolo[4,5-b]pyridine
DMAPBO	2-(4′-*N*,*N*-dimethylaminophenyl)benzoxazole
DMAPBI	2-(4′-*N*,*N*-dimethylaminophenyl)benzimidazole
DMABN	4-(Dimethylamino)benzonitrile
t-DMASBI	2-(4′-*N*,*N*-Dimethylaminostyryl)benzimidazole
t-DMASBT	2-(4′-*N*,*N*-Dimethylaminostyryl)benzothiazole
t-DMASIP-b	2-(4′-*N*,*N*-Dimethylaminostyryl)imdazo[4,5-b]pyridine
t-DMASIP-c	2-(4′-*N*,*N*-Dimethylaminostyryl)imdazo[4,5-c]pyridine
DMF	*N*,*N*-Dimethylformamide
DMSO	Dimethylsulfoxide
EA	Electron affinity
Em	Emission wavelength
Exc	Excitation wavelength
FTNMR	Fourier transforms nuclear magnetic resonance
HF	Hartree-Fock

HOMO	Highest occupied molecular orbital
IC	Internal conversion
ICT	Intramolecular charge transfer
IP	Imidazopyridine
ImNH	1-Methyl-2-(4′-(*N*,*N*-dimetylaminophenyl)imidazo[4,5-b]pyridine
ISC	Inter system crossing
LC-MS	Liquid chromatography-mass spectrometry
LUMO	Lowest unoccupied molecular orbital
MC	Monocation
MCP	Micro-channel plate
NMR	Nuclear magnetic resonance
PICT	Planar intramolecular charge transfer
PIE	Pseudo-phase ion-exchange
PMT	Photomultiplier Tube
PIP	2-Phenylimidazo[4,5-b]pyridine
PyN-Me	*N*,*N*-Dimethyl-4-(4-methyl-4*H*-imidazo[4,5-b]pyridin-2-yl) benzenamine
RICT	Rehybridized intramolecular charge transfer
SDS	Sodium dodecyl sulfate
TAC	Time-to-amplitude converter
TC	Trication
TCSPC	Time correlated single photon counting
TD	Time dependent
TDDFT	Time dependent density functional theory
TICT	Twisted intramolecular charge transfer
TLC	Thin layer chromatography
TX-100	Triton X-100
UV	Ultra violet
ZINDO	Zerner's intermediate neglect of differential overlap

List of figures

List of tables

List of charts and schemes

Chapter 1

Introduction

1.0. Introduction

This chapter gives a brief introduction to luminescence in particular molecular fluorescence and also to important photoprocesses, intramolecular charge transfer (ICT) and photoisomerization. The scope of present work is presented in the end of the chapter.

1.1. Luminescence

Luminescence is the emission of light by excited molecule. Among different types of luminescence, photoluminescence is most common. In photoluminescence, excitation of the species takes place by absorption of a photon that causes the absorbing species to go to a higher energy electronic excited state. Then de-excitation of photon occurs by emission.

1.2. Molecular fluorescence

Absorption of photon by a molecule may result in its electronic excited state. The emission process that occurs from the excited singlet state to the ground state is known as fluorescence. The decay time of fluorescence is approximately 10^{-9} to 10^{-7} s. The efficiency of fluorescence is measured in terms of quantum yield which is defined as fraction of the molecules that fluoresce. Generally the energy emitted is less than the energy of the photon absorbed by the molecule due to vibrational relaxation. The loss in energy of emitted photon causes a red shift in the fluorescence known as Stokes shift.

1.3. Radiative and nonradiative transitions

The transitions that occur in the electronic state can be explained with the help of Perrin's-Jablonski diagram (**Figure 1.1**). Upon absorption of photon, the molecules go from the ground state (S_0) to the higher singlet states (S_1, S_2, S_3 etc.). The absorption of photon is very fast (10^{-15} s) compared to all other processes. It brings the molecule to one of the vibrational levels of the singlet excited state from which the possible de-excitation processes take place.

1.3.1. Internal conversion

It is a nonradiative transition that occurs between two electronic states of same spin multiplicity. In solution state, the internal conversion (IC) process is followed by vibrational relaxation towards the lowest vibrational state of the corresponding electronic state. The time scale for IC is 10^{-13}-10^{-11} s.

1.3.2. Fluorescence

Generally fluorescence emission occurs from S_1 state and does not depend on the excitation wavelength which is known as Kasha's rule. The difference between the vibrational levels in the ground state and the excited state are similar, thus in most cases fluorescence emission resembles the absorption spectrum (mirror image rule). Other de-excitation processes those take place in the excited state such as IC, intersystem crossing (ISC), vibrational relaxation, photoisomerization, photoionization, photodissociation, proton transfer, charge transfer, electron transfer, excimer or exciplex formation compete with fluorescence. Generally fluorescence occurs in 10^{-8}-10^{-10} s.

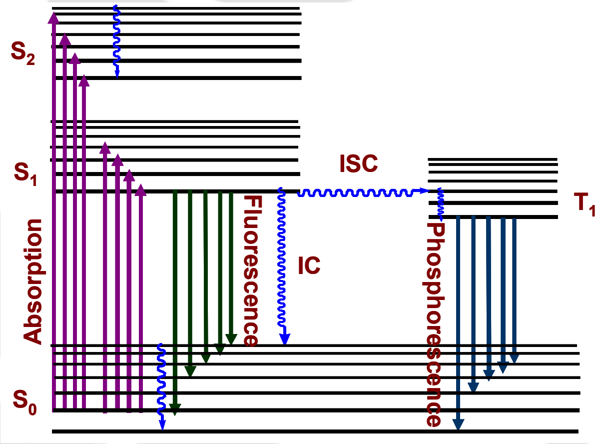

Figure 1.1. Perrin's-Jablonski diagram.

1.3.3. Inter system crossing

It is a nonradiative transition that occurs between two isoenergetic vibrational levels belonging to two electronic states of different spin multiplicity. Although it is a forbidden transition it occurs due to spin orbit coupling and the time scale for ISC is 10^{-7}-10^{-9} s.

1.3.4. Phosphorescence

Radiative de-excitation that occurs from the triplet state (T_1) to the ground state (S_0) is known as phosphorescence. Alike ISC, due to spin orbit coupling phosphorescence can take place. The life time of the phosphorescence is very long and is comparatively longer than fluorescence.

1.4. Fluorescence quantum yield

Fluorescence quantum yield (Φ_f) can be defined as the fraction of the excited molecules that returns to the ground state by fluorescence. It is related to the radiative rate and nonradiative rate and can be defined as follows.

$$\Phi_{\mathrm{f}} = \frac{k_{\mathrm{r}}}{k_{\mathrm{r}}+k_{\mathrm{nr}}} \tag{1.1}$$

where k_r and k_{nr} are the radiative and the nonradiative rates respectively.

1.5. Fluorescence lifetime

The kinetics of the de-excitation process can be well understood with the help of time resolved fluorescence. The time resolution of the order of femtoseconds can be achieved with the help of laser or light emitting diode as the light source. For a very simple system which exhibits a single emission, the fluorescence intensity decay, I(t), can be represented as follows

$$\mathrm{I(t)} = \mathrm{I}_0 e^{-t/\tau} \tag{1.2}$$

where I_0 is the initial intensity and τ is the fluorescence lifetime. The fluorescence life time is defined as the average time spent by the fluorophore in the excited state before de-excitation to the ground state. The fluorescence lifetime is related to both radiative and nonradiative rates. For multiemittive system where more than one species are present in the excited state, instead of monoexponential decay it results in multiexponential and the decay is represented as

$$\mathrm{I}(t) = \sum_{i=1}^{n} a_i e^{-t/\tau_i} \tag{1.3}$$

where a_i and τ_i are i^{th} pre-exponential factor and the lifetime in the multiexponential decay respectively. Pre-exponential factors can be either positive or negative. For multiexponential decays it is useful to calculate the average lifetime ($\bar{\tau}$). $\bar{\tau}$ can be calculated using the following equation.

$$\bar{\tau} = \frac{\sum a_i \tau_i^2}{\sum a_i \tau_i} \tag{1.4}$$

1.6. Intramolecular charge transfer

Excited state intramolecular charge transfer (ICT) is a fundamental process that occurs in several natural systems and is a key mechanism in photochemistry and photobiology. Absorption of photon by molecules having both donor and acceptor moieties separated by a spacer, triggers the charge transfer from the donor to the acceptor in the excited state. This leads to the formation of the ICT state and the emission occurs from both locally excited state and ICT state.[1-5] However, non emissive ICT state and single emission only from ICT state were also observed in few cases.[6-10]

Although several mechanisms were proposed to explain the origin of dual fluorescence in *p*-(*N,N*-dimethylamino)benzonitrile (DMABN, **1**) in polar solvents, this time it is well established that the red shifted longer wavelength fluorescence is because of the photoinduced ICT process. However, controversy still persists about the molecular structure of the emitting ICT state. Different ICT mechanisms suggesting a twisted ICT (TICT)[2,3] or a wagged ICT (WICT) state,[11] or a rehybridized ICT (RICT),[12,13] or a planar ICT (PICT),[5,14] being responsible for the longer wavelength fluorescence were proposed. But, now, only TICT and PICT models are leading models prevailing to explain the structure of the molecule in the ICT state. In the PICT model a planar structure is proposed for ICT emitting species, where as in the TICT model the electron donor is twisted with respect to rest of the molecule at an angle close to 90º. Although direct detection of the structure of the emitting species is found to be experimentally difficult, convincing indirect evidences have been reported for both TICT and PICT mechanisms.[15,16] Recent quantum mechanical calculations revealed that DMABN and its analogues have two charge transfer states in addition to the locally excited state.[17] Depending on the molecular structure the emission may arise from the locally excited-PICT states or the locally excited-TICT states or the charge transfer PICT-TICT states. It was proposed that the ICT state is formed by the transfer of an electron from a covalently linked donor group to an anti-bonding orbital of the π-electron system of benzene. The distortion of the benzene ring to a quinoid or an antiquinoid structure occurs due to change in charge distribution of the molecule in the ICT state. Among the ICT states, the decoupled twisted geometry is expected to have larger dipole moment compared to the planar geometry.

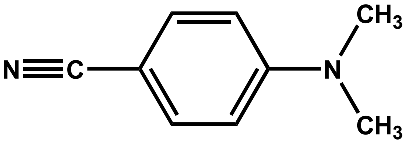

1

1.7. Factors influencing the ICT emission

The ICT emission mainly depends on three different factors namely; polarity, viscosity and hydrogen bonding capacity.

1.7.1. Polarity and viscosity

Since the formation of ICT state involves charge separation, increase in polarity leads to increase in the rate of formation and stabilization of the ICT state, in other word the ICT state will be favored in polar media. The polarity also affects the nonradiative decay rate from the ICT state to the low lying triplet state and/or ground state. For example in DMABN, since the lowest triplet state does not have an appreciable charge transfer character as TICT singlet state, thus the dipole moment of DMABN in the TICT state is more than that in triplet state.[1,2] With rise in polarity the energy gap between the TICT state and the triplet state decreases. According to energy gap law of nonradiative transition,[18,19] the decrease in energy gap between the triplet and singlet state will increase the rate of ISC. The triplet yield of DMABN and related molecules increases, as the polarity of the medium increases.[20] As a result, polarity affects the ICT emission in two opposing ways i.e. the increase of the ICT process tends to increase the ICT emission. On the other hand, the increase in nonradiative process from the ICT state tends to decrease it. Thus in general, increase in polarity does not affect the ICT emission monotonically.[1,2,21-24]

5-(4-dimethylamino-phenyl)-penta-2,4-dienoic acid methyl/ethyl esters (**2**) exhibit single emission in nonpolar solvent and dual emission in polar solvent.[25] Large solvatochromic shift of the emission band and very high dipole moment value indicate that the ICT process is strongly dependent on the polarity of the medium.

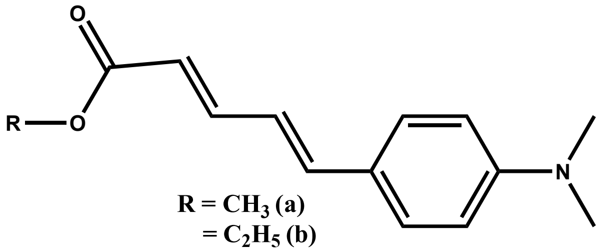

2

Styryl push-pull compound, 2-[4-(dimethylamino)styryl]-1-methylquinolinium iodide found to exhibit a strong solvent polarity-dependent characteristic.[26] It is reported that upon increasing the solvent polarity as well as hydrogen bonding ability the ICT state is stabilized progressively. However after some critical point the ICT state becomes the ground state as a result the further stabilization with solvents results in a blue shift causing the negative solvatochromism. Complex fluorescence is obtained from 9-aminoacridine derivative (**3**) and is ascribed to emission of the acridine chromophore from the ICT state in addition to the locally excited singlet state.[27] The ICT emission is readily quenched by addition of water and is due to changes in the keto-amine/enol-imine equilibrium of the dye.

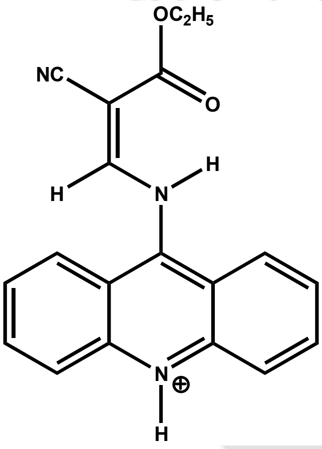

3

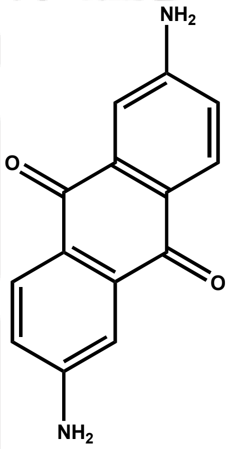

4

The spectral characteristics of 2,6-diamino-9,10-anthraquinone (**4**) results in unusual deviations in less polar aprotic solvents in compared to those in higher polar aprotic solvents.[28] It was inferred that the dye adopts a PICT structure in medium to higher polarity solvents, where the lone pair of amino group is in resonance with the anthraquinone moiety, but in less polar solvent a nonplanar structure is predicted as a result the lone pair electrons of the amino group is not in good resonance with the anthraquninone moiety. A triphenylamine derivative with weak acceptor group (**5**) is found to be sensitive to the polarity of the medium.[29] Increase in the solvent polarity causes bathochromic shift in the emission spectra due to increase in ICT character in the emitting singlet state. Among the three substituted polyhydroquinoline derivatives (**6**), an additional large Stokes shifted fluorescence band is observed in **6c** due to presence of dimethylamino donor group which facilitates the ICT process upon increasing the solvent polarity of the medium.[30] It was suggested that in **6c** the ICT structure is formed may be due to 1,3-H migration in the excited state.

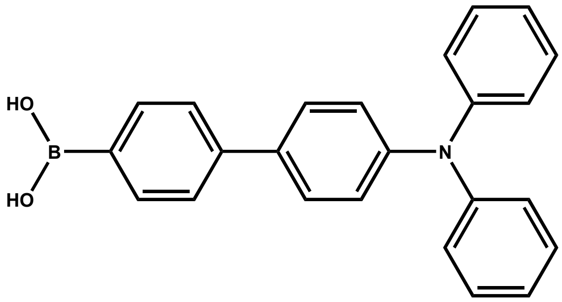

5

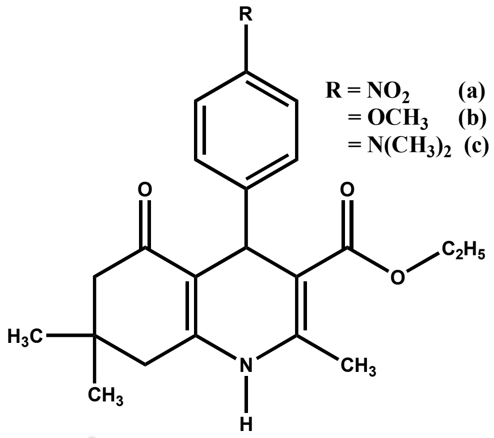

6

Biologically active molecule Rhaponticin (**7**) shows the increased Stokes shift in polar solvents suggested due to ICT character that corresponds to π → π* transitions.[31]

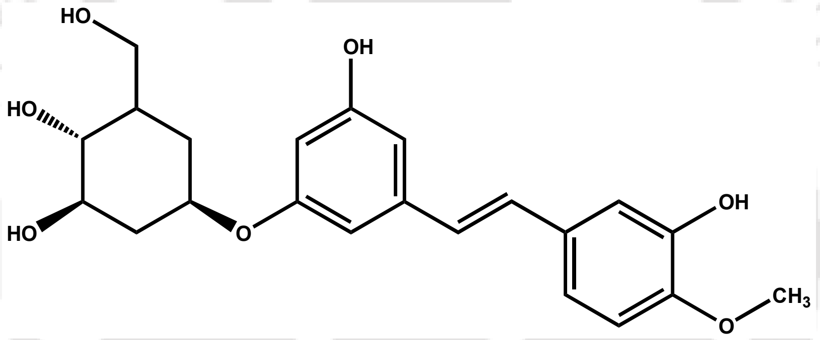

7

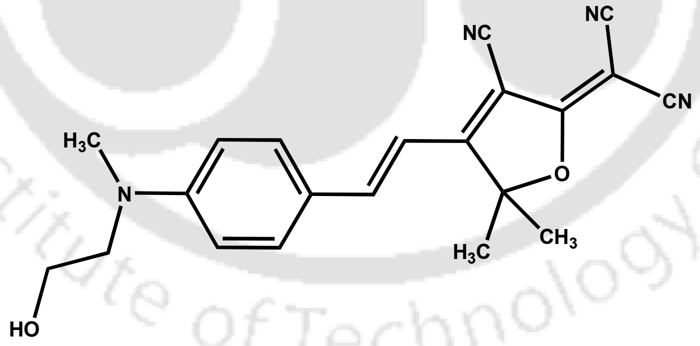

8

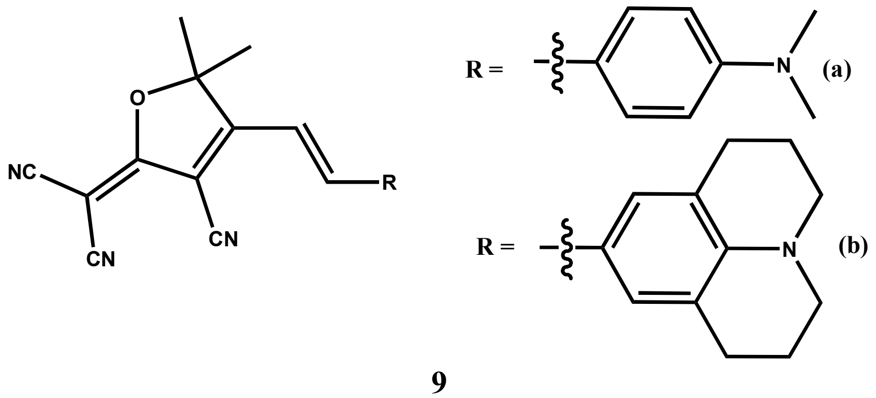

9

A push-pull styryl dye **8** is found to exhibit positive solvatochromism upon increasing the polarity of the solvent.[32] A comparative study of similar structural backbone like **8** is carried out by varying the donor moiety.[33] Although both the dyes exhibited the ICT properties, due to the presence of more electron donating group in dye **9b** (julolidine moiety), it exhibits a very strong positive solvatochromism than the molecule having dimethylamino group as an electron donor group **9a**. The spectral characteristics of a coumarin-6 dye (**10**) reveals a linear correlation with the solvent polarity of moderate to higher polarity nature except in nonpolar solvent.[34] This unusual behavior is depicted due to the formation of a non-planar structure in nonpolar medium whereas in polar medium the dye is planarized, as a result the ICT character increases upon increasing the polarity.

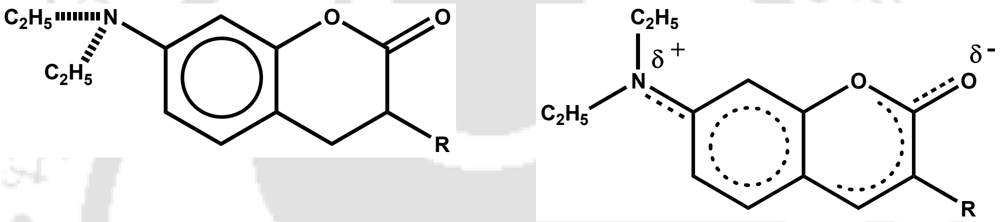

nonplanar structure Planar ICT structure

10

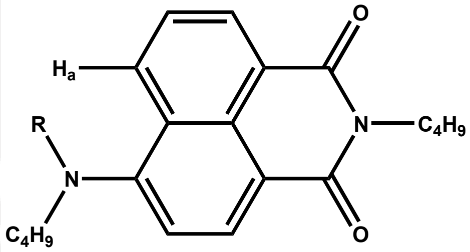

11. **(a)** R = CH_3, **(b)** R = H

In addition to the polarity effect, TICT involves twisting motion of the donor group with respect to the rest of the moiety; therefore viscosity also affects the TICT process. But the polarity and viscosity are opposing each other. Upon increasing the viscosity of the medium the barrier in twisting increases and thus the formation of TICT state is expected to be less favored. Molecules having small rotating group, TICT process is almost independent of viscosity even up to moderate viscosity.[35,36] However at very high viscosity the TICT process may be affected as friction plays an important role.[37-39] On contrary, when the rotating group is bulky, upon increasing the viscosity the rate constant drastically decreases thus affecting the TICT process.[40] Therefore, these kinds of molecules can act as excellent probes for microviscosity.[41-46]

The fluorescence spectrum of **11a** is more sensitive towards the polarity and viscosity of the medium in comparison to **11b**.[47] In polar solvent such as ethanol, the fluorescence efficiency of **11a** is almost completely quenched whereas **11b** emits strong fluorescence. This behavior was attributed to the additional nonradiative path that arises due to TICT state. The formation of TICT state is facilitated by the steric repulsion of the methyl group and peri hydrogen (H_a) so that twisting of 4-amino group occurs with respect to the napthalimide ring.

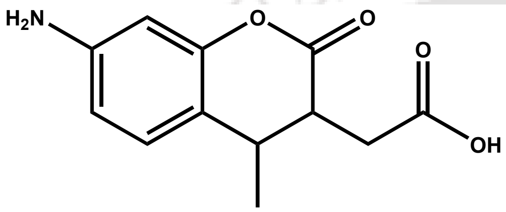

12

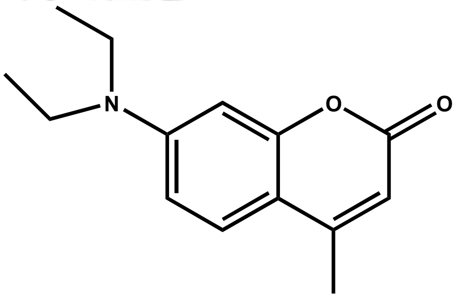

13

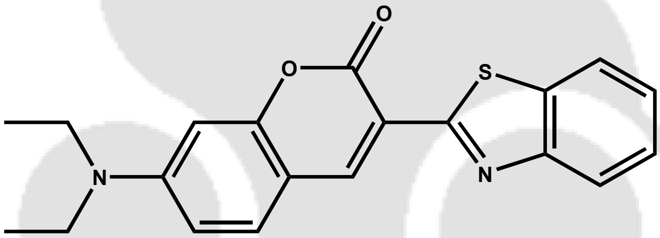

14

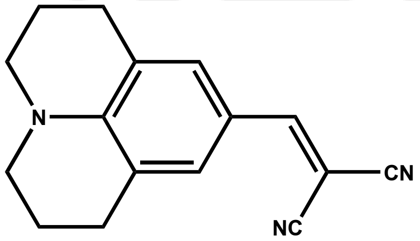

15

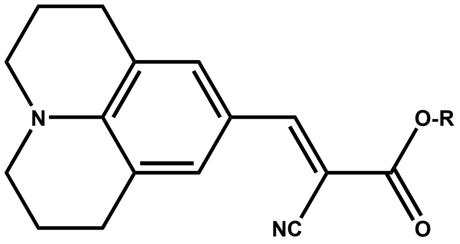

$R = (CH_2CH_2O)_2CH_2CH_3$

16

Haidekker et al. studied the effect of solvent polarity and viscosity on the fluorescence properties of molecular rotors and some related probes.[6] They reported that the emission wavelength of Coumarins (**12-14**) was influenced by solvent polarity; however neither viscosity nor polarity influenced the emission intensity. DMABN shows a complicated effect which is affected by both solvent polarity and viscosity which is very difficult to separate the effect individually on the emission intensity. The emission intensities of the molecular rotors **15** and **16** are found to be highly dependent on the viscosity whereas very low sensitivity towards solvent polarity. Therefore molecular rotors can act as excellent microviscosity probes even in environments where polarity changes are expected.

Compounds containing *p*-*N*,*N*-dialkylaminobenzylidene cyanoacetate motif can serve as fluorescent non-mechanical viscosity sensors due to the formation of TICT in the excited state.[48] The fluorescence response of a few substituted 2-phenylbenzo[g]quinoxalines (**17**) having a rotatable phenyl moiety suggests only **17d** and **17e** which have stronger electron-donating groups exhibit sensitivity towards viscosity.[49] It indicates that strong electron donating group substituted at the phenyl ring leads to high sensitivity towards the viscosity. Hence it can be used as very good viscosity-sensitive fluorescent probes.

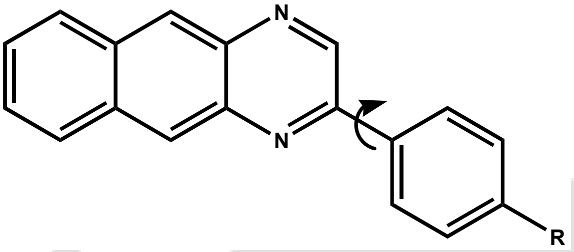

a. R = Cl
b. R = H
c. R = OCH_3
d. R = OH
e. R = $N(CH_3)_2$

17

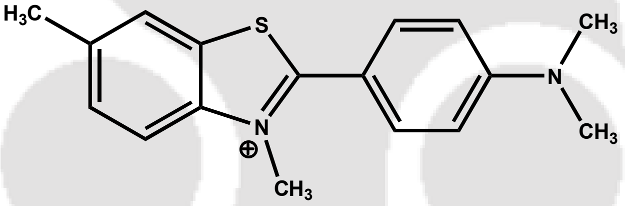

18

The studies of the spectral characteristics of thioflavin T (**18**) in different viscous solvents suggest that a high local microenvironment is responsible for the enhancement of the thioflavin T emission.[50-53] It is ascribed that the nonemissive TICT state is formed by the torsional rotation of the anilino ring with respect to the benzothiazole moiety. The formation of a nonemissive TICT state occurs that is mainly controlled by the viscosity of the environment. Therefore it behaves as a very good sensor for viscosity.[51-55]

1.7.2. Role of hydrogen bonding

Apart from polarity and viscosity, hydrogen bonding also plays an important role for the formation and stabilization of the ICT state. On the basis of hydrogen bond formation at donor or acceptor moiety, the role of hydrogen bonding on ICT can be subdivided into two different categories.

1.7.2.1 Role of hydrogen bonding with electron donor

Cazeau-Dubroca et al. suggested that the hydrogen bonding of the solvent with charge donor moiety results in twisted conformer in the ground state and such twisted conformers upon excitation emit TICT fluorescence.[56-59] The model was challenged by the observation of longer wavelength emission in non-hydrogen bonding polymer matrices and a free volume model was put forward to account the dual emission of DMABN and related molecules in rigid matrices.[60] But Cazeau-Dubroca argued that the presence of water traces introduced in the matrices is responsible for the dual fluorescence of DMABN in non-hydrogen bonding polymer. They extended their hypothesis further to assign the ICT emission in aprotic solvents to the traces of water present in the solvents.[61] Few others also supported the Cazeau-Dubroca's model, but no clear evidence was provided to substantiate the promoting effect of hydrogen bonding of solvents with the electron donor in the formation of the ICT state.[62-64] The pre-twisted conformer formed by hydrogen bonding of solvent with donor moiety as a precondition for the formation of TICT state in DMABN is also severely challenged.[65] Few groups suggested that the ground state hydrogen bonding at the amino nitrogen does not promote rather inhibits the formation of the ICT state in DMABN.[66,67]

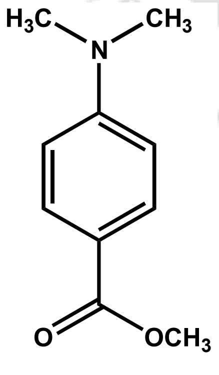

19

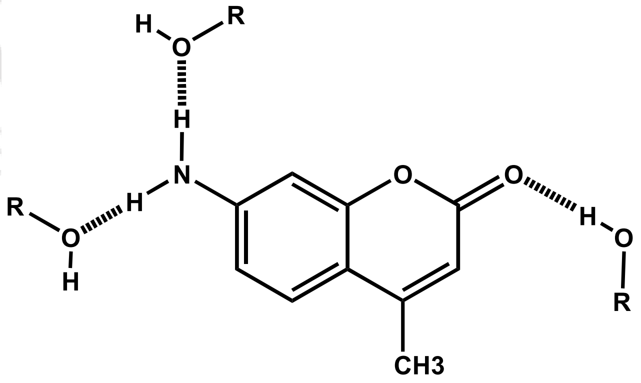

20

Recently Dreuw *et al.* studied the role of water in the ICT emission of 4-(dimethylamino)methylbenzoate (**19**).[68] Based on the theoretical calculation they predicted that in gas phase it is the dimethylamino nitrogen hydrogen bonded complex that is responsible for the ICT emission but not the carboxylate hydrogen bonded molecule. The hydrogen bond of the solvent with dimethylamino nitrogen acts as energy accepting channel in the gaseous phase. The stabilization energy of the ICT state is used for breaking the hydrogen bond.

Interestingly in some of the aminocoumarins, different type of hydrogen bonding between the amino group and the solvents is proposed in the ground state, in which the electron donating amino group acts as a hydrogen bond donor (**20**).[69,70] However, such hydrogen bonds rather increase the electron donating capacity of the amino group, thus favor the formation of the ICT state. Datta et al. showed that the ICT emission of 3-aminoquinoline (**21**) was favored in aprotic solvents such as dimethyl sulfoxide by similar type of hydrogen bonding (**22**).[71] On the other hand hydrogen bonding inhibits the ICT emission of **21** in protic solvents, where the charge donor acts as hydrogen bond acceptor **23**, but the protonation of the acceptor enhances the ICT process **24**.

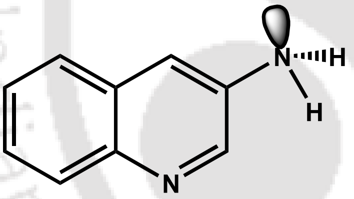

21

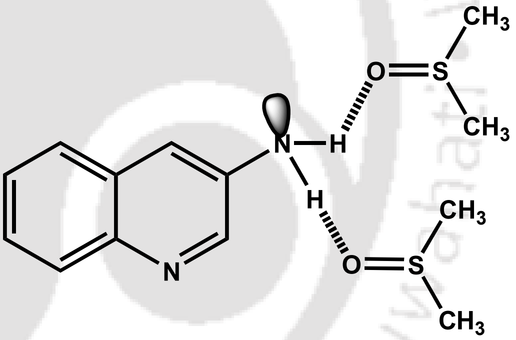

22

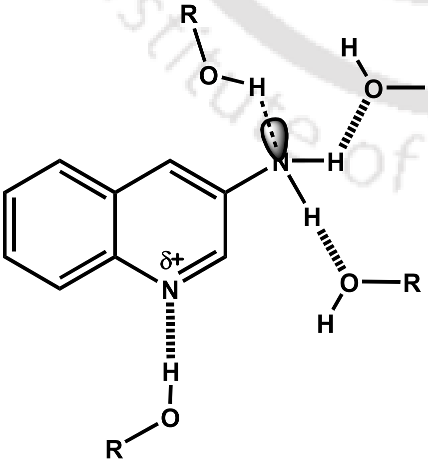

23

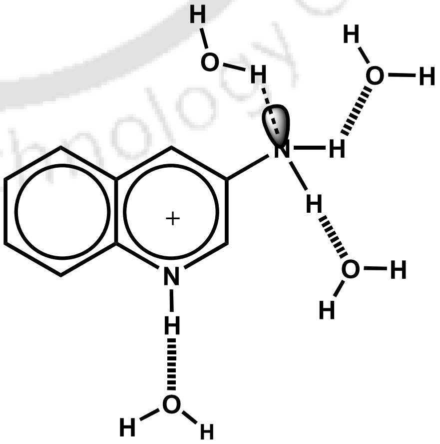

24

It is reported that in a number of substituted 1,8-naphthalimides and naphthalic anhydrides, the introduction of electron-donating substituents induce a charge transfer in the excited state.[72] Introduction of amino group in the napthalimide ring (**25b**) drastically changes the photophysical properties in compared to the unsubstituted analogue (**25a**).[73] This is due to the lowering of the singlet excited state with respect to the triplet state. In **25a**, the intermolecular hydrogen bonding plays a prominent role. In its analogue **25b**, in aprotic solvent, ICT plays an important role, whereas in presence of protic solvent, hydrogen bonding predominates over the ICT.

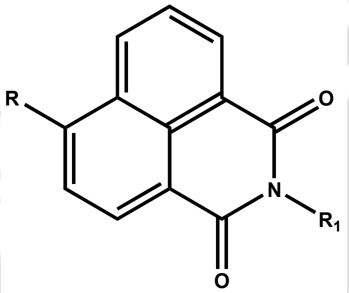

R = H, $R_1 = C_5H_{10}SeCN$ (a)
R = NH_2, $R_1 = C_5H_{10}Br$ (b)

25

1.7.2.2 Role of hydrogen bonding with electron acceptor

Hydrogen bonding with the electron acceptor increases the flow of charge from the donor to the acceptor, thereby favors the ICT process. In several molecules the hydrogen bond with electron acceptor enhances the ICT process, already exhibited by the molecule. In few other molecules it induces the ICT process and in these molecules the hydrogen bond with acceptor is a prior requirement for the formation of the ICT state.

Direct observation of the formation of hydrogen bond between methanol and the cyano group in the ICT state of DMABN was reported.[74] Despite strong interaction between the solvent molecules, the charge separation in the ICT state favors the formation of hydrogen bond between DMABN and methanol, so that the majority of the molecules become hydrogen-bonded. Zhao and Han demonstrated that the hydrogen bond between the cyano group and methanol is strengthened in the TICT state, which can facilitate the deactivation of the excited DMABN in methanol via internal conversion.[75]

The photophysics of 4-dialkylaminopyrimidines (**26-28**) were studied by Herbich et al.[66,67,76] They reported that 4-dimethylaminopyrimidine (**26**) emits clear dual fluorescence in presence of protic solvents or Zn^{2+} ions. Other 4-

dialkylaminopyrimidines **27** and **28** exhibit single exponential decays resulting from the ICT emissions indicating only one kind of hydrogen bonded complex that induces the formation of the ICT state and is assigned to the interaction via the pyrimidine nitrogen *para* to the amino moiety (**29**). The spectral characteristics in terms of energetics and kinetics of the 1:1 complexes with Zn^{2+} are similar to those of hydrogen bonded complexes with protic solvent molecules and thus it is assumed that the structures are similar in both cases (**29** and **30**).

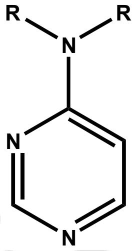

R = CH_3 **26**
R = C_2H_5 **27**

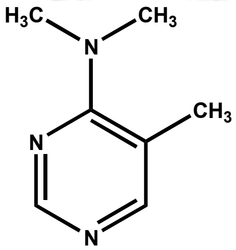

28

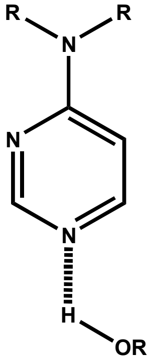

29

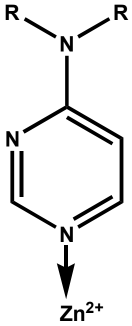

30

Aminophenylpyridoimidazoles are interesting class of molecules, where hydrogen bonding is absolutely essential to obtain dual emission. Fasani et al. were the first to show that 2-(4'-aminophenyl)-pyridoimidazoles (**31** and **32**) emit single emission from locally excited state in nonpolar and polar aprotic solvents, but dual emission from both locally excited state and ICT state in alcoholic solvents.[77] They hypothesized that the hydrogen bonding of protic solvents with imidazole nitrogen and 'NH' hydrogen twists the pyridoimidazole group with respect to the rest of the molecule which results in the formation of the TICT state. This is contrary to reports that the hydrogen bonding of the solvent with acceptor make it more planar with the spacer, which facile the charge flow from the spacer to the acceptor.[78,79] The hydrogen bonding induced TICT emission from 2-(4′-*N,N*-dimethylaminophenyl) pyridoimidazoles (**33** and **34**) were also studied. But it is reported that the hydrogen

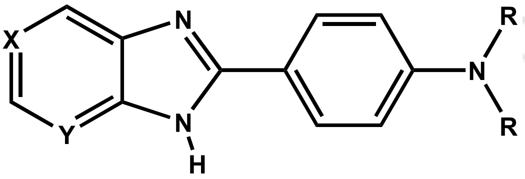

X = N, Y = CH, R = H **31**
X = CH, Y = N, R = H **32**
X = N, Y = CH, R = CH_3 **33**
X = CH, Y = N, R = CH_3 **34**

bonding with pyridine nitrogen plays an important role in the formation and stabilization of the TICT state.[79-86]

The ICT emission of *N*,*N*-dimethylaminophenyl(phenyl)acetylene (**35**) is significantly quenched in protic solvents due to the lowering of the energy gap between the ICT and the low lying states as the hydrogen bonding of the solvent with the acceptor stabilizes the ICT state.[87] *trans*-(4-Monoethylaminophenyl)-acrylonitrile (**36**) in non polar solvents shows normal emission only, whereas in polar aprotic solvents it shows dual emission.[88] The large Stokes shifted band is the ICT band and is further red shifted with increasing polarity of the solvent but with decrease in intensity. In protic solvents with increasing hydrogen bonding capacity the quantum yields decrease, but a linear relationship between the fluorescence maxima of the ICT band and the hydrogen bonding parameter[89] was observed. This shows hydrogen bonding interaction is responsible for the large Stokes shift in the ICT band which leads to enhanced nonradiative decay from the ICT state.

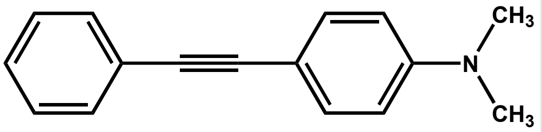

35

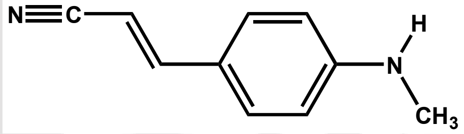

36

1.8. Effect of microheterogeneous environments

As the ICT process is very much sensitive towards the nature of the environments,[90] the confined environments such as micelles, reverse micelles, cyclodextrins and proteins significantly affect the photophysical process that occurs in the molecules.

The ICT process of ethyl ester of *N*,*N*-dimethylaminonaphthyl-(acrylic)-acid is investigated in various micellar environments.[91] It is found that the sensitivity of the ICT band is greater in the micellar environment rather than the local excited emission band. Due to the change in viscosity and strong binding of the molecule with micelles, the nonradiative rate decreases as a result the fluorescence intensity increases. The ICT property of *trans*-ethyl-*p*-(dimethylamino)cinnamate is used to probe different micelles.[92] The intensity of the ICT fluorescence band is increased with a blue shift upon addition of surfactants. It is suggested that the fluorophore resides in the interface region in all micellar environments, but comparatively it penetrates more towards the micellar core in presence of nonionic micelle than in ionic micelle. The ICT fluorescence of 3-(4'-dimethylaminophenyl)-1-(2-furanyl)prop-2-en-1-one and the corresponding thienyl derivative in aqueous micellar solutions undergoes strong hypsochromic shift with a greater enhancement in the fluorescence quantum yield due to reduced polarity of the environment.[93,94] The ICT emission of 4-(*p*-*N*,*N*-dimethyl-aminophenylmethylene)-2-phenyl-5-oxazolone experiences a hypsochromic shift with enhancement in intensity in sodium dodecyl sulfate (SDS) and cetyl trimethylammonium bromide (CTAB) micelles than in aqueous medium. Due to the less polar medium, the ICT state is destabilized inside micelles, as a result the energy gap between the emitting ICT state and ground state increases, which produces blue shift of the spectra.[95] The shift and intensity of ICT band of 2-(4-(dimethylamino)styryl)-1-methylpyridinium iodide is different in different micelles due to difference in the binding location.[96] DMAPIP-b selectively emits dual fluorescence from both locally excited state and TICT state in SDS and triton X-100 (TX-100) whereas in CTAB no TICT emission is observed.[85] This behavior is attributed to the variation in the extent of hydrogen bonding capacity experienced by the fluorophore in different micelles.

6-propionyl-2-dimethylaminonaphthalene shows a clear ICT emission at higher w_0 value in aerosol OT (AOT) reverse micelle whereas in cationic benzyl-*n*-hexadecyl dimethylammonium chloride reverse micelle the ICT emission is not clear.[97] It is speculated that in both reverse micelles the molecule remains at the reverse micelle interface. However the hydrogen bond accepting carbonyl group of the molecule remains towards the hydrocarbon tails, far from water pool and polar head group in AOT reverse micelle whereas in cationic reverse micelle the orientation is just opposite. As a result the hydrogen bonding interaction is obstructed in AOT whereas its strong in cationic reverse micelle resulting a clear ICT emission in AOT. The retardation of the ICT process of 2,6-*p*-toluidinonapthalene sulfonate occurs inside the water pool of the AOT reverse micelle than in bulk water is due to the lower static polarity of the water pool compared to the bulk water.[98] The rate of TICT emission of 4-(1-morpholenyl)benzonitrile in AOT reverse micelles increases with increase in water pool size due to increase in CT character upon increasing w_0 value because of the increase in average polarity of the medium.[99] However, the TICT emission is less pronaounced in compared to the bulk water because of the extra restriction arises from the enhanced rigidity of the solvent molecules due to confinement as a result the rotation of the donor group (morpholenyl group) is hindered.[99] The dynamics of the ICT process of nile red inside the water nanopool of the reverse micelle is slow compared to that in bulk water due to the lower static polarity of the water pool.[100] The ICT rate and solvation dynamics of coumarin 490 in AOT reverse micelle is found to be decreased compared to that in bulk water.[101] Similar behavior was also reported for some coumarin derivatives in aqueous and non-aqueous reverse micellar environments.[101-104] The ICT fluorescence anisotropy of 3-acetyl-4-oxo-6,7-dihydro-12*H*-indolo-[2,3-a]quinolizine decreases drastically with increase in the core size of AOT reverse micelle.[105]

The reduction in the rate of ICT of 3-acetyl-4-oxo-6,7-dihydro-12*H*-indolo-[2,3-a] quinolizine occurs within the hydrophobic interior of albumins.[106] Fluorescent molecules containing both a hydroxystyryl and a cyanopyranyl moieties were found to exhibit very weak fluorescence emission in the absence of protein, whereas a large Stokes shift and dramatic increase of fluorescence intensity and red emission observed upon addition of BSA caused by the ICT.[107] It is reported that the ICT exhibiting halogenated squaraine dyes show high selectivity toward site II of serum albumins with appreciably high association constant.[108] This shows that these squaraine dyes can be used as potential noncovalent protein labeling and photodynamic therapeutic agents. A polarity sensitive ICT molecule (*E*)-3-(4-methylamino-phenyl)-acrylic acid ethyl ester is reported to act as a probing agent to stabilize BSA.[109] ICT emitting 4-aminonaphthalimide-based ratiometric fluorescent probe is designed for the quantification of BSA by a ratiometric and colorimetric way with high sensitivity.[110] It is reported that a fluorescent probe having styryl, sulfonyl and cyanopyranyl moieties interacts with the protein via noncovalent interaction.[111] The fluorescence intensity enhanced drastically upon binding with the protein owing to ICT nature of the emission.

The restricted environment inside the cyclodextrin (CD) cavity as well as the hydrophobic nature affects, the spectral characteristics of the ICT molecules drastically.[112] The ICT fluorescence intensity of *trans*-ethyl-*p*-(dimethylamino) cinnamate and its acid derivative was found to increase with a blue shift in the presence of cyclodextrins.[113] The spectral modulations of an ICT molecule ethyl ester of *N*,*N*-dimethylaminonaphthyl-(acrylic)-acid occurs upon encapsulation in the water and DMF solution of β-CD nanocavities.[114] *p*-dimethylaminoacetophenone does not have any TICT emission in aqueous solution, whereas in α-CD solution, both the locally excited and TICT emission are enhanced.[115] The behavior is attributed due to the formation of a 1:2 complex in which the molecule is entirely trapped by two α-CD molecules. The increase in the intensity of the TICT band of *p-N,N*-dimethylaminobenzaldehyde relative to the locally excited band is found to be maximum in α-CD and minimum in γ-CD medium due to the difference in polarity of the CDs.[116,117] The relative retardation of nonradiative rate for TICT emission of nile red[118] results in the presence of both β-CD and γ-CD compared to pure water and the rate is much higher in β-CD than in γ-CD. The little retardation in the nonradiative rate of nile red in presence of γ-CD is attributed to the formation of hydrogen bonds between the hydroxyl groups of γ-CD with the molecule.[118] Upon encapsulation in CD cavity, the charge transfer fluorescence of 3-acetyl-4-oxo-6,7-dihydro-12*H*-indolo-[2,3-a]quinolizine exhibits hypsochromic shift.[119] The nonradiative deactivation rate of the fluorophore also decreases in the nanocavities which lead to an increase in both fluorescence yield and lifetime.

1.9. Photoisomerization and ICT

Push–pull styryl dyes have received considerable attention because of their wide applications in various fields.[120-125] In these molecules, presence of the donor and the acceptor moiety facilitates ICT emission; additionally presence of the olefinic double bond causes excited state torsional rotation about carbon–carbon double bond results in *trans–cis* photoisomerization. Photoisomerization is a very important phenomenon that occurs in several biological processes. For example photoisomerization of retinal plays a key role in vision (**Chart 1.1**).[126,127] It is reported that styrylpyridines are useful as imaging agent in the living human brain of patients suffering from Alzheimer's disease.[128] Styryl dyes show very high first-order hyperpolarizability, thus can act as very efficient materials for the applications in molecular electronics.[129,130] The photophysical and photochemical properties of these molecules are of key interest to many researchers.[131-137]

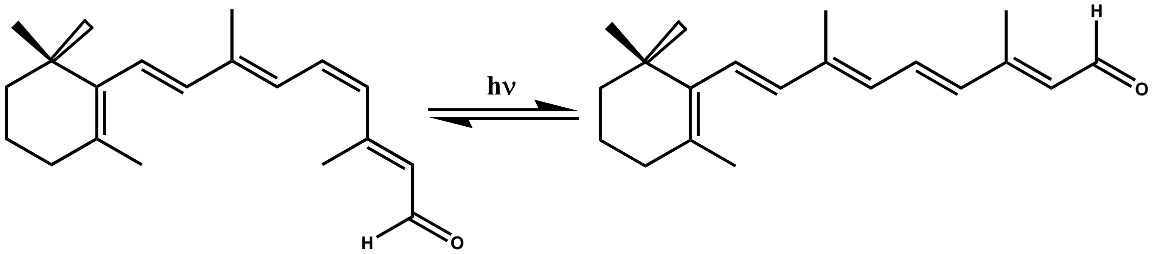

Chart 1.1. **Photoisomerization of retinal in the vision process.**

In push-pull styryl compounds the main deactivation process arises due to the photoisomerization process which competes with the fluorescence emission.[138-142] The fluorescence quantum yield of 1-(9-Anthryl)-2-(4-Pyridyl)ethenes in polar solvents drastically reduced and the photoisomerization quantum yield increased due to the stabilization of ICT excited state.[143] The fluorescence quantum yield of *trans*-4-dimethylamino-4′-cyanostilbene increases upon increasing the polarity of the solvent and decreasing the temperature due to decrease in the photoisomerization process.[144,145] Nonheterocyclic push–pull aromatic systems are extensively studied, however the heterocycle based push–pull aromatic systems are scarily reported.[146-151] Ho et al. studied the substitution effects on the ICT behavior of some styrylheterocycles[146] and suggested that due to the presence of strong donor dimethylamino group, ICT emission occurs on those molecules. Fayed et al. studied benzothiazole and benzoxazole derived push–pull styrenes[148,149] and butadienes[150] (**37** and **38**) with *N*,*N*-dimethylaminophenyl group as donor. It is revealed that all these molecules exhibit ICT emission and interesting prototropic equilibria. Fayed et al. established the utility of benzazole derived push–pull butadienes to probe the micelles.[152] Saha et al. and Purkayastha et al. extend studies on *trans*-2-[4′-(dimethylamino)styryl]benzothiazole (*t*-DMASBT)[153,154] (**37b**) and elaborated its utility as fluorescent probe for various microheterogeneous systems.[155,156] However Saha et al. predicted that isomerization takes place only in nonpolar solvent like dioxane, but no isomerization takes place in polar viscous solvent like glycerol. Our result suggests that **37b** undergoes isomerization not only in nonpolar solvents, but also in viscous polar solvent including glycerol even at room temperature.[157,158]

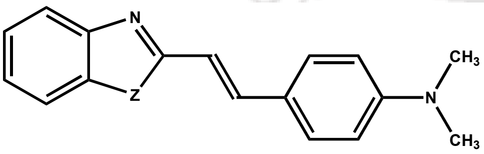

(a) X = O

(b) X = S

37

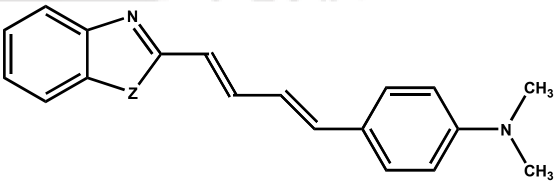

(a) X = O

(b) X = S

38

1.10. Scope of the present work

It is already explained earlier that ICT has been a topic of growing interest both in photochemistry and photobiology as it is a possible mechanism for several biological processes and chemical energy conversion. In the present thesis the photoinduced ICT process of a few organic bichromophoric molecules are studied in various homogeneous and microheterogeneous environments.

DMAPIP-b is a biologically active molecule and it acts as an inhibitor for aurora kinases.[159] It also has interesting photophysical characteristics. It emits dual emission only in protic solvents. The shorter and the longer wavelength emissions are attributed to the normal and the TICT emissions, respectively.[82] The dual emissive nature and its sensitivity towards the environment make DMAPIP-b as an excellent ratiometric probe to investigate various microheterogeneous systems including protien.[83,85,160] Although it is reported that the hydrogen bonding with pyridyl nitrogen plays a vital role in the formation of the TICT in protic environment, the mechanism of the process is not clearly understood. To understand the mechanism of the formation of TICT state in DMAPIP-b, the photophysical characteristics of some analogues of DMAPIP-b are investigated (**Chapter 3**). As discussed earlier, push-pull styryls have wide applications in various fields.[161-165] In order to understand the effect of introducing olefinic double bond in DMAPIP-b on the spectral characteristics of the system *trans*-2-[4'-(dimethylamino)styryl]imidazo[4,5-b]pyridine (*t*-DMASPI-b) was synthesized and studied in solvents of different polarity, viscosity and hydrogen bonding capacity (**Chapter 4**). The water confined in the reverse micelles mimic biological water and its characteristics are different from the bulk water. Since, the dual emission of DMAPIP-b strongly depends on the nature of the protic media the photophysics of DMAPIP-b was examined in reverse micelles (**Chapter 5**).

Imidazoles and oxazoles are important class of heterocyclic compounds. Varieties of drug molecules have the imidazole and oxazole frameworks and these heterocyclic frames play important role in the interactions of those drugs with proteins. Therefore, a comparative study on the interactions of proteins with imidazoles and oxazoles will be useful for the design and discovery of drug. Serum albumins are the most abundant transport proteins[166,167] found in the blood plasma and can bind with various biologically relevant substances like bilirubin, bile salts, certain metals, hormones and a variety of therapeutic drugs.[168-170] Owing to the easy availability and the similarities with human serum albumin, BSA is considered as a model protein. Since, ICT emission is more sensitive, the interactions of ICT emitting imidazoles and oxazoles, 2-(4′-*N*,*N*-dimethylaminophenyl)benzimidazole (DMAPBI) and its other analogues with BSA are studied to understand the fundamental interaction between these heterocyclic derivatives and BSA (**Chapter 6**).

Developing high sensitive and selective sensors for the detection of metal ions in biological and environmental fields is an active area of research. A variety of divalent metal ions are known to be involved in the structural, catalytic and regulatory aspects of the biological system and some such metal ions serve as prognostics of certain human diseases.[171] Although a large number of studies have been performed on the sensing ability of fluorescent molecules toward different metal ions, still to get selective and sensitive fluorophore is highly challenging. Substantial amount of chemosensors developed for metal ion sensing have heterocylic derivatives. Since ICT emission is sensitive to the environment, several ICT based metal sensors have been developed. Thus, a comparative study of ICT emitting DMAPBI and its oxazole analogues are explored to understand the effect of heteroatom on their potential for metal ion sensing ability (**Chapter 7**).

The effect of micelles on prototropic equilibriums are well studied and understood.[172-175] However, the role of micelles on the site of protonation is also an interesting subject which did not receive much attention. Therefore, the effect of anionic, cationic and nonionic micelles on the protonation sites of push-pull styryl derivatives, *t*-DMASBT, *trans*-2-[4'-(dimethylamino)styryl]imidazo[4,5-c]pyridine (*t*-DMASIP-c) and *t*-DMASIP-b are investigated (**Chapter 8**).

Chapter 2

Materials, methods and instrumentations

Indian Institute of Technology Guwahati

2.0. Introduction

This chapter provides the details of the chemicals and the solvents used for the syntheses of the fluorophores and the experimental work carried out in the present thesis work. Also the procedure followed for the syntheses, experiments, theoretical calculations and analyses of the data were briefly described in this chapter. The chapter ends with details of the instruments used and a brief description of the major instruments.

2.1. Materials

The details of the solvents and chemicals used for performing the syntheses as well as experiments are given below.

2.1.1. Solvents

- Acetonitrile (HPLC grade, Spectrochem India)
- 1-Butanol (HPLC grade, Spectrochem India)
- Cyclohexane (HPLC grade, Rankem India)
- Diethyl ether (HPLC grade, Spectrochem India)
- Dimethylformamide (DMF, HPLC grade, Rankem India)
- Dimethylsulfoxide (DMSO, HPLC grade, Rankem India)
- 1, 4-Dioxane (AR grade, Spectrochem India)
- Ethanol (ACS grade, Merck)
- Ethyl acetate (HPLC grade, Rankem India)
- Glycerol (AR grade, Rankem India)
- Glycol (AR grade, Rankem India)
- Methanol (HPLC grade, Rankem India)
- 1-Propanol (AR grade, Rankem India)
- 2-Propanol (HPLC grade, Rankem India)
- Tetrahydrofuran (THF, HPLC grade, Rankem)
- Water (Millipore)

The solvents were transparent in the spectral region of interest and were used as received.

2.1.2. Metal salts

- Barium perchlorate hydrate, $Ba(ClO_4)_2.xH_2O$ (Sigma Aldrich)
- Cadmium nitrate hydrate, $Cd(NO_3)_2.xH_2O$ (Merck)
- Calcium perchlorate tetrahydrate, $Ca(ClO_4)_2.4H_2O$ (Sigma Aldrich)
- Cobalt chloride hexahydrate ($CoCl_2.6H_2O$) (Merck)
- Copper perchlorate hexahydrate, $Cu(ClO_4)_2.6H_2O$, (Sigma Aldrich)
- Lithium perchlorate, $LiClO_4$ (Sigma Aldrich)
- Magnesium perchlorate hexahydrate, $Mg(ClO_4)_2.6H_2O$ (Sigma Aldrich)
- Nickel perchlorate hexahydrate, $Ni(ClO_4)_2.6H_2O$ (Sigma Aldrich)
- Silver nitrate, $AgNO_3$ (Sigma Aldrich)
- Sodium perchlorate monohydrate, $NaClO_4.H_2O$ (Sigma Aldrich)
- Pottasium perchlorate, $KClO_4$ (Sigma Aldrich)
- Zinc perchlorate hexahydrate, $Zn(ClO_4)_2.6H_2O$ (Sigma Aldrich)

2.1.3. Other chemicals

- Aerosol OT (AOT, Sigma Aldrich)
- 2-Aminophenol (Himedia)
- 2-Aminothiophenol (Sigma Aldrich)
- 2-Amino-3-hydroxypyridine (Sigma Aldrich)
- Bovine serum albumin (BSA, Merck India)
- Cetyltrimethylammonium bromide (CTAB, Sigma Aldrich)
- Chloroform-d (Sigma Aldrich)
- β-Cyclodextrin (β-CD, Sigma Aldrich)
- 4-Dimethylaminocinnamic acid (Sigma Aldrich)
- 2,3-Diaminobenzene (Sigma Aldrich)
- 2,3-Diaminopyridine (Sigma Aldrich)
- 3,4-Diaminopyridine (Sigma Aldrich)
- Diphosphorous pentoxide (Merck India)
- Dimethylsulfoxide-d_6 (Sigma Aldrich)
- Di-sodium hydrogen phosphate anhydrous (Merck)
- Iodomethane (Merck India)
- Methyl-d_3 alcohol-d (Sigma Aldrich)
- *ortho*-Phenylenediamine (Merck India)
- *ortho*-Phosphoric acid (AR grade, Rankem India)

- Phosphorous oxychloride (Spectrochem)
- Potassium hydroxide (Merck India)
- Silica gel (60-120 mesh) (Merck India)
- Silica gel for thin layer chromatography (Merck India)
- Silica gel GF254 (Merck India)
- Sodium dihydrogen phosphate dihydrate (Merck)
- Sodium dodecyl sulfate (SDS, Sigma Aldrich)
- Sodium hydroxide (Merck India)
- Sodium sulfate anhydrous (Merck India)
- Sulfuric acid (AR grade, Rankem India)
- Triton X-100 (TX-100, Sigma Aldrich)

2.1.4. Synthesis

2.1.4.1. Syntheses of 2-(4′-*N*,*N*-dimethylaminophenyl)oxazolo[4,5-b]pyridine and 2-(4′-*N*,*N*-dimethylaminophenyl)benzoxazole

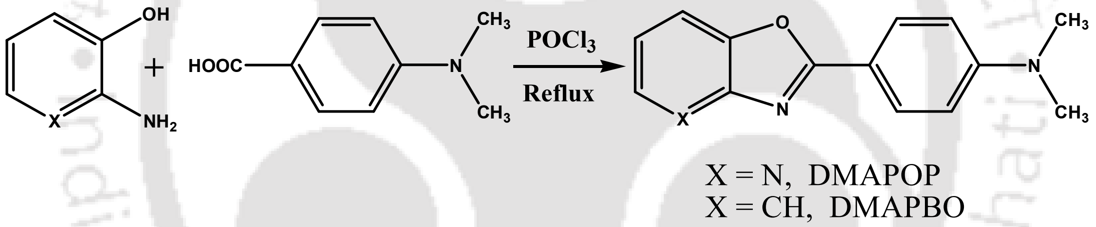

Scheme 2.1. Syntheses of DMAPOP and DMAPBO.

2-(4'-*N*,*N*-Dimethylaminophenyl)oxazolo[4,5-b]pyridine (DMAPOP) was synthesized by refluxing equivalent amount of 2-amino-3-hydroxypyridine and *p*-(*N*,*N*-dimethylamino)benzoic acid in $POCl_3$ for 8 h (**Scheme 2.1**).[159] Then the reaction mixture was cooled to room temperature and poured to ice cold water. The mixture was neutralized by concentrated NaOH solution. The precipitates were collected and purified by column chromatography. 2-(4′-*N*,*N*-Dimethylaminophenyl)benzoxazole (DMAPBO) is synthesized following the same procedure using 2-aminophenol instead of 2-amino-3-hydroxypyridine.

DMAPOP: **^{1}H NMR** (400 MHz, $CDCl_3$, ppm) δ 8.46 (d, J = 4.4 Hz, 1H); 8.14 (d, J = 8 Hz, 2H); 7.86 (d, J = 16.4 Hz, 1H); 7.16 (dd, J = 8.8 Hz, 1H); 6.75 (d, J = 16.4 Hz, 2H); 3.07 (s, 6H).

LCMS (M+1): 241.11.

DMAPBO: **^{1}H NMR** (600 MHz, CD_3OD, ppm) δ 8.13 (d, J = 9 Hz, 2H); 7.70 (d, J = 7.8 Hz, 1H); 7.52 (d, J = 7.8 Hz, 1H); 7.29 (m, 2H); 6.79 (d, J = 9 Hz, 2H); 3.08 (s, 6H).

HRMS (M+1): 239.1289.

2.1.4.2. Syntheses of 2-(4′-*N*,*N*-dimethylaminophenyl)benzimidazole, 2-(4′-*N*,*N*-dimethylaminophenyl)imidazo[4,5-b]pyridine and 2-phenylimidazo[4,5-b] pyridine

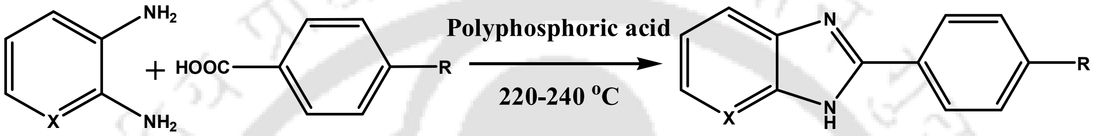

X = N, R = $N(CH_3)_2$, DMAPIP-b
X = CH, R = $N(CH_3)_2$, DMAPBI
X = N, R = H, PIP

Scheme 2.2. Syntheses of DMAPIP-b, DMAPBI and PIP.

2-(4′-*N*,*N*-Dimethylaminophenyl)benzimidazole (DMAPBI), 2-(4′-*N*,*N*-dimethylaminophenyl)imidazo[4,5-b]pyridine (DMAPIP-b) and 2-phenylimidazo[4,5-b]pyridine (PIP) were synthesized following the reaction scheme shown in **Scheme 2.2**.[176,177] Equimolar mixture of appropriate diamine and acid were heated in polyphosphoric acid at 220-240 ºC for 5 h. The reaction mixture was cooled to room temperature and poured to ice cold water and stirred well. The acidic solution was then neutralized with aqueous KOH solution. The precipitates were suctioned by vacuum and dried overnight in desiccator. The dried precipitate was dissolved in methanol by heating. The solution was filtered and the solvent was evaporated by rotavapor. Then the crude was purified by column chromatography using silica gel as stationary phase and varying percentage of ethyl acetate in hexane as eluent. The identities and purity of the synthesized compounds were confirmed by either HRMS or LCMS and NMR.

DMAPIP-b: **^{1}H NMR** (400 MHz, CD_3OD), δ: 8.24 (d, 1H, J = 5 Hz), 8.12 (d, 2H, J = 9 Hz), 7.96 (d, 1H J = 8 Hz), 7.14 (dd, 1H, J = 8,5 Hz), 6.74 (d, 2H, J = 9 Hz), 3.05 (s, 6H).

LCMS (M+1) 239.12.

DMAPBI: ^{1}**H NMR** (600 MHz, CD_3OD, ppm) δ 7.93 (d, *J* = 8.4 Hz, 2H); 7.59 (d, *J* = 7.8 Hz, 2H); 7.22 (m, 2H); 6.76 (d, *J* = 8.4 Hz, 2H); 3.03 (s, 6H).

HRMS (M+1): 238.1457.

PIP: ^{1}**H NMR** (400 MHz, $CDCl_3$, ppm) δ 8.41 (d, 1H); 8.26 (d, 2H); 8.15 (d, 1H); 7.58 (m, 3H); 7.30 (m, 1H).

LCMS (M+1): 196.10.

2.1.4.3. Synthesis of *N*,*N*-dimethyl-4-(4-methyl-4*H*-imidazo[4,5-b]pyridin-2-yl) benzenamine

N,*N*-Dimethyl-4-(4-methyl-4*H*-imidazo[4,5-b]pyridin-2-yl)benzenamine (PyN-Me) was synthesized by irradiating the mixture of DMAPIP-b and methyl iodide by microwave (200 W) using the procedure given in the literature[86,178] and followed by a treatment with ammonia solution (**Scheme 2.3**).[179] The compound was purified by preparative thin layer chromatography. The identity of the compound was confirmed using NMR and mass data.

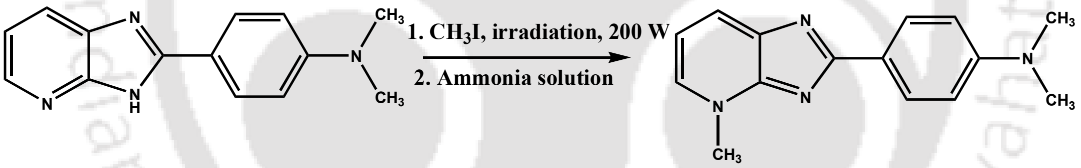

Scheme 2.3. Synthesis of PyN-Me.

^{1}**H NMR** (400 MHz, $CDCl_3$, ppm) δ 7.71 (1H, d), δ 7.53 (2H, d), δ 7.26 (3H, m), δ 6.99 (1H, d), δ 4.19 (3H, s), δ 3.15 (6H, s).

LCMS (M + 1): 253.06.

2.1.4.4. Synthesis of 1-methyl-2-(4′-(*N*,*N*-dimethylaminophenyl)imidazo[4,5-b]pyridine

1-Methyl-2-(4′-(*N*,*N*-dimetylaminophenyl)imidazo[4,5-b]pyridine (ImNH-Me) was synthesized by following the literature procedure for alkyl substitution of similar compounds.[86,180] DMAPIP-b and methyl iodide (4:9) was dissolved in a solvent mixture of 3 ml dimethylformamide and 1 ml tetrahydrofuran. Powdered KOH was added and heated at 40 °C for 24 h (**Scheme 2.4)**. The compound was extracted with dichloromethane and purified by column chromatography. The identity of the compound was confirmed by NMR and mass data.

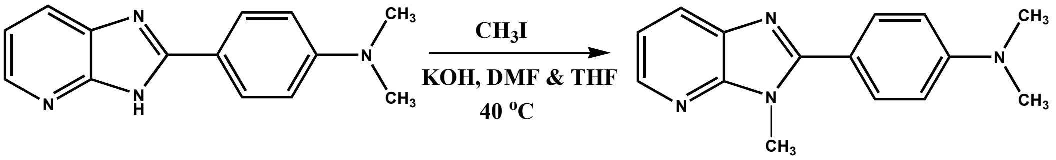

Scheme 2.4. Synthesis of ImNH-Me.

^{1}H NMR (400 MHz, CDCl$_3$, ppm) δ 8.35 (1H, d), δ 8.02 (1H, d), δ 7.77 (1H, t), δ 7.22 (2H, d), δ 6.83 (2H, d), δ 4.00 (3H, s), δ 3.07 (6H, s).
LCMS (M+1): 253.08.

2.1.4.5. Synthesis of *trans*-2-[4'-(dimethylamino)styryl]benzothiazole

t-DMASBT was synthesized by procedure reported by Fayed et al.[149] A solution of *p*-dimethylamino benzaldehyde (0.002 mmol) in dry DMF (4 mL) was added dropwise to a solution of 2-methylbenzothiazole (0.003 mmol) and powdered KOH (0.02 mmol) in 8 ml of dry DMF with continuous stirring. The mixture was stirred at 140 °C (**Scheme 2.5**). After 48 h the mixture was cooled to room temperature and dilute HCl (10%) was added to make it weakly acidic. The compound was extracted by dichloromethane. The compound purified by column chromatography was further purified by preparative thin layer chromatography using hexane-ethyl acetate mixture. The synthesis and purification of the compound were carried under red light to avoid photoisomerization.

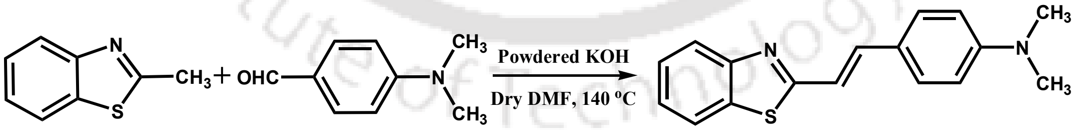

Sc

heme 2.5. Synthesis of *t*-DMASBT.

^{1}H NMR (400 MHz, CD$_3$OD), δ 7.87 (d, *J* = 7.6 Hz, 1H); 7.75 (d, *J* = 8.4 Hz, 1H); 7.42-7.35 (m, 4H); 7.25 (t, *J* = 7.6 Hz, 1H); 7.14 (d, *J* = 16 Hz, 1H); 6.65 (d, *J* = 8.8 Hz, 2H); 2.96 (s, 6H).
HRMS (M+1): 281.1178

2.1.4.6. Syntheses of *trans*-2-[4'-(dimethylamino)styryl]imidazo[4,5-b]pyridine and *trans*-2-[4'-(dimethylamino)styryl]imidazo[4,5-c]pyridine

trans-2-[4'-(Dimethylamino)styryl]imidazo[4,5-b]pyridine (*t*-DMASIP-b) and *trans*-2-[4'-(dimethylamino)styryl]imidazo[4,5-c]pyridine (*t*-DMASIP-c) were synthesized by the same procedure used for the synthesis of DMAPBI and related molecules and the schematic representation is shown in **Scheme 2.6**. However purifications of these styryl compounds were carried out by column chromatography followed by preparative thin layer chromatography. Same as in benzothiazole analogue, red light environment is maintained throughout the synthesis and purification to avoid the isomerization. The identities and purity were confirmed by HRMS and NMR.

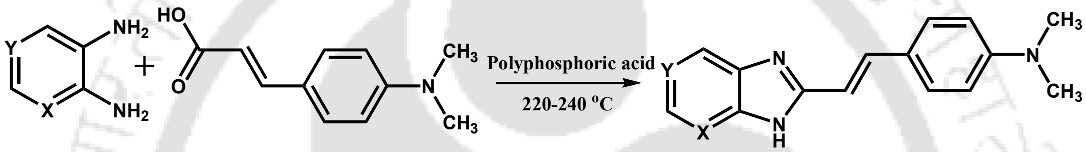

X = N, Y = CH, *t*-DMASIP-b
X = CH, Y = N, *t*-DMASIP-c

Scheme 2.6. Syntheses of *t*-DMASIP-b and *t*-DMASIP-c.

***t*-DMASIP-b: ^{1}H NMR** (400 MHz, CD_3OD, ppm): δ 8.10 (d, J = 4.4 Hz, 1H); 7.72 (d, J = 8 Hz, 1H); 7.49 (d, J = 16.4 Hz, 1H); 7.32 (d, J = 8.8 Hz, 2H); 7.06 (dd, J_1 = 5.2 Hz, J_2 = 8 Hz, 1H); 6.74 (d, J = 16.4 Hz, 2H); 6.56 (d, J = 8.8 Hz, 1H), 2.82 (s, 6H).

HRMS (M+1): 265.1479.

***t*-DMASIP-c: ^{1}H NMR** (600 MHz, $CDCl_3$, ppm): δ 8.28 (d, J = 6 Hz, 1H); 8.24 (d, J = 5.4 Hz, 1H); 8.09 (s, 1H); 7.60 (d, J = 16 Hz, 1H); 7.36 (m, 2H); 7.05 (d, J = 9 Hz, 1H); 6.83 (d, J = 16 Hz, 1H); 6.62 (d, J = 8.2 Hz, 1H); 2.95 (s, 6H).

HRMS (M+1): 265.1468.

2.2. Sample preparation

2.2.1. In solvents

The main stock solution of the compound of concentration 1 x 10^{-3} M was prepared in methanol. From the stock solution 50-100 µl was pipette out to 10 ml volumetric flasks. The solution was kept in oven for overnight at 50 °C for complete removal of methanol. Then 10 ml of experimental solvent/solution was added to volumetric flask. For pK_a measurements of dilute phosphoric acid and NaOH solution were used for maintaining the required pH. The fluorophore concentrations were 5-10 μM for any absorption or fluorescent measurement unless otherwise mentioned. The styryl dyes solutions were prepared in red light conditions.

2.2.2. In micelles

The stock solutions of surfactant were prepared in 100 ml volumetric flask by dissolving appropriate amount of surfactant (**Figure 2.1**) in millipore water. Appropriate amount of surfactant solution and water were added to the fluorophore in the volumetric flask. The pH of the solutions were adjusted by adding dilute sulfuric acid or sodium hydroxide solution.

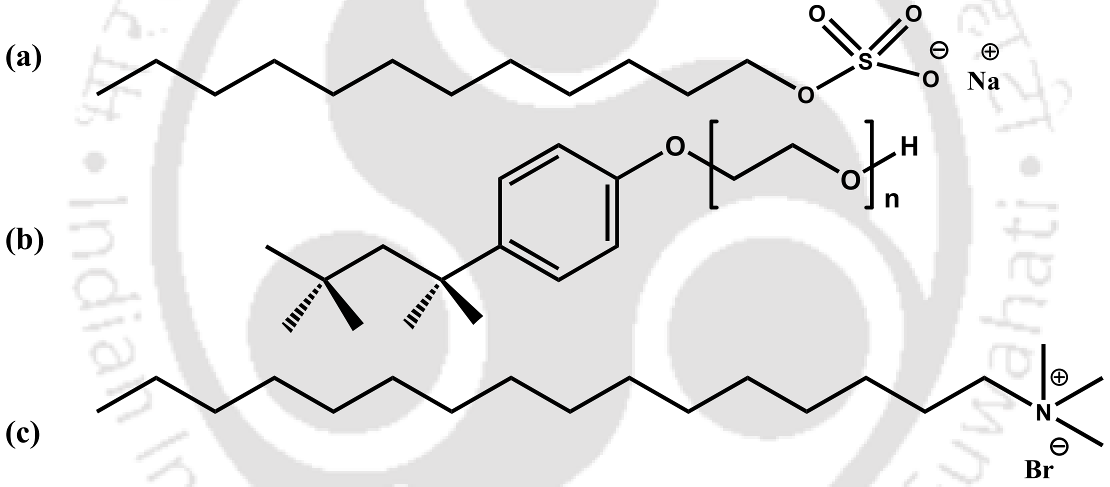

Figure 2.1. Structures of (a) SDS, (b) TX-100 and (c) CTAB.

2.2.3. In reverse micelles

AOT/*n*-heptane/water reverse micelles were prepared by mixing desired amount of water, *n*-heptane-AOT solution. The water quantity in the reverse micellar system is represented in terms of molar ratio (w_0) of water to the surfactant. The fluorophore concentration (5 μM) and the AOT concentration (0.1 M) were kept fix and the water quantity were varied. The structure of AOT is shown in **Figure 2.2**.

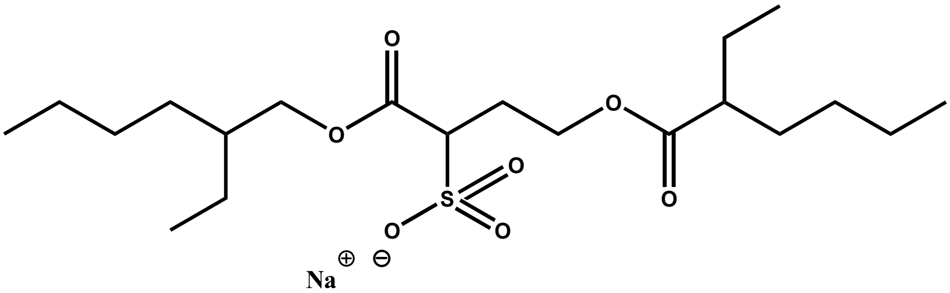
Figure 2.2. Structure of AOT

2.2.4. Metal ion solutions

Metal perchlorates of lithium, sodium, potassium, magnesium and copper were used as source of their respective metal ions. Nitrate salts of cadmium and silver were used as source for corresponding metal ion. Cobalt chloride was used as source of cobalt ion. The fluorophore concentrations were ~ 5 μM. For metal ion titration, by keeping the fluorophore concentrations fixed, the concentrations of metal ions were varied by adding appropriate amount of metal ion solution and solvent. Acetonitrile was used as solvent for these studies.

2.2.5. Protein samples

10 mM phosphate buffer of pH 7.0 was prepared by using monosodium phosphate and disodium phosphate in appropriate amount and is used for all protein sample solutions. Millipore water was used for the sample preparation. All the spectral measurements were preformed at the solute concentration of 5 μM (fixed). The protein concentrations were varied by adding appropriate amount of protein solution and buffer.

2.3. Methods

2.3.1. Quantum yield

Quantum yield of fluorescence (Φ_f) is defined as the ratio of the number of photons emitted to the total number of photons absorbed and is represented as follow.

$$\Phi_f = \frac{\text{Number of photons emitted}}{\text{Number of photons absorbed}} \qquad \textbf{(2.1)}$$

For the determination of the fluorescence quantum yields the absorbance of the sample were kept at 0.1. In the present work quinine sulphate in 1N sulphuric acid is used as a standard whose quantum yield is 0.55.[181] The quantum yield is calculated by using the following equation:

$$\frac{\Phi_s}{\Phi_r} = \frac{I_s A_r n_s^2}{I_r A_s n_r^2} \tag{2.2}$$

where I_s and I_r represent the area obtained from the emission spectra of the sample and reference respectively. The area under the curves are determined from λ_{ex} + (5 or 10) nm till the wavelength where the intensity is negligible. A_s and A_r are the absorbance values for the sample and reference respectively. n_s and n_r are the refractive indices for the sample and the reference solution respectively.

2.3.2. Determination of ionization constant

The acid dissociation constant or the pK_a is a measure of the strength of an acid or a base. pK_a value of the dye in a given medium provides knowledge about both nature of the probe and the medium. The Hammett equation is commonly used for the determination of ionization constant of the dissociation reaction of an acid in aqueous medium and is given below.

$$BH^+ + H_2O \rightleftharpoons B + H_3O^+ \tag{2.3}$$

$$H_0 = pK_a + \log\frac{[B]}{[BH^+]} \tag{2.4}$$

where [BH$^+$] and [B] are molar concentration of conjugate acid and base, respectively. H_0 is called Hammett's acidity function and is defined in the following equation

$$H_0 = -\log\frac{a_{H^+} f_B}{f_{BH^+}} \tag{2.5}$$

where f_B and $f_{BH}{}^+$ are the acidity coefficient of conjugate base and acid respectively. $a_H{}^+$ is the activity of the proton. For dilute solution, H_0 is replaced by pH. A plot of pH versus $\log\frac{[B]}{[BH^+]}$ is a straight line with unit slope and the pH = pK_a when [B] = [BH$^+$]. The factor $\frac{[B]}{[BH^+]}$ can be determined from following relation.

$$\frac{[B]}{[BH^+]} = \frac{[A_B - A]}{[A - A_{BH^+}]} \tag{2.6}$$

where A_{BH}+ and A_B are the absorbance (at the analytical wavelength) of the pure BH$^+$ and B respectively and A is absorbance (at same wavelength) of any solution in which BH$^+$ is partially ionized.

$$\frac{[B]}{[BH^+]} = \frac{[B]}{[C]-[B]} \tag{2.7}$$

where [C] is the molar concentration of compound in experimental solution.

$$[B] = \frac{A(\lambda_1)\varepsilon_{BH}^{+}(\lambda_2) - A(\lambda_2)\varepsilon_{BH}^{+}(\lambda_1)}{\varepsilon_B(\lambda_1)\varepsilon_{BH}^{+}(\lambda_2) - \varepsilon_B(\lambda_2)\varepsilon_{BH}^{+}(\lambda_1)} \tag{2.8}$$

ε is the molar extinction coefficient and for the calculation generally two wavelengths were considered (λ_1 and λ_2) at both side of the isosbestic point of the absorption spectra at different pH.

2.3.3. Quantum mechanical calculation

For the ground state optimization and to calculate the molecular parameters, the molecular geometries were optimized by employing gradient corrected exchange functional of Becke[182] and the correlation functional of Lee, Yang and Paar (LYP)[183] (B3LYP) using density functional theory (DFT) method. For the entire calculations 6-31G(d,p) basis set with restricted shell wavefunctions is employed.[184,185] To verify the minimum energy nature of the stationary points vibrational frequency analyses were performed. The excitation energies were obtained by vertical excitations of optimized ground states by time dependent DFT (TDDFT) method. Since it has been reported that the geometries and the molecular properties obtained at the configuration interaction singles (CIS) level are quite reasonable and correct, at least as a first approximation for a number of molecules,[186,187] the geometry optimization in the excited state is performed by CIS method. TDDFT method is employed on these optimized geometries to obtain the emission energies. The computational calculations were performed using Gaussian 03.[188]

2.3.4. Docking study

For docking studies the amino acid sequence of bovine serum albumin (BSA) protein was obtained from the NCBI website.[189] The 3D model of the BSA protein was built using the 3D structure 1AO6 chain 'A' as template using the ESyPred3D18 web server. This template shares 72.4% identities with the BSA sequence. Following is the BSA sequence which was used to generate the 3D model. >gi|3336842|emb|CAA76847.1| bovine serum albumin [Bos taurus]. The minimum energy ligand molecules are obtained from the DFT optimized geometries by

Gaussian software and were used in docking study. Docking calculations were carried out by autodock 4.2 software.[190] Binding sites were automatically detected by the docking software. AutoDock 4.2 uses the Lamarckian genetic algorithm to search for the optimum binding site of small molecules to the protein. To recognize the binding sites in BSA, docking study were done by using the grid box 40, 40, 40 along X, Y and Z coordinates with grid spacing as 0.375 Å and grid center was set to 30.314, 32.063 and 24.976 Å along X, Y and Z axis respectively. The following parameters also kept fixed for all the three molecules. Genetic algorithm (GA) population size: 150; maximum number of energy evaluations; 250 0000, maximum number of runs; 200 considered for each molecule. The conformation with the lowest binding energy and of highest clustering was same for all the cases and those conformations have considered for further analysis. The data were examined by PyMOL software.[191]

2.4. Instruments

2.4.1. Absorption measurements

The modern absorption spectrometers consist of following components: light source, monochromator, detector, amplifier and recording devices. A beam of light from the source is separated into its component wavelengths by a monochromator. Each monochromatic beam splits into two beams; sample beam and reference beam by a half-mirrored device. The sample beam passes through a cuvette containing the sample solution. The reference beam passes through an identical cuvette containing the reference solvent. The intensities of these beams are then measured by detectors and compared. The intensity of the reference beam is generally defined as I_0 and the intensity of the sample beam is defined as I. Finally the spectrophotometer scans automatically all the component wavelengths with a short time period. The block diagram of UV-visible spectrophotometer is shown in **Scheme 2.7**.

In the present work, absorption spectra were recorded with the help of a Cary 100 double beam spectrometer. Deuterium and tungsten lamps are used as light sources and photomultiplier tube (PMT) is used as detector.

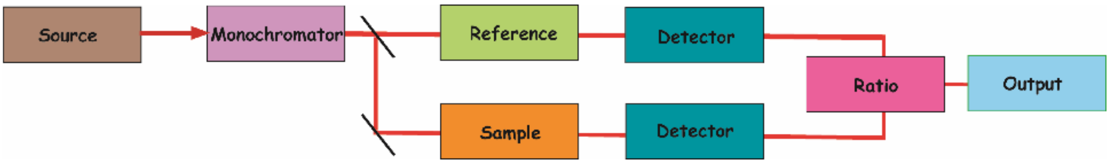

Scheme 2.7. Block diagram for UV-visible spectroscopy.

2.4.2. pH measurements

The pH of different solutions were measured using Jenway (model No 3510) pH meter. Before any measurement, the pH meter was calibrated using three different standard buffer solutions (pH 4, pH 7 and pH 10) within a range of ± 0.02 pH units.

2.4.3. Steady state fluorescence measurements

Fluorescence spectral measurements were carried on Edinburgh Instruments FSP 920, Jobin Yon Spex Fluoromax 4, Fluorolog 3 and Cary Eclipse instruments depending on the availability of the same. The block diagram for steady state fluorimeter (FSP 920) is shown in **Scheme 2.8**.

Optical System

The most common light source for fluorimeter is xenon arc lamp, as xenon light provides relatively uniform intensity over a broad spectral range from the ultraviolet to the near infrared region. Two monochromators are used for the selection of the excitation wavelength and emission wavelength. Motorized monochromator is used for automatic scanning of wavelengths. The monochromators are controlled by the electronic devices and the computer. The optical module contains various parts: sample holder, shutters, polarizers (not always), beam splitter etc. The beam splitter is made up with a quartz plate reflecting a few percent of the exciting light towards a quantum counter or a photodiode.

The emission spectrum is obtained by fixing the excitation wavelength (λ_{exc}) and it reflects the variations of fluorescence intensity as a function of the wavelength at which the fluorescence is observed (λ_{em}). The excitation spectrum reflects the variations of fluorescence intensity as a function of λ_{exc} with fixed λ_{em}. The spectra are recorded as a function of wavelength and not wavenumber due to the following reason. The monochromators of spectrofluorimeters are equipped with gratings, thus for a given width of the input and output slits, the monochromators operate at a constant bandpass expressed in wavelength.

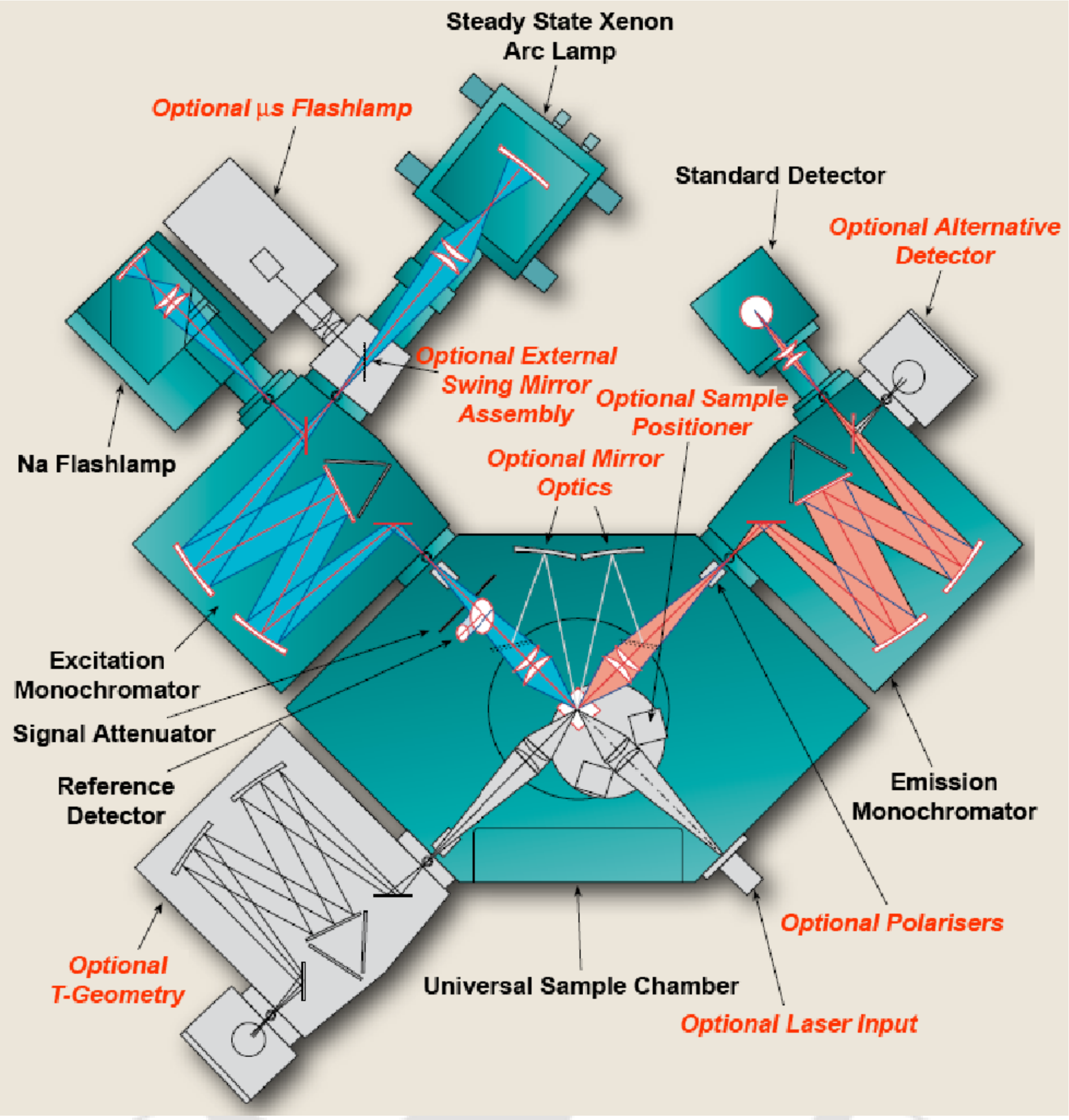

Scheme 2.8. Block diagram of FSP 920 steady state fluorescence spectrophotometer. (Diagram was obtained from the catalogue of Edinburgh instruments FSP 920)

The fluorescence spectra have to be corrected for the distortion by the wavelength dependence of several components of the instrument.

Correction for emission spectra

Since emission spectrum depends on efficiency of the emission monochromator and the response of the photomultiplier tube (PMT) it is necessary to correct the emission spectra. Basically correction factors are calculated using a calibrated tungsten lamp or a standard fluorescence dye whose corrected emission spectrum is reported. For the instruments used in the thesis work, the correction factors are provided by the supplier.

Correction for excitation spectra

Excitation spectrum is mainly affected by the variations of the intensity of the exciting light which is due to the wavelength dependency of the lamp intensity and of the transmission efficiency of the excitation monochromator. Since the quantum counter overcomes the wavelength dependence of the sensitivity of the reference photomultiplier, the ratio of the fluorescence signal from the sample to that from the quantum counter or photodiode (as a function of the excitation wavelength) provides in principle corrected excitation spectra. However, for a very accurate measurement, for example comparison of the absorption spectra to the excitation spectra such correction procedures may be insufficient. This behavior is due to the wavelength dependence of optical parts (e.g. focal length of lenses) may introduce some distortion into the excitation spectrum as it is not same. Thus the correction factor is obtained using a known fluorescent compound absorbing in the same wavelength region that of the fluorescent molecule to be studied and whose absorption spectrum should be identical to the corresponding excitation spectrum. The ratio obtained for the excitation spectrum to the absorption spectrum of the reference compound (using the quantum counter) provides the correction factors that can be used. However the excitation spectra recorded using the photo-diode instead of quantum counter is generally further corrected, as the wavelength response of the photodiode is not strictly flat over the whole wavelength range available. However, for the fluorimeters used in the present thesis, the correction files are supplied by the manufacturer.

FSP 920 and Fluorolog 3 are equipped, 450 W xenon arc lamp with double excitation monochromator. Other instruments used for the measurements have single excitation monochromator. Fluoromax 4 has 150 W xenon arc lamp as light source. But Cary Eclipse employs 75 W pulsed xenon lamp as light source. All these instruments have Hamamastu red sensitive PMT as detector.

2.4.4. Fluorescence lifetime measurements

Two different methods, frequency-domain and time-domain are used to determine the fluorescence lifetime.[192-197] Time-domain time correlated single photon counting (TCSPC) method is widely used (**Scheme 2.9**).

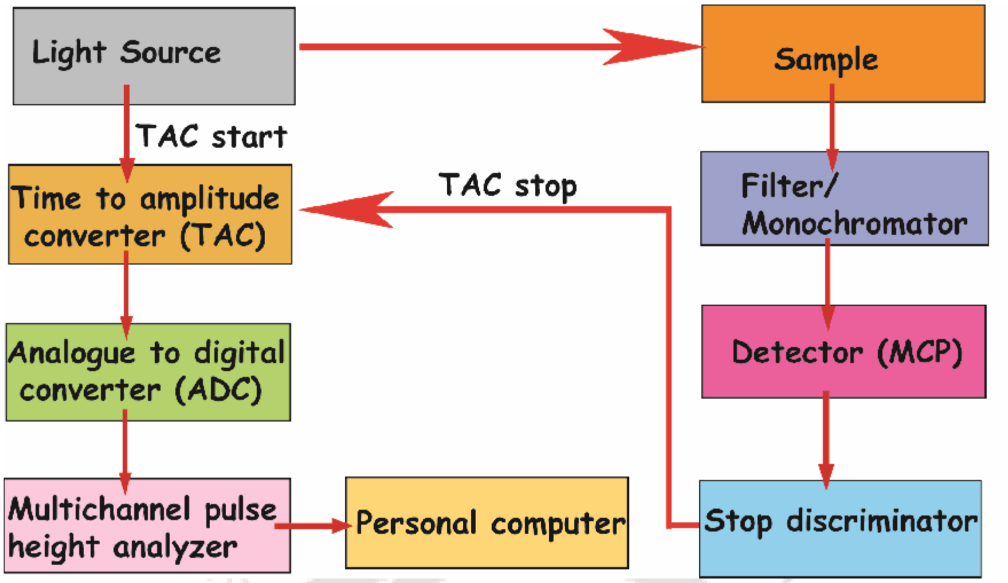

Scheme 2.9. Block diagram for time-correlated single photon counting (TCSPC)

In the present work also TCSPC method is used. In this method the sample to be analyzed is excited with a short light pulse from the source with sufficient delay between pulses. Flash lamp, pulsed laser, laser diode or LED used as the light source for this method. Upon excitation, the molecules emit photons at different relaxation times; thus the decay time of single molecules must have a certain rate rather than occurring at a specific time with excitation. The principle of TCSPC is the detection of single photons and the measurement of their arrival times with respect to a reference signal from the light source. TCSPC method is composed with two pulses namely start signal pulse and the stop signal pulse, splits from the light source beam into two paths. The start signal pulse travels to a photomultiplier tube (PMT) or micro-channel plate (MCP) photomultiplier that activates the time-to-amplitude converter (TAC). The stop signal pulse travels through the sample and the growth of ramp signal in TAC is stopped by this pulse. TAC output is amplified using an amplifier and this analogue pulse height corresponding to a measured time of the signal goes through further processing to convert to the digital pulse through the analogue to digital converter (ADC).The TCSPC needs a high repetitive light source to accumulate a sufficient number of photons since this is a statistical method and required many numbers of statistical data precision. The time measurement of the start and stop sequence will be represented by an increase of a memory value in a histogram. Thus, this experiment must be repeated many times to gather the sufficient photons in the full range of delays between excitation and emission. The resulting histogram counts versus the time channels will represent the curve of fluorescence decay profiles. In most cases, the TCSPC technique has limits for the temporal resolution and lifetime range measurable for the fluorescence lifetimes. Deconvolution procedure is used to derive the fluorescence temporal profiles with the instrument response using nonlinear least-squares fittings.

For the fluorescence lifetime measurements, Edinburgh Lifespec II instrument with 375 nm laser diode from Edinburgh having pulse width of 90 ps as light source is used. Lifespec II employs Hamamatsu MCP detector that has response time of 50 ps. The fluorescence decay was analyzed by reconvolution method using software provided by Edinburgh. The fluorescence decay was analyzed by tail fitting method using software provided by Edinburgh

2.4.4 Other instruments

FT NMR spectra were recorded in $CDCl_3$ or CD_3OD with tetramethylsilane as the standard for ^1H (400 MHz) Mercury, Varian instruments and ^1H (600 MHz) from Bruker instruments. High resolution mass spectrometry (HRMS) instruments from Agilent technologies and liquid chromatography-mass spectrometry (LCMS) from Waters instruments (Q-Tof Premier) are used for recording the mass spectra. Oriel 300 W ozone free xenon arc lamp was used for photochemical irradiation experiments. The xenon lamp source has F/1,2 element type condenser and transmittance range 200-2500 nm with output diameter of 33 mm.

Chapter 3

Spectral characteristics of a few pyridazole analogous organic bichromophoric molecules: An understanding towards the mechanism of twisted intramolecular charge transfer emission of 2-(4′-*N*,*N*-dimethylaminopheny)imidazo[4,5-b]pyridine

3.0. Introduction

Recent studies on DMAPIP-b by our group revealed that it has interesting fluorescence characteristics.[82] It exhibits single emission in nonpolar and polar aportic solvents, but dual emission in polar protic solvents. The relative intensity of the longer wavelength emission depends upon the protic nature of the solvent. It was reported that the dual emission of DMAPIP-b in protic solvent is due to the formation of TICT state. It was also suggested that the hydrogen bonding of the protic solvents with pyridyl nitrogen plays a crucial role in the formation of TICT state in DMAPIP-b.[82,84,198] The dual emission and its sensitivity towards environment make DMAPIP-b as an attractive probe to investigate various microheterogeneous systems including protien.[83,85,86,160] However, despite the fact that the shorter and the longer wavelength emissions are attributed to normal and TICT emission, respectively, still the mechanism of the formation of TICT state in protic environment is not clearly understood.

To understand the mechanism of the formation of TICT state in DMAPIP-b, the photophysical characteristics of some analogues of DMAPIP-b are investigated in this chapter. **Chapter 3** is divided into two sections. In first section the effect of oxazole ring substitution is studied. In section two, studies on imidazole analogues, *N*,*N*-dimethyl-4-(4-methyl-4*H*-imidazo[4,5-b]pyridin-2-yl)benzenamine (PyN-Me), *N*,*N*-dimethyl-4-(3-methyl-3*H*-imidazo[4,5-b]pyridin-2-yl)benzenamine or 1-methyl-2-(4′-(*N*,*N*-dimetylaminophenyl)imidazo[4,5-b]pyridine (ImNH-Me) and 2-phenylimidazo[4,5-b]pyridine (PIP) are described.

3.1.0. Photophysical study of 2-(4'-*N*,*N*-dimethylaminophenyl)oxazolo[4,5-b]pyridine in different solvents and at various pH

Recently Mac et al. studied the fluorescence properties of several oxazolo[4,5-b]pyridines including 2-(4'-*N*,*N*-diethylaminophenyl)oxazolo[4,5-b]pyridine (DEAPOP, **Chart 3.1**) and found that the dyes posses charge transfer character in the ground as well as the excited states. DEAPOP has oxazole ring instead of imidazole ring in DMAPIP-b. However, they did not observe dual emission from any of the molecules including DEAPOP, but their studies are restricted to nonpolar and polar aprotic solvents.[7] They also studied the prototropic equilibria of DEAPOP and found two absorption bands due to the formation of two kinds of monocations. On the other hand they reported only one fluorescence spectrum corresponds to one of the monocation.

Therefore, the spectral characteristics of 2-(4'-*N*,*N*-dimethylaminophenyl) oxazolo[4,5-b]pyridine (DMAPOP) in solvents having different polarity and hydrogen bond capacity and at different pH in aqueous medium are investigated. The main objectives of the studies are to investigate (i) the effect of protic solvents on the fluorescence characteristics of DMAPOP and (ii) understand the excited state prototropic equilibria of DMAPOP.

DMAPIP-b

R = CH_3, DMAPOP
R = C_2H_5, DEAPOP

Chart 3.1. Structures of DMAPOP and related molecules.

3.1.1. Solvent effect on absorption and fluorescence spectra

The absorption and the fluorescence spectral data of DMAPOP are compiled in **Table 3.1**. **Figure 3.1** depicted the fluorescence spectra of DMAPOP in different solvents. The fluorescence spectrum is structured in nonpolar solvents. Upon increasing the polarity and the hydrogen bonding capacity of the solvents, the vibrational progression becomes blurred with a little bathocromic shift. The bathochromic shift is more pronounced in DMAPOP than the corresponding imidazole derivative.[82] For example from cyclohexane to methanol 22 nm shift in the absorption spectra and 43 nm shift in the fluorescence spectra are observed for DMAPOP (**Table 3.1**). On the other hand the bathochromic shifts are only 14 nm and 35 nm in the absorption and fluorescence spectra of DMAPIP-b, respectively.[82] In polar medium, the red shift is observed in the electronic transition of the type π-π* due to greater stabilization of ππ* state by increase in intramolecular charge transfer. Therefore it is clear that the substitution of electronegative oxygen increases the charge flow from the dimethylamino group to the oxazolopyridine moiety. Further the absorption spectrum of DMAPIP-b in water was blue shifted with respect to that in methanol owing to greater hydrogen bonding tendency of water (than methanol) with dimethylamino nitrogen. But no such hypsochromic shift was observed in the absorption spectral maxima of DMAPOP, substantiates the increased charge flow from dimethylamino group to oxazolopyridine moiety.

Table 3.1. Longest wavelength absorption maxima (λ_{max}^{ab}, nm), fluorescence emission maxima (λ_{max}^{em}, nm), Stokes shift ($\bar{\nu}_{SS}$, cm^{-1}), fluorescence quantum yield (Φ_f), lifetime (τ, ns), radiative rate constant (k_r, s^{-1}) and nonradiative rate constant (k_{nr}, s^{-1}) of DMAPOP in different solvents.

Solvents	λ_{max}^{ab}	λ_{max}^{em}	$\bar{\nu}_{SS}$	Φ_f	τ	k_r (10^8)	k_{nr} (10^8)
Hexane	341, 358 (sh)	364, 384, 407 (sh)	3284	0.96	1.2	8.1	0.4
Cyclohexane	343, 360 (sh)	366, 386, 408 (sh)	3248	0.94	1.2	7.8	0.5
Dioxane	354	404	3496	0.99	1.3	7.6	0.01
Ether	352	397	3220	0.88	1.3	7.0	1.0
DMF	362	424	4039	0.88	1.4	6.4	0.9
Acetonitrile	358	418	4010	0.86	1.5	5.6	0.9
Methanol	365	429	4087	0.60	1.1	5.2	3.6
Ethanol	364	427	4053	0.83	1.5	5.6	1.1
1-Propanol	366	425	3793	0.94	1.5	6.1	0.4
2-Propanol	362	421	3871	0.99	1.5	6.4	0.1
Butanol	364	420	3663	0.94	1.5	6.2	0.4
Glycol	373	438	3979	0.51	1.0	4.9	4.7
Glycerol	376	442	3971	0.90	1.5	6.2	0.7
Water	365	448	5076				

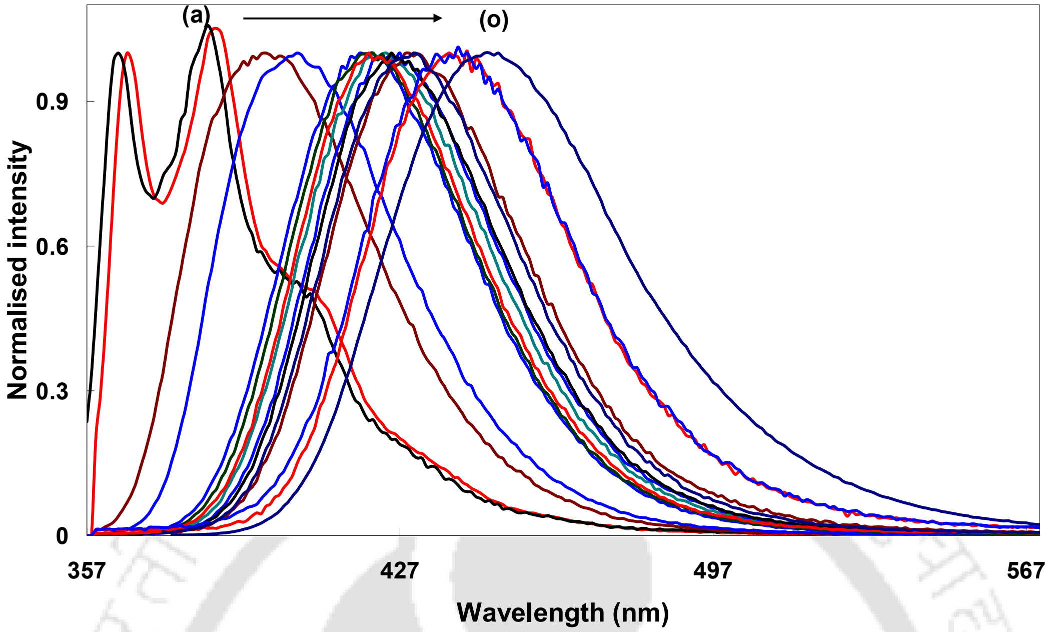

Figure 3.1. Normalized fluorescence spectra (λ_{exc} = 350 nm) of DMAPOP in (a) hexane, (b) cyclohexane, (c) ether, (d) dioxane, (e) acetonitrile, (f) 2-propanol, (g) butanol, (h) dimethyl formamide, (i) ethanol, (j) 1-propanol, (k) dimethyl sulfoxide, (l) methanol, (m) glycol, (n) glycerol and (o) water.

Multiple linear regression analysis proposed by Abraham et al. is preformed to identify the modes of solvation of the absorption and emission energies.[199] The value of the solvent parameters were taken from the literature.[200] The multiparametric approach separates the different solvent parameters. It also gives the information about specific contribution of each solvent parameter. Thus, the absorption and the fluorescence spectral data are analyzed using multiple linear regression method employing the following equation.

$$E = E_0 + s\pi^* + a\alpha + b\beta \quad \textbf{(3.1)}$$

where E is the absorption/fluorescence energy in cm^{-1}, E_0 is the value independent of solvent, π^* is the polarity/polarizability parameter of the solvents, α is the index of hydrogen bond donating ability of the solvent and β is the index of hydrogen bond accepting capacity of the solvent and *s*, *a* and *b* coefficients are the measure of the sensitivity to each individual contributing parameter. The positive sign indicates the destabilization and negative sign indicates stabilization of the system. The multiple linear regression analysis using the absorption and fluorescence spectral data give following equations.

$$E\ (A) = 29158 - 1131\ \pi^* - 524\ \alpha - 867\ \beta \qquad \textbf{(3.2)}$$

$$E\ (F) = 25970 - 2192\ \pi^* - 1029\ \alpha - 498\ \beta \qquad \textbf{(3.3)}$$

where E (A) and E (F) are absorption and fluorescence band maxima in cm^{-1} respectively. Good correlations are found for E (A) and E (F) with Taft's π^*, α and β values. The regression value obtained for absorption and fluorescence data were 0.97 and 0.99 respectively. E_0 values are also in good agreement with the experimental values obtained in nonpolar solvent. Negative values of π^*, α and β indicate all the three parameters contribute to the stabilization of both ground state and excited state of the molecule. A good linear variation is also observed between the fluorescence maxima and the $E_T(30)$ values[201] (**Figure 3.2**).

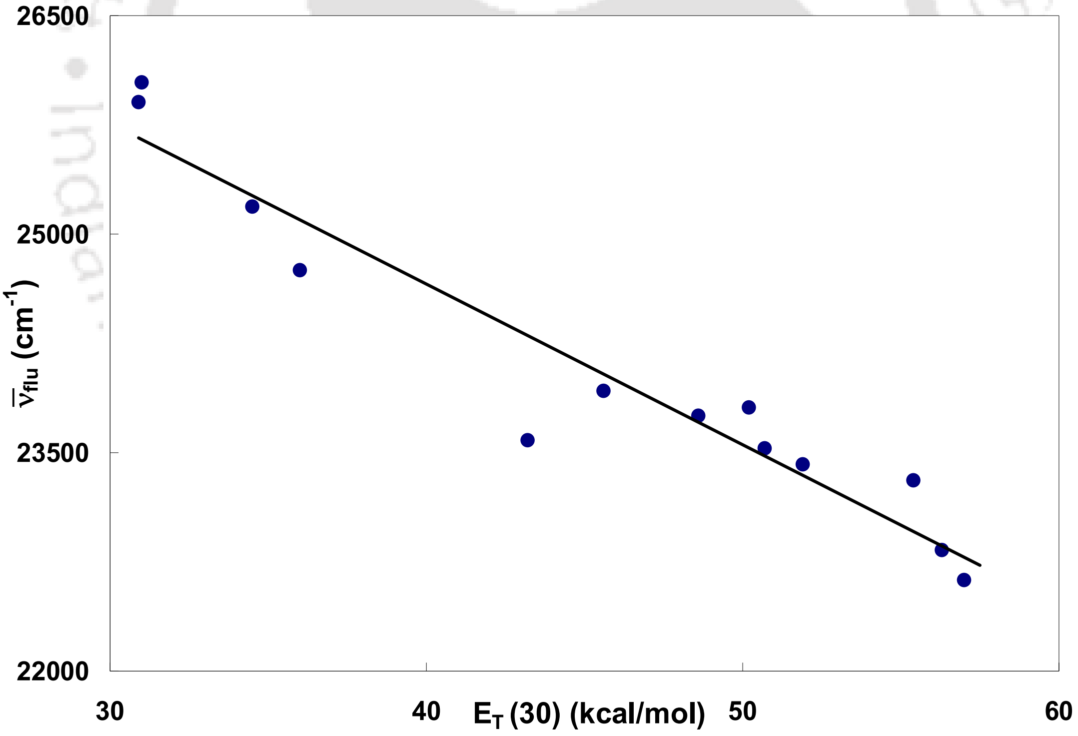

Figure 3.2. Plot of $\bar{\nu}_{flu}$ versus $E_T(30)$ parameters.

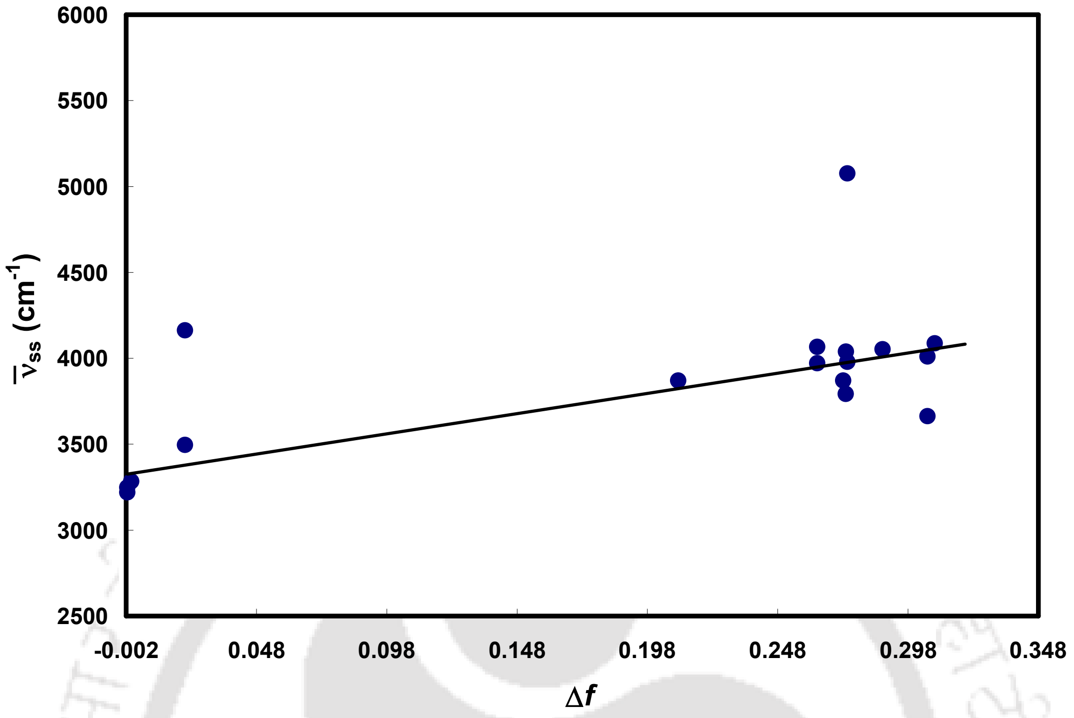

Figure 3.3. Lippert-Mataga plot for DMAPOP.

The Lippert-Mataga plot[202] was constructed (**Figure 3.3**) by using the relation

$$\bar{\nu}_{SS} = [2(\mu_e - \mu_g)^2/hca^3]\,\Delta f + \bar{\nu}_{SS}^{\circ} \qquad \textbf{(3.4)}$$

where $\bar{\nu}_{SS}$ is the Stokes shift, the superscript "°" indicates the absence of solvent, μ_g and μ_e are dipole moments in the ground state and the excited state, respectively, *a* is Onsager cavity radius. The orientation polarizability Δ*f* is defined as

$$\Delta f = [(\varepsilon - 1) / (2\varepsilon + 1)] - [(n^2 - 1) / (2n^2 + 1)] \qquad \textbf{(3.5)}$$

where ε and *n* are solvent dielectric constant and refractive index respectively. The geometrical optimization of DMAPOP was done by DFT method using Gaussian 03 software to calculate the μ_g.[188] The μ_e value was calculated from the slope of Lippert-Mataga plot and using the μ_g value 5.9 D, obtained from the DFT calculation. The μ_e value thus obtained is 10.6 D. The value is little higher than 10.4 D reported for DEAPOP.[7]

Fluorescence quantum yields of DMAPOP measured in different solvents are presented in **Table 3.1** and the variation of quantum yield with solvent polarity parameter $E_T(30)$ is shown in **Figure 3.4**. It is clear from the plot that fluorescence quantum yield of

DMAPOP decreases with increase in polarity of the solvents and the decrease is less prominent in nonpolar and polar aprotic solvents. But in case of polar protic solvents the change is much prominent with steep slope. The significant decrease of quantum yield observed upon increasing the protic nature of medium suggests the differential contribution of charge transfer and hydrogen bonding interactions.[203] Owing to greater viscosity of the solvent DMAPOP exhibits higher quantum yield in glycerol.

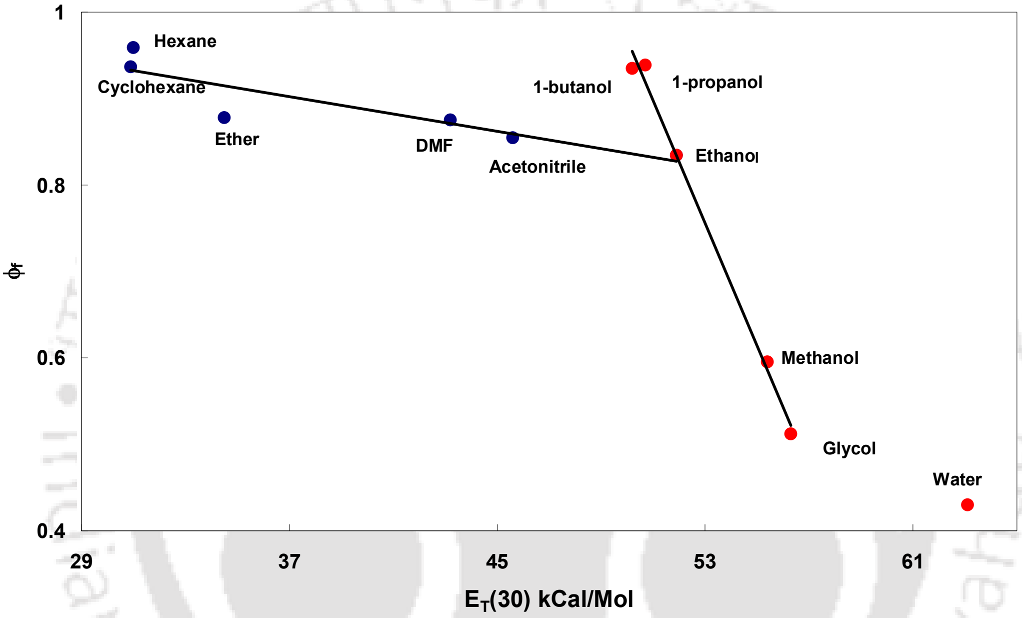

Figure 3.4. Variation of fluorescence quantum yield of DMAPOP as a function of solvent polarity parameter.

Radiative (k_r) and nonradiative (k_{nr}) rate constants are calculated from fluorescence quantum yields and lifetimes values of DMAPOP in different solvents to understand the effect of solvation on the dynamics of the excited state. The k_r and k_{nr} values are tabulated in **Table 3.1**. Logarithm of (k_r/k_{nr}) of DMAPOP is plotted against the solvent polarity parameter $E_T(30)$ (**Figure 3.5**). Two different straight lines are obtained, one for aprotic solvent and the other for protic solvents. In both cases upon increasing the polarity, the logarithmic ratio of radiative to nonradiative rate decreases but steeper slope is obtained in case of protic solvents. It indicates that the radiative and nonradiative rates are more sensitive toward protic solvents. It may be the hydrogen bonding interaction in polar protic environments enhances the stabilization of the S_1 state of DMAPOP as a result the nonradiative relaxation rate increases.[203]

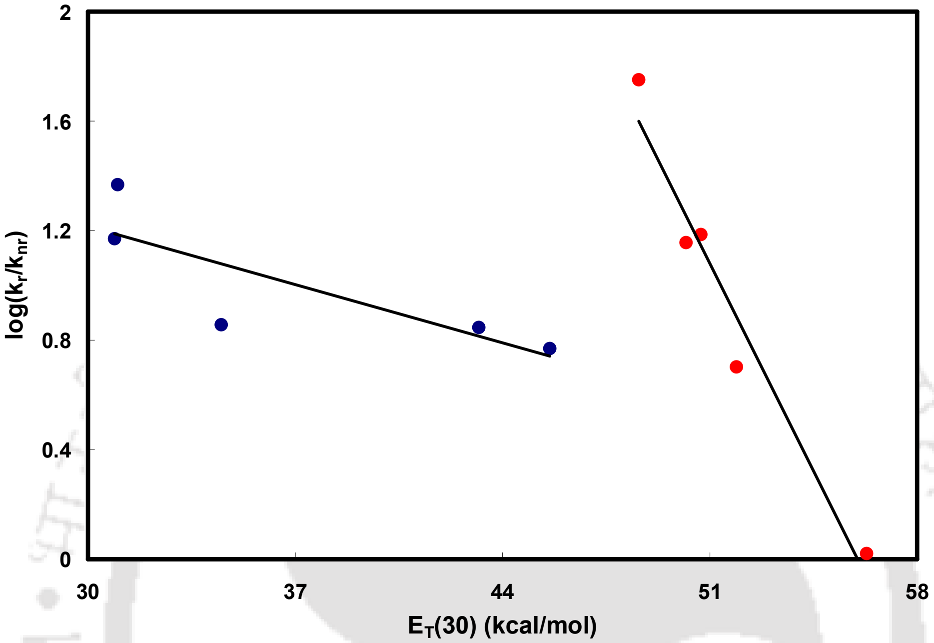

Figure 3.5. Plot of log(k_r/k_{nr}) versus $E_T(30)$ in various solvents.

Striking difference between DMAPOP and its imidazole analogue, DMAPIP-b is the absence of longer wavelength emission in protic solvents in DMAPOP. The single exponential decays in protic solvents further substantiate the presence of single excited state species in DMAPOP. Earlier studies indicate that the hydrogen bonding of the solvent with pyridyl nitrogen plays a major role in the formation of TICT state in DMAPIP-b.[82] The present study suggests that 'NH' group of imidazole nitrogen may also play an important role in the formation of TICT state in DMAPIP-b. One possibility that comes in mind is the proton transfers from imidazole 'NH' nitrogen to pyridyl nitrogen coupled charge transfer. Yoon et al. proposed such a model to explain the formation of TICT emission in 4-(*N*,*N*-dimethylamino)salicylic acid in nonpolar solvent.[204] Further investigations on dual fluorescence of DMAPIP-b are presented in the next section .

3.1.2. Prototropic equilibria

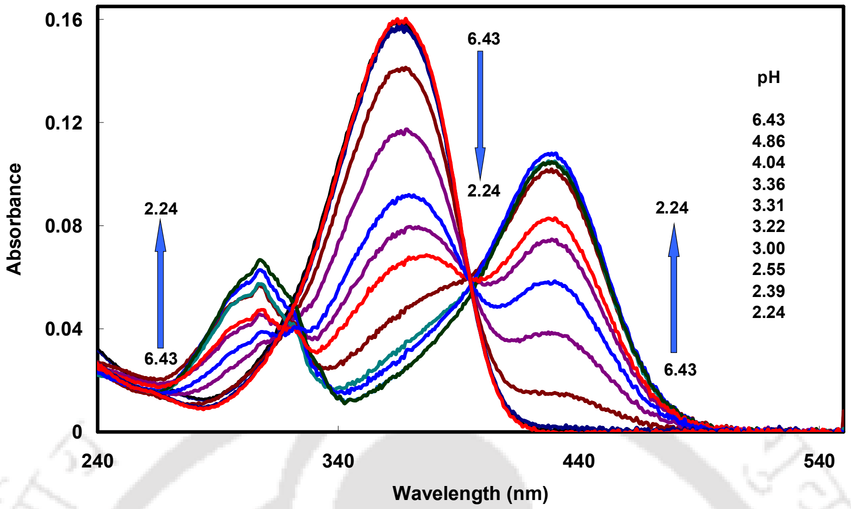

Figure 3.6. Absorption spectra of DMAPOP for neutral monocation equilibrium in water.

Different possible cations those can be formed by the protonation of basic nitrogens in DMAPOP are presented in **Scheme 3.1**. Upon decreasing the pH two new bands appear in the absorption spectra of DMAPOP with two quasi isosbestic points at 324 nm and 395 nm (**Figure 3.6**). This indicates the formation of two different kinds of monocations. The emission spectra are quite complicated. Excitation at 324 nm, isosbestic point resulted in a two band systems with a quasi isoemissive point at 412 nm (**Figure 3.7a**). This suggests an equibrium between the neutral and the monocation. On the other hand the fluorescence spectrum corresponds to the neutral molecule is predominantly observed when excited at the red side isosbestic point (λ_{exc} = 395 nm, not shown). The intensity of the neutral fluorescence band decreases with increase in acid concentration. However excitation at the red absorption band (λ_{exc} = 430 nm) produces an additional weak emission at 560 nm (**Figure 3.7b**). With decrease in pH, the intensity of the 560 emission also increases at the cost of the neutral emission. The spectral data are compiled in **Table 3.2**. This clearly establishes that two kinds of monocations are present in both ground and excited states.

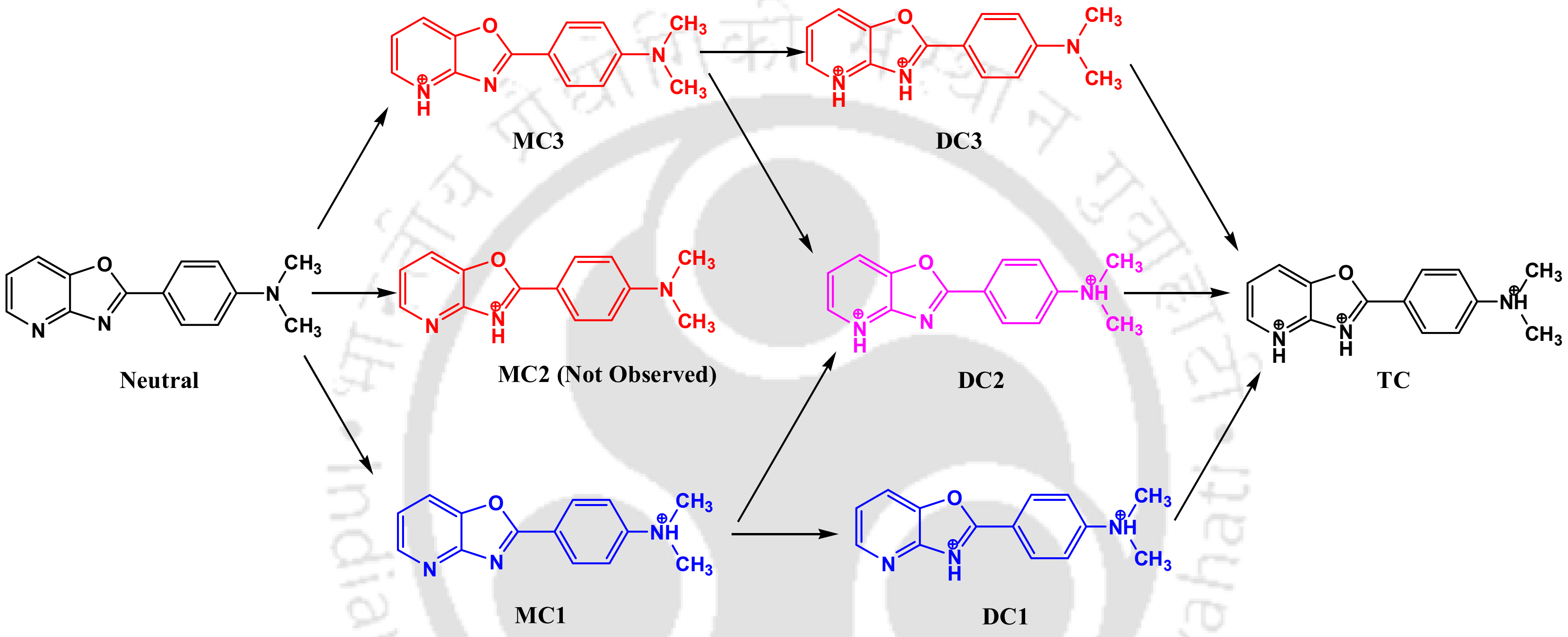

Scheme 3.1: Prototropic reactions of DMAPOP.

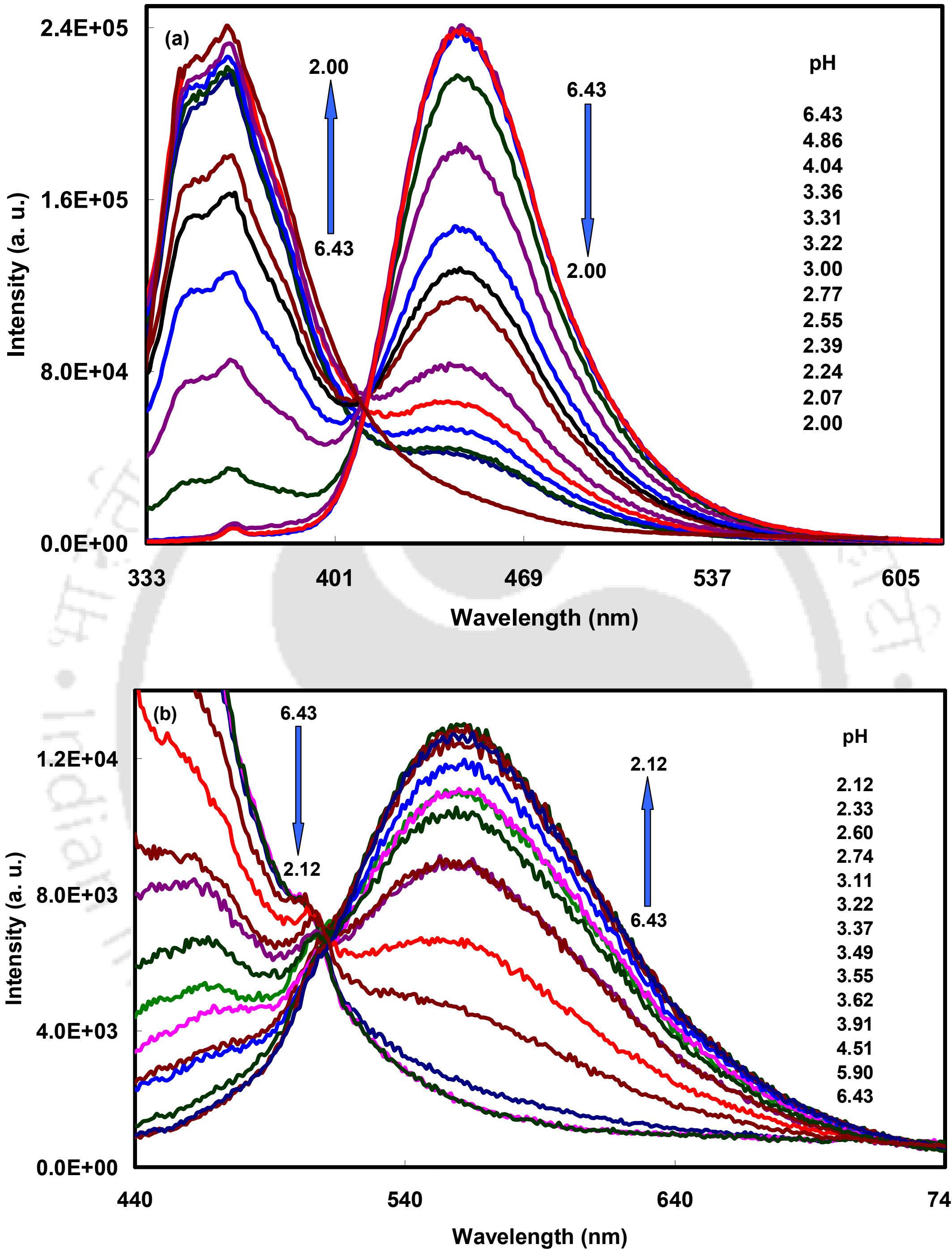

Figure 3.7. Emission spectra of DMAPOP by (a) λ_{exc} = 324 nm and (b) λ_{exc} = 430 nm (the shoulder peak at 506 nm is due to water Raman) at different pH.

Table 3.2. Absorption band maxima (λ_{max}^{ab}, nm), excitation band maxima (λ_{max}^{exc}, nm) and emission band maxima (λ_{max}^{em}, nm) for different prototropic species in water.

Species	λ_{max}^{ab}	λ_{max}^{exc}	λ_{max}^{em}
Neutral	365	366	447
MC3	428	428	560
MC1	306	308, 321	350, 365
DC3		595	700
DC2		360	480
DC1	317, 331	319, 332	360, 375
TC	325	327	354, 370, 384

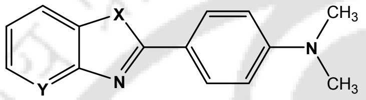

X = NH, Y = CH, 2-(4'-N,N-dimethylaminophenyl)benzimidazole
X = O, Y = CH, 2-(4'-N,N-dimethylaminophenyl)benzoxazole
X = NH, Y = N, 2-(4'-N,N-dimethylaminophenyl)imidazo[4,5-b]pyridine
X = O, Y = N, 2-(4'-N,N-dimethylaminophenyl)oxazolo[4,5-b]pyridine

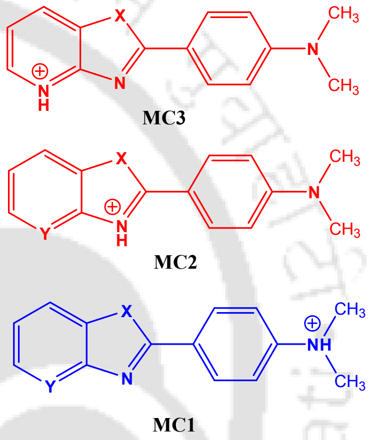

Chart 3.2. Structures of monocations of DMAPOP and related molecules.

Protonation of the dimethylamino nitrogen leads to blue shift and that of ring nitrogens leads to red shift. The shift is more prominent in case of protonation at pyridyl nitrogen than imidazole nitrogen.[83,85,205,206] Therefore the blue shifted band at 308 nm in the absorption spectrum and the corresponding fluorescence spectrum at 350 nm can be assigned to the monocation formed by the protonation of dimethylamino nitrogen i.e. MC1 (**Scheme 3.1**). Based on the following facts the red shifted absorption and the fluorescence spectra are assigned to the monocation formed by the protonation of pyridyl nitrogen (MC3) rather than the oxazole nitrogen (MC2). (i) Due to higher charge transfer character, large Stokes shift is expected in the fluorescence spectrum of MC3 than MC2. The observed Stokes shift (5500 cm^{-1}) for the monocation is more close to that of MC3 of DMAPIP-b rather than MC2 of DMAPIP-b and the Stokes shift is also much higher than that obtained for monocation formed by the protonation of azole nitrogen (1850 cm^{-1}) in 2-(4′-*N*,*N*-dimethylaminophenyl)benzoxazole (**Chart 3.2**).[83,85,207,208] (ii) The pK_a value

(3.35) obtained for DMAPOP is higher than that of oxazole nitrogen protonation (2.35) in 2-(4'-*N*,*N*-dimethylaminophenyl)benzoxazole.[207] This is consistent with the fact that pyridyl nitrogen protonation has higher pK_a value for the neutral-monocation equilibrium than that of azole nitrogen protonation.[82,205-207]

Table 3.3: pK_a values of neutral-monocation of different molecule along with site of protonation (see Chart 3.2 for monocation labelling).

Molecule	pK_a	Monocation formed
2-(4′-*N*,*N*-dimethylamino phenyl)benzimidazole[a]	5.60	MC2 >> MC1
2-(4′-*N*,*N*-dimethylamino phenyl)benzoxazole[b]	2.35	MC1 > MC2
DMAPIP-b[c]	5.40	MC2 > MC3
DMAPOP	3.35	MC3 > MC1

[a]Ref. 206, [b]Ref. 207, [c]Ref. 82,83

The results of neutral-moncation equilibrium of DMAPOP and other related molecules (**Chart 3.2**) from the literature are summarized in **Table 3.3**. In 2-(4′-*N*,*N*-dimethylaminophenyl)benzimidazole due to increase in charge flow from dimethylamino nitrogen to azole nitrogen, protonation predominantly occurs at imidazole nitrogen and a small amount of protonation occurs at dimethylamino nitrogen.[208] When the >NH group was replaced by oxygen, it reduces the charge density on azole nitrogen in 2-(4′-*N*,*N*-dimethylaminophenyl)benzoxazole and protonation at the azole nitrogen decreases and that at the dimethylamino increases.[207] On the other hand when nitrogen is substituted in benzene ring (DMAPIP-b), no protonation occurs at dimethylamino nitrogen and it occurs at the azole nitrogen with small amount at pyridyl nitrogen. In DMAPOP the pyridyl nitrogen is introduced in benzene ring and the >NH group was replaced by oxygen, the formation of MC2 (i.e. protonation at azole nitrogen) is completely terminated and the protonation at pyridyl nitrogen dominates over that at dimethylamino nitrogen (**Chart 3.2**). It appears that substitution of more electronegative oxygen decreases the electron density on the azole nitrogens. This is substantiated by the lower pK_a values for the neutral-monocation equilibrium of oxazoles compared to those of imidazoles (**Table 3.3**). Since presence of pyridyl nitrogen also decreases the electron density on the azole nitrogen, azole nitrogen could not be protonated in DMAPOP. May be due to higher electron density on diethylamino group (over dimethylamino group), in DEAPOP the protonation at diethylamino group was more facile than that at pyridyl nitrogen.[7]

Decreasing the pH of solution below 2 causes a decrease in the absorbance of MC3 and the absorption spectrum of MC1 also undergoes bathochromic shift with increase in absorbance (**Figure 3.8**).

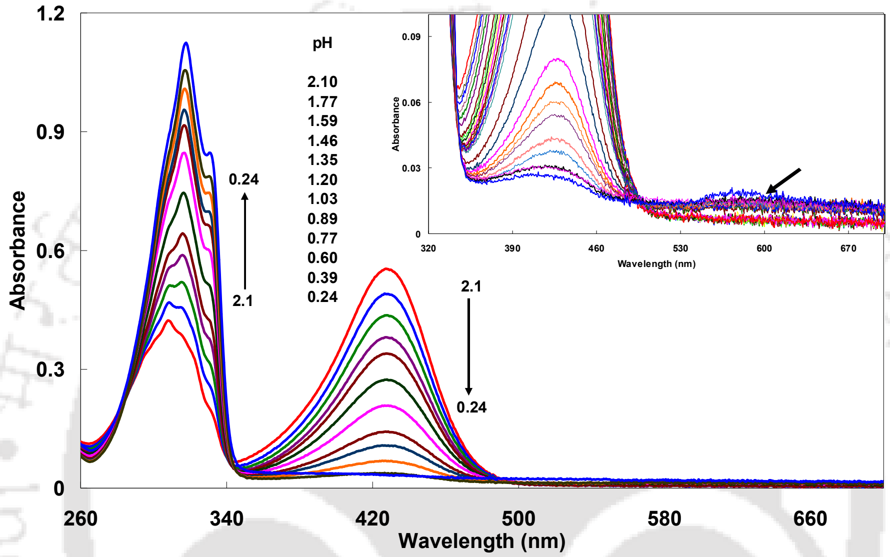

Figure 3.8. Absorption spectra of DMAPOP for monocation(s)-dication(s) equilibrium in water (Inset shows the expanded spectra).

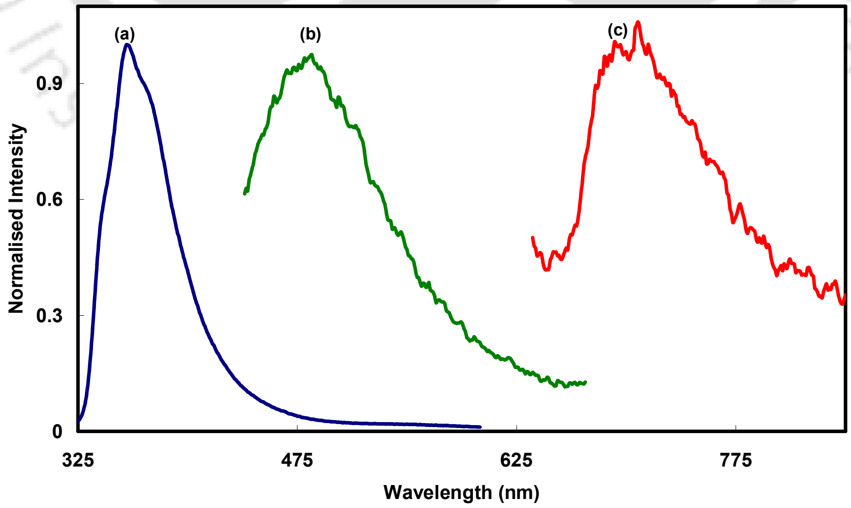

Figure 3.9. Normalised emission spectra of DMAPOP for all three dications at pH 0.18, (a) $\lambda_{exc} = 316$ nm (DC1), (b) $\lambda_{exc} = 428$ nm (DC2) and (c) $\lambda_{exc} = 620$ nm (DC3).

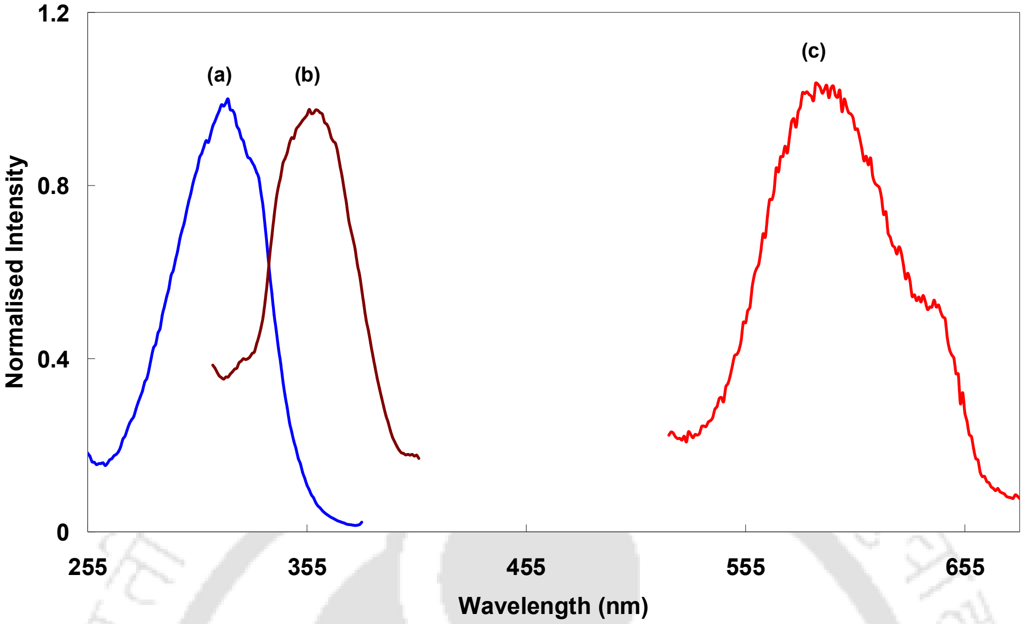

Figure 3.10. Normalised excitation spectra of DMAPOP at pH 0.18, (a) λ_{em} = 387 nm (DC1), (b) λ_{em} = 470 nm (DC2) and (c) λ_{em} = 710 nm (DC3).

At pH 0.18, a clear structured band is observed at 317 nm with a long tailing on the red side. These changes are consistent with shifting of the equilibrium towards dication from monocation. The absence of isosbestic point shows the complicate nature of the equilibrium. Three distinguished fluoresence spectra were obtained at pH 0.18 while exciting at 316 nm, 428 nm and 620 nm (**Figure 3.9**). In the absorption spectra of dications, though non zero absorbance is obtained at around 600 nm, no clear band is observed. However the excitation spectra recorded clearly shows a band at 595 nm (**Figure 3.10**). The excitation spectra of all the three emission bands at dicationic pH (0.18) are given in **Figure 3.10**. The fluorescence data along with respective excitation spectral data are compiled in **Table 3.2**. Three type of dications are possible (**Scheme 3.1**). Large red shift in the excitation and the emission spectra shows that both ring nitrogens were protonated, therefore emission band at 702 nm and the corresponding excitation band at 595 nm can be assigned to DC3, which is formed from MC3. The excitation band at 360 nm and the fluorescence band at 480 nm are blue shifted with respect to those of MC3 and red shifted to those of MC1 and these bands can be assigned to DC2 formed by the protonation of both pyridyl and dimethylamino nitrogens. Last excitation band at 319 nm and the emission band at 360 nm can be assigned to DC1 and as expected it is red shifted with respect MC1 and blue shifted compared to MC3 and other dications. The large shift in the emission spectrum of DC3 compared to other dication may be due to higher charge transfer in DC3, where both protonation occurred at the acceptor ring nitrogens and on the other hand the protonation at dimethylamino nitrogen (donor) will retard the charge transfer in DC2 and DC1. The fluorescence spectra of DMAPOP at pH lower than 0.18 are shown in **Figure 3.11**. The spectral changes indicate the shifting of equilibrium towards trication. In concentrated sulhphuric acid at H_0 = -9.4, single excitation and single emission spectra were obtained (**Figure 3.12**). These spectra confirm the formation of trication by protonation of all three nitrogens. For comparison purpose the fluorescence spectra of all the prototropic species of DMAPOP (**Scheme 3.1**) are complied in **Figure 3.13**.

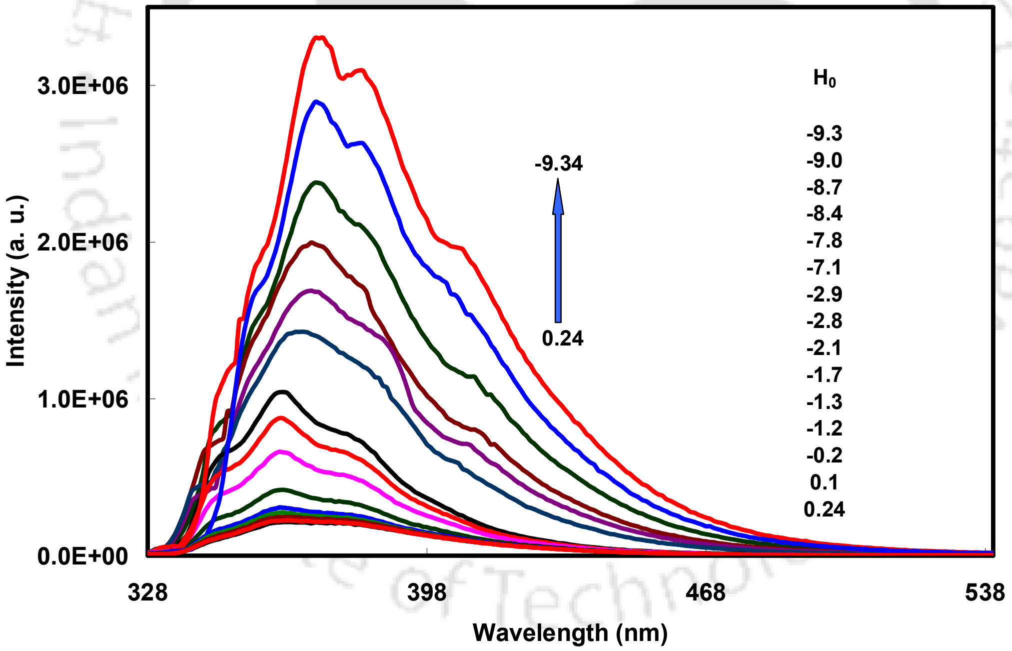

Figure 3.11. Emission spectra for dication – trication equilibrium of DMAPOP (λ_{exc} = 318 nm).

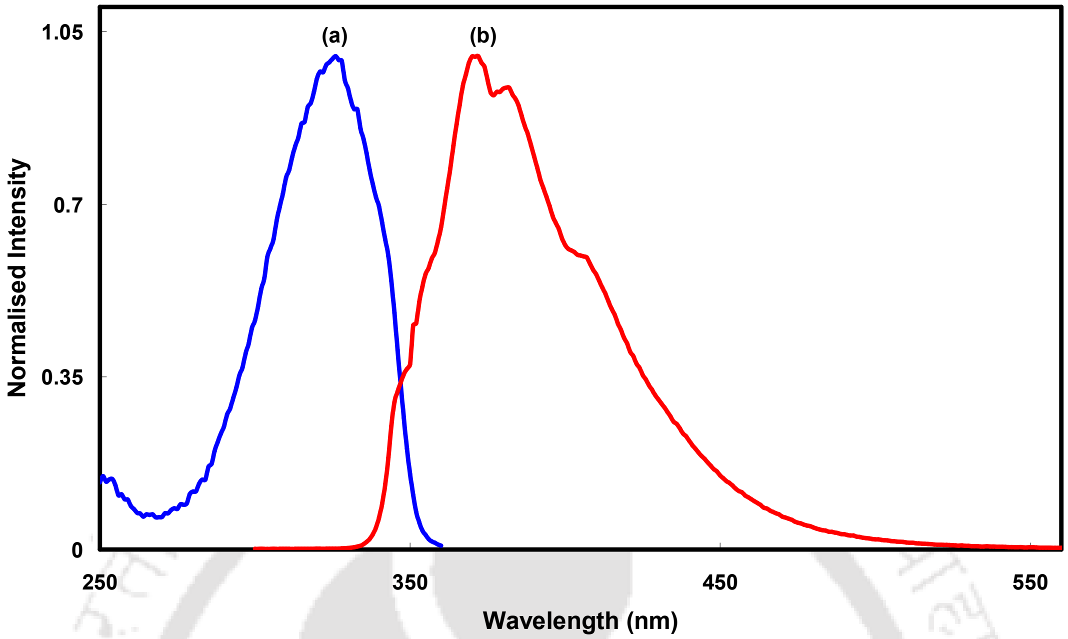

Figure 3.12. Normalised excitation and emission spectra of DMAPOP for trication (in conc. H_2SO_4), (a) λ_{em} = 370 nm and (b) λ_{exc} = 320 nm.

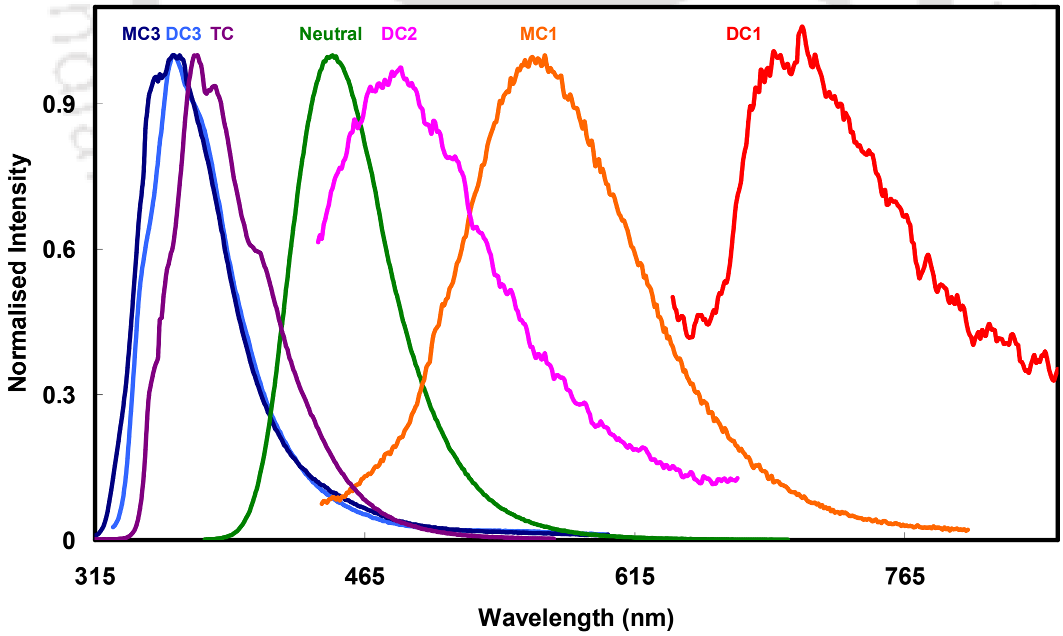

Figure 3.13. Normalised emission spectra for all the prototropic forms of DMAPOP.

3.1.3. Conclusion

The emission characteristics of DMAPOP are significantly different from those of its imidazole analogue, DMAPIP-b, in protic solvents. DMAPOP emits single emission from the ICT state in both protic and aprotic solvents. No protic solvent induced dual emission is observed in DMAPOP. Multiparametric regression analysis suggested that all the three solvent parameters contribute to the stabilization of both ground and excited states. However the relative contribution of dipolar interactions and hydrogen-bond donating ability of the solvent enhanced in the excited state and while that of the accepting ability of solvents is reduced in the excited state. The quantum yield decreases in polar protic solvents due to increase in the nonradiative rate by hydrogen bonding interactions. DMAPOP also forms two kinds of monocations in the ground and the excited states. But unlike DMAPIP-b, monocations are formed by protonation of pyridyl and dimethylamino nitrogens. Although the dicationic equilibrium is dominated by DC1, other two dications DC3 and DC2 also exist in aqueous medium.

3.2.0. Double proton transfer induced twisted intramolecular charge transfer emission in 2-(4'-*N*, *N*-dimethylaminophenyl)imidazo[4,5-b]pyridine

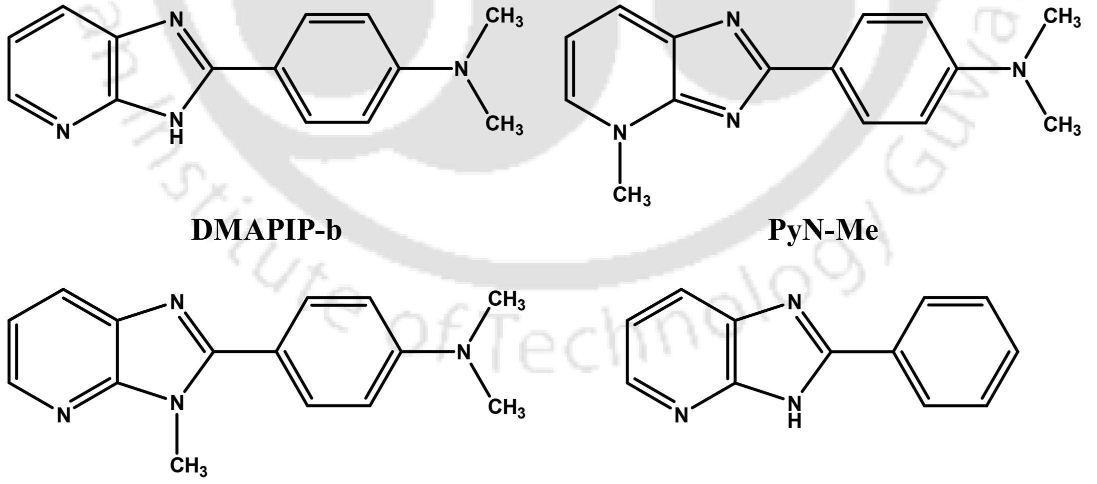

Chart 3.3. Structures of DMAPIP-b, PyN-Me, ImNH-Me and PIP.

As mentioned earlier, it was established that the hydrogen bonding of the solvent with pyridyl nitrogen plays a major role in the formation of TICT state in DMAPIP-b.[82] As discussed in the previous section (**Section 3.1**), studies on DMAPOP suggest that 'NH' group of imidazole nitrogen may also have a role in the formation of TICT state in DMAPIP-b. Therefore, to understand the mechanism of dual emission of DMAPIP-b, the photophysical characteristics of related molecules (**Chart 3.3**) *N*,*N*-dimethyl-4-(4-methyl-4*H*-imidazo[4,5-b]pyridin-2-yl)benzenamine (PyN-Me), *N*,*N*-dimethyl-4-(3-methyl-3*H*-imidazo[4,5-b]pyridin-2-yl)benzenamine or 1-methyl-2-(4′-(*N*,*N*-dimetylamin ophenyl)imidazo[4,5-b]pyridine (ImNH-Me) and 2-phenylimidazo[4,5-b]pyridine (PIP) are investigated.

3.2.1. Absorption spectra of methyl derivatives

Table 3.4. Absorption band maxima (λ_{max}^{ab}, nm), fluorescence band maxima (λ_{max}^{em}, nm) of PyN-Me, ImNH-Me and DMAPIP-b[1].

Solvents	λ_{max}^{ab}			λ_{max}^{em}		
	DMAPIP-b	**PyN-Me**	**ImNH-Me**	**DMAPIP-b**	**PyN-Me**	**ImNH-Me**
Cyclohexane	336, 352	333, 349, 366	323,332	359, 379, 398	373, 393, 419	362, 381, 401
Dioxane	340	346, 362	324,333	383	401	392
DMF	346	347, 361	337	428	402	414
DMSO		347, 362	339		403	421
Acetonitrile	345	343, 358	331	407	395, 430	412
Methanol	350	341, 355	335	414, 506	402	428
Ethanol	350	343, 356	336	413, 494	397	421
1-Propanol	349	343, 355	336	410, 486	398	418
2-Propanol	346	343, 356	336	408	395	415
Butanol	348	343, 357	336	407, 475	399	414
Glycerol	360	343, 356	343	446	406	441

[1]From ref. 82.

To understand the role of pyridyl nitrogen and the imidazole >NH group in the dual emission of DMAPIP-b, the methyl derivatives, PyN-Me and ImNH-Me (**Chart 3.3**) were synthesized. The absorption spectral data of methylated derivatives in different solvents are compared with DMAPIP-b in **Table 3.4**. The absorption spectra of all three molecules are structured in nonpolar solvent. But in polar solvent the vibrational structure in the absorption spectra of ImNH-Me are blurred with a bathochromic shift, as that of

DMAPIP-b. However, in contrast to other two molecules, the absorption spectra of PyN-Me is more structured in polar solvents also. The absorption spectra of PyN-Me is less sensitive towards the polarity of the environment (7 nm shift), whereas the solvatochromic shift in the absorption spectra of ImNH-Me is comparatively larger (20 nm shift) than that of PyN-Me and comparable to that of DMAPIP-b (24 nm shift). The Structureless absorption band in polar solvent and the larger solvatochromic shift suggest the occurrence of charge transfer in ImNH-Me. On the other hand, the small solvatochromic shift and structured spectra indicate less charge transfer in PyN-Me.

As discussed in the previous section (**Section 3.1**) that the multiparamateric approach separates the different solvent parameters [200] and it gives information about specific contribution of each solvent parameter. Thus, the spectral data are analyzed by using multiple linear regression analysis to identify the different modes of solvation and are compared with DMAPIP-b.

The multiple linear regression analysis using the absorption spectral data reported resulted in following equations.

$$E\ (\text{DMAPIP-b}) = 29860 - 966\,\pi^* - 900\,\alpha + 84\,\beta\ (r = 0.98) \qquad \textbf{(3.6)}$$

$$E\ (\text{ImNH-Me}) = 31150 - 731\,\pi^* - 418\,\alpha - 802\,\beta\ (r = 0.96) \qquad \textbf{(3.7)}$$

$$E\ (\text{PyN-Me}) = 28721 + 474\,\pi^* + 540\,\alpha - 271\,\beta\ (r = 0.96) \qquad \textbf{(3.8)}$$

A good linear correlation is obtained for all the molecules (regression ≥0.96). The value of E_0 obtained from this approach is also very good agreement with that of the experimental value in nonpolar cyclohexane. As expected due to charge transfer character, the polarity/polarizability parameter stabilizes DMAPIP-b and ImNH-Me. In addition, the hydrogen bond donating capacity of the solvent also stabilizes both DMAPIP-b and ImNH-Me. On the other hand, in PyN-Me where the pyridyl nitrogen is blocked and not available for hydrogen bonding, the coefficient of α becomes positive. Therefore, it is clear that the hydrogen bonding of the protic solvent with pyridyl nitrogen stabilizes the molecule more than that with the imidazole nitrogen. Large negative values of "*s*" and "*a*" for DMAPIP-b indicate that the dipolar interaction and hydrogen bond donating ability of the solvent contribute more for the stabilization of DMAPIP-b than ImNH-Me.

3.2.2. Fluorescence spectra of methyl derivatives

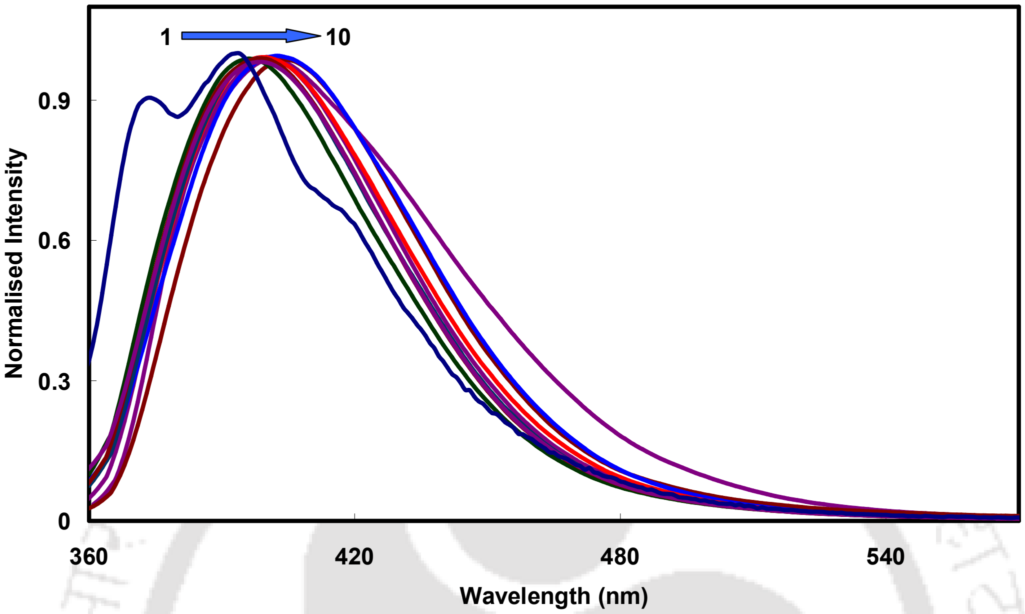

Figure 3.14. Normalised emission spectra of PyN-Me in different solvents: (1) cyclohexane, (2) 2-propanol, (3) 1-propanol, (4) butanol, (5) dioxane, (6) ethanol, (7) DMF, (8) methanol, (9) DMSO and (10) glycerol.

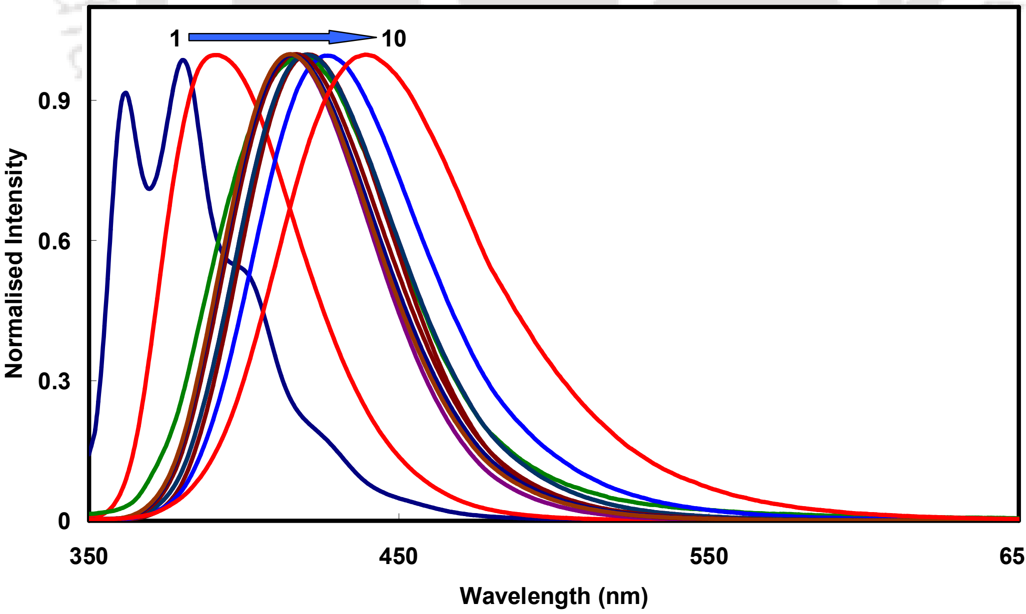

Figure 3.15. Normalised emission spectra of ImNH-Me in different solvents: (1) cyclohexane, (2) dioxane, (3) 2-propanol, (4) DMF, (5) ethylene glycol, (6) n-propanol, (7) ethanol, (8) DMSO, (9) methanol and (10) glycerol.

Like DMAPIP-b, in methyl derivatives also, the emission bands are structured in nonpolar solvents and upon increasing the polarity of the medium it becomes structureless with a red shift (**Figures 3.14** and **3.15**). The spectral shift of ImNH-Me is higher (60 nm, **Table 3.4**) and is comparable to that of shorter wavelength emission of DMAPIP-b (67 nm, **Table 3.4**). From this it can be inferred that like in DMAPIP-b the locally excited state of ImNH-Me also has charge transfer character. On the other hand, the bathochromic shift is small in the fluorescence spectra of PyN-Me (13 nm, **Table 3.4**) which indicates that PyN-Me is less sensitive towards the polarity of the medium.

The fluorescence spectral data are also analyzed using the SCM approach, which results in the following equations.

$$E\ (\text{DMAPIP-b}) = 26900 - 2628\ \pi^* - 836\ \alpha - 593\ \beta\ (r = 0.93) \qquad \textbf{(3.9)}$$

$$E\ (\text{ImNH-Me}) = 26453 - 2547\ \pi^* - 1922\ \alpha + 377\ \beta\ (r = 0.98) \qquad \textbf{(3.10)}$$

$$E\ (\text{PyN-Me}) = 25210 - 318\ \pi^* + 561\ \alpha - 476\ \beta\ (r = 0.67) \qquad \textbf{(3.11)}$$

The fluorescence spectral analysis also shows linear correlation in all the molecules and the values of E_0 also match well with the values in nonpolar solvent. As expected, the contribution from π^* is also high for ImNH-Me and comparable to that of DMAPIP-b.

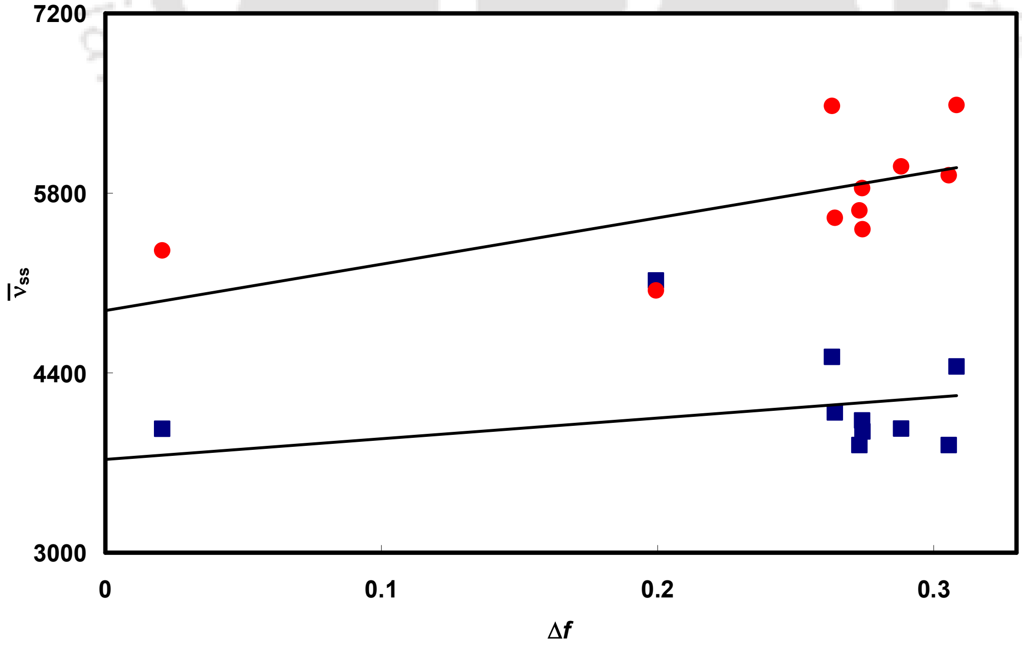

Figure 3.16. Lippert-Mataga plot for ImNH-Me (●) and PyN-Me (■).

Table 3.5. DFT optimized parameters of DMAPIP-b, ImNH-Me, PyN-Me and PIP.

Molecules	Ground state Energy (eV)	Excitation energy[a] (eV)	Emission energy[a] (eV)	μ_g (D)	φ_1^b	φ_2^b
DMAPIP-b	-20707.0821	3.82 (3.69)	3.57 (3.27)	5.07	2.54 (0.11)	6.77 (3.23)
ImNH-Me	-21776.7682	3.88 (3.84)	3.53 (3.25)	4.77	29.3 (0.53)	7.70 (4.32)
Py-Me	-21776.5134	3.16 (3.56)	3.09 (3.16)	2.64	0.00 (0.01)	0.04 (0.04)
PIP	-17061.3840	4.23 (4.04)	3.83 (3.65)	1.74	2.28 (0.02)	

[a]Values in parentheses are experimental values in cyclohexane. [b]Values in parentheses are those of excited state. φ_1 - the torsional angle of phenyl ring with the imidazopyridyl ring. φ_2 - the torsional angle of dimethylamino group with the phenyl ring.

The Lippert-Mataga plot[202] was constructed for ImNH-Me and PyN-Me (**Figure 3.16**). The excited state dipole moments are estimated from the slope and the ground state dipole moment (**Table 3.5**) calculated by DFT method. The excited state dipole moment thus obtained for ImNH-Me and PyN-Me are 11.24 D and 5.99 D, respectively. The excited state dipole moment of ImNH-Me is comparable to that of DMAPIP-b (12.20 D, small difference in excited state dipole moment of DMAPIP-b with earlier value[82] is because of the small difference in the ground state dipole moment predicted by *ab* initio and DFT calculations).

Table 3.6. Fluorescence quantum yield (Φ_f) and lifetime (τ_f, ns) of methyl derivatives.

Solvent	Φ_f		τ_f	
	PyN-Me	ImNH-Me	PyN-Me	ImNH-Me
Cyclohexane		0.819	1.22	1.17
Dioxane	0.385	0.896	1.27	1.42
Ethylacetate	0.343	0.291	1.28	1.31
DMF	0.453	0.931	1.41	1.61
DMSO	0.278	0.733	1.05	1.63
Acetonitrile	0.369	0.883	1.42	1.74
Methanol	0.472	0.223	1.78	0.57
Ethanol	0.453	0.808	1.67	1.87
1-Propanol	0.469	0.921	1.62	1.81
2-Propanol	0.433	0.917	1.58	1.87
Butanol	0.479	0.980	1.60	-
Glycerol	0.469	0.275	1.54	1.10

The fluorescence quantum yields and the lifetime of methylated molecules are compiled in **Table 3.6** and the variation of quantum yield with the $E_T(30)$ parameter is shown in **Figure 3.17**. The fluorescence quantum yield of PyN-Me varies very little with the nature of the environment, whereas the fluorescence quantum yield of ImNH-Me were reduced in protic solvents and is lowest in methanol. The fluorescence lifetime also attenuated in methanol (**Figure 3.18** and **Table 3.6**). The same behavior is observed for DMAPIP-b, whose shorter wavelength emission decay time is very low in methanol (0.31 ns) compared to other solvents (1.50 ns in acetonitrile).[82] However, the fluorescence lifetime of PyN-Me in methanol is comparable to those in other solvents and that of ImNH-Me in methanol is less compared to those in other solvents. From this, it can be inferred that the hydrogen bonding of the solvent with pyridyl nitrogen leads to fluorescence quenching.

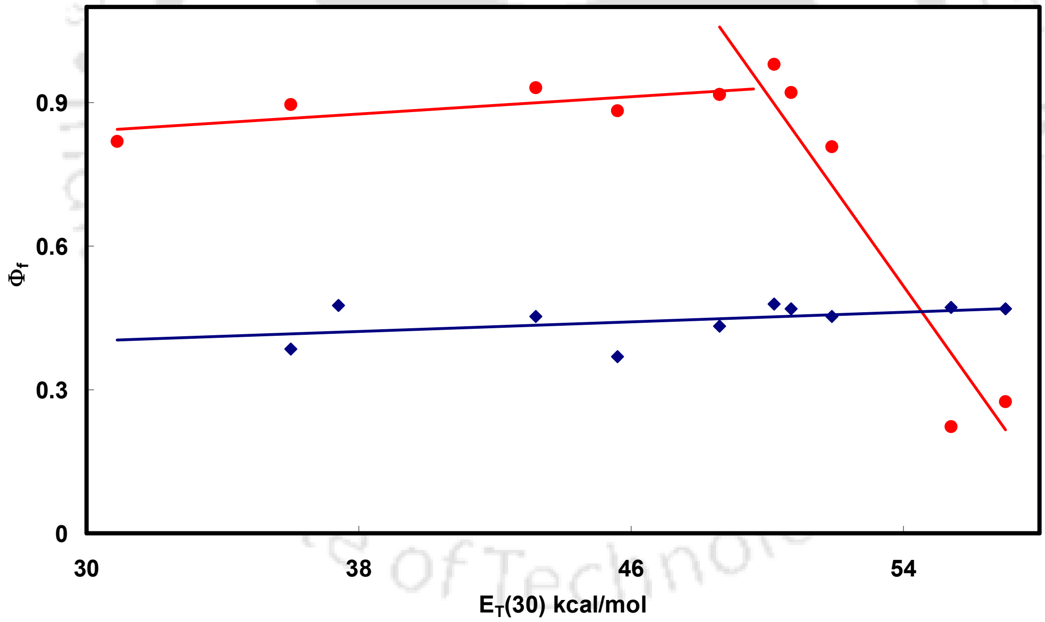

Figure 3.17. Plot of quantum yield versus $E_T(30)$ parameters for ImNH-Me (●) and PyN-Me (♦).

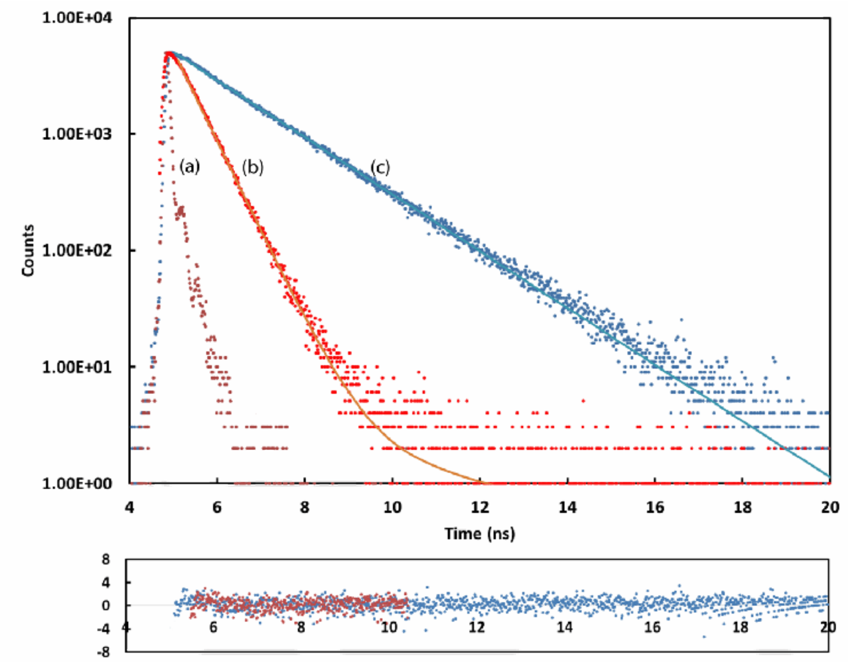

Figure 3.18. (a) The instrument response function and the fluorescence decays of (b) ImNH-Me and (c) PyN-Me in methanol along with fitted curves and residue plot.

Interestingly, both methyl derivatives exhibit single emission not only in aprotic solvents but also in protic solvents. However, DMAPIP-b emits dual emission in protic solvents.[82] In PyN-Me, the pyridyl nitrogen is prevented from hydrogen bonding. On the other hand, in ImNH-Me, the imidazole >NH group is substituted by >N-Me and therefore the >NH group is not available for hydrogen bonding. The absence of dual emission in PyN-Me and ImNH-Me shows that both pyridyl nitrogen and the >NH group are vital for the dual emission of DMAPIP-b in protic solvents. One such possibility is transfer of a proton from the >NH group to pyridyl nitrogen to form a tautomer (**Scheme 3.2**). Such solvent assisted intermolecular proton transfer in the excited state occurs in several molecules.[209-211]

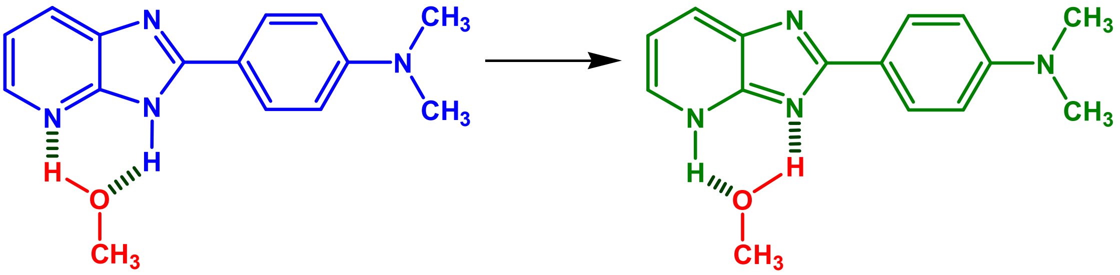

Scheme 3.2. Solvent assisted proton transfer.

3.2.3. Spectral characteristics of 2-phenylimidazo[4,5-b]pyridine

Table 3.7. Absorption band maxima (λ_{max}^{ab}, nm) and fluorescence band maxima (λ_{max}^{em}, nm) of PIP.

Solvent	λ_{max}^{ab}	λ_{max}^{em}
Cyclohexane	307, 321	324, 340, 358, 374
Dioxane	308, 321	328, 344, 360, 377
Ethylacetate	306, 320	326, 341, 357, 378
Ether	298, 307, 320	324, 340, 357, 374
DMF	308, 321	328, 343, 358, 377
Acetonitrile	307, 319	328, 343, 359, 378
Methanol	307, 320	328, 343, 358, 378
1-Propanol	306, 320	328, 343, 359, 378
2-Propanol	307, 320	327,341,359,378
Butanol	307, 321	328, 343, 358, 377
Glycerol	312, 322	332, 348, 362, 382

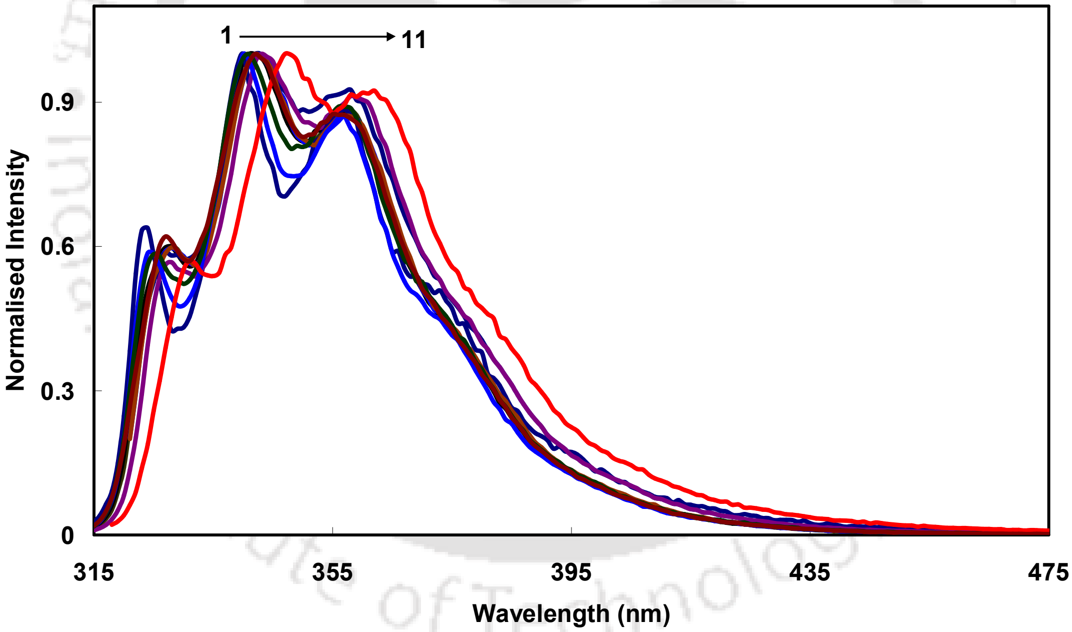

Figure 3.19. Normalised emission spectra of PIP in different solvents: (1) cyclohexane, (2) dioxane, (3) ether, (4) ethyl acetate, (5) DMF, (6) acetonitrile, (7) methanol, (8) 1-propanol, (9) 2-propanol, (10) butanol and (11) glycerol.

To verify the proton transfer hypothesis, the spectral characteristics of PIP (**Chart 3.3**), the molecule without a charge donor dimethylamino group, are investigated (**Table 3.7**). The absorption and the fluorescence band maxima are blue shifted compared to

DMAPIP-b and the methylated derivatives due to the absence of charge donating dimethylamino group. The solvatochromic shift is also very small compared to other molecules and the fluorescence spectra also possess well resolved vibrational structure (**Figure 3.19**). Markedly, no dual emission is observed in any solvent including protic solvents such as methanol. Despite the fact that both pyridyl nitrogen and the >NH group are freely available for hydrogen bonding, PIP exhibits single emission. Therefore, it can be concluded that the electron donating group is absolutely necessary for the dual emission in protic solvents and the longer wavelength emission originates from the charge transfer state. Further, strong positive solvatochromic behavior of the longer wavelength emission of DMAPIP-b and the higher dipole moment of its emitting state (**section 3.2.5**) also substantiate the conclusion that the state is a charge transfer state.

3.2.4. Effect of deprotonation of >N-H proton

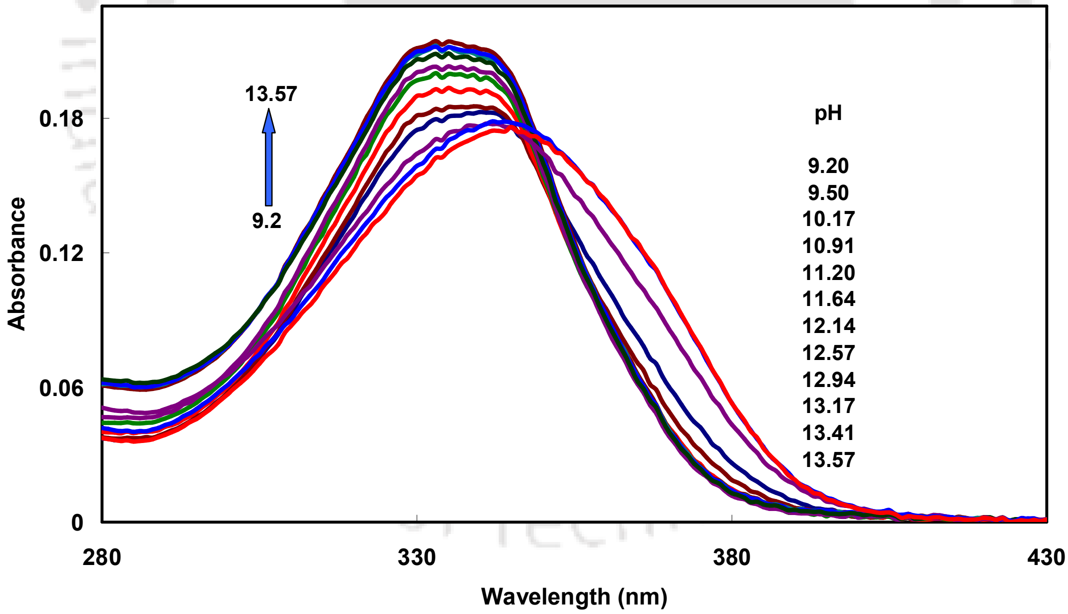

Figure 3.20. Absorption spectra of DMAPIP-b for neutral-anion equilibrium.

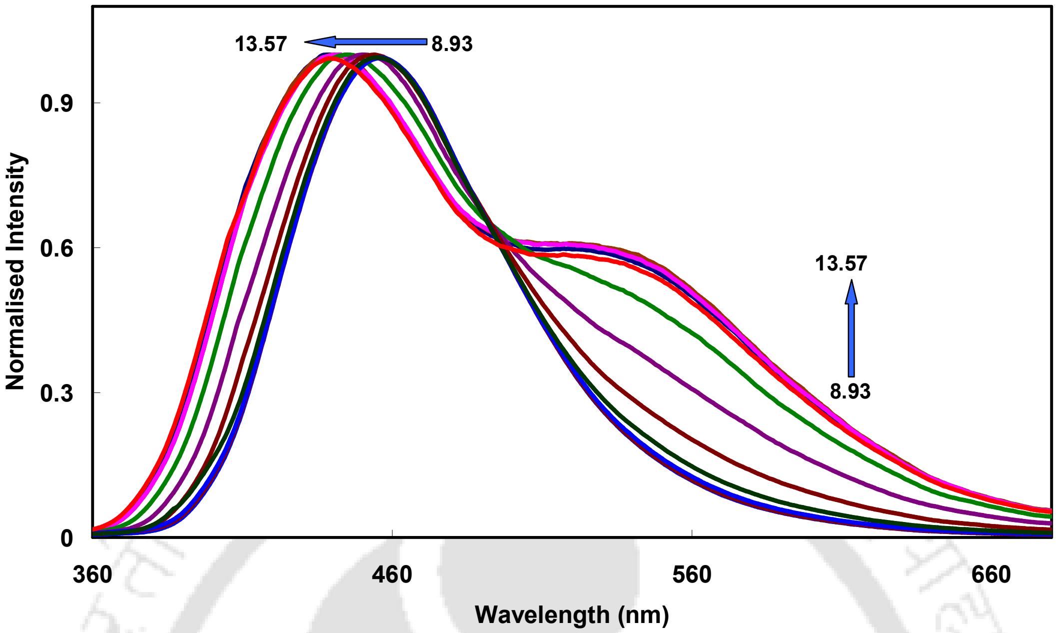

Figure 3.21. Normalised emission spectra (λ_{exc} = 349 nm) of DMAPIP-b for neutral-anion equilibrium.

To get further insight about the role of >NH proton in the dual emission, the neutral-anion equilibrium of DMAPIP-b was investigated. At pH 9.0, the molecule is in neutral form.[82] Upon increasing the pH, the absorption spectrum is blue shifted with a hyperchromic effect (**Figure 3.20**). DMAPIP-b has only one acidic proton (>NH). The spectral changes are consistent with the deprotonation of the >NH group to form an anion. The blue shift is also observed in absorption spectra of similar molecules when the imidazole >NH group is deprotonated.[205,206] The effect of pH on the fluorescence spectra is shown in **Figure 3.21**. The fluorescence spectrum of DMAPIP-b has an emission band in water at 451 nm with a long tail. With increasing pH of the solution, the normal emission band is blue shifted and a band emerges at the longer wavelength side. However, the most interesting change is the emergence of longer wavelength emission upon deprotonation. At higher pH, two different lifetimes are observed for DMAPIP-b when monitored at 425 and 545 nm (**Table 3.8**). Compared to shorter wavelength, when monitored at longer wavelength, the relative amplitude of the short lifetime species decreases, while that of the long lifetime species increases. This indicates that the longer wavelength emitting state has a longer lifetime and the shorter wavelength emitting species has a shorter lifetime. This is consistent with the lifetimes of the neutral form of DMAPIP-b.[82] The observation of clear dual emission in an anion suggests that the deprotonation may be one of the important steps in the formation of the longer wavelength emitting state in DMAPIP-b.

Table 3.8. Fluorescence lifetime (τ, ns) of the monoanionic form of DMAPIP-b and the values in parenthesis are relative amplitude.

Monitoring wavelength (nm)	τ_1	τ_2	χ^2
425	0.37 (30.44)	2.79 (69.56)	1.05
545	0.39 (20.14)	2.81 (79.86)	0.95

3.2.5. Double proton transfer induced TICT emission

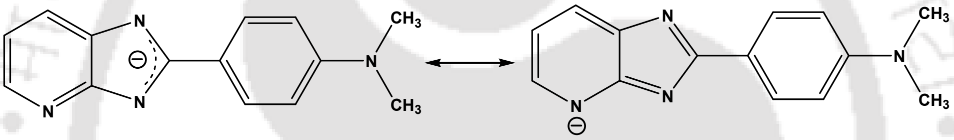

Scheme 3.3. Resonance stabilization of the anionic form of DMAPIP-b.

The studies suggest that both pyridyl nitrogen and the imidazole >NH group play an important role in the dual emission of DMAPIP-b in protic solvents. The charge donor is absolutely essential and the longer wavelength emission is from the ICT state. The dipole moment of the longer wavelength fluorescence emitting state was estimated by both solvatochromic (24.6 D) and thermochromic (25.5 D) methods.[212] The value is much higher than that of the shorter wavelength emitting state (12.2 D). On the basis of the theoretical calculations, it was reported in the literature that the dipole moment of the TICT state is much higher than the planar ICT state.[17] Very high dipole moment of the longer wavelength emitting state of DMAPIP-b clearly suggests that the ICT state is a TICT state. The enhanced dual emission in the anion reveals that the formation of the TICT state in protic solvent involves the deprotonation of an imidazole >NH proton. On the basis of these results, it is hypothesized that the formation of the TICT state is induced by solvent assisted (double) proton transfer from imidazole >NH to pyridyl nitrogen. The dissociation of a proton from the >NH group will produce a negative charge on the pyridyl nitrogen by resonance (**Scheme 3.3**); abstraction of a proton by pyridyl nitrogen results in proton transfer. It is reported that the excited state intramolecular proton transfer is accompanied by a torsional rotation of the tautomer, leading to the formation of a twisted charge transfer state in number of molecules.[213-216] However, in contrast to DMAPIP-b, the formation of a tautomer in those systems is an intramolecular process and torsional motion of the tautomer directs to a nonemissive charge transfer state.

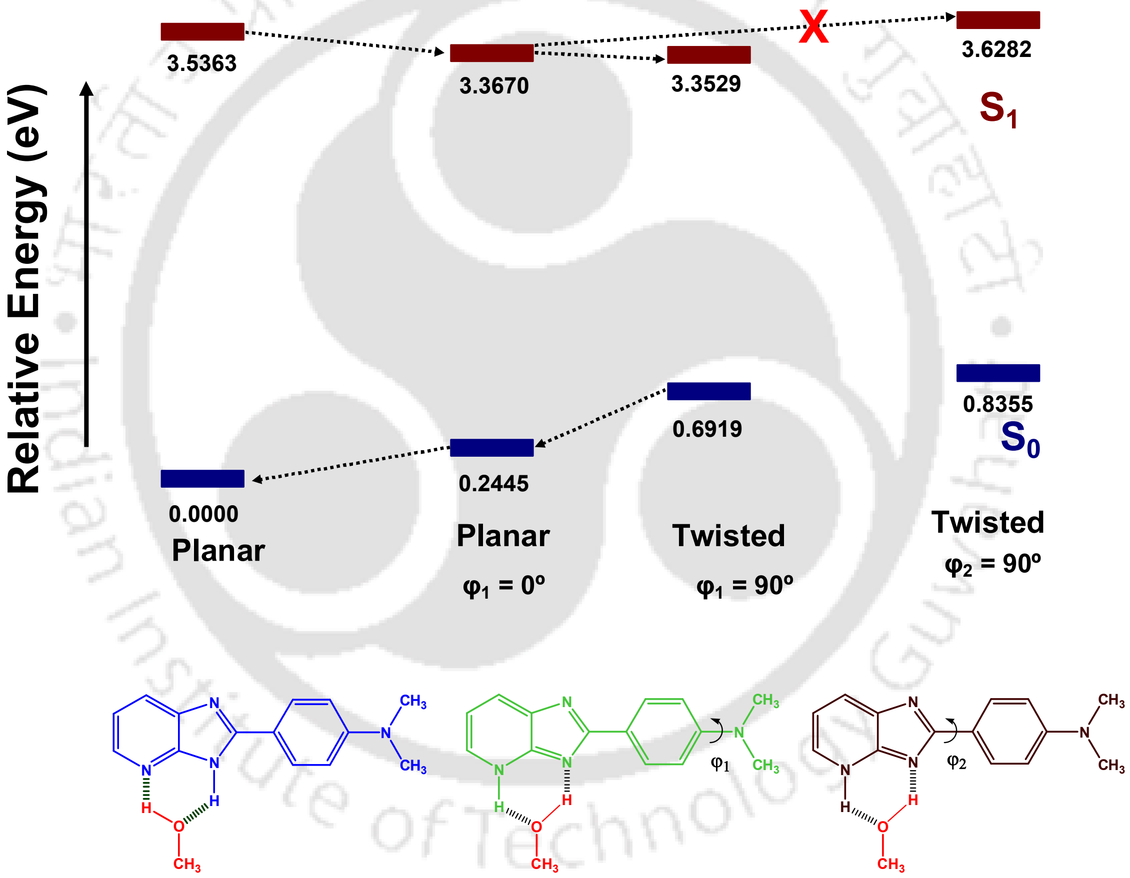

Scheme 3.4. Energy level diagram of DMAPIP-b and its tautomer (the cross indicates that the path is energetically not favored).

To verify the hypothesis, the structures of methanol-DMAPIP-b complexes are optimized and the energy level diagram was constructed (**Scheme 3.4**). The energy level diagram shows that the excited state energy of the planar tautomer is less than that of the normal form. The TICT state can be formed by rotation of either the dimethylamino group or the dimethylaminophenyl ring. The calculations indicate that the energy of the dimethylaminophenyl ring twisted state is higher than that of the planar state and the energy of the twisted state is even higher than that of the locally excited state. Therefore, the formation of the TICT state by twisting of the dimethylaminophenyl ring is not a favored process. On the other hand, the energy of the dimethylamino group twisted state of the tautomer is lower than that of the planar state. This suggests that the TICT state is formed by the twisting of the dimethylamino group rather than the dimethylaminophenyl ring. The experimental emission energy of the longer wavelength fluorescence (2.46 eV)[82] is in better agreement with the emission energy predicted from the twisted state (2.66 eV) than the predicted energy from the planar state (3.12 eV).[82] This supports the proposed mechanism. Yoon et al. reported that the excited state proton transfer promotes the formation of the TICT state in 4-*N*,*N*-dimethylaminosalicylic acid and 4-aminosalicylic acid which has a weak electron donating group also emits TICT emission due to formation of a phototautomer.[204,217] They also demonstrated that the TICT emission of 4-*N*,*N*-dimethylaminosalicylic acid is enhanced inside the cyclodextrin cavity due to enhancement in the intramolecular hydrogen bond which favors the formation of phototautomer. Recently, Guchhait et al. also proposed such proton transfer assisted charge transfer in some photochromic Schiff bases.[218] Nonetheless, in DMAPIP-b, the formation of a tautomer is a double proton transfer process assisted by a protic solvent molecule not an intramolecular process.

3.2.6. Conclusion

Both PyN-Me and ImNH-Me exhibit single emission not only in aprotic solvents but also in protic solvents. The absence of dual emission in PyN-Me where pyridyl nitrogen is prevented from hydrogen bonding with protic solvents emphasizes that the hydrogen bonding with pyridine nitrogen is crucial for the dual emission of DMAPIP-b in protic solvents. On the other hand, the absence of dual emission in ImNH-Me suggests that the hydrogen bonding with hydrogen of the imidazole >NH group is also playing an important role in the process. The absence of dual emission in PIP substantiates the conclusion that the longer wavelength emitting state is an ICT state. The higher dipole moment indicates that the ICT emitting state is the TICT state. The enhancement of longer wavelength emission at higher pH illustrates that the formation of a charge transfer state involves the deprotonation of imidazole >NH hydrogen. The dual emission of DMAPIP-b in protic solvents is due to formation of the TICT state that is induced by double proton transfer. The energy level diagram obtained by theoretical calculation supports the hypothesis.

Chapter 4

Photoinduced intramolecular charge transfer in *trans*-2-[4'-(dimethylamino)styryl]imidazo[4,5-b]pyridine

4.0. Introduction

In **chapter 3**, it is illustrated that the TICT emission of DMAPIP-b is induced by double proton transfer followed by charge transfer process. The process is assisted by protic solvent molecules and the hydrogen bonding at both pyridyl nitrogen and the imidazole >NH group are prerequisite for the stabilization of the TICT state in DMAPIP-b. Therefore, no TICT emission is observed when >NH is replaced by oxygen. Herein, the study was extended to a newly synthesized molecule *trans*-2-[4'-(dimethylamino)styryl]imidazo[4,5-b]pyridine (*t*-DMASIP-b, **Chart 4.1**). The main objective of the study is to examine the effect of introducing ethylenic double bond between donor and acceptor on the TICT emission and other spectral characteristics of the molecule. The *trans* and *cis* forms of DMASIP-b are shown in **Chart 4.1**.

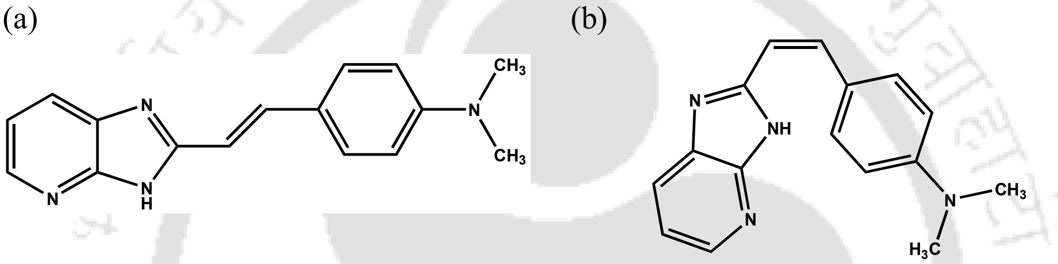

Chart 4.1. Structures of (a) *trans*-DMASIP-b and (b) *cis*-DMASIP-b.

4.1. Absorption spectra

Table 4.1. Longest wavelength absorption maxima (λ_{max}^{ab}, nm), fluorescence maxima (λ_{max}^{em}, nm), Stokes shift ($\bar{\nu}_{SS}$, cm^{-1}) and fluorescence quantum yield (Φ_f) of *t*-DMASIP-b in different solvents.

Solvent	λ_{max}^{ab}	λ_{max}^{em}	$\bar{\nu}_{SS}$	Φ_f
1. Cyclohexane	375, 394 (sh)	415, 438, 453	3836	0.026
2. Dioxane	381	450	4024	0.038
3. Ether	375	449	4395	0.030
4. Ethylacetate	380	459	4529	0.019
5. 1-Butanol	390	479	4767	0.036
6. 1-Propanol	391	485	4957	0.031
7. Ethanol	391	489	5175	0.028
8. Acetonitrile	384	492	5716	0.031
9. Methanol	391	500	5575	0.030
10. Glycerol	403	513	5321	0.790

The UV-visible absorption spectra were recorded in different solvents and the data are compiled in **Table 4.1**. In cyclohexane the absorption spectrum of *t*-

DMASIP-b is broad and less structured with respect to well resolved structure of DMAPIP-b (**Figure 4.1**). This suggests that *t*-DMASIP-b has higher conjugation than DMAPIP-b. The spectral band maxima of *t*-DMASIP-b are also largely red shifted (40 nm) in all the solvents compared to those values of DMAPIP-b. On increasing solvent polarity absorption spectrum of *t*-DMASIP-b undergoes a red shift with complete loss of vibrational structure. This feature is same as observed in DMAPIP-b.[82]

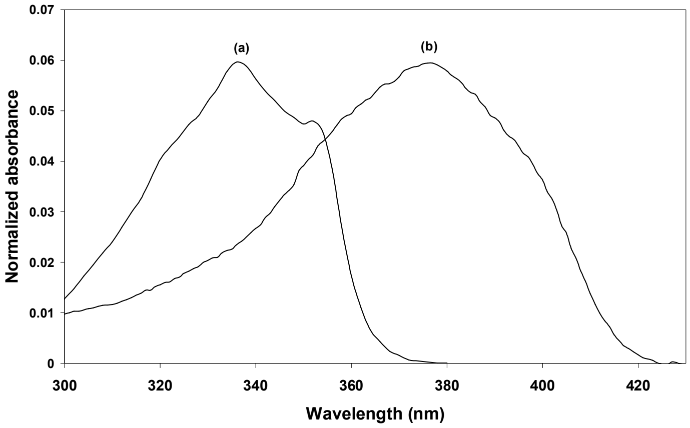

Figure 4.1. Absorption spectra of (a) DMAPIP-b and (b) *t*-DMASIP-b in cyclohexane.

4.2. Fluorescence spectra

The emission spectra of *t*-DMASIP-b in few selected solvents of different polarities are shown in **Figure 4.2** and data from all the solvents are compiled in **Table 4.1**. In cyclohexane the emission spectrum is sharp and has well resolved vibronic structure compared to that of absorption spectrum. Such less structured absorption spectrum and well structured sharp emission spectrum were also found in DMAPIP-b.[82] The vibrational frequency observed for *t*-DMASIP-b (1276 cm^{-1}) is also close to that of DMAPIP-b and other 2-phenyl substituted benzazoles.[219] All these spectral characteristics indicate the structural similarities of *t*-DMASIP-b with 2-phenyl substituted benzazoles. The vibrational structure diminishes with a red shift on increasing polarity of the solvent. The fluorescence spectrum of *t*-DMASIP-b (same as DMAPIP-b)[82] is independent of λ_{exc} in all solvents. It supports the theoretical predictions (see **Section 4.4**) that *t*-DMASIP-b is present in only one isomeric form (isomer I, **Chart 4.2**). This can be explained by the repulsive effect of lone pair of electrons in imidazole and pyridyl nitrogens.

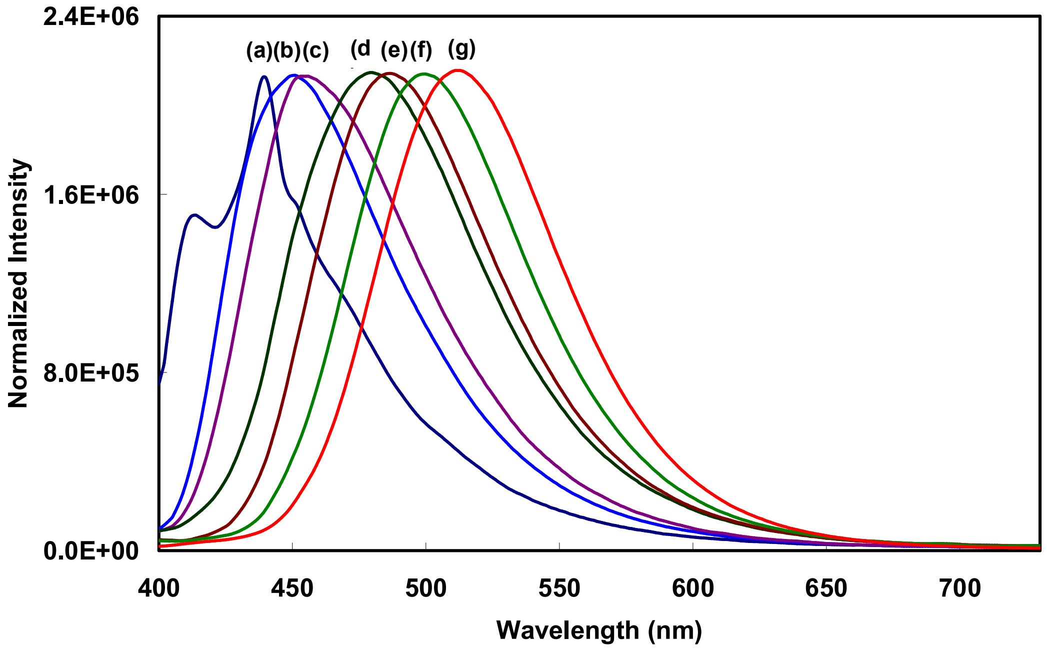

Figure 4.2. Normalized fluorescence spectra of DMASIP-b in (a) cyclohexane, (b) dioxane, (c) ethylacetate, (d) *n*-butanol, (e) acetonitrile, (f) methanol and (g) glycerol.

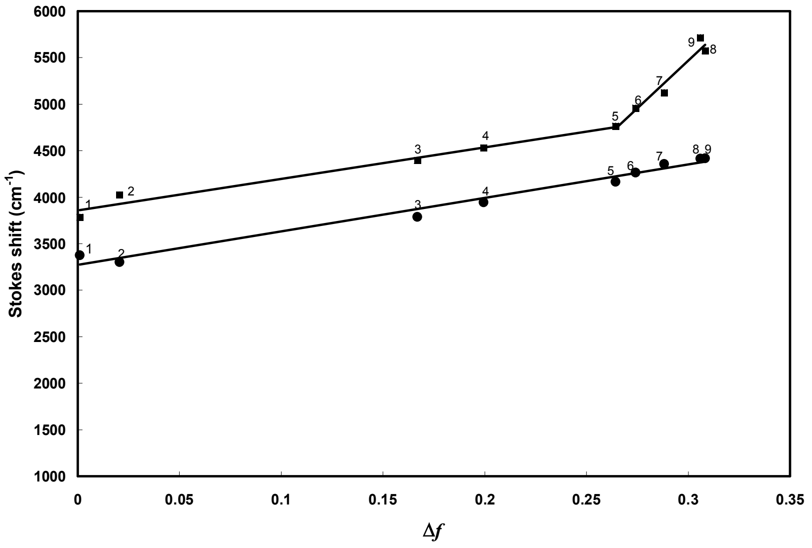

Figure 4.3. Lippert-Mataga plot of *t*-DMASIP-b (■) and DMAPIP-b (●, data from ref 82 and only shorter wavelength emission band maxima is used for calculating Stokes shift in protic solvents).

The significant difference between the emission spectra of DMAPIP-b[82] and *t*-DMASIP-b is the single emission band of *t*-DMASIP-b in protic solvents. Other striking difference is found in the Lippert plot (**Figure 4.3**). The Lippert-Mataga plot[202] (**equation 3.4**) was constructed as explained in **Section 3.1.1**. Attempt to construct a single straight line for *t*-DMASIP-b using data from all the solvents resulted in poor fit. However, very good fit was found for separate plot with nonpolar (r = 0.99) and polar (r = 0.98) solvents (**Figure 4.3**).

The Lippert-Mataga plot in polar solvents is much steeper (20485 cm^{-1}) than that for the same in nonpolar solvents (3380 cm^{-1}), indicating a large dipolar change between ground and excited states in polar solvent than in the nonpolar solvent. On the other hand, in the case of DMAPIP-b single straight line is good enough to show the linear correlation (r = 0.99) for the same set of solvents. Using 6.2 Å for the Onsager radius of *t*-DMASIP-b, the Lippert-Mataga plot gives the difference in dipole moments between the two states in nonpolar and polar solvents as 8.8 D and 22.5 D respectively. Considering the ground state dipole moment as 6.1 D (obtained by DFT calculation)[188] the excited state dipole moments were found to be 14.9 D and 28.6 D in nonpolar and polar media, respectively. All these results reveal that in polar solvent, the excited state from which *t*-DMASIP-b emits is different from the one from which it emits in nonpolar solvents. High dipole moment for the emitting state in polar solvents suggests that it is having appreciable charge transfer character than the emitting state in nonpolar solvents.

4.3. Nature of the emitting states

Since the size of *t*-DMASIP-b and DMAPIP-b are different, it is difficult to compare the charge transfer between the two fluorophores. Higher dipole moment of *t*-DMASIP-b may be due to large charge separation or more charge transfer character. The solvent polarity parameter π* will be a very good indication. To get a clear idea about the individual contribution of solvent effects the multiple linear regression analysis[199] (**equation 3.1**, **Section 3.1.1**) using the absorption and fluorescence spectral data were performed and represented below.

$$E\ (A) = 26884 - 217\ \pi^* - 268\ \alpha - 1250\ \beta\ (r = 0.76) \qquad \textbf{(4.1)}$$

$$E\ (F) = 23006 - 2472\ \pi^* - 1250\ \alpha - 166\ \beta\ (r = 0.97) \qquad \textbf{(4.2)}$$

The E_0 values obtained from multiple liner regression approach are nearly same with the experimental values obtained in cyclohexane. The above equations illustrate that all the three parameters π*, α and β contribute to the stabilization of both ground state as well as excited state. The stabilization by hydrogen bond donating capacity of the solvent (α) is more in DMAPIP-b in the ground state (**equation 3.6**, **Section 3.2.1**), however in the excited state, it is more in *t*-DMASIP-b. But the contribution from the polarity/polarizability parameter π* is maximum for DMAPIP-b in both ground and excited state and the value is higher in the excited state. This indicates the contribution from the dipolar interaction in DMAPIP-b is more enhanced in the excited state. This is a clear indication of increase in ICT in the excited state. The contribution of π* is less in the stabilization of *t*-DMASIP-b compared to the contribution of same in the stabilization of DMAPIP-b in both ground state and excited state (**Section 3.2**). The lower negative value of π* in *t*-DMASIP-b compared to that in DMAPIP-b indicates that the ICT from donor to acceptor in *t*-DMASIP-b is lesser than that in DMAPIP-b. From this, it may be concluded that the charge transfer character is less in *t*-DMASIP-b. In addition no dual emission is observed from *t*-DMASIP-b in any solvent including protic solvents. The solvatochromic shift for *t*-DMASIP-b between cyclohexane and methanol is 2830 cm^{-1} and for DMAPIP-b between cyclohexane and methanol 2230 cm^{-1} (normal emission) and is 6620 cm^{-1} (TICT emission).[82] Therefore, it is clear that the emitting state in polar solvent has appreciable charge transfer character; but unlike DMAPIP-b in protic solvent, it is not a TICT state.

In donor-acceptor systems, upon excitation, transfer of an electronic charge from a donor to an acceptor leads to a charge separation that results in an ICT state. In the planar ICT model, the highly dipolar planar quinoid structure is formed in the emitting state.[220,221] Cogan et al.[17] predicted that in many cases the planar conformation of ICT excited state is lower in energy than that of the locally excited state and fluorescence can be observed from planar structures. Though the dipole moment of the planar ICT state is lesser that that of TICT state, it is higher than that of normal excited state. The higher excited state dipole moment observed for *t*-DMASIP-b in polar solvents suggests that the molecule is emitting from the ICT state. The emission of DMAPIP-b in nonpolar solvents can be assigned as the emission from the normal excited state.

Since the emitting state in polar solvent has different origin, the dipole moment in the excited state for polar solvents can be calculated using the fluorescence data from the following **equation 4.3**,[1]

$$\bar{\nu}_f = \bar{\nu}_f^{0} - [2\mu_e(\mu_e - \mu_g)/hca^3]\,\Delta f' \qquad \textbf{(4.3)}$$

$$\Delta f' = [(\varepsilon - 1)/(2\varepsilon + 1)] - (1/2)[(n^2 - 1)/(2n^2 + 1)] \qquad \textbf{(4.4)}$$

where $\bar{\nu}_f$ is the fluorescence maximum, all other parameters have same meaning as defined earlier in **Section 3.1.1**. The linear fit (r = 0.93) thus obtained (**Figure 4.4**) gives the excited state dipole moment 27.4 D for the ICT state.

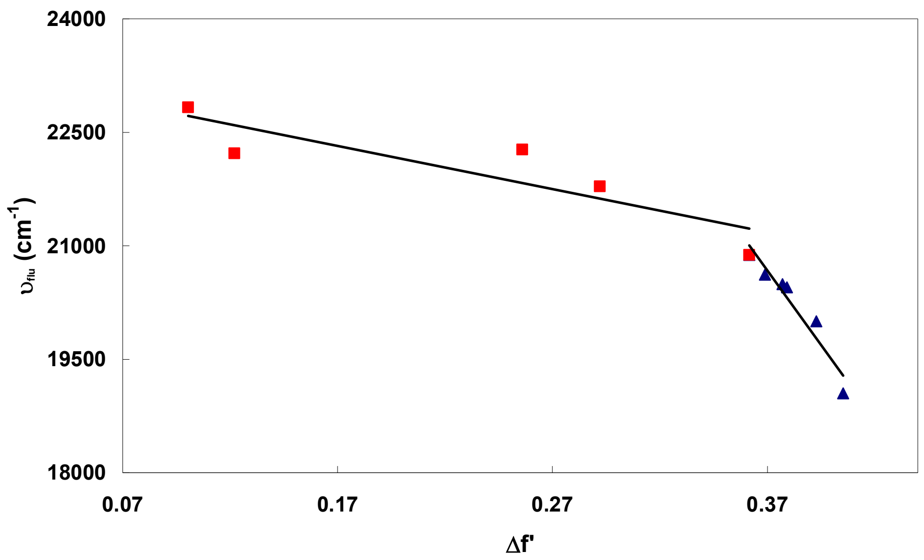

Figure 4.4. The plot of fluorescence maxima (cm^{-1}) against solvent polarity parameter Δf′.

4.4. Computational calculations

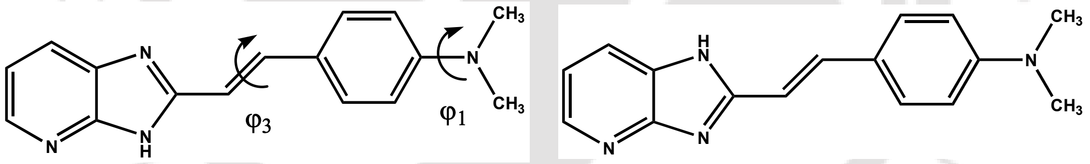

E = - 838.3723 a. u.
μ_g = 6.1 D
Isomer I

E = - 838.3653 a. u.
μ_g = 8.3 D
Isomer II

Chart 4.2. Structures of the isomers of *t*-DMASIP-b.

Computational calculations have been performed to further rationalize the experimental results. Two isomeric forms are possible for *t*-DMASIP-b (**Chart 4.2**). DFT calculations predict that isomer I is more stable than isomer II in any solvent. However isomer II is more polar than isomer I (**Chart 4.2**). But the relative population of isomer II is less than 2% even in polar solvents (calculated using Boltzmann distribution law). Thus isomer II was not considered for any further discussion. The optimized parameters of the ground state and the excited state are compiled in **Table 4.2**. The calculations predict that the structure of *t*-DMASIP-b is also nearly planar like DMAPIP-b,[82] with small dihedral angle of 6° between dimethylamino group and the phenyl group. The theoretical excitation and emission energy obtained by TDDFT is in good agreement with the experimental values (**Table 4.2**).

Table 4.2. Optimized molecular parameters of *t*-DMASIP-b.

	Ground State	Excited state
Energy (a. u.)	-838.372	-838.250
Phenyl/dimethylamino dihedral angle (^{o})	6.0	0.05
Phenyl/ethylenic group dihedral angle (^{o})	0.6	0.02
Imidazopyridine/ ethylenic group dihedral angle (^{o})	0.6	0.01
Theoretical transition energy[1] (nm)	372 (375)	408 (415)

[1] Values in parentheses are experimental values in cyclohexane.

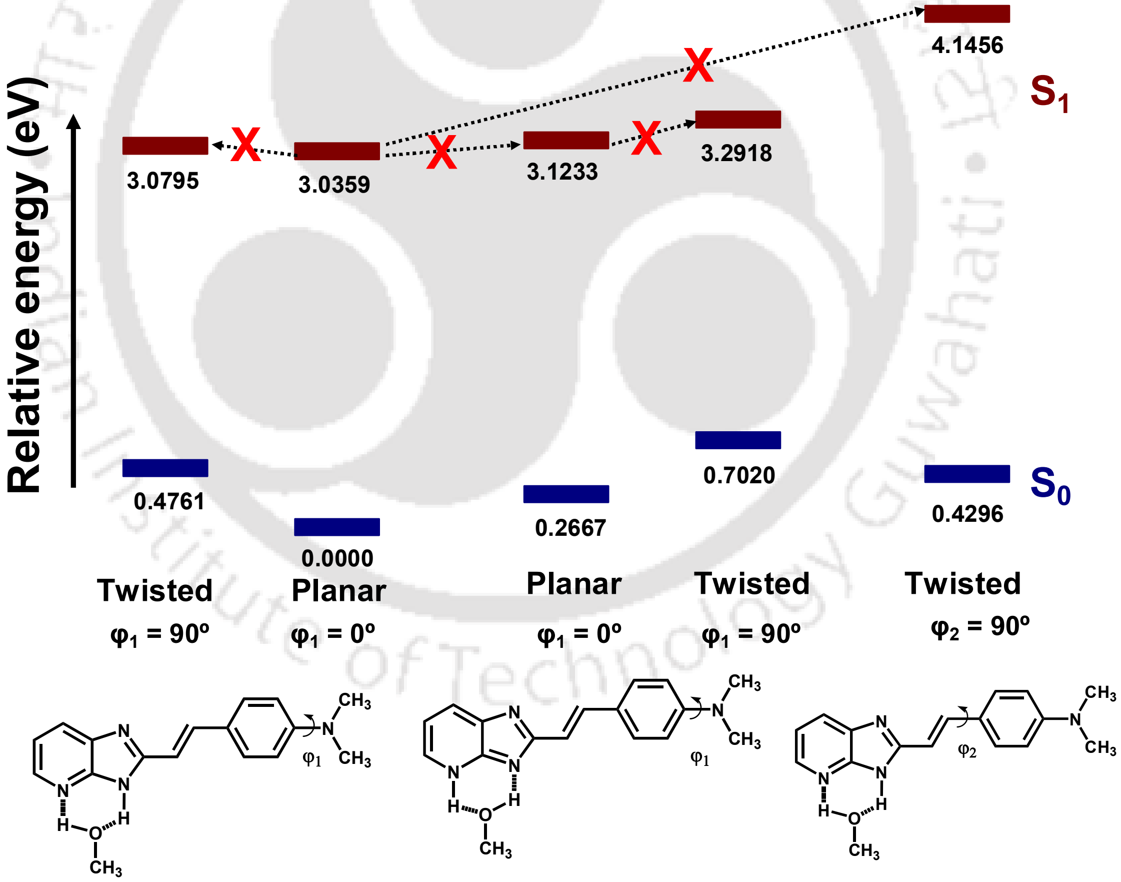

Scheme 4.1. Energy level diagram of *t*-DMASIP-b and its tautomer (the cross indicates the path is energetically not favored).

As in DMAPIP-b (**Section 3.2.5**), the structures of methanol-*t*-DMASIP-b complexes are optimized and the energy level diagram was constructed (**Scheme 4.1**).

But, unlike DMAPIP-b, the excited state of the normal form is more stable than the planar tautomer. The energy of the twisted tautomers are further higher than the planar tautomer. The normal planar form is more stable than its twisted form. Therefore, neither normal form of the complex nor the tautomeric form of the complex emits TICT emission. Lesser hydrogen bond accepting capacity of the solvent with *t*-DMASIP-b (-166) in the excited state than that with DMAPIP-b (-593) might have contributed to the absence of double proton transfer in *t*-DMASIP-b.

4.5. Fluorescence quantum yield and isomerization

The fluorescence quantum yield of *t*-DMASIP-b is low in non-viscous solvent and is very high in viscous solvent glycerol (**Table 4.1**). The quantum yield of *t*-DMASIP-b in glycerol was found to be ~26 times greater than that of non-viscous solvent such as methanol. In the literature similar type of viscosity effect on the fluorescence quantum yield is reported for other push-pull styryl molecules.[148,154] This is attributed to the restriction on twisting of the olefinic double bond that leads to isomerization. Therefore, the effect of viscosity will be much higher on the twisting of carbon-carbon double bond[222] that decreases the photoisomerization and increases the fluorescence quantum yield. To identify the isomerization path of *t*-DMASIP-b the potential energy surface for the isomerization was theoretically constructed by rotating the ethylenic double bond (**Figure 4.5**). The result indicates that the

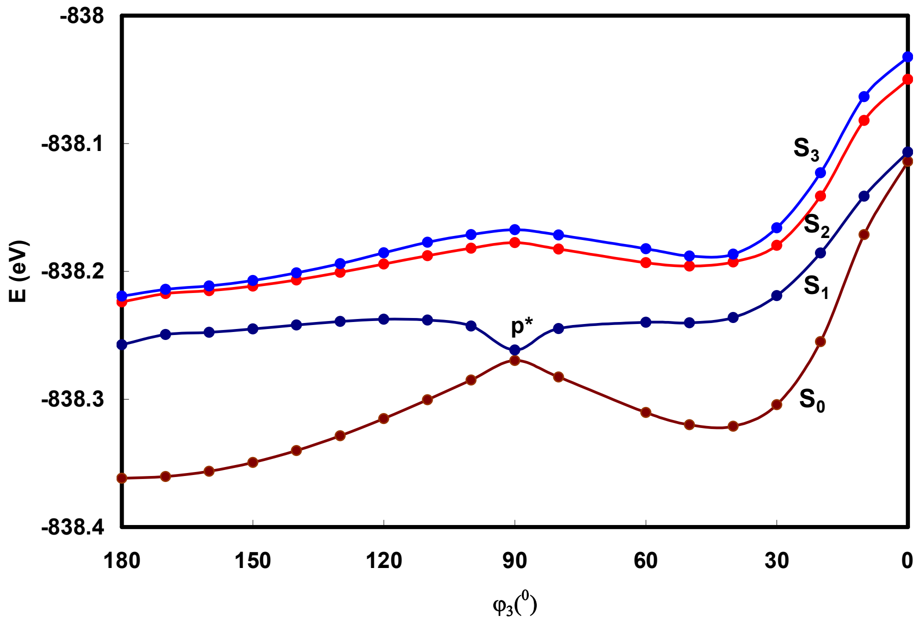

Figure 4.5. Potential energy surfaces simulated for photoisomerization of *t*-DMASIP-b in different electronic states.

photoisomerization occurs via phantom state in a nonradiative way and there is a very small barrier for the rotation of the *trans* isomers to reach the phantom state and a very little or no barrier for the *cis* isomers to reach the perpendicular geometry.

For further confirmation, the irradiation experiments have been carried out (using cut-off filter 420 nm) in nonpolar solvent dioxane, polar aprotic solvent acetonitrile, polar protic solvent methanol and polar viscous solvent glycerol. The reaction was followed by UV-visible absorption spectra (**Figure 4.6**). In all the solvents, upon irradiation hypochromic effect is observed in the absorption spectra and spectral shifts occur at the shorter wavelength. In addition, a clear isosbestic point is observed. Such a blue shift and hypochromic effect are due to the formation of *cis* isomer.[157] The present study, depicted that in all the solvents media upon irradiation the *trans* isomer is converted to its *cis* isomer and the presence of the isosbestic point suggests the existence of 1:1 equilibrium between the *trans* and the *cis* isomers. In all the solvents the photostationary state was reached within a minute.

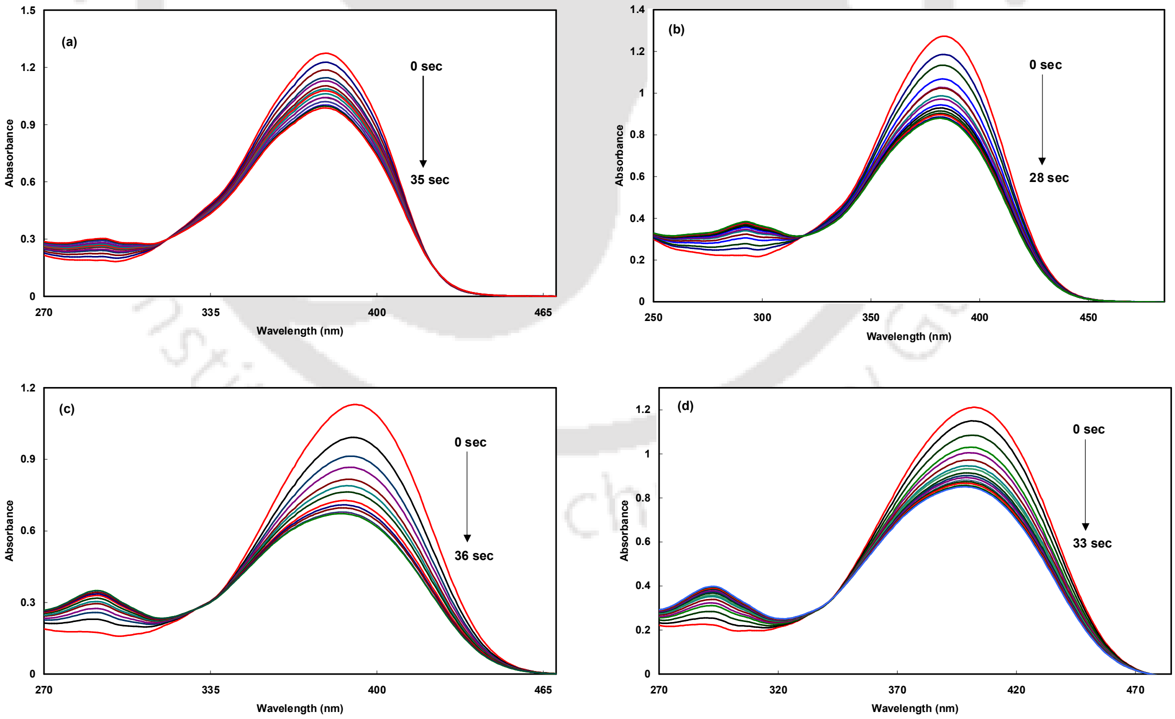

Figure 4.6. Irradiation (using 420 nm cut-off longpass filter) of *t*-DMASIP-b in (a) dioxane, (b) acetonitrile, (c) methanol and (d) glycerol (followed by UV-visible spectra).

It is observed that the content of *trans* isomer is more in dioxane and methanol. The difference in behavior observed is either real or due to the spectral shifts that results in the change in the incident light excitation-ratio of the two isomers. Thus the absorbance ratio of the sample after reaching the photostationary state (after irradiation i.e. A_{ai}) to that of *trans* isomer (before irradiation i.e. A_{bi}) at λ_{max}^{ab} were calculated. and A_{ai}/A_{bi} ratio follows the order: methanol (0.59) < acetonitrile (0.70) ~ glycerol (0.71) < dioxane (0.78). However, the absorption maxima of the *trans* isomer of *t*-DMASIP-b in the above solvents follows the order: dioxane (380 nm) < acetonitrile (385 nm) < methanol (392 nm) < glycerol (403 nm). Hence, it may be depicted that due to solvent effect, the amount of *trans* isomer present in dioxane and methanol at photostaionary state is more.

4.6. Effect of temperature on the spectral characteristics of *t*-DMASIP-b

The rate constant for the formation of the ICT state is mainly depends on temperature due to the vibronic coupling.[1] On the other hand, it is shown that the solvent parameters such as viscosity and polarity and the solute parameters such as twist angle of ground state, rotating volumes, molecular shape and electronic nature are established to determine the rate for this process.[1] With rise in temperature, the intensity of the ICT emission is expected to increase due to the enhancement in the formation of the ICT state. However, rise in temperature favors the photoisomerization also.[141,142] Hence the increase in photoisomerization quantum yield leads to decrease in fluorescence quantum yield as it competes with the ICT process.

The effect of temperature on the spectral characteristics of *t*-DMASIP-b is investigated in a few selected solvents (**Figure 4.7** and **Figure 4.8**). The absorption spectra show hypochromic effect and hypsochromic shift upon increase in temperature in all the solvents except glycerol and quasi-isosbestic point is observed (**Figure 4.7** for dioxane is shown as representative). However in glycerol the absorption maximum remains almost unaffected.

The steady state emission spectra of *t*-DMASIP-b were also recorded as a function of temperature (**Figure 4.8**). The fluorescence spectrum undergoes a blue shift with increase in temperature in solvents like dioxane, acetonitrile and methanol, whereas bathochromic shift was observed in glycerol.

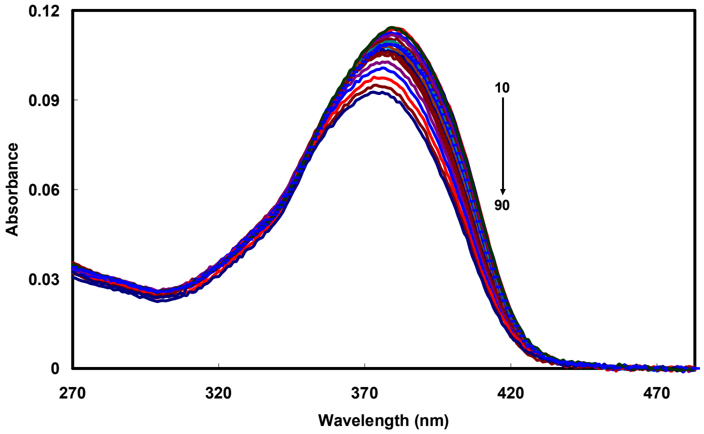

Figure 4.7. Absorption spectra of *t*-DMASIP-b at different temperature in dioxane.

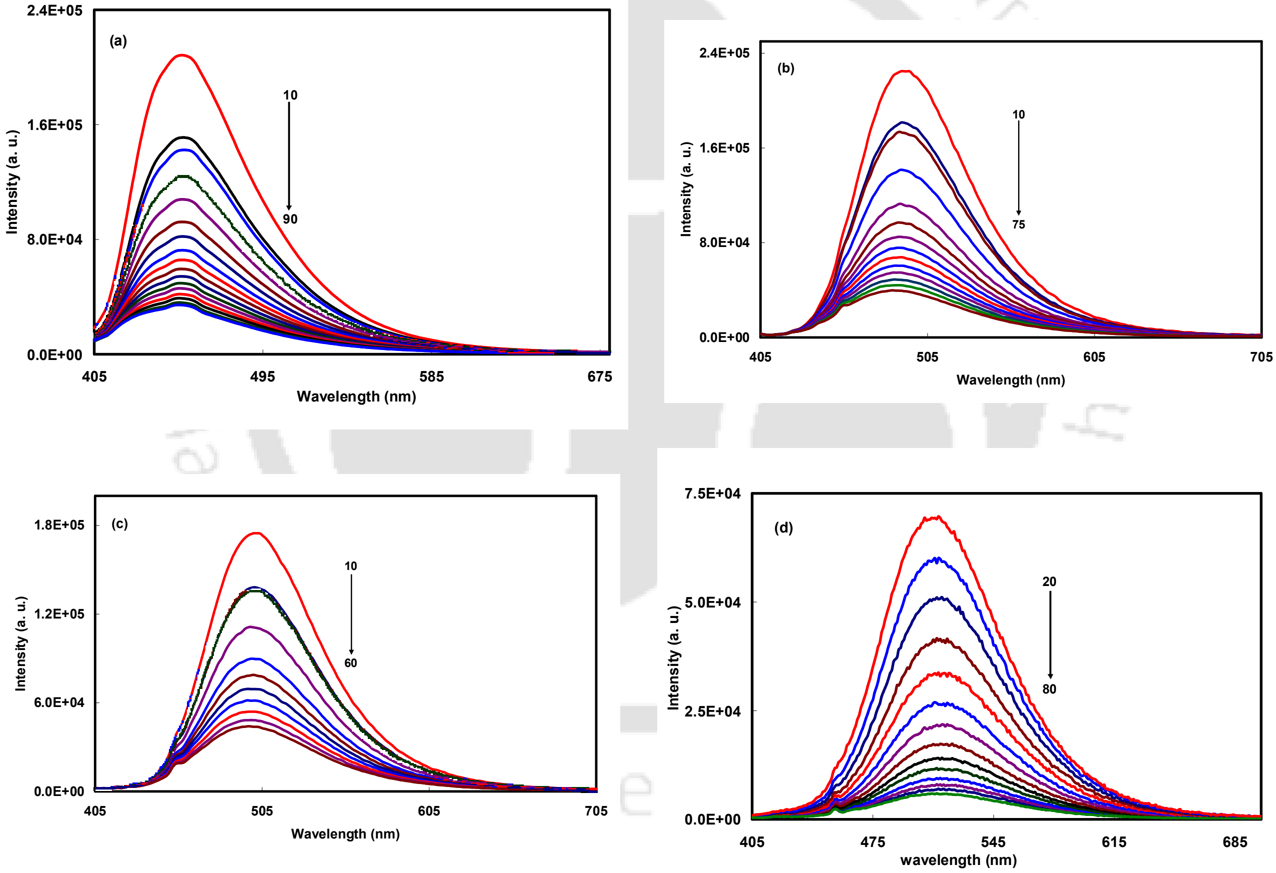

Figure 4.8. Fluorescence emission spectra (λ_{exc} = 400 nm) of *t*-DMASIP-b at different temperatures in (a) dioxane, (b) acetonitrile, (c) methanol and (d) glycerol.

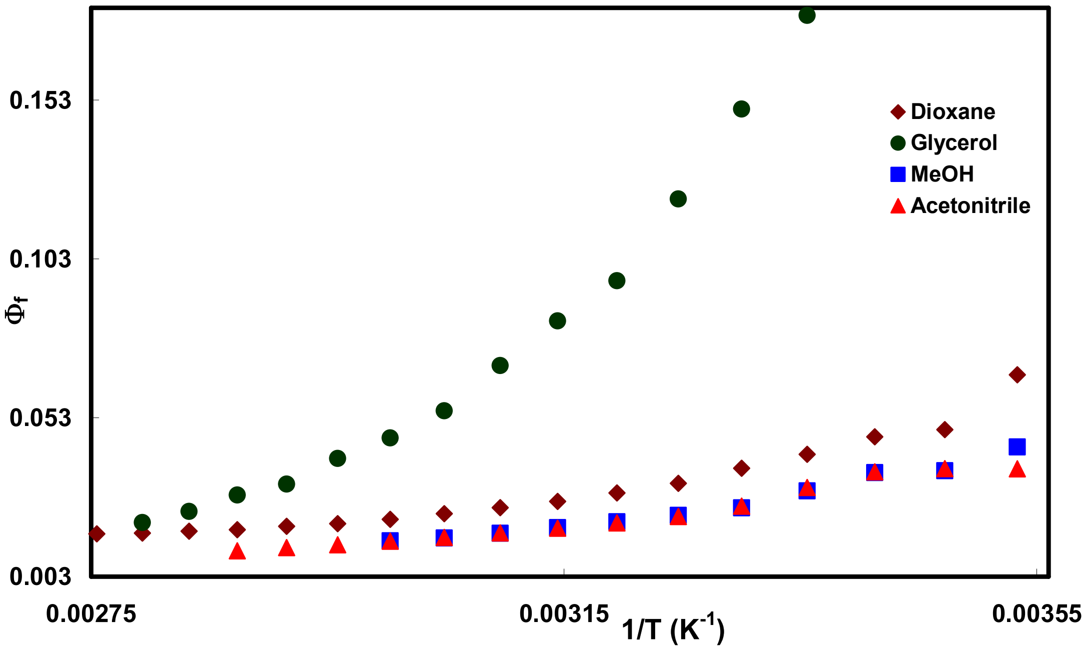

Figure 4.9. Temperature dependence of fluorescence quantum yield (Φ_f) of *t*-DMASIP-b in different solvents.

The steady state emission spectra of *t*-DMASIP-b were also recorded as a function of temperature (**Figure 4.8**). The fluorescence spectrum undergoes a blue shift with increase in temperature in solvents like dioxane, acetonitrile and methanol, whereas bathochromic shift was observed in glycerol. Upon increasing the temperature, the fluorescence quantum yield decreases continuously in all the solvents (**Figure 4.9**). Same behavior was observed for *trans*-stilbene and its analogues due to enhanced isomerization.[154,141,142,222-229] Upon increasing the temperature the movement of the molecule becomes more facile so that the nonradiative decay route through rotation of double bond i.e. the isomerization is more favorable. In summary, the fluorescence quantum yield decreases with increase in temperature, whereas it increases with increase in viscosity. Thus it is attributed that in highly viscous solvent like glycerol, both fluorescence and isomerization processes are coupled with changing temperature.[142,222,224]

The increase in temperature (T) leads to decrease of the permittivity ε and the refractive index *n* of the solvent as given by the empirical formulas.[230]

$$\varepsilon(T) = \varepsilon_0(T_0) - \alpha(T-T_0) - \beta(T-T_0)^2 - \gamma(T-T_0)^3 \qquad \textbf{(4.5)}$$

$$n(T) = n_0(T_0) - a(T-T_0) - b(T-T_0)^2 \qquad \textbf{(4.6)}$$

where the parameters α, β, γ as well as *a* and *b* are solvent dependent constants. This explains the hypsocromic effect observed in dioxane, acetonitrile, methanol and glycerol. On contrary, bathochromic shift is observed in glycerol. It may be due to the fact that the solvent reorientation around the dipole becomes more facile due to reduced viscosity of the solvent at higher temperature.

4.7. Effect of pH

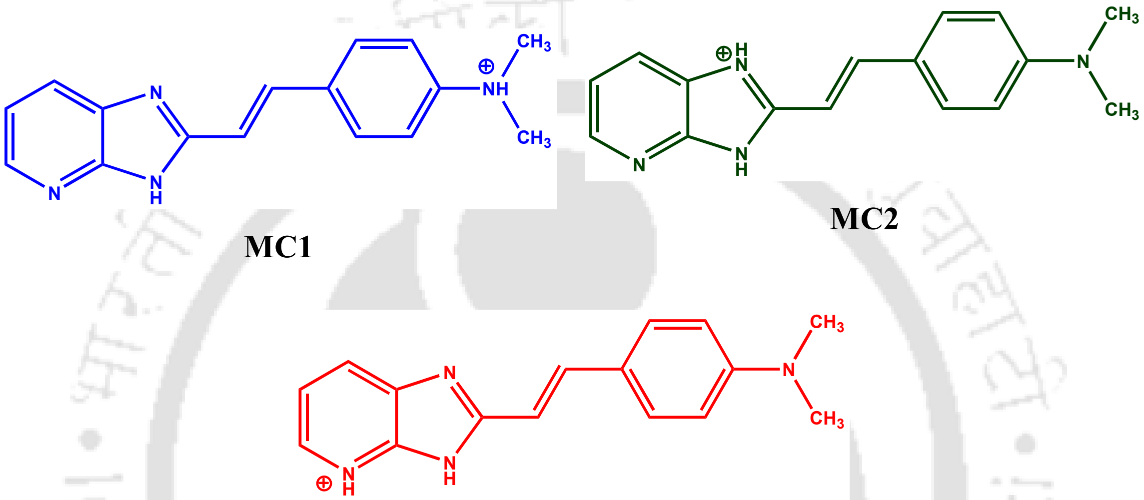
MC1
MC2
MC3

Chart 4.3. Structures of possible monocations of *t*-DMASIP-b.

Upon increasing the acid concentration protonation takes place at imidazole nitrogen and dimethylamino nitrogen of DMAPIP-b to form two kinds of monocations in both ground state and first excited state.[82,83] Alike DMAPIP-b, *t*-DMASIP-b also has three basic centers where protonation can take place. Protonation at dimethylamino nitrogen, imidazole nitrogen and pyridyl nitrogen are labeled as MC1, MC2 and MC3, respectively (**Chart 4.3**). Since the introduction of double bond in DMAPIP-b affected its spectral characteristics, it will be quite interesting to study the effect on the prototropic equilibrium.

As mentioned in **Section 3.1.2** that the formation of MC2 and/or MC3 will cause red shift as it will increase the conjugation of the system by increasing the withdrawing nature of the acceptor group and MC3 is expected to produce more red shift than MC2. But formation of MC1 causes a blue shift in the spectrum as it decreases the conjugation of the system, as upon protonation the lone pair electron of dimethylamino nitrogen will be no longer easily available for stabilization by resonance.[148,154,205,206,231-233]

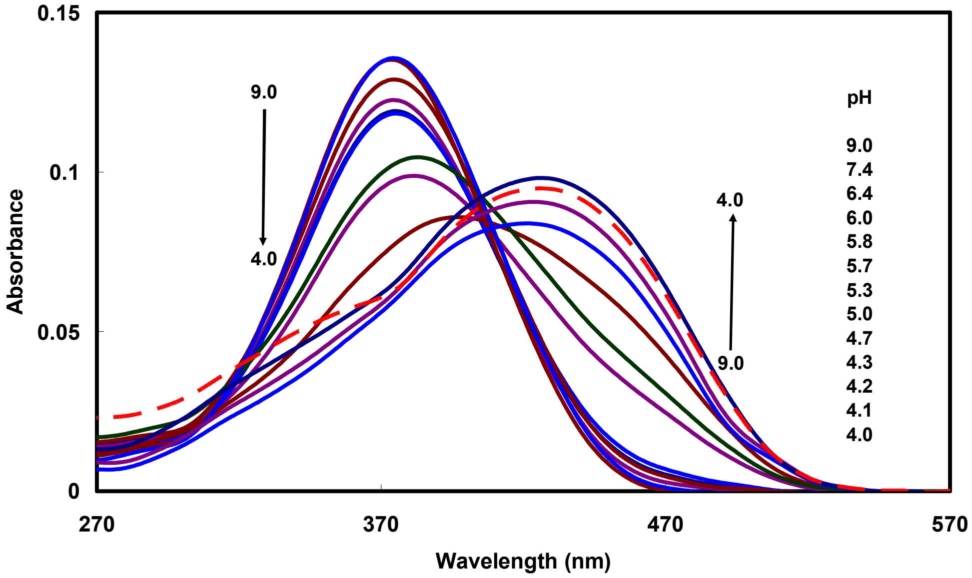

Figure 4.10. UV visible spectra of *t*-DMASIP-b for neutral - monocation equilibrium in aqueous medium (the spectrum at pH 4.0 is shown as dotted line).

Figure 4.10 shows the effect of pH on the absorption spectrum of *t*-DMASIP-b. It is observed that upon increasing the acid concentration, the absorbance of the original band appears at 375 nm decreases monotonically with appearance of a new band at the red side of the original band at 432 nm. No isosbestic point is observed in the absorption spectra indicating that the prototropic equilibrium is not exactly one to one conversion and there may be more than one new species is formed. It is observed that the new band obtained at 432 nm increases up to pH 4.1. Upon further addition of acid the absorbance of the monocationic band decreases.

The results indicate that in the ground state upon increasing the acid concentration, protonation takes place at the ring nitrogen and no protonation takes place at the dimethylamino nitrogen. The pK_a value is calculated for the neutral-monocation equilibrium using Henderson–Hasselbach equation from the absorption spectral data and is found to be 5.2 (plot is not shown). The pK_a value obtained for *t*-DMASIP-b is close to the value obtained for DMAPIP-b (5.4)[82] for the neutral monocation equilibrium.

Upon increasing the acid concentration, the intensity of the fluorescence band decreases with a bathochromic shift (**Figure 4.11**). The results indicate, same as in the ground state, in the excited state also, protonation takes place at ring nitrogen but not at dimethylamino nitrogen. For further confirmation of the monocation formation is MC2 and/or MC3, emission spectra were recorded at cationic pH (pH 4.1), monitoring at various wavelengths. The spectral shift occurs from 530 nm to 554 nm (**Figure 4.12**).

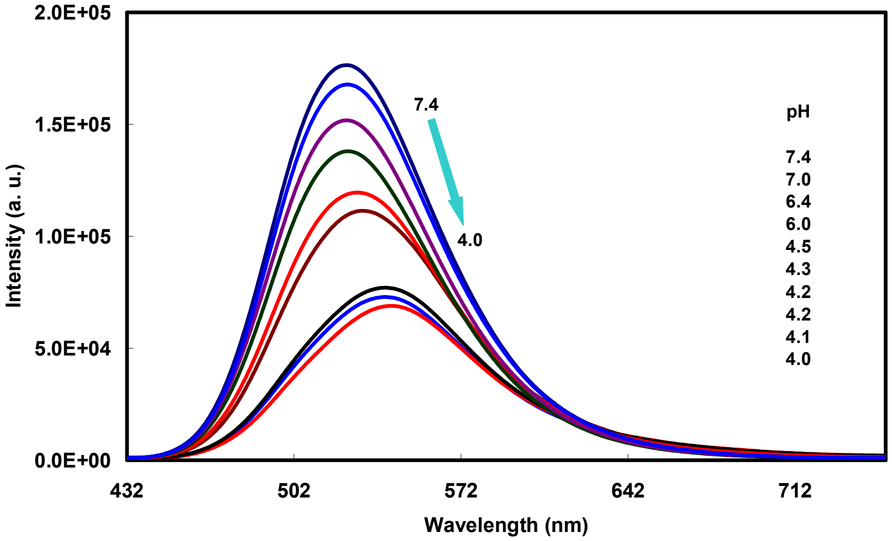

Figure 4.11. **Emission spectra (λ_{exc} = 428 nm) of *t*-DMASIP-b in aqueous medium for neutral-monocation equilibrium at pH range 9.0 to 4.0.**

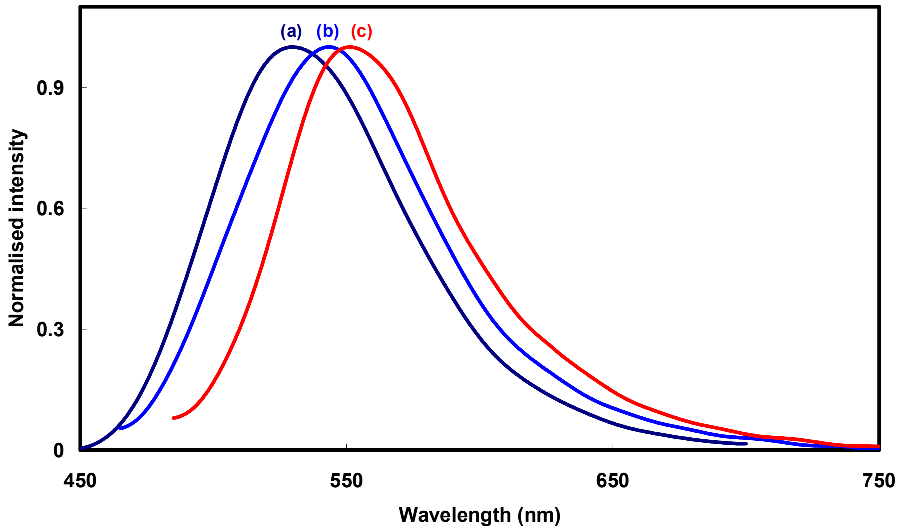

Figure 4.12. Normalised emission spectra of *t*-DMASIP-b in aqueous medium at cationic pH (4.1): (a) λ_{exc} = 440 nm, (b) λ_{exc} = 460 nm and (c) λ_{exc} = 480 nm.

It is already stated earlier that both MC2 and MC3 (**Chart 4.3**) will cause bathochromic shift and the shift is more pronounced upon protonation at pyridyl nitrogen than at imidazole nitrogen due to increase in conjugation. Therefore, it can be concluded that both MC2 and MC3 are formed. The pK_a^* was calculated using fluorimetric titration method and was found to be 4.36 that is less than that of pK_a (5.2). This indicates that in the excited state the monocation becomes more acidic and proton dissociation takes place from monocation at lower pH which shifts the equilibrium.

4.8. Conclusion

Presence of carbon-carbon double bond in *t*-DMASIP-b strongly perturbs the photophysics of the molecule. In contrast to DMAPIP-b, *t*-DMASIP-b emits single emission in all solvents including protic solvents. However, the emitting states of *t*-DMASIP-b in nonpolar and polar solvents are different. From the solvatochromic approach it is observed that among the three solvent parameters the maximum contribution of stabilization arises from the dipolar interaction in the excited state. The emitting state in polar solvents is a planar ICT state and not a TICT state. Theoretical calculations further substantiates the energy of the TICT state is higher than planar states. Both experimental and theoretical results also indicate that introduction of the olefinic double bond hinders not only the stabilization of the TICT state, but also the solvent assisted proton transfer process. The *trans-cis* photoisomerization competes with the fluorescence process in both nonpolar and polar solvents. Reasonably very high fluorescence quantum yield obtained in glycerol is due to hindrance of isomerization by the restricted twisting motion of the olefinic double bond. The isomerization of *t*-DMASIP-b occurs via a nonadiabatic path. The irradiation experiments suggest that the photostationary state is solvent dependent and further studies are required to understand the solvent dependence of photoisomerization. Temperature effect studies reveal that upon increase in temperature the quantum yield decreases due to increase in the competing nonradiative processes. The effect of introduction of olefinic double bond affects the prototropic equilibrium also. Unlike in DMAPIP-b, in *t*-DMASIP-b protonation takes place at imidazole nitrogen (MC2) and pyridyl nitrogen (MC3).

Chapter 5

Spectral characteristics of 2-(4′-*N*,*N*-dimethylaminophenyl)imidazo[4,5-b]pyridine in aerosol OT reverse micelle

5.0. Introduction

Surfactant molecules, dissolved in nonpolar solvents in the presence of water form aggregates known as reverse micelle.[234-236] It is spherical in shape and the arrangement of the polar head group and nonpolar tail are opposite to that of micelle. In reverse micelle the hydrophilic head group projects towards the core whereas the hydrophobic chain projects towards the nonpolar oil phase (**Figure 5.1**). Hence, reverse micelle is also known as inverted micelle. The size of a reverse micelle is measured in terms of molar ratio of added water to surfactant (w_0 = [water]/[surfactant]). Upon increasing the w_0 value the polarity as well as the average aggregation number of the surfactant increases whereas the microviscosity of the solubilized water decreases. It is reported in literature that in aerosol OT (AOT)/*n*-heptane/water reverse micelle, the radius of water nanopool is approximately $2w_0$.[237,238] In reverse micelles, the water nanopool exists in two different forms, bound water and free water. In the water nanopool the peripheral water surrounded by the polar head group is known as bound water or confined water, whereas the water molecule present at the central position or inner core remains apart from the polar head group, known as free water.[238,239] The properties of bound water and free water are different from bulk water. The confined water pool mimics water inside protein, biomembranes, enzymes etc.[240-242] This is due to the presence of localized charged boundaries surrounding the confined water. Hence reverse micelles are one of the rudimentary models of such confined water.[243-246]

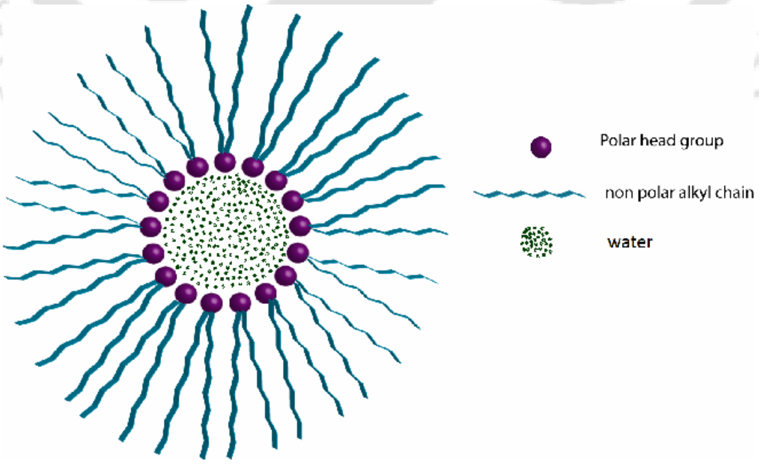

Figure 5.1. Structure of reverse micelle

Reverse micelles are also widely used to modulate the photophysics of the fluorophores. To get a broad idea on the effect of the surfactant-water interaction on the structure and dynamics of the encapsulated water molecules, the effect of reverse micelles is extensively studied.[247-257] The spectral characteristics of ICT molecules are also widely studied in reverse micelles[97-105,258-262] which serve as models for biological membrane. Study of *p*-*N*,*N*-dimethylaminobenzoic acid in cationic CTAB reverse micelle and anionic AOT reverse micelle suggests that the molecule remains at the reverse micelle-water pool interface with its diemethylamino group resides near the hydrocarbon chains and the carboxylic group reside near the polar head group and interacts electrostatically.[260,261] The ICT emission of *p*-*N*,*N*-dimethylaminobenzoic acid in AOT reverse micelle was found to be weaker than that obtained in CTAB reverse micelle. The lifetime of 1-anilino-8-napthalenesulfonate in AOT reverse micelle was found to be longer than that in bulk aqueous medium.[262] In AOT reverse micelle, the ICT emission of *p*-*N*,*N*-dimethylaminobenzoic acid is less than that of DMABN.[102] This was attributed due to the increase in the nonradiative rate from the hydrogen-bonded ICT complex of *p*-*N*,*N*-dimethylaminobenzoic acid. The ICT process of nile red is reduced due to lower polarity of the reverse micellar water pool.[100]

Proton transfer exhibiting molecules are also widely studied in the reverse micellar environment.[263-266] Double proton-transfer reaction between the 7-hydroxyquinoline and water molecule is studied in the AOT reverse micellar enviornment.[244] The excited state intramolecular proton transfer (ESIPT) in AOT reverse micelle was controlled by core solvents.[267] In the presence of aprotic solvent such as acetonitrile, the intermolecular hydrogen bonding of 3-hydroxyflavone-AOT complex become more prominent that reduced the ESIPT. However in the presence of protic solvent like methanol or water, extensive solvation of the AOT head group takes place, thus the intermolecular hydrogen bond between 3-hydroxyflavone and AOT is disrupted, resulting enhancement of the ESIPT process.[268] The rate of proton transfer from the photoacid 8-hydroxy-1,3,6-pyrenetrisulfonic acid to water was found to depend on the size of the reverse micelle.[269]

Among the reverse micelles, AOT reverse micelle is most widely used as it can solubilize more water. As mentioned in the previous chapter, the longer wavelength emission of DMAPIP-b is due to double proton transfer induced charge transfer process which requires assistance of protic solvent molecule. Both proton transfer and ICT process strongly depend on the nature of the protic solvents. Since the water pool in reverse micelle is different from bulk water, it is interesting to study this proton transfer induced charge transfer process in reverse micelle. Therefore, the photophysics of DMAPIP-b is explored in the most common AOT/*n*-heptane/water reverse micelle to find how confined water affects the proton transfer induced charge transfer process of DMAPIP-b. Such a study will also be useful to understand the properties of confined water in biological system.

5.1. Absorption spectra

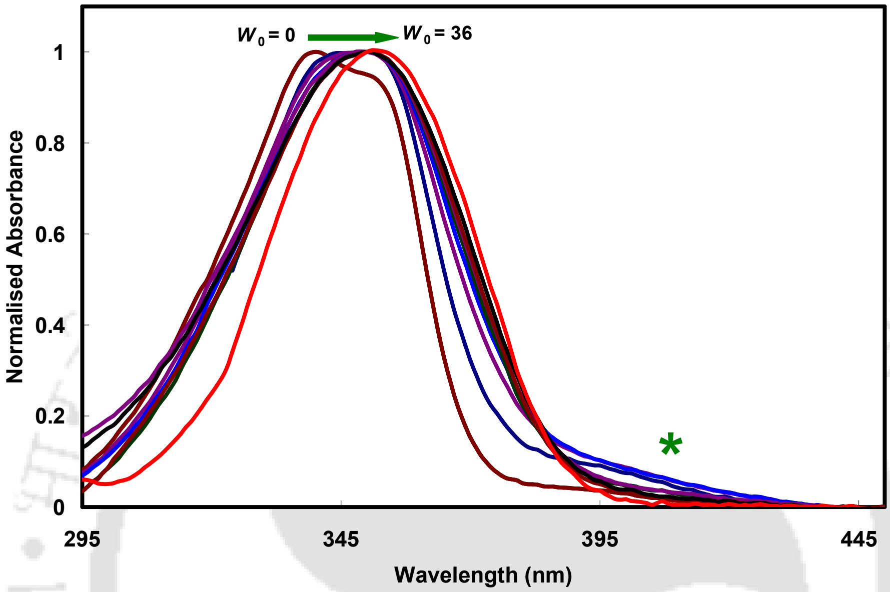

Figure 5.2. Normalised absorption spectra of DMAPIP-b in AOT (0.1 M)/*n*-heptane as a function of added water (w_0).

The anionic reverse micelle is formed by adding water to the surfactant AOT solution in *n*-heptane. **Figure 5.2** shows the absorption spectra of DMAPIP-b in AOT reverse micelle as a function of w_0 and the data are compiled in **Table 5.1**. It is observed that at $w_0 = 0$ the absorption spectrum is structured and upon increasing the w_0 values it becomes structure less with a bathochromic shift from 339 nm to 352 nm (**Figure 5.2**). This indicates the interaction of the dye molecule with the environment and it makes the system more stable. In addition to the main band at 339 nm, a band emerges near 400 nm (marked as * in **Figure 5.2**). The absorbance of the 400 nm band increases with initial addition of water and reaches the maximum at $w_0 = 6.2$. With further increase in water amount, its absorbance reduces and at higher w_0 value the band is not observed. From these results it may be concluded that at lower water content a species is present in addition to the neutral form of DMAPIP-b. The decrease in absorbance of the 400 nm band with increase in w_0 value specifies that the species absorbing at 400 nm is affected by the increase in size of the water nanopool.

Table 5.1: Absorption maxima (λ_{max}^{ab}, nm), emission maxima (λ_{max}^{em}, nm), and fluorescence lifetime (τ, ns) of DMAPIP-b in AOT reverse micelle at various w_0.

w_0	λ_{max}^{ab}	λ_{max}^{em}	λ_{em} = 400 nm		λ_{em} = 515 nm	
			τ	χ^2	τ	χ^2
0	339, 351	382	1.13 (59.1) 1.64 (40.9)	1.08	1.74 (48.7) 2.56 (51.3)	1.03
1.8	339, 351	389	0.96 (65.2) 1.53 (34.8)	1.18	0.80 (16.3) 2.27 (83.7)	1.00
3.1	343, 351	394	0.76 (69.7) 1.40 (30.3)	1.19	0.52 (9.4) 1.91 (90.6)	1.08
6.2	346, 351	403	0.57 (74.5) 1.07 (25.5)	1.09	1.32	1.12
8	348	408	0.51 (73.2) 0.95 (26.8)	1.09	0.57 (8.5) 1.26 (91.5)	1.14
12	351	413	0.47 (79.9) 0.88 (20.1)	0.9	0.90 (14.1) 1.10 (85.9)	1.07
15	351	415	0.46 (85.1) 0.90 (14.9)	0.97	0.77 (31.4) 1.14 (68.6)	1.09
18	351	418	0.43 (72.1) 0.71 (27.9)	0.95	0.59 (15.2) 1.04 (84.8)	1.13
24	352	420	0.41 (82.8) 0.79 (17.2)	1.05	0.76 (66.5) 1.29 (33.5)	1.23
36	352	421	0.41 (88.1) 0.88 (11.9)	1.01	0.77 (84.1) 1.62 (15.9)	1.13

5.2. Fluorescence spectra

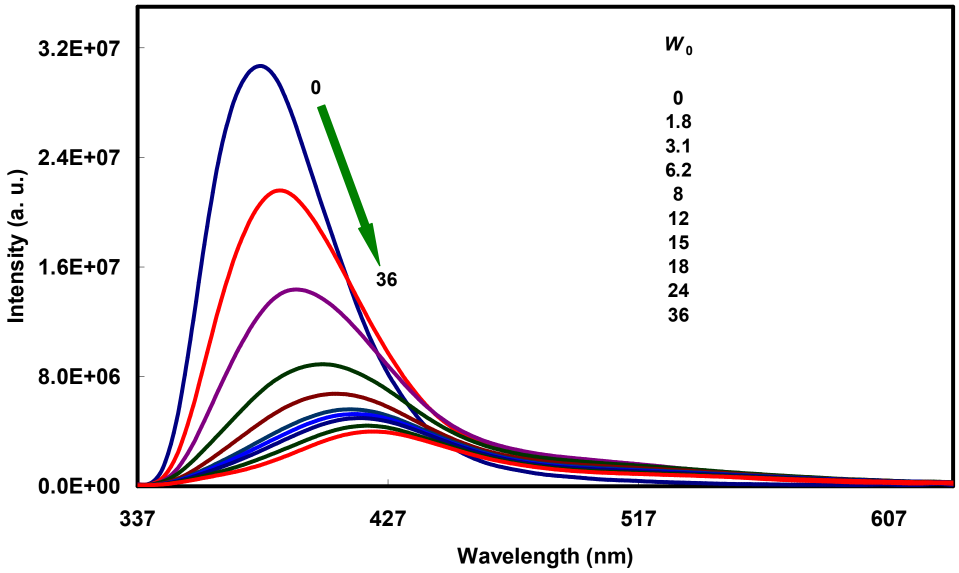

Figure 5.3. Fluorescence spectra of DMAPIP-b in AOT (0.1 M)/*n*-heptane as a function of added water (w_0) (λ_{exc} = 327 nm).

The emission spectra of DMAPIP-b in AOT reverse micelle at different w_0 are recorded by exciting at different wavelengths. The emission spectra at λ_{exc} = 327 nm is shown in **Figure 5.3**. It is found that at $w_0 = 0$, the band is appeared at 380 nm with a long tail. Upon increasing the water amount a bathocromic shift is observed. However upon increasing the size of water pool the fluorescence intensity decreases continuously and the effect is more significant up to $w_0 = 8$. Although the intensity decreases continuously with further increase in the pool size, the effect is very less significant in compared to initial addition of water. The red shift is also more pronounced for the initial increase in water pool size and is less for further additions. At $w_0 = 0$, there is a very less restriction on surfactant's rotational mobility present in the solution.[175,270] Upon continuously increasing the water amount, it becomes solubilized inside the core region and also the water pool size of the reverse micellar system increases. Thus the polarity of the medium increases upon increasing the w_0 value and hence causes the bathochromic shift of the spectra. Although no clear dual band is observed in the emission spectra only a long tail is present at the longer wavelength. Very small increase in fluorescence intensity is observed at the tail for initial additions of water in the reverse micellar system. On further increase in water content, the change in intensity is negligible, but the relative intensity at longer wavelength emission is enhanced. However, the longer wavelength emission with respect to the shorter wavelength emission is more prominent at lower water content upon exciting at longer wavelengths. The emission spectra obtained by exciting at 402 nm at different w_0 are shown in **Figure 5.4**.

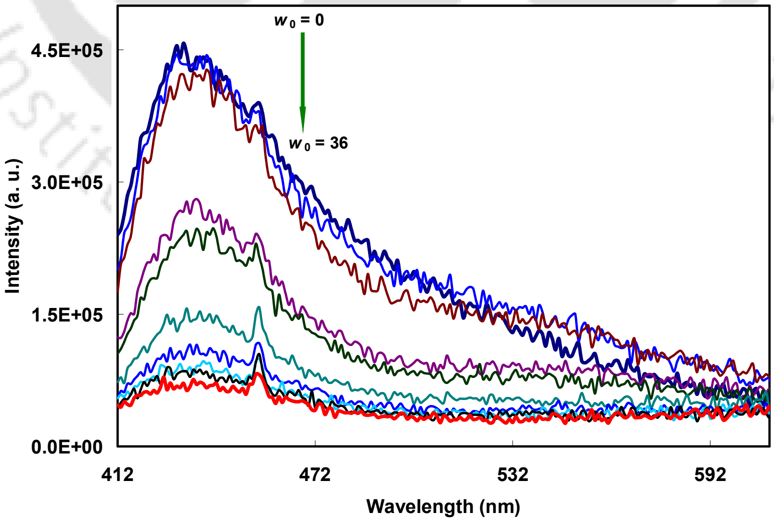

Figure 5.4. Fluorescence spectra of DMAPIP-b in AOT (0.1 M)/*n*-heptane as a function of added water (w_0) (λ_{exc} = 402 nm).

The excitation spectra recorded at different wavelengths have same features as those of the absorption spectra i.e. appearance of a band at 400 nm in addition to the main band. The 400 nm band is more prominent when monitored at 550 nm (**Figure 5.5**). The intensity of the band obtained at 400 nm increases up to w_0 = 3.1 and upon further increase of the water amount, the band intensity gradually diminishes.

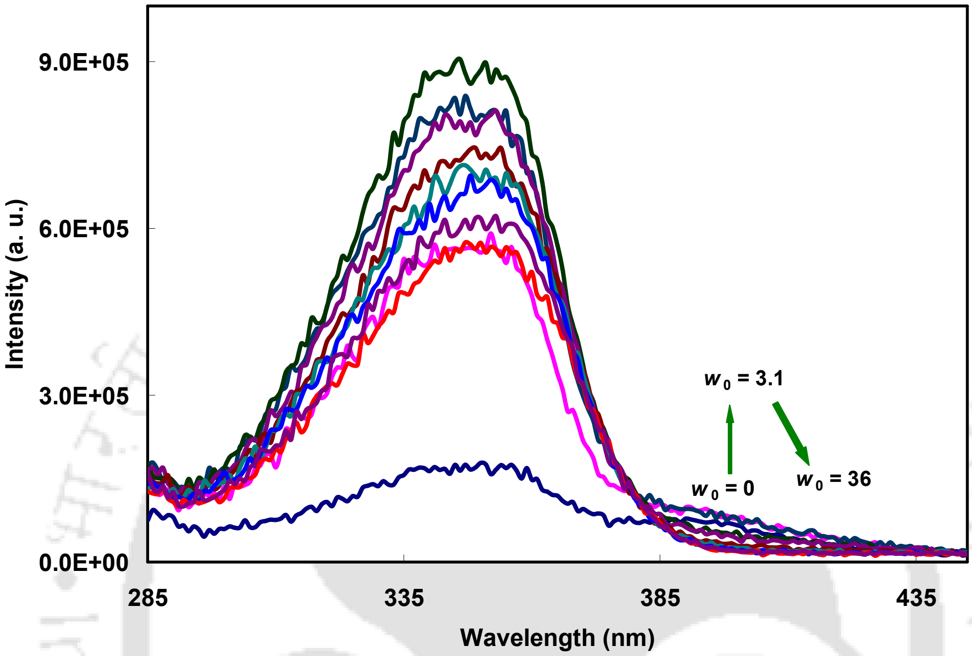

Figure 5.5. Excitation spectra (λ_{em} = 550 nm) of DMAPIP-b in AOT/*n*-heptane/ as a function of added water (w_0).

Bathochromic shifts are observed in the absorption and fluorescence spectra of DMAPIP-b upon protonation of ring nitrogen. According to pseudophase ion-exchange model,[175,85] the cations and the protons tend to concentrate near the polar head group of the anionic micelle. Since AOT is an anionic micelle, it is more facile to protonate the molecule at the micelle phase due to the presence of protons near the anionic head group. The pK_a value of DMAPIP-b in anionic micelle, SDS is found to be more than that in aqueous medium.[85] Therefore, the 400 nm band can be assigned to the formation of monocation by the protonation of ring nitrogen. The absorption maximum of the monocation of DMAPIP-b in aqueous medium is 386 nm.[82,85] The red shift observed in AOT reverse micelle is due to the presence of anionic polar head group present near the fluorophores. This stabilizes the monocations more by electrostatic interaction. Such interactions between the anionic head groups of the micelles and the monocations of DMAPIP-b were observed in anionic SDS micelle. The band maximum observed at 394 nm for the monocationic form of DMAPIP-b in

SDS micelle is in close agreement with present band maximum. The formation of monocation even at $w_0 = 0$ suggests the presence of trace amount of water in AOT reverse micelle even before the initial addition of external water. This trace amount of water may be from the AOT or the hydrocarbons. Other groups also found the presence of trace amount of water droplet in AOT and presence of such water in trace amounts was indeed suggested as a prerequisite for the formation of aggregates in organic solvents.[271-275] The polarity of the reverse micelles increases with increase in water amount. Despite that, the intensity of the monocationic band decreases at higher water content shows the decrease in the relative population of monocation at higher water amount. One reason could be smaller dipole moment of the monocation formed by the protonation of imidazole nitrogen than the neutral form of DMAPIP-b.[83] Other reason is due to different location of the fluorophores (See **Section 5.4**).

To verify the presence of the TICT emission, the intensity ratio plot of the longer wavelength to shorter wavelength emission is constructed as a function of w_0 (**Figure 5.6**). From the plot it is clear that upon increasing the water content (w_0) the intensity ratio increases. Although protonation takes place at lower amount of water, the rate decreases at higher quantity of water. Nevertheless, the relative intensity of the longer wavelength emission increases with increase in w_0, even after complete shrinking of monocatonic band. Therefore, it is clear that DMAPIP-b emits from TICT state also. The lifetime data further supports the occurrence of TICT emission in AOT reverse micelle (see later).

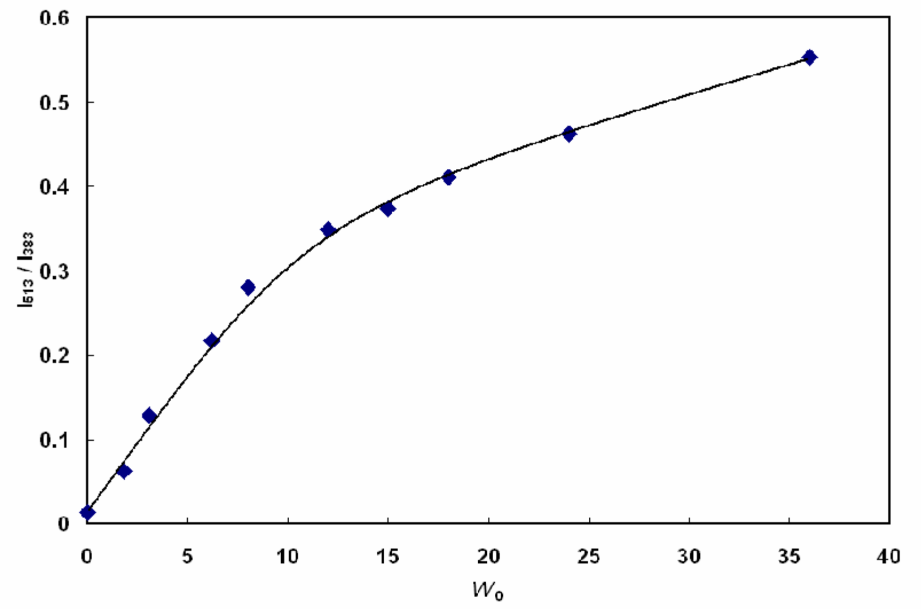

Figure 5.6. The intensity ratio of longer wavelength to shorter wavelength emission in AOT/*n*-heptane as a function of added water (w_0).

5.3. Quantum yield and lifetime

The variation of quantum yields with w_0 values are plotted in **Figure 5.7** (the refractive indices for AOT reverse micelle at different w_0 values are interpolated using the literature[276] values). With increase in water content there is a very sharp decrease in quantum yield of the shorter wavelength emission. But the longer wavelength emission is affected less with variation in water content. The sharp decrease in quantum yield indicates that the environment of the fluorophore is changing upon increasing the size of the water nanopool.

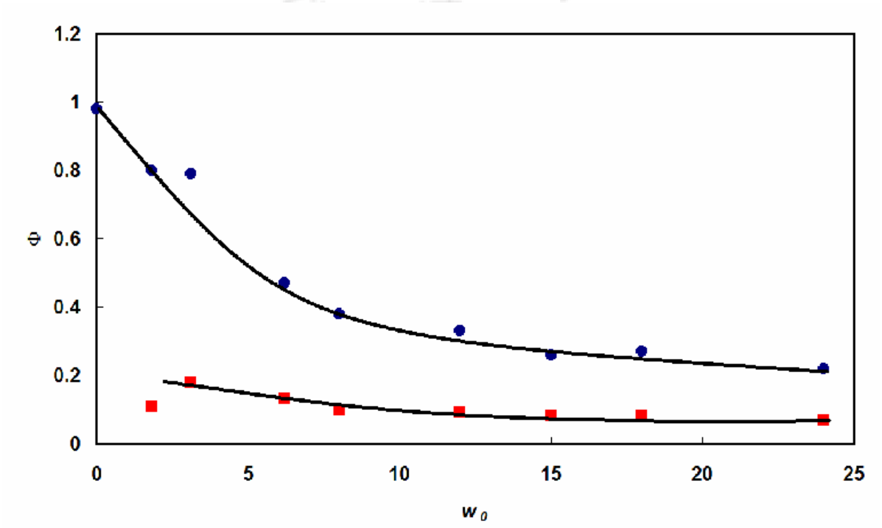

Figure 5.7. Plot of quantum yield (Φ) as a function of w_0 (● and ■ indicate the quantum yield of the normal and the TICT bands respectively, the error in calculation of quantum yield is upto 10%).

Fluorescence lifetime is a very good method to explore the position of the molecule inside the reverse micellar environment.[192,277-280] The lifetime data monitoring at two different wavelengths (400 nm and 515 nm) are compiled in **Table 5.1**. Monitoring at the shorter wavelength band maximum, two different lifetimes observed in all the solutions. The lifetime of both components are shortened upon increasing the water content. Upon monitoring at the longer wavelength (515 nm), it is observed that the lifetime as well as the relative amplitude of the shorter lifetime component decreases up to w_0 = 3.1 and at w_0 = 6.2, the lifetime for the shorter lifetime component is not at all observed. Further addition of water results in biexponenital decay again. From the result it is inferred that from the beginning the shorter lifetime arises due to the monocation and the other lifetime is due to the normal emission. Decrease in relative amplitude of the shorter component indicates that the cationic form gradually decreases and is not observed at w_0 = 6.2. Further addition of water gives dual emission, which arises from the TICT state and the locally excited state.

5.4. Location of the fluorophore

The fluorophore can locate in reverse micelle in any of the three regions; organic phase, micellar phase or water nanopool. The location of the fluorophore depends on factors such as structure of the micelle, water content in the solution and micropolarity. From the absorption and fluorescence spectral characteristics it can be inferred that the microenvironment around DMAPIP-b is changed with the addition of water content. This observation indicates that water is accessible to the fluorophore and suggests that the molecule resides either in the water nanopool or the micellar phase near the water pool. The fluorescence quantum yield of DMAPIP-b decreases steeply up to $w_0 = 6.2$ and upon further addition of water, it gradually decreases in the microemulsion (**Figure 5.5**). It is reported that the fluorescence quantum yield for the normal emission decreases steeply for the initial addition of water when the molecule is present in the water pool of the reverse micelle.[270] All these facts indicate that DMAPIP-b is present in the surfactant-water interface in the bound water region of the reverse micelle and upon addition of water the fluorophore moves towards core of the water nanopool. This was substantiated by the presence of monocation at lower w_0 values and its absence at higher w_0 values. For initial addition of water only bound water is formed,[244] so the absorbance of the monocation band increases due to increase in proton concentration near the polar head group. Upon further addition of water, the pool size increases as a result free water starts to form. The fluorophore moved away from the polar head group towards the water pool and the monocation-neutral equilibrium shifted toward the neutral form. This was substantiated by the decrease in the absorbance at 400 nm with increase in water quantity in reverse micelle and the bathochromic shift of normal emission band. Similar bathochromic shifts were observed in other molecules also when they shift towards the free water pool.[259,281] The absence of monocation at higher w_0 suggests that the free water of the anionic reverse micelle is less acidic than the bound water.

The normal emission maximum in reverse micelles, are nearly 30 nm hypsochromically shifted than that in neat water (**Table 5.1**). This suggests that polarity of the water in nanopool of the reverse micelle is less than that of bulk water and is same as that of methanol-water mixture.

It is well known from the literature[82,83,85,205-208,270] and also explained in earlier chapters that protonation and/or hydrogen bond formation at dimethylamino nitrogen results blue shift of the spectra and that of ring nitrogens causes red shift. Both absorption and fluorescence spectra of DMAPIP-b are bathochromically shifted in AOT reverse micelles with increase in w_0 value. Thus, it can be inferred that ring nitrogens are involved in hydrogen bonding. It is also found that in cyclodextrin[83] and normal micelle,[85] the dimethylamino group of DMAPIP-b was oriented towards the hydrophobic region and the imidazopyridine ring prefers the hydrophilic region. Similar orientation is expected in AOT reverse micelle at lower w_0 values, where the imidazopyridine ring resides near the polar head group and water and the dimethylamino group projects towards the hydrophobic chain in the nonpolar solvent. However, at higher w_0 value, the fluorophore is fully entrapped in the water nanopool as the size increases. As mentioned earlier, DMAPIP-b acts as an inhibitor for aurora kinases.[159] It is reported that the pyridyl nitrogen and imidazole >NH group play an important role in the binding interaction with aurora-A kinase through hydrogen bonding. Moreover, as mentioned in **Chapter 3**, the hydrogen bonding of the protic solvents with pyridyl nitrogen and imidazole >NH are crucial for TICT emission. The observation of TICT emission shows that in confined water also, hydrogen bonding takes place. Thus, alike in neat protic solvent, in confined water also double proton transfer followed by charge transfer takes place.

5.5. Conclusion

In AOT/*n*-heptane/water reverse micelle DMAPIP-b exists both in neutral and monocationic form at lower w_0 values and resides in the micellar phase near the polar head group. The presence of two forms depends upon the size of the water pool. Upon addition of water, the fluorophore shifts towards the core and at large pool size the neutral-monocation equilibrium shifts towards neutral form. At higher w_0, DMAPIP-b present only in neutral form. This suggests that the bound water of the AOT reverse micelle is more acidic than the free water. Although, the polarity of the reverse micelle increases with increase in w_0, even at $w_0 = 36$, the polarity of the confined water in nanopool is less than that of bulk water and is same as that of methanol-water mixture. DMAPIP-b emits dual emission in reverse micelle due to double proton transfer induced TICT emission. Both normal and TICT emission are quenched by water.

Chapter 6

Interactions of a few dimethylaminophenyl substituted azoles with bovine serum albumin: role of heteroatoms

6.0. Introduction

Serum albumins are globular proteins found abundant in plasma.[168,282,283] They bind to a variety of bioactive molecules by hydrophobic, hydrophilic and ionic interactions which help them to carry steroids, fatty acids and thyroid hormones. Among them BSA is the most studied model protein because of its easy availability and structural homology with human serum albumin.[284] BSA is a heart shape protein (**Figure 6.1**). The tertiary structure of BSA has three domains I, II and III, each domain is divided into two sub domains IA, IB; IIA, IIB and IIIA, IIIB respectively. Site-I is situated in the hydrophobic core of sub domain IIA, whereas site-II is situated near the sub domain IIIA.[168,285] The specific physiological activity of the ligands upon binding with serum albumin originates from the presence of two major and structurally selective binding sites, namely site-I and site-II and site-I is influenced by strong hydrophobic interactions whereas site-II involves hydrophobic, hydrogen bonding and electrostatic interactions.[286] Besides these structural demarcations, BSA has two tryptophan units namely Trp-158 and Trp-237. Trp-158 residue is located in the hydrophilic subdomain IB near the surface of the albumin molecule, thus subdomain IB is exposed to solvent environment. Trp-237 is located deep in the hydrophobic cavity of subdomain IIA.

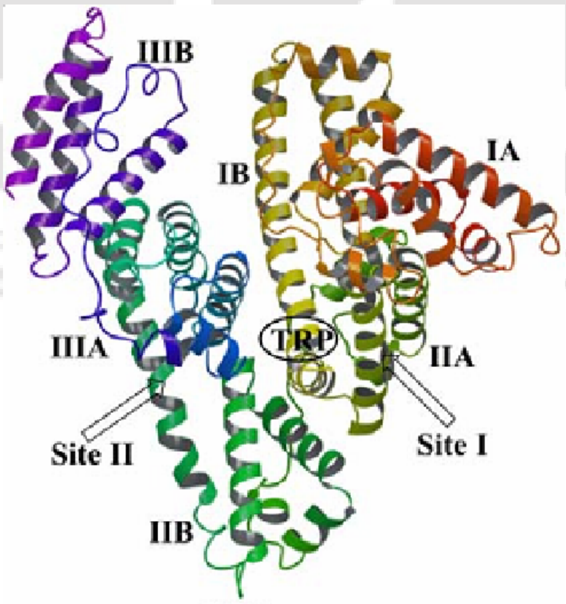

Figure 6.1. Structure of BSA protein.

Studies on interactions of small organic molecules with BSA have attracted much attention for understanding many biological systems as well as immobilization of proteins. Such studies can provide useful information about locations and characteristics of different binding sites. Therefore, these investigations attracted many researchers to employ, fluorescence spectroscopy using solvent polarity sensitive fluorescence probes to understand / study these proteins.[109,287-298] Easily handled fluorescent probes showed high spectral response to the changes in the polarity of their local surroundings and one such situation arises when they bind to BSA. Such studies also give crucial information about ligand-protein interactions which will have significant importance in pharmacology and drug discovery.

The environment inside the proteins are quite different from that of the bulk medium. The polarity, viscosity and hydrogen bonding capacity inside the protein are completely different. Thus, studying the interaction of proteins with the ligand molecules is an interesting research area. Few studies on the interactions of ICT fluorophores with serum albumin are reported in literature.[110,299-301] Studies on series of rigid and flexible dipolar molecules demonstrated that the enhancement in fluorescence of the flexible systems is more than the rigid system due to reduction in the internal motion of the flexible systems.[295] The interaction between few pyrrolizine derivatives and BSA were investigated.[302] The study revealed that the substituents on the benzene ring influence the binding affinity of pyrrolizine derivatives with BSA. Recent studies indicate that the presence and position of long alkyl chain on the ligand strongly affects the interaction of ligand with BSA.[160]

Benzimidazoles and benzoxazoles are very important class of molecules having wide application in medicinal chemistry. Numerous reports are available on the pharmaceutical importance of these azole derivatives. For example some 2-[(benzotriazol-1/2-yl)methyl]benzimidazoles and 2-arylbenzimidazoles are reported to act as antiviral and antiproliferative.[303-306] Niewiadomy et al. developed some biologically active benzimidazole deivatives and established the cytotoxicity in vitro against the four human cancer cell lines namely rectal, bladder, lung and breast.[307] Some benzimidazole sugar conjugates show anti-inflammatory and analgesic activities.[308] Benzoxazole derivative, 1,3-benzoxazole-4-carbonitirle acts as a support for β-1,6-glucan synthesis inhibitors with potent antifungal activity against candida species.[309] Some benzazole derivatives were found to have inhibition potential towards human cyclooxygenase-2 enzyme.[310] A new benzoxazole derivative was reported to act as anticancer and antichronic inflammatory agents and specific anti-breast cancer agent.[311] Oxazole derivatives are used as anti-inflammatories, analgesics, anti-pyretics and antagonists.[312-315] DMAPIP-b and some other pyridoimidazole derivatives act as inhibitor for aurora kinases.[159] Hence, it will be interesting to study the fundamental interactions between those benzazoles and proteins. Hence a comparative study of the interaction between ICT emitting ligands DMAPBI, DMAPBO and DMAPOP (**Chart 6.1**) with BSA were performed.

The spectral characteristics of DMAPBI and DMAPBO are reported in literature[206,207] and that of DMAPOP is discussed in **Section 3.1**. All ligands are highly sensitive to the environment. The interaction of BSA with DMAPIP-b was already studied using fluorescence technique.[160] Therefore, the interactions of BSA with DMAPBI, DMAPBO and DMAPOP are compared with that of DMAPIP-b. Since no molecular docking studies are carried out with any of these ligands including DMAPIP-b, the molecular docking studies are also performed with all four ligands for better understanding.

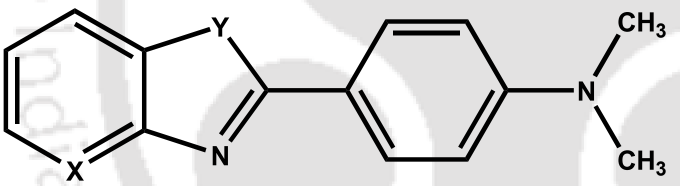

X = CH, Y = NH, DMAPBI
X = N, Y = NH, DMAPIP-b
X = CH, Y = O, DMAPBO
X = N, Y = O, DMAPOP

Chart 6.1. Structures of DMAPBI and analogous molecules.

6.1. Absorption spectra

Absorption spectra of DMAPBI, DMAPBO and DMAPOP are recorded in phosphate buffer of pH 7.0 at different concentrations of BSA (0-80 μM). The absorption spectra of DMAPBI, DMAPBO and DMAPOP show absorption band at 332 nm, 341 nm and 368 nm respectively. Although the effect of BSA on the absorption spectral maxima is very little in all three ligands, with increase in BSA concentration the absorbance of both DMAPBI and DMAPBO increases. On the other hand for initial additions of BSA till 22 μM a small decrease in absorbance is observed in the spectrum of DMAPOP, but the absorbance increases with further addition of BSA. The results suggest the presence of some interactions between BSA and the ligands.

6.2. Fluorescence spectra

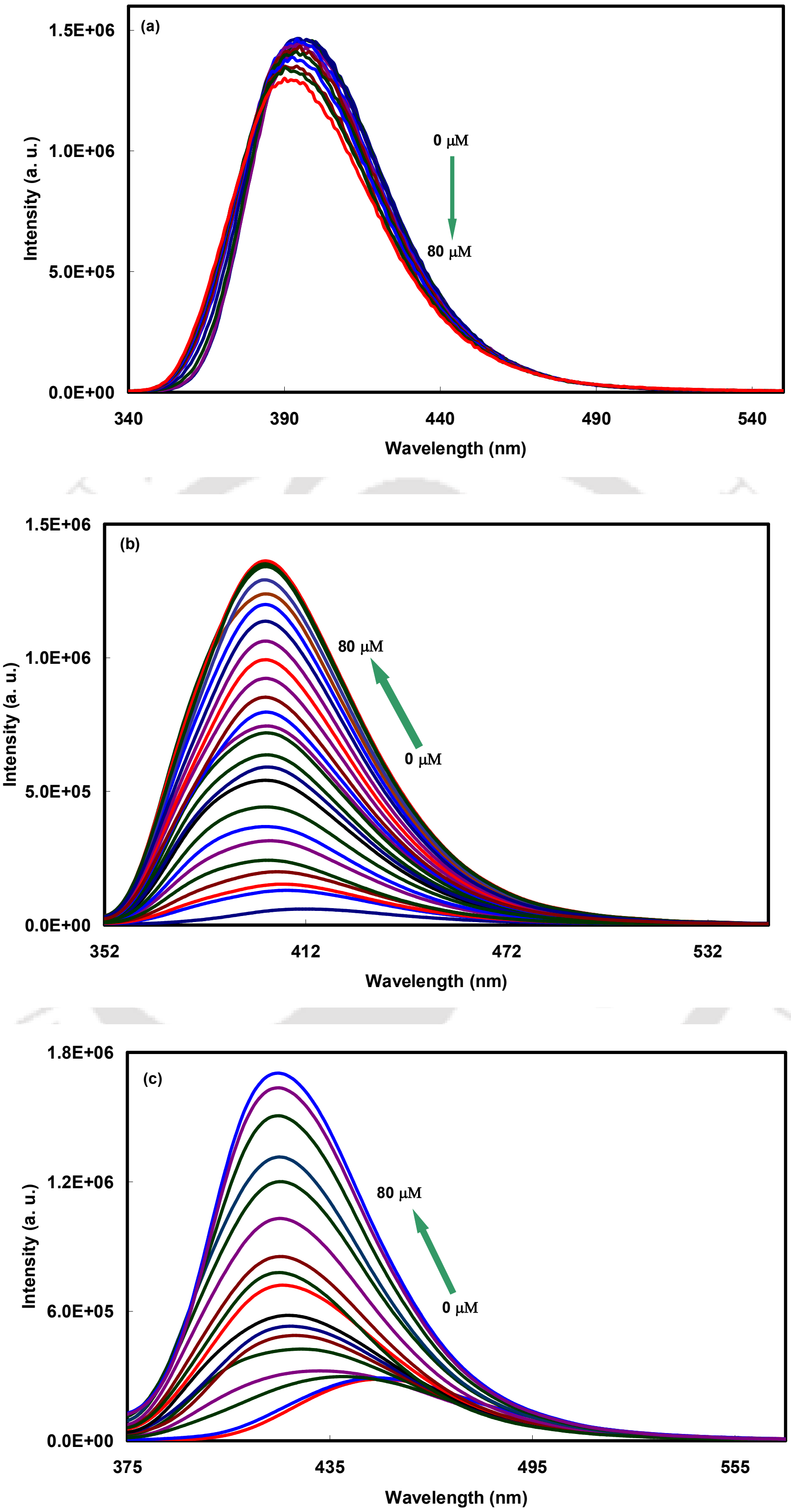

Figure 6.2. Emission spectra of the ligands as a function of BSA concentration: (a) DMAPBI (λ_{exc} = 330 nm), (b) DMAPBO (λ_{exc} = 342 nm) and (c) DMAPOP (λ_{exc} = 365 nm).

Since the fluorescence spectra are more sensitive than the absorption spectra, to investigate further the nature of interactions of these fluorophores and BSA, were investigated using the fluorescence technique. The effect of BSA on the fluorescence spectra of the ligands are depicted in **Figure 6.2**. In the absence of BSA, DMAPBI, DMAPBO and DMAPOP exhibit fluorescence bands at around 399 nm, 413 nm and 451 nm respectively (**Table 6.1**).

Table 6.1. Fluorescence band maxima (λ_{max}^{em}, nm) in absence and presence of BSA and spectral shift.

Flurophores	λ_{max}^{em}		Spectral shift (nm)
	In buffer	In BSA (80 μM)	
DMAPBI	399	392	7
DMAPBO	413	401	12
DMAPOP	451	420	31

Although in most cases, addition of BSA results in enhancement of fluorescence intensity. The fluorescence intensity of DMAPBI decreases with increase in concentration of BSA. On the other hand huge enhancement in intensities is observed in the fluorescence spectra of DMAPBO and DMAPOP with increase in concentration of BSA. But blue shifts are observed in the fluorescence spectra of all three ligands. As mentioned earlier that the emitting state of all three ligands have substantial amount of ICT character, upon increasing the polarity of the environment bathochromic shifts were observed in the fluorescence spectra of all these ligands.[206,207] The bathochromic shifts were observed due to stabilization of the ICT emitting state through dipolar and hydrogen bonding interactions. The observed hypsochromic shifts in the emission spectra of the ligands in presence of BSA indicate that the ligands are moving into hydrophobic environment from hydrophilic environment. The stronger stabilization of the ICT state by dipolar interaction decreases the energy gap between emitting state and low lying triplet state and/or ground state. By energy gap law decrease in energy gap increases the nonradiative decay. Therefore, all these ligands have weak emission in water due to stronger stabilization of ICT state. Upon moving from hydrophilic environment (water) to hydrophobic BSA, the dipolar interactions decrease which destabilize the ICT state. This increases the energy gap between ICT and low lying state. In other words, it is expected to reduce the nonradiative decay and increase the radiative emission. Thus, the fluorescence intensities of DMAPBO and DMAPOP increase in presence of BSA.

The decrease observed in the fluorescence intensity of DMAPBI with increase in concentration of BSA is unusual.

Two different factors affect the fluorescence intensity (i) the increase in the hydrophobicity of the environment (ii) hydrogen bonding with heteroatom. As reported in the literature and explained earlier that the increase in the hydrophobicity decreases the nonradiative decay in all these ligands. On the other hand, hydrogen bonding with heteroatoms quenches the fluorescence.[206] Inside BSA, these two factors are opposing each other. Since, DMAPIP-b, DMAPBO and DMAPOP are present much deeper inside the hydrophobic pocket as suggested by spectral shift, the enhancement of fluorescence intensity due to hydrophobicity predominates over the fluorescence quenching by hydrogen bonding. On the other hand, the environment of DMAPBI is less hydrophobic as suggested by the spectral shift, therefore quenching owing to hydrogen bonding dominates over the enhancement in fluorescence caused by the hydrophobicity. Further, the change in the fluorescence intensity of DMAPBI is much smaller compared to those of its analogues. The binding location predicted by docking studies also supports the hypothesis. The different orientation of DMAPBI in BSA compared to its analogues (see later) might also have a role in this difference in behaviour.

6.3. Binding constant

To investigate the extent of binding of different ligands with BSA, association constant or binding constants are calculated. The Benesi-Hildebrand plot was constructed for calculating the binding constant of DMAPBO and DMAPOP with BSA using the following equation.[316]

$$1/\left(I-I_0\right)= 1/\{(I_\infty-I_0)K\left[BSA\right]\} + 1/(I_\infty-I_0) \qquad \textbf{(6.1)}$$

where I_0 and I are the intensity of the fluorophores in the absence and presence of BSA, respectively. I_∞ is the fluorescence intensity when all the guest molecules are complexed. K is the binding constant. The plot for DMAPOP is shown as representative (**Figure 6.3**).

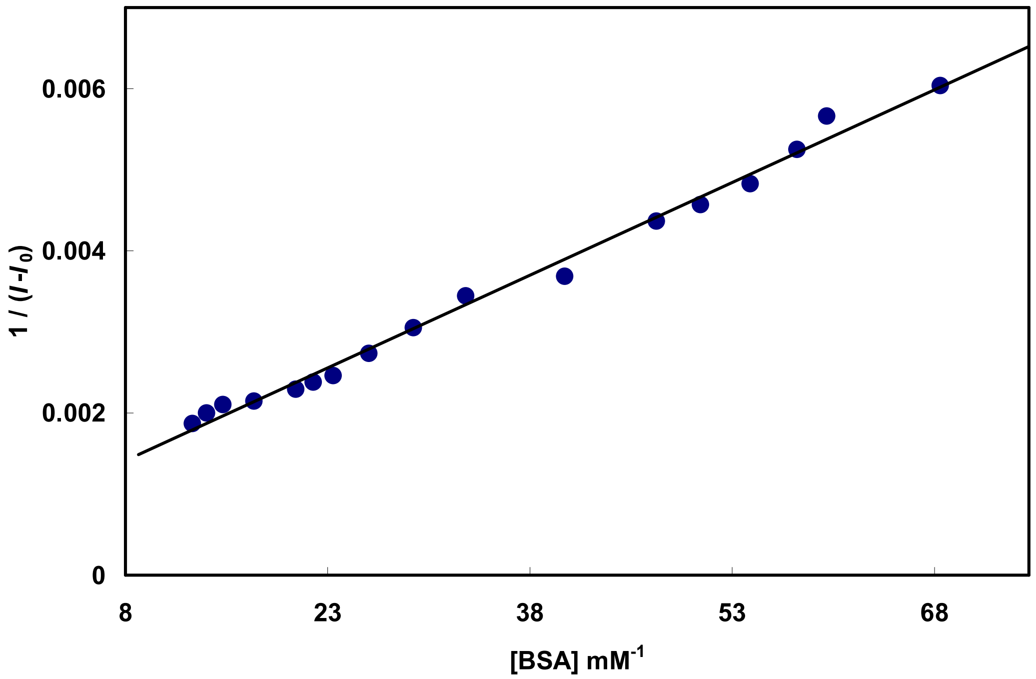

Figure 6.3. Benesi-Hildebrand plot for DMAPOP.

Since, the fluorescence intensity of DMAPBI decreases with increase in BSA concentration, following equation is used to calculate the binding constant.[193]

$$\frac{I_0}{I} = 1 + K_s[Q] \qquad \textbf{(6.2)}$$

The plot thus obtained is shown in **Figure 6.4** and the binding constants obtained for all three molecules are tabulated along with that of DMAPIP-b (**Table 6.2**).

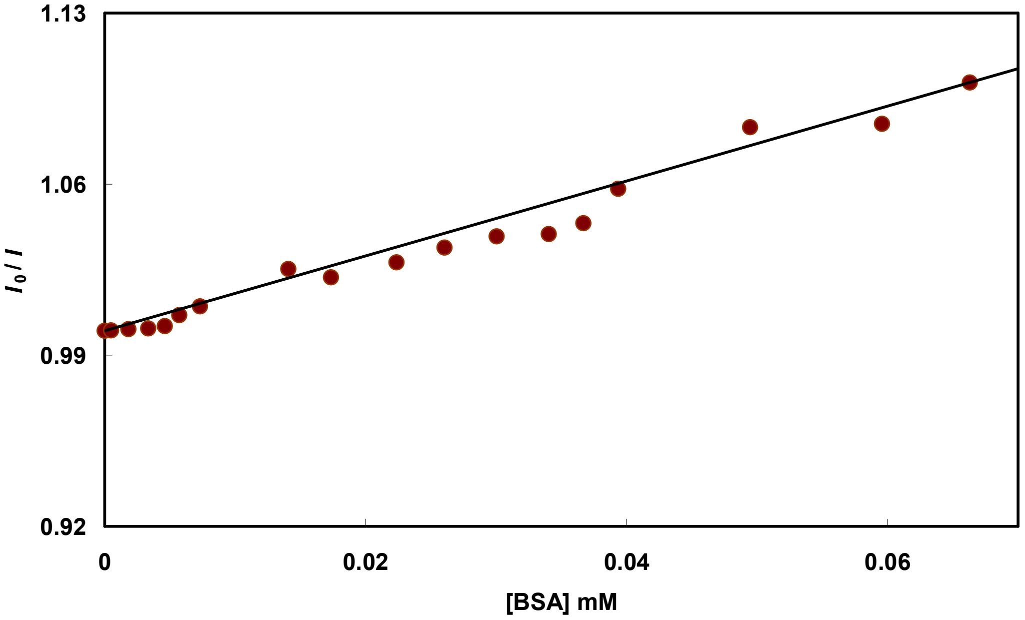

Figure 6.4. The binding constant plot for DMAPBI.

Table 6.2. The binding constant of ligands with BSA.

Molecules	Binding constant (*K*, M^{-1})
DMAPBI	1.5×10^3
DMAPIP-b[a]	4.3×10^3
DMAPBO	7.5×10^3
DMAPOP	13×10^3

[a] The binding constant value was taken from ref 160 for comparison purpose

The binding constants reveal that the oxazoles have stronger binding affinity than the imidazoles (**Table 6.2**). The presence of extra nitrogen in the heterocyclic ring enhanced the binding affinity. The binding constant of DMAPOP is ~ 2 times more than that of DMAPBO and that of DMAPIP-b is ~ 3 times more than that of DMAPBI. On the other hand, DMAPBO binds 5 times more stronger than DMAPBI and DMAPOP binds ~ 3 times more stronger than DMAPIP-b.

6.4. Molecular docking study

To understand more on molecular binding, docking studies were carried out. As docking studies of DMAPIP-b were not performed earlier; therefore, those were also performed and compared with the other molecules. It is well known that when the molecules bind at hydrophilic pockets of proteins no spectral shift were observed in the fluorescence spectra.[160,295] On the other hand, blue shifts are observed when molecules enter the hydrophobic pocket of proteins.[160,295] The fluorescence studies clearly indicate the ligands are in the hydrophobic environment (**Section 6.2**). This was substantiated by docking studies (**Figure 6.5**).

It is observed that in DMAPBI, the dimethylamino group projects towards the hydrophobic core whereas in other three molecules, the projection is opposite to that of DMAPBI (**Figure 6.5**). This difference in orientations can be explained as follow. It is reported in the literatures, both DMAPBI and DMAPIP-b form inclusion complexes with β-CD.[208,83] In both inclusion complexes, the dimethylaminophenyl group was present inside the hydrophobic basket and the heterocyclic ring was present outside the β-CD nanocavity. The azole nitrogen was located near the rim and forms hydrogen bond with rim hydroxyl group of the host and/or water present near the rim. Thus, it is clear that the dimethylaminophenyl prefers the hydrophobic environment and heterocyclic ring prefers the hydrogen bonding environment. Therefore, it is no surprise that the dimethylaminophenyl ring of DMAPBI is present inside the protein cavity and the heterocyclic ring is projected outside (**Figure 6.5a**). BSA is a protein consists of the amino acid residues, unlike in β-CD cavity hydrogen bond formation can take place inside the protein cavity also. DMAPBI has only one basic center (azole nitrogen) in its heterocyclic ring to accept the hydrogen bond. On the other hand, DMAPIP-b has one extra heteroatom, pyridyl nitrogen which also forms hydrogen bond with amino acid residue. This stabilizes the presence of heterocyclic ring inside the cavity, in other word the opposite fashion of orientation of the ligand in BSA (**Figure 6.5b**). DMAPBO is also orientated with heterocyclic ring inside and dimethylaminophenyl group outside (**Figure 6.5c**). But unlike DMAPIP-b no extra pyridyl nitrogen is present in DMAPBO, but the >NH group of DMAPBI is replaced by –O–. The more electronegative oxygen forms stronger hydrogen bond than nitrogen (see later), this might have given the extra stabilization for the presence of heterocyclic ring inside in the BSA cavity. Same orientation of DMAPOP is consistent with the argument of DMAPOP and DMAPIP-b which has both oxygen atom and pyridyl nitrogen (**Figure 6.5d**).

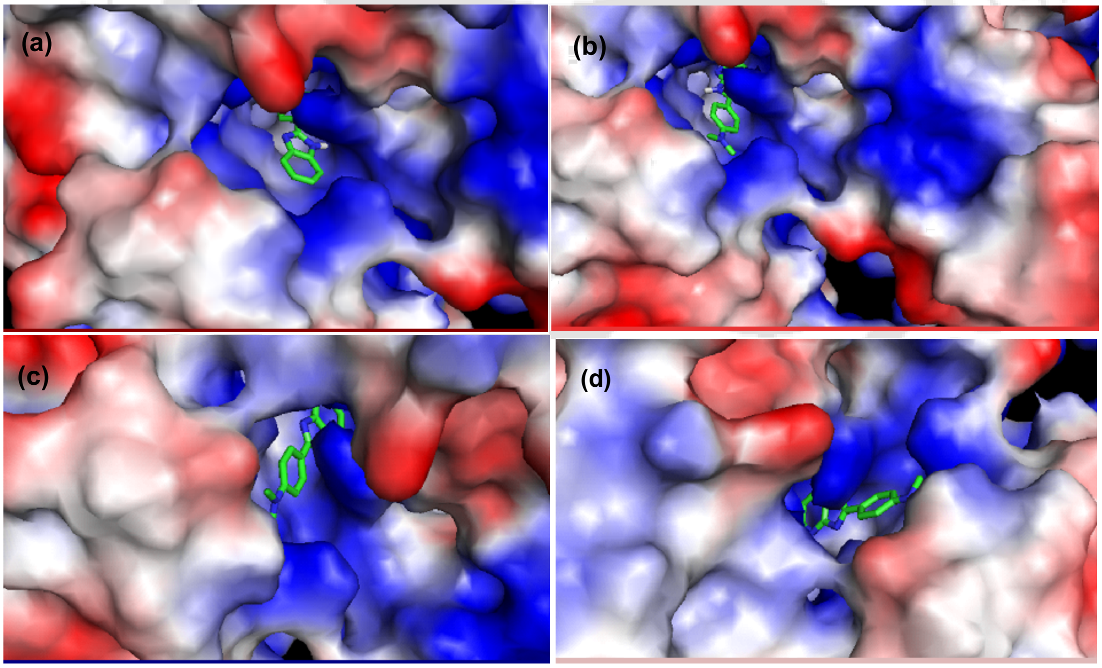

Figure 6.5. Docking pose of (a) DMAPBI, (b) DMAPIP-b, (c) DMAPBO and (d) DMAPOP with BSA.

The ligands interact with hydrophobic and polar amino acid residues via hydrogen bonding and van der Waals interaction. DMAPBI resides at the site containing the residues Arg-218, Tyr-475, Asp-474, Leu-221, Arg-222, Trp-237, Ser-225 etc. within 4 Å distance (**Figure 6.6a**).

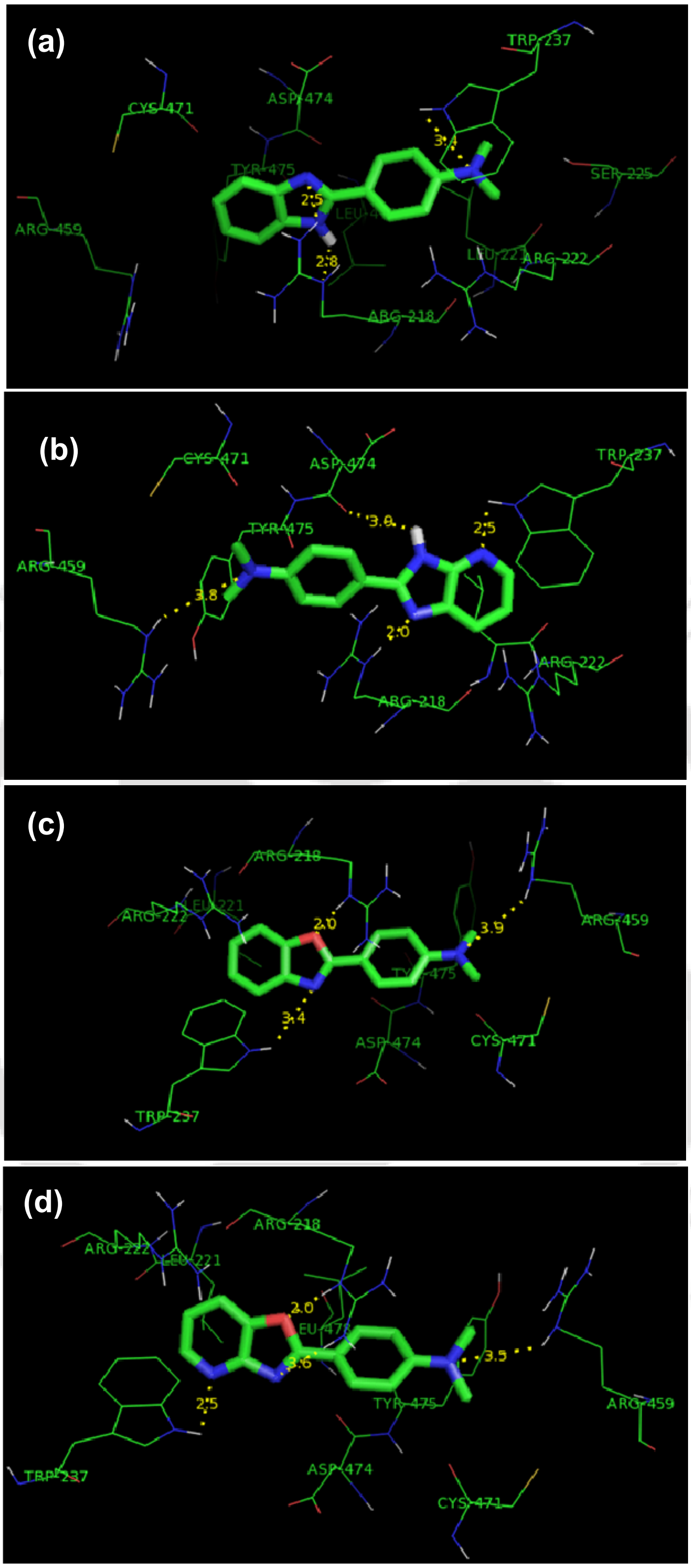

Figure 6.6. Molecular docking analysis results: amino acid residues surrounding the ligands within 4 Å distance: (a) DMAPBI, (b) DMAPIP-b (c) DMAPBO and (d) DMAPOP.

DMAPIP-b resides near Arg-218, Trp-237, Asp-457 and Arg-459 etc (**Figure 6.6b**). DMAPBO resides at the site containing the residues Arg-218, Arg-459, Arg-222, Asp-474, Tyr-475, Trp-237 and Cys-471 etc (**Figure 6.6c**). Similarly DMAPOP resides at the site containing the residues Trp-237, Arg-218, Arg-459, Leu-475, Asp-474 and Cys-471 etc within 4 Å distance from the ligands (**Figure 6.6d**). DMAPBI forms one hydrogen bond with polar Arg-218 residue through the azole nitrogen (2.5 Å, **Figure 6.6a**). On the other hand, DMAPIP-b forms two hydrogen bonds one with polar residue Arg-218 through the imidazole nitrogen (2 Å) and another one with the hydrophobic residue Trp-237 via the pyridyl nitrogen (2.5 Å, **Figure 6.6b**). Alike DMAPBI, DMAPBO forms one hydrogen bond with the polar Arg-218 residue; however the distance is shorter than that of DMAPBI. The hydrogen bond formation takes place via azole oxygen (2 Å, **Figure 6.6c**). Alike DMAPIP-b, DMAPOP forms two hydrogen bonds one with polar residue Arg-218 through the oxygen atom of azole ring (2 Å) and another one with the hydrophobic residue Trp-237 with the pyridyl nitrogen (2.5 Å, **Figure 6.6d**). From the results it can be inferred that BSA acts as hydrogen bond donor and the ligands acts as hydrogen bond acceptor and oxygen forms stronger hydrogen bond than nitrogen. DMAPOP and DMAPIP-b enter more deeply into the hydrophobic pocket of BSA as it forms hydrogen bond with Trp-237 residue which is present in the hydrophobic pocket of BSA and other two ligands are not forming the hydrogen bond with the Trp-237 unit. This result agrees well with the experimental result of higher spectral shift in DMAPIP-b[160] and DMAPOP (**Table 6.1**).

Table 6.3. Change in free energy ΔG (kcal/mol) and other energies obtained from docking studies (kcal/mol). The data obtained from the experiments are included in the parenthesis.

Molecules	ΔG	$E_{intermolecular}$	$E_{internal}$	$E_{torsional}$
DMAPBI	-5.30 (-4.26)	-5.90	-0.25	0.6
DMAPIP-b	-5.38 (-4.95)[a]	-5.97	-0.24	0.6
DMAPBO	-5.65 (-5.28)	-6.25	-0.28	0.6
DMAPOP	-5.77 (-5.45)	-6.37	-0.26	0.6

[a] Ref. 160

The different energies obtained from the docking study of protein-ligand interactions are presented in **Table 6.3**. The intermolecular energy ($E_{intermolecular}$) is the energy obtained by interaction of the ligand with the protein in the docked compounds. It is directly proportional to the change in free energy of binding. The internal energy ($E_{internal}$) of the ligand is defined as the sum of internal van der Waals and electrostatic energy. Torsional energy ($E_{torsional}$) mainly depends on the number of flexible bonds present in the ligand. Since the flexible bonds (number of torsions) are same for all four molecules the torsional energies obtained in all the cases are same. The intermolecular energy and torsional energy combined together results the free energy of binding. As the torsional energy is same for all molecules, thus the difference in binding energies arises from the difference in the intermolecular energy. Thus, from the data obtained, it can be depicted that among the four molecules, the binding interaction is maximum for DMAPOP and is minimum for DMAPBI (**Table 6.3**). The change in free energy obtained from experiment is also in good agreement with the predicted energy. Thus both from experimental and docking studies, it is inferred that the strength of ligand protein interaction follows the order DMAPOP > DMAPBO > DMAPIP-b > DMAPBI.

6.5. Conclusion

The interaction of BSA with DMAPBI, DMAPBO and DMAPOP was investigated and compared with DMAPIP-b. The docking studies were performed for all four ligand molecules. The fluorescence intensity of DMAPBI decreases in BSA. On the other hand, enormous increases in fluorescence intensities are observed in those of DMAPBO and DMAPOP in BSA. This difference is mainly due to difference in the binding locations of the ligands and orientation in binding location. The hypsochromic shift in the fluorescence spectra of all four ligands suggests that these ligands bind in the hydrophobic pocket of BSA. From the study, it is inferred that the replacement of imidazole >NH group by oxygen atom increases the binding ability of the fluorophore with BSA due to increase in hydrogen bond accepting ability of the oxygen. Replacement of benzene ring by pyridine ring also increases the binding ability due to increase in hydrogen bond accepting nature of the ligand. Due to these, the binding constant increases in the order: DMAPBI < DMAPIP-b < DMAPBO < DMAPOP which also supports the argument. Docking study also substantiates the experimental results. The studies reveal that BSA act as hydrogen bond donor and the hydrogen bonding also plays a crucial role in the orientation and location of the molecular binding.

Chapter 7

Sensing ability of a few dimethylaminophenyl substituted azoles toward metal ions: role of heteroatoms

7.0. Introduction

Sensing of metal ions by optical method is an active area of research. It has wide application in chemistry, biochemistry and environmental science.[317-321] Among various optical methods fluorescence technique is mostly used due to high sensitivity, easy to handle, low cost and less time consuming. The complex formation between the ligand and metal cation is a lewis acid-base type reaction where metal ion acts as a lewis acid and ligand acts as a lewis base. As the complexed cation affects the efficiency of ICT, it is anticipated that the interaction of cations with the ICT ligand, changes the spectral characteristics of the ligand. Numerous works have been reported on the sensing ability of ICT molecules toward different metal cations.[322-324] The interaction of two new cruciform chromophores with metal ion indicates the spectral properties of the cruciforms change via switching of the ICT band.[322] Qian et al. developed an ICT based selective sensor for Cu^{2+} with 1,8-naphthalimide derivative.[325] A novel ICT based dual emission of coumarin-alkyne derivative was rationally designed for the ratiometric detection of gold ion.[326]

Previously in our group, the sensing ability of a dual ICT fluorophore DMAPIP-b in different metal cations is studied. It is found that DMAPIP-b acts as an excellent sensor toward Zn^{+2} where Zn^{+2} is coordinated with both pyridiyl and azole nitrogen.[327] In order to find out the effect of heteroatom replacement on metal coordination and the sensing ability towards different metal cations of ICT sensors, in the present study the sensor molecules chosen are having same donor group like DMAPIP-b i.e. (dimethylamino group), but the acceptor moieties are different (**Chart 7.1**). Thus, the effect of metal ion on the spectral characteristics of DMAPBI, DMAPBO and DMAPOP are studied and compared with DMAPIP-b to investigate the effect of hetero atom replacement.

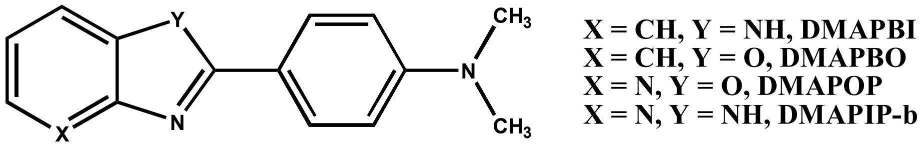

Chart 7.1. Structures of DMAPBI and analogous molecules.

As mentioned in previous chapter, in all the three molecules, the emission occurs from the ICT state in polar solvents. However the studies of the metal sensing ability of these molecules are not yet explored. Although huge amount of works have been reported on the sensing ability of the fluorescent molecules toward different metal ions, to obtain selective and sensitive fluorescent ICT molecule is still a challenge. Therefore, a comparative study may be useful for designing novel sensor for metal ions.

7.1. Absorption spectra

The absorption spectra of DMAPBI, DMAPBO and DMAPOP were recorded at various concentrations of different metal cations. Throughout the experiments, the concentrations of metal ions were considered up to 5 mM unless otherwise mentioned.

7.1.1. Alkali and alkaline earth metal ions

Except K^+, addition of all other alkali and alkaline earth metal ions change the spectral characteristics of DMAPBI (**Table 7.1**). Upon increasing the concentration of Li^+, Na^+, Ba^{+2} and Ca^{+2}, the absorbance of the fluorophore's band at 331 nm decreases and a new band starts to appear at the red side around 377 nm with appearance of a quasi-isosbestic point. Even at higher metal ion concentration, the original band as well as the new red side band coexists. As a representative, effect of addition of Li^+ ion on the absorption spectra of DMAPBI is shown in **Figure 7.1a** and plot of absorbance at both sides of the isosbestic point over concentration is shown in **Figure 7.1b**.

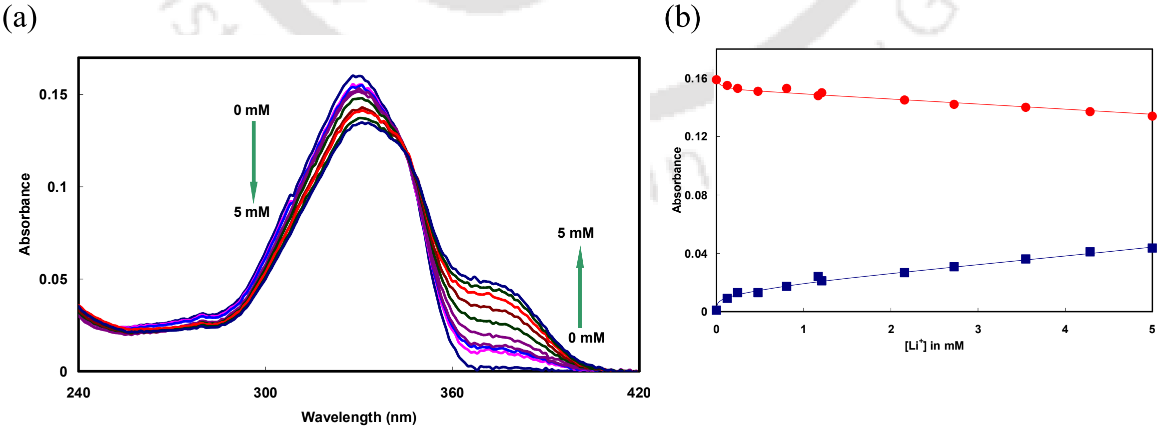

Figure 7.1 (a) Absorption spectra of DMAPBI in presence of Li^+. (b) Plot of absorbance at maxima, ● 330 nm and ■ 379 nm.

Addition of Mg^{+2} affects the spectral characteristics of DMAPBI more as compared to other alkali and alkaline earth metal ions. Alike observed in presence of other alkali and alkaline earth metal ions, upon increasing the Mg^{+2} concentration, the absorbance of the original band at 331 nm decreases and a new band emerges at the longer wavelength side (370 nm) of the original band. The absorbance of the new band monotonically increases with appearance of a clear isosbestic point (**Figure 7.2a**). However unlike other alkali and alkaline earth metal ions, at higher Mg^{+2} concentration, the 331 nm band corresponds to the free molecule diminishes completely and at its expense the new band having band maxima at 377 nm reaches its maximum. Plot of absorbance at both sides of the isosbestic point over concentration is shown in **Figure 7.2b**.

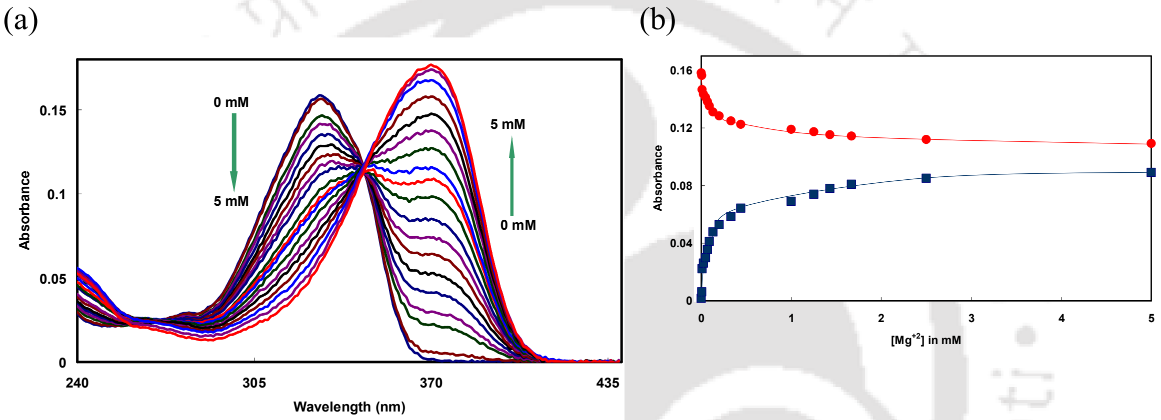

Figure 7.2 (a) Absorption spectra of DMAPBI in presence of Mg^{+2}. (b) Plot of absorbance at maxima, ● 330 nm and ■ 370 nm.

However, the spectral characteristics of DMAPBO remain unaffected in the presence of alkali and alkaline earth metal ions except Li^+. Addition of Li^+ results in a very minor spectral change. At a very high metal ion concentration, small increase in absorbance is observed at a shorter wavelength (blue shift). However the band is not clearly visible. The result implies the existence of very weak interaction between the ligand and Li^+.

The spectral property of DMAPOP also remains almost unaffected except for a few exceptions discussed below. Alike in DMAPBO, addition of Li^+ results in a very minor change of the spectra at a very high metal ion concentration. However unlike DMAPBO, the increase in absorbance is observed at longer wavelength side of the ligand band (430 nm). The result indicates a very weak interaction between DMAPOP and Li^+. Very high concentration of Mg^{+2} results in a very small increase in the absorbance at the red side indicating very weak interaction occurs between DMAPOP and Mg^{+2}.

7.1.2. Transition metal ions

The effect of the transition metal ions such as Ag^{+}, Co^{+2}, Cd^{+2}, Ni^{+2}, Zn^{+2} and Cu^{+2} on the absorption spectral characteristics of all three molecules are investigated. The effect of Ag^{+} and Cd^{+2} ions on the absorption spectra of DMAPBI are similar to those observed upon addition of alkali and alkaline earth metal ions such as Li^{+}, Na^{+}, Ba^{+2} and Ca^{+2}. i.e. upon increasing the Ag^{+} or Cd^{+2} ion concentration, the absorbance of the band corresponds to the free ligand decreases and a new band emerges at the red side with an isosbestic point. On the other hand, the effect of Co^{+2}, Ni^{+2} and Zn^{+2} are more significant on the absorption spectra of DMAPBI and are same as the effect of Mg^{+2}. Upon increasing the concentration of these metal ion concentrations, not only the absorbance of the free ligand band decreases with emergence of a new band at the red side with appearance of a clear isosbestic point, but also the free ligand band diminishes completely at higher metal ion concentration. This indicates that DMAPBI has stronger affinity towards Co^{+2}, Ni^{+2} and Zn^{+2} ions than Ag^{+} and Cd^{+2}. The spectral changes observed with addition of Cu^{+2} (**Figure 7.3a**) is also similar to those of Mg^{+2}, Co^{+2}, Ni^{+2} and Zn^{+2} ions.

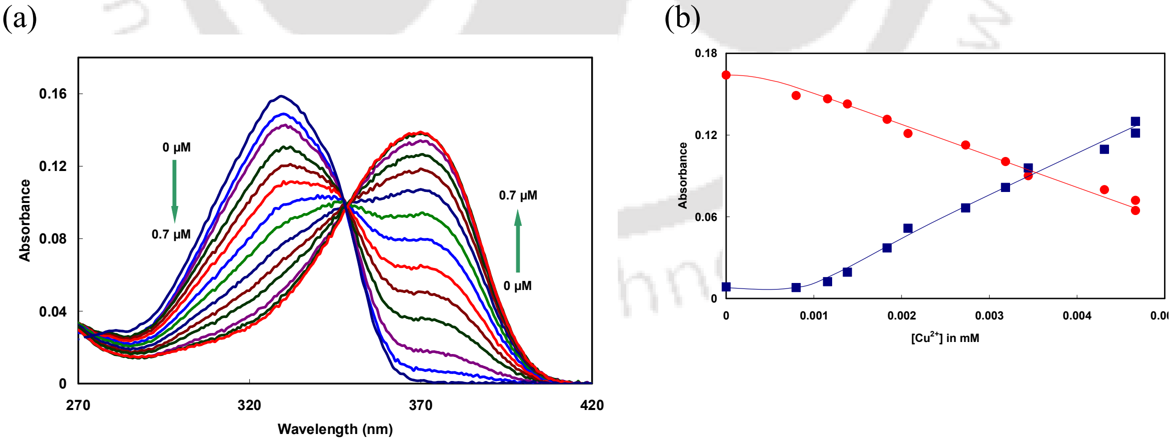

Figure 7.3 (a) Absorption spectra of DMAPBI in presence of Cu^{+2}. (b) Plot of absorbance at maxima, ● 330 nm and ■ 370 nm.

However, the ligand-metal complex formation is completed at a very lower metal ion concentration (~ 0.7 µM). Thus it can be stated that among these metal ions under investigations, the sensitivity of the absorption spectra of DMAPBI is maximum towards Cu^{+2}. Plot of absorbance at maxima over concentration is shown in **Figure 7.3b**.

Addition of Co^{+2}, Cd^{+2} and Zn^{+2} do not affect the spectral characteristics of DMAPBO even at very high concentration. The change in the spectral properties of DMAPBO is very less in presence of Ag^{+} and Ni^{+2} ions even at very high metal ion concentration. The new band is observed only at higher concentration of Ag^{+} and Ni^{+2}. Addition of Ag^{+} results in the new band at the shorter wavelength side of the free ligand band, whereas upon addition of Ni^{+2} a new band appears at the longer wavelength side. But band was not very prominent in either case. This concludes a very weak interaction takes place upon addition of Ag^{+} and Ni^{+2} with DMAPBO.

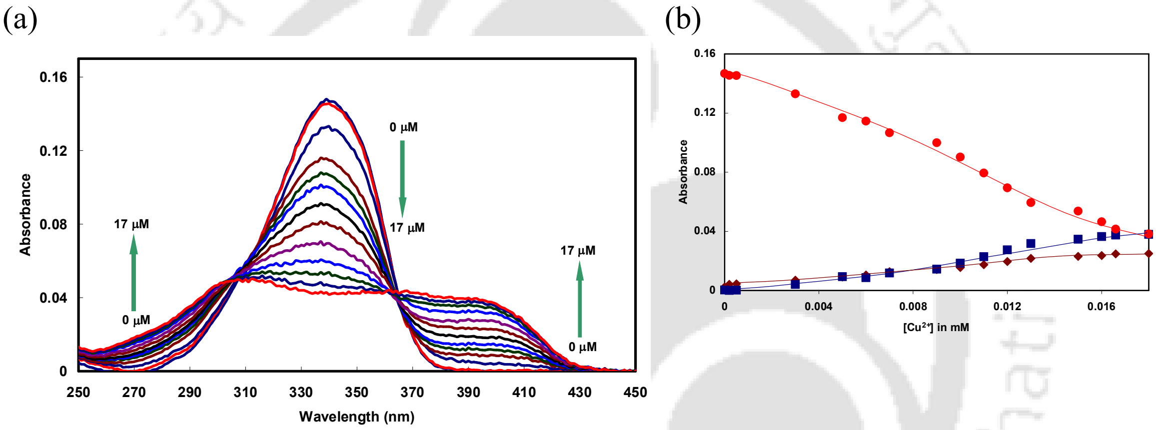

Figure 7.4 (a) Absorption spectra of DMAPBO in presence of Cu^{+2}. (b) Plot of absorbance at maxima, ● 340 nm, ♦ 280 nm and ■ 398 nm.

Addition of Cu^{+2} causes a very significant change on the spectral properties of DMAPBO. Even at lower concentration, the spectral properties of DMAPBO changes drastically. Upon increasing the metal ion concentration, the absorbance of the free ligand band decreases with appearance of two new bands at both sides of the original band and the absorbance of the new bands increase monotonically with appearance of two distinct isosbestic points at 305 nm and 368 nm (**Figure 7.4a**). It is also observed that the complex formation is completed upon addition of ~ 17 µM of Cu^{+2}. Plot of absorbance at maxima over concentration is shown in **Figure 7.4b**. Like DMAPBI, DMAPBO also shows higher sensitivity towards Cu^{+2} than other metal ions. However, the sensitivity of benzoxazole derivative (DMAPBO) towards Cu^{+2} is less in comparison to the corresponding benzimidazole derivative (DMAPBI).

Very little change is observed in the absorption spectrum of DMAPOP upon addition of Ag^+. Unlike DMAPBO, upon increasing the Ag^+ concentration, a small decrease in the absorbance of the molecular band is observed with appearance of a weak band at the shorter wavelength side and broadening of the spectra occurs at the longer wavelength. Unlike the absorption spectrum of DMAPBO, the absorption spectrum of DMAPOP is affected by the addition of Cd^{+2} ions. Addition of Cd^{+2} produces two clear bands at both sides (295 nm and 398 nm) of the free ligand band. With increase in Cd^{+2} concentration, the absorbance of both new bands increase at the cost of free ligand's absorption band with two clear isosbestic points (**Figure 7.5a**). Plot of absorbance at maxima over concentration is shown in **Figure 7.5b**.

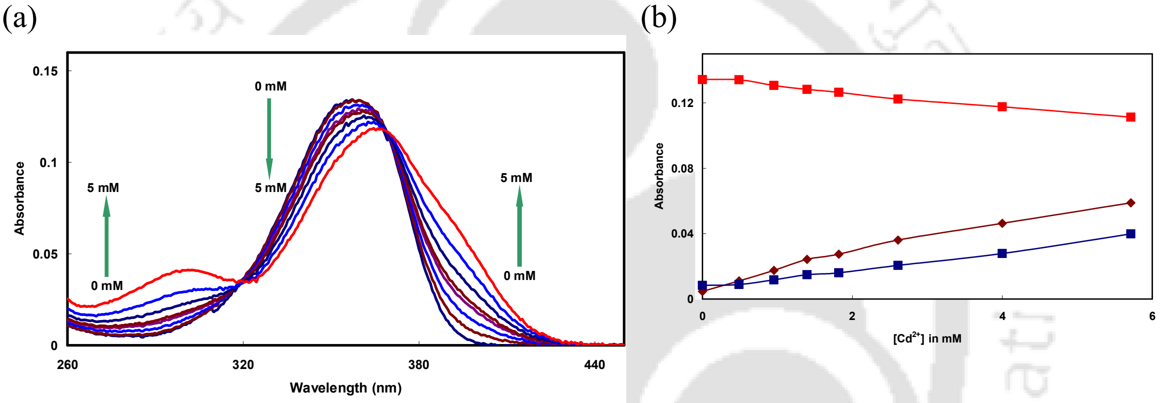

Figure 7.5 (a) Absorption spectra of DMAPOP in presence of Cd^{+2}. (b) Plot of absorbance at maxima, ● 357 nm, ♦ 395 nm and ■ 295 nm.

The spectral properties of DMAPOP are affected upon addition of Co^{+2} and new band is obtained at the red side (398 nm) of the uncomplexed form. Ni^{+2} also produces a bathochromic shift and the absorbance of the new band increases with increase in concentration of Ni^{+2} with appearance of a quasi-isosbestic point. At higher metal ion concentration the original band diminishes completely. Like its other analogues, DMAPOP also has higher sensitivity towards Cu^{+2} which affects drastically the spectral characteristics of DMAPOP even at a very low concentration. Alike in DMAPBO, in DMAPOP also addition of Cu^{+2} ion results in decrease in the absorbance of the original band with appearance of two new bands obtained one at longer wavelength (427 nm) and other at shorter wavelength (308 nm) of the original band (357 nm) with two distinct isosbestic points and the complex formation saturated at ~ 8.4 μM (**Figure 7.6a**). Plot of absorption maxima at both sides of the isosbestic point over concentration is shown in **Figure 7.6b**.From the result it can be inferred that the sensitivity of DMAPOP toward Cu^{+2} is more than DMAPBO but less than DMAPBI.

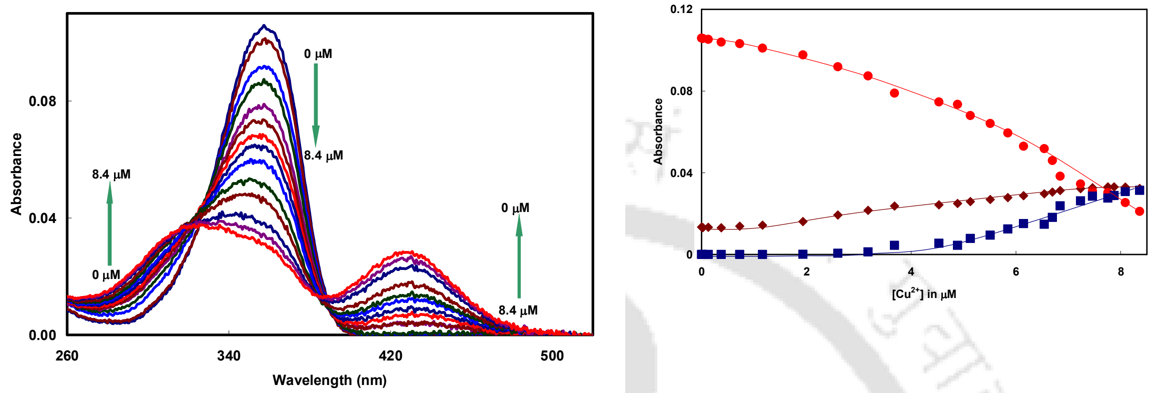
(a) (b)

Figure 7.6 (a) Absorption spectra of DMAPOP in presence of Cu^{+2}. (b) Plot of absorbance at maxima, ● 357 nm, ♦ 307 nm and ■ 430 nm.

The effect of Zn^{+2} on the absorption spectrum of DMAPOP is not only different from those of DMAPBI and DMAPBO; it is also quite different from the effect of other metal ions. For initial addition of Zn^{+2} a new band is observed at 435 nm and it's absorbance increases upto ~ 1.4 mM concentration of metal ion. On further increasing the Zn^{+2} concentrations, a clear band emerges at 390 nm (**Figure 7.7a**). Plot of absorbance at maxima over concentration is shown in **Figure 7.7b**.

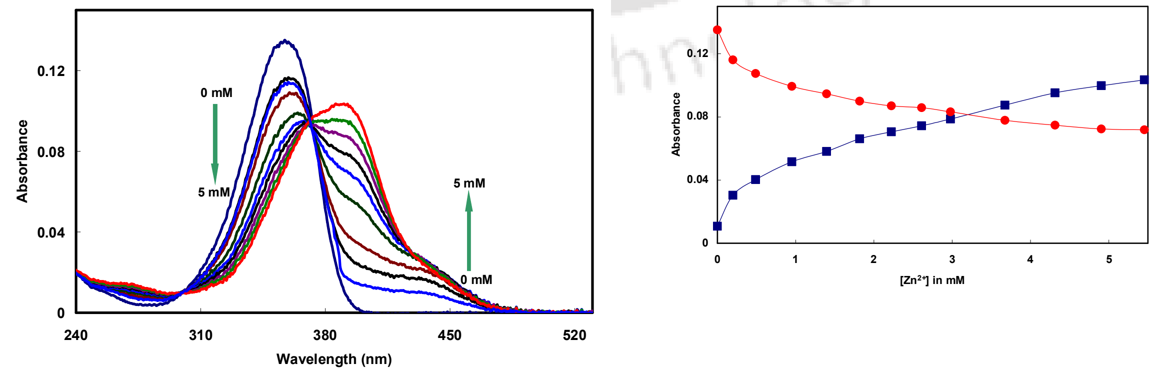
(a) (b)

Figure 7.7 (a) Absorption spectra of DMAPOP in presence of Zn^{+2}. (b) Plot of absorbance at maxima, ● 357 nm and ■ 390 nm.

7.2. Fluorescence spectra

7.2.1. Alkali and alkaline earth metal ions

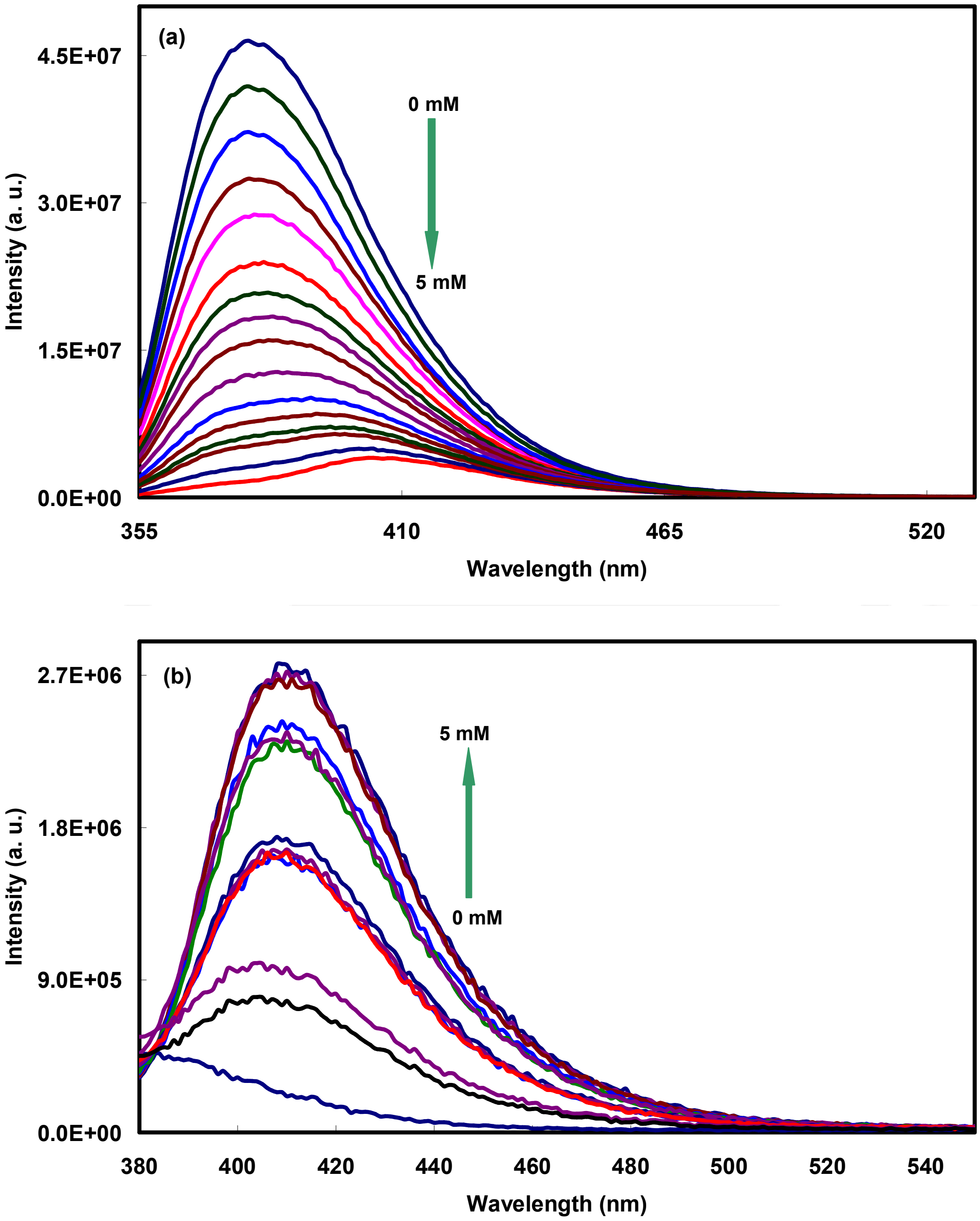

Figure 7.8. Fluorescence spectra of DMAPBI in presence of Mg^{+2}: (a) $\lambda_{exc} = 330$ nm and (b) $\lambda_{exc} = 370$ nm.

Insignificant changes are observed in the fluorescence spectra of DMAPBI in presence of Li^+, Na^+ and K^+ ions 330 nm. But exciting at 370 nm results in a weak band emerges at 397 nm (figure not shown). This indicates that there is a very weak interaction of DMAPBI with Li^+, Na^+ and K^+. However more significant changes are obtained upon addition of Ba^{+2}, Ca^{+2} and Mg^{+2}. The effect of Mg^{+2} on the fluorescence spectra are shown in **Figure 7.8** as representative. When excited at 330 nm, a band is obtained at 380 nm (**Figure 7.8a**). Upon increasing the concentration of the metal ion the intensity of the original band decreases monotonically and at higher concentrations of Mg^{+2} the band broadens and shifted towards red side. This indicates the mixing of two bands. At very high concentration the original band diminishes and the new red shifted band become more prominent. But, when excited at 370 nm, the new red shifted band starts to appear even for the initial addition of metal ion and the intensity of the band increases with increase in metal ion concentration (**Figure 7.8b**). Although effect of other two alkaline earth metal ions are also same, but the magnitude is less. The change in the spectral intensity are in the order $Ba^{+2} < Ca^{+2} < Mg^{+2}$. However, the alkali and alkaline earth metal ions fail to produce any significant change in the fluorescence spectra of DMAPBO and DMAPOP.

7.2.2. Transition metal ions

Addition of Ag^{+} ion in DMAPBI solution results in decrease in the emission intensity of the original band without any shift or appearance of new band by exciting at the ligand's band maximum (λ_{exc} = 330 nm). However upon exciting at the longer wavelength (λ_{exc} = 370 nm), a new band arises at 410 nm. DMAPBI shows more sensitivity towards Ni^{+2}, Co^{+2}, Cd^{+2} and Zn^{+2} than alkaline earth metal ions and Ag^{+}. Upon increasing the concentration of Ni^{+2}, the intensity of the free ligand band at 380 nm decreases and the spectra broadens and a new band emerges at 402 nm (figure not shown). The new band becomes more prominent with increase in Ni^{+2} concentration and the original band diminishes slowly. By exciting at 370 nm the appearance of the new band occurs and the intensity increases with increase in concentration. Similar behaviour is also found upon addition of Co^{+2}, Cd^{+2} and Zn^{+2}. However the saturation of the new band reaches at 3.6 mM, 1.1 mM and 0.9 mM concentration of Co^{+2}, Cd^{+2} and Zn^{+2} respectively.

Same as in the absorption spectra, addition of Cu^{+2} affects drastically the fluorescence spectral characteristics of DMAPBI. Upon exciting at the isosbestic point (345 nm), the intensity of the molecular band at 380 nm decreases gradually and like in Co^{+2} and Cd^{+2}, the spectra broaden and the band is shifted towards the longer wavelength (404 nm) upto addition of 8 μM of Cu^{+2}. Upon further addition (> 8 μM) of Cu^{+2}, the intensity of the red shifted band increases and is saturated at concentration 50 µM (**Figure 7.9a**, inset). Upon exciting at 370 nm, the new red shifted band starts to appear even for the initial addition of Cu^{+2} and the intensity of the band increases with increase in metal ion concentration (**Figure 7.9b**).

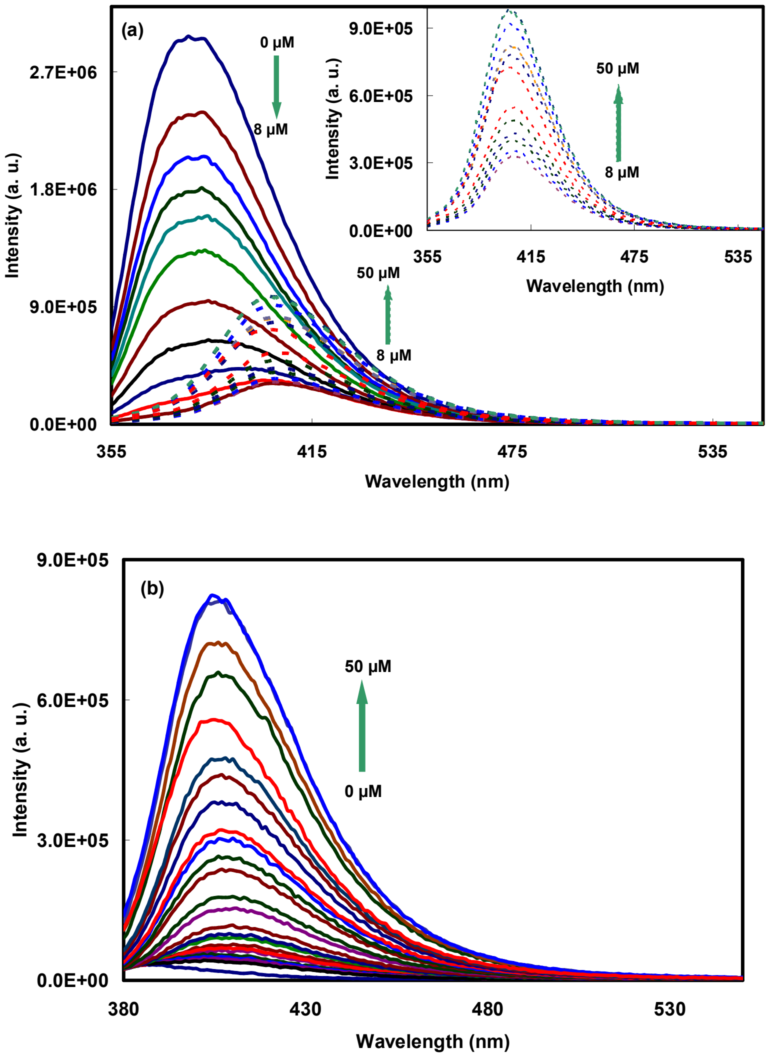

Figure 7.9. Fluorescence spectra of DMAPBI in presence of Cu^{+2}: (a) $\lambda_{exc} = 345$ nm and (b) $\lambda_{exc} = 370$ nm.

No significant change in the fluorescence spectra is observed upon addition of Ag^{+}, Cd^{+2}, Co^{+2} and Zn^{+2} to DMAPBO solution which indicates that there is negligible or no interaction of DMAPBO with these metal ions. However upon addition of Ni^{+2}, the fluorescence intensity decreases and the quenching is observed without any shift or emergence of any new band. On the other hand, Cu^{+2} affects drastically the spectral properties of DMAPBO even at a very lower concentration. When excited at the blue side isosbestic point (305 nm), the intensity of the original band at 394 nm decreases with a hypsochromic shift. At 63 µM of Cu^{+2} the original band diminishes completely and the band at 368 nm is prominent and also got saturated (**Figure 7.10a**). Exciting at the red side isosbestic point (368 nm) resulted only in quenching of fluorescence without any shift or emergence of any new band (figure not shown). On addition of Cu^{+2}, same as in the emission spectra, the intensity of the excitation spectra (obtained by monitoring at 450 nm) decreases gradually with a blue shift (**Figure 7.10b**).

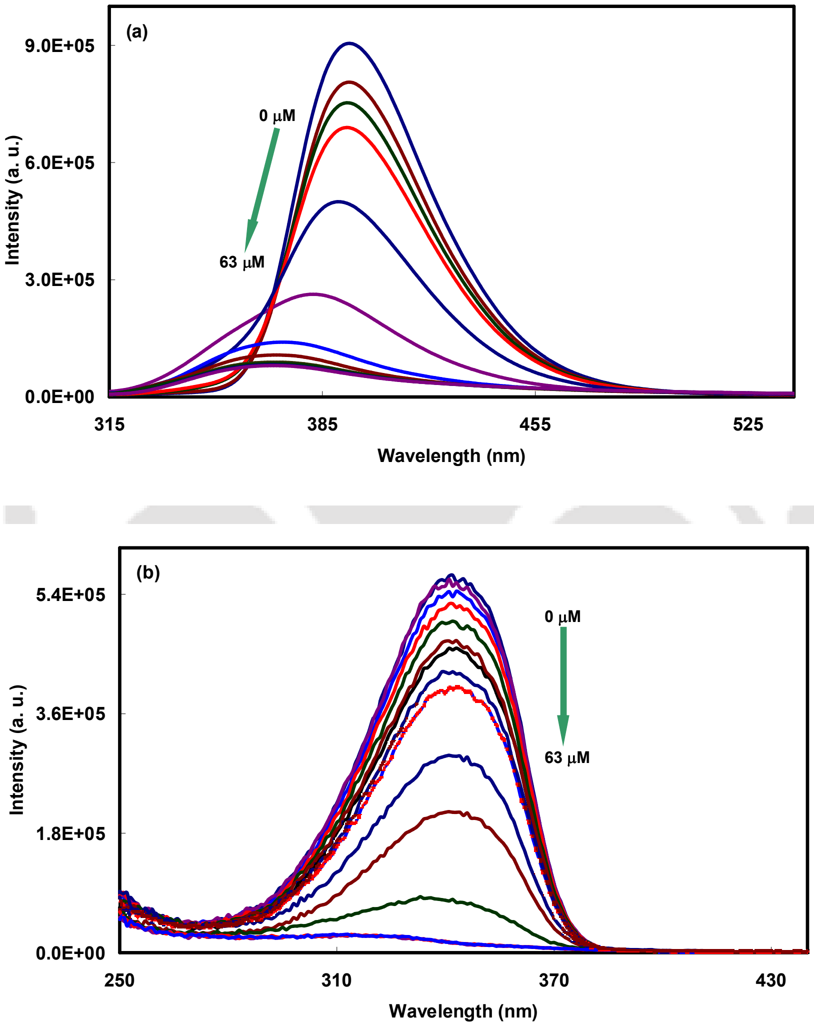

Figure 7.10. (a) Emission spectra (λ_{exc} = 305 nm) and (b) excitation spectra (λ_{em} = 450 nm) of DMAPBO in presence of Cu^{+2}.

The fluorescence intensity of DMAPOP decreases with addition of Ag^{+} when excited at 305 nm and 345 nm without appearance of any new band. However upon exciting at 390 nm, the ligand's emission band at 420 nm decreases with emergence of a new band at the red side with appearance of a quasi-isoemissive point at around

434 nm (**Figure 7.11a**). Plot of emission intensity at maxima over concentration is shown in **Figure 7.11b**.

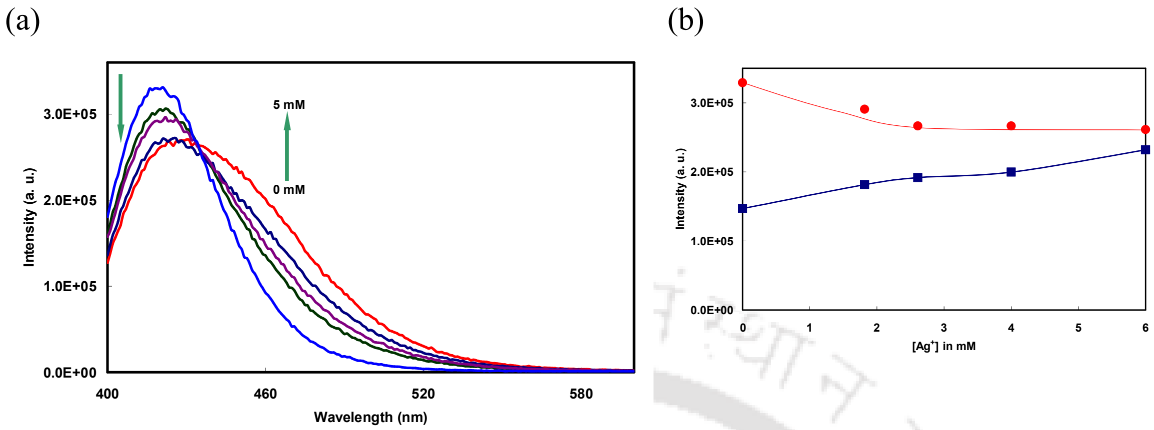

Figure 7.11 (a) Fluorescence spectra of DMAPOP in presence of Ag$^+$ (λ_{exc} = 390 nm). (b) Plot of absorbance at maxima, ● 420 nm and ■ 450 nm.

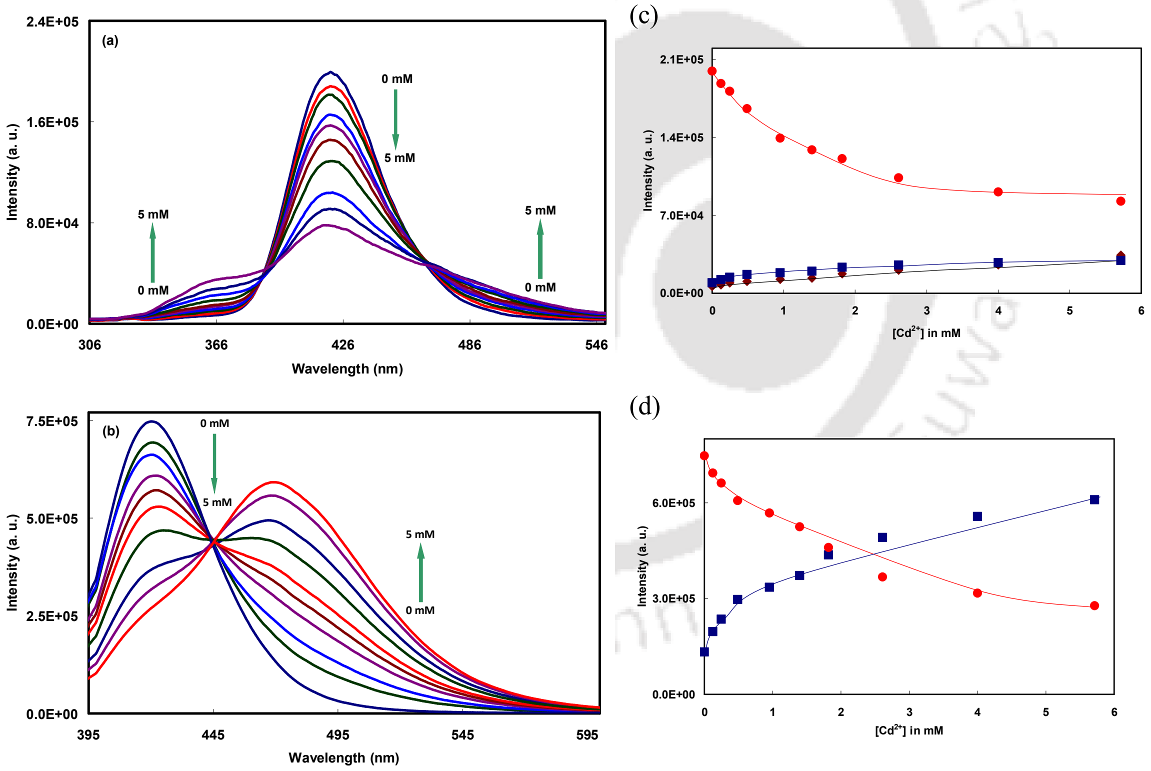

Figure 7.12. Fluorescence spectra of DMAPOP in presence of Cd^{+2}: (a) λ_{exc} = 297 nm and (b) λ_{exc} = 385 nm. (c) Plot of emission intensity at maxima, ● 420 nm, ♦ 360 nm and ■ 498 nm (λ_{exc} = 297 nm). (d) Plot of emission intensity at maxima, ● 420 nm and ■ 470 nm (λ_{exc} = 385 nm).

Fluorescence titration of Cd^{+2} on DMAPOP is shown in **Figure 7.12**. When excited at 300 nm, the single emission band system is slowly replaced by two bands system. Although, the red shifted band appears as a tail when excited at 300 nm (**Figure 7.12a**), it appears as a clear band upon excitation at 380 nm (**Figure 7.12 b**). The excitation spectra (not shown) behaviour also correlates well with the emission spectra. Plot of emission intensity at maxima over concentration is shown in **Figure 7.12c** and **Figure 7.12d**.

The effect of Ni^{+2} on DMAPOP is same as that on DMAPBO. The fluorescence spectrum is quenched with increase in concentration of Ni^{+2}, without any spectral shift or appearance of new band (figure not shown). Co^{+2} also quenches the fluorescence spectra of DMAPOP without any shift (figure not shown). Upon increasing Zn^{+2} concentration, the intensity of the free ligand emission band decreases with emergence of a new band at the red side (498 nm). At higher Zn^{+2} concentration the intensity of the molecular band decreases drastically and the new band obtained at the red side becomes much more prominent (**Figure 7.13a**). Plot of emission intensity at maxima over concentration is shown in **Figure 7.13b**.

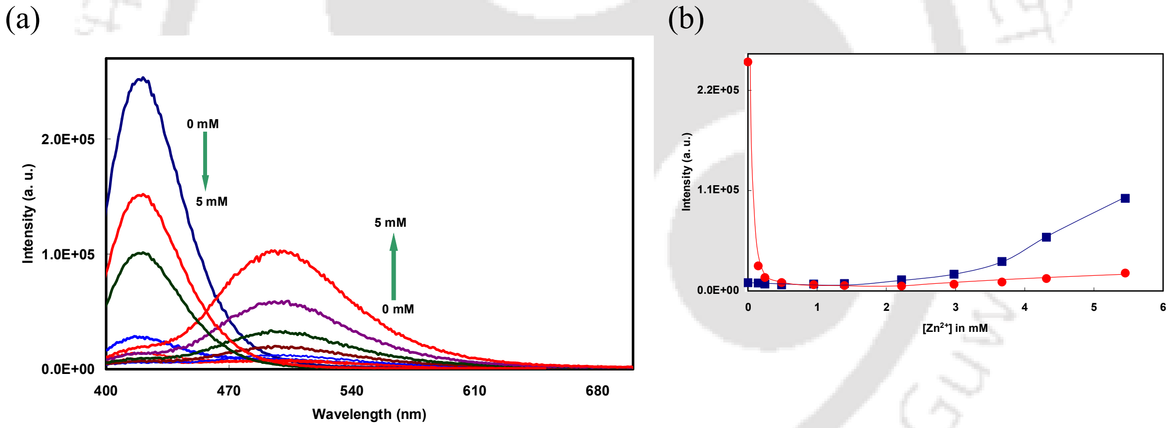

Figure 7.13 (a) Fluorescence spectra of DMAPOP in presence of Zn^{2+} (λ_{exc} = 390 nm). (b) Plot of emission intensity at maxima, ● 420 nm and ■ 500 nm.

The effect of Cu^{2+} on DMAPOP is same as that on DMAPBO. The fluorescence spectra obtained by exciting at both quasi-isosbestic points (323 nm and 387 nm) in presence Cu^{2+} ion lead to quenching of the 420 nm fluorescence band of uncomplexed DMAPOP (**Figure 7.14**). However, a new band appears at 380 nm upon excitation at 323 nm (**Figure 7.14a**) and no such new band emerges upon excitation at the red side isosbestic point **Figure 7.14b**.

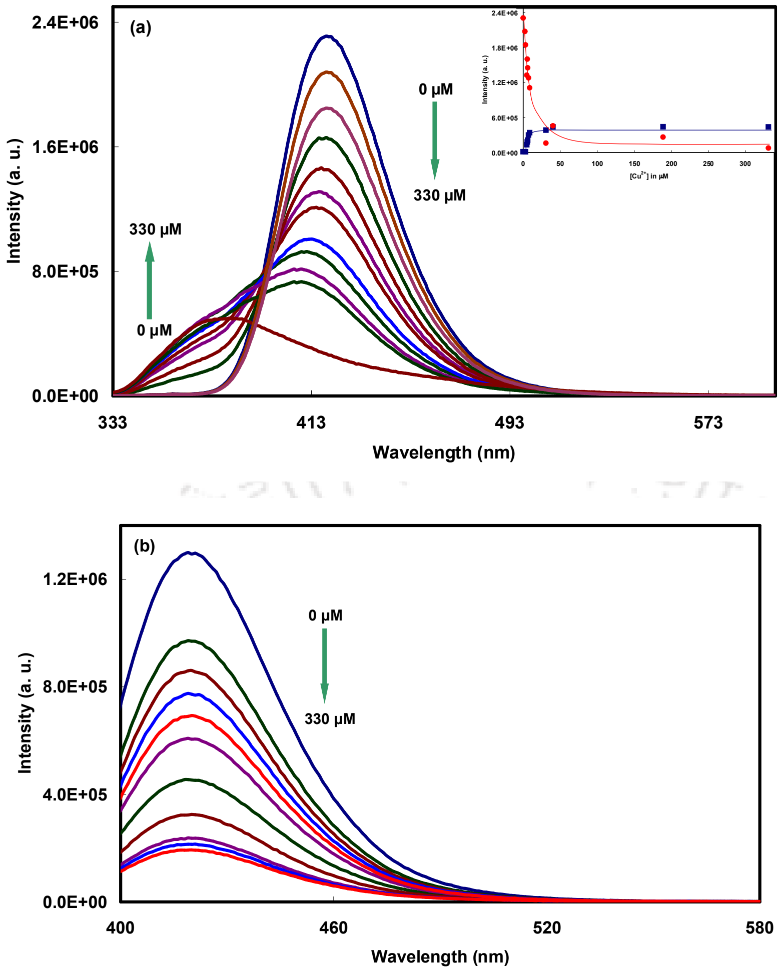

Figure 7.14. Fluorescence spectra of DMAPOP in presence of Cu^{+2}: (a) λ_{exc} = 323 nm (Inset shows plot of emission intensity at maxima, ● 420 nm and ■ 365 nm (λ_{exc} = 387 nm).

7.3. Discussion

7.3.1. Complex formation

The absorption band maxima and fluorescence band maxima for all the three molecules in the presence of metal ions are compiled in **Table 7.1**. DMAPBI and DMAPBO have two basic centers i.e. azole nitrogen and dimethylamino nitrogen. In addition to azole nitrogen and dimethylamino nitrogen DMAPOP contains one more basic center i.e. pyridyl nitrogen. It is well established in the literature and also explained in previous chapters that the binding of cations (protons) through the dimethylamino group results in blue shift and those through ring nitrogens produce red shift.[82,83,85,205-208] The bathochromic shift is more when cation binds at the pyridyl nitrogen than when it binds at the azole nitrogen.

.

Table 7.1. Absorption maxima (λ_{max}^{ab}, nm) and fluorescence maxima (λ_{max}^{em}, nm) of DMAPBI, DMAPBO and DMAPOP in presence of a series of metal ions studied.

Metal ion	DMAPBI		DMAPBO		DMAPOP	
	λ_{max}^{ab}	λ_{max}^{em}	λ_{max}^{ab}	λ_{max}^{em}	λ_{max}^{ab}	λ_{max}^{em}
No metal	330	379	340	394	358	420
Li^{+}	378	410	298 (weak)	394	433	420
Na^{+}	378	410	340	394	358	420
K^{+}	330	410	340	394	358	420
Ba^{+2}	377	410	340	394	358	420
Ca^{+2}	377	410	340	394	358	420
Mg^{+2}	370	410	340	394	394 (weak)	437
Co^{+2}	370	410	340	394	399	420
Cd^{+2}	377	410	340	394	295, 395	370, 470
Ag^{+}	370	410	308 (weak)	394	308	431
Ni^{+2}	370	410	379 (weak)	394	372	420
Zn^{+2}	370	410	340	394	390, 440	500
Cu^{+2}	370	403	298, 397	370	309, 430	379

Addition of metal ion causes bathochromic shift in both absorption and fluorescence spectra of DMAPBI's band. This indicates that all the metal ions interact with DMAPBI through the azole nitrogen. As the charge flow from the dimethylamino group to the imidazole ring, the charge on the azole nitrogen increases. Thus, the coordination of metal ions occurs only through the azole nitrogen, but none of the metal ion interacts at dimethylamino nitrogen of DMAPBI due to less charge density at the dimethylamino nitrogen.

As indicated by the absorption and fluorescence spectra, metal ions such as Na^+, K^+, Mg^{+2}, Ca^{+2}, Ba^{+2}, Co^{+2}, Cd^{+2} and Zn^{+2} do not interact with DMAPBO. The formation of blue shifted band at very high concentrations of Li^+ and Ag^+ implies weak interaction of the fluorophore with the metal ion via dimethylamino nitrogen. On the other hand, appearance of a weak red shifted band upon addition of Ni^{+2} in the absorption spectra suggests the binding of metal ion at azole nitrogen of DMAPBO. However, the quenching of fluorescence spectra results without any appearance of new band shows that the binding becomes weaker in the excited state. The quenching of the fluorescence is due to the interaction of ligand with the paramagnetic Ni^{+2} The formation of two new bands in the absorption spectra on addition of Cu^{+2}suggests that the metal ion binds at both dimethylamino nitrogen and azole nitrogen to form two 1:1 complexes with DMAPBO.

The metal ions like Na^+, K^+, Ca^{+2} and Ba^{+2} do not bind with DMAPOP. Addition of Ag^+ results a weak band at shorter wavelength side with broadening of the spectra at longer wavelength of the absorption spectra of DMAPOP with respect to the molecular band. However, no emission band is observed at the shorter wavelength side, but the longer wavelength band is appeared at higher concentration. This suggests that although in ground state DMAPOP interacts with Ag^+ via both dimethylamino nitrogen and azole nitrogen, but in the excited state the dissociation of the dimethylamino coordinated complex takes place. The bathochromic shift is observed in the absorption spectra of DMAPOP upon complexation with Mg^{+2}, Co^{+2} and Ni^{+2} are more than that observed upon complexation with Li^+. This shows that Mg^{+2}, Co^{+2} and Ni^{+2} form complexes through azole nitrogen and complexation with Li^+ occurs via pyridyl nitrogen. From the formation of two red shifted absorption bands upon complexation with Zn^{+2}, it can be inferred that it forms two kinds of 1:1 complexes by coordination through each ring nitrogen. Similarly, from the spectral shifts it can be inferred that Cd^{+2} and Cu^{+2} also form two 1:1 complexes, but in the presence of Cd^{+2} binding occurs via dimethylamino and azole nitrogens, and in the presence of Cu^{+2} binding occurs via dimethylamino and pyridyl nitrogens, respectively. The binding sites of the metal ions with different fluorophores are summarized in **Table 7.2**.

Table 7.2. The coordination site of different metal ions on DMAPBI, DMAPBO and DMAPOP.

Metal ion	DMAPBI	DMAPBO	DMAPOP
Li^{+}	Azole nitrogen	Dimethylamino nitrogen (weak interaction)	Pyridyl nitrogen (weak interaction)
Na^{+}	Azole nitrogen	-	-
K^{+}	Azole nitrogen	-	-
Ba^{+2}	Azole nitrogen	-	-
Ca^{+2}	Azole nitrogen	-	-
Mg^{+2}	Azole nitrogen	-	Azole nitrogen (weak interaction)
Co^{+2}	Azole nitrogen	-	Azole nitrogen
Cd^{+2}	Azole nitrogen	-	Dimethylamino nitrogen and Azole nitrogen
Ag^{+}	Azole nitrogen	dimethylamino (weak interaction)	Dimethylamino nitrogen and Azole nitrogen
Ni^{+2}	Azole nitrogen	Azole nitrogen (weak interaction)	Azole nitrogen
Zn^{+2}	Azole nitrogen	-	Azole nitrogen and Pyridyl nitrogen
Cu^{+2}	Azole nitrogen	Dimethylamino nitrogen and Azole nitrogen	Dimethylamino nitrogen and Pyridyl nitrogen

The changes observed in the fluorescence spectral characteristics are more than those in the absorption spectral characteristics. However, in general, higher concentrations of metal ions were required to reach the saturation limit in the fluorescence spectra compared to the absorption spectra in all the fluorophores. The interaction becomes weaker in the excited state because of the difference in charge distribution in the excited state and the ground state.

7.3.2. Comparative sensitivity

From the results discussed above it can be depicted that the sensitivity of DMAPBI and its analogous are higher toward transition metal ions than alkali and alkaline earth metal ions. Among the three ligands, the sensitivity toward different metal cations is highest for DMAPBI and is lowest for DMAPBO. Again, unlike in other molecules in DMAPBI, the metal ions are binding only at azole nitrogen and interact with almost all metal ions. The selectivity improves upon replacing the >NH group of the heterocyclic ring by oxygen. But, when electron withdrawing nitrogen was introduced in benzene of the benzoxazole the selectivity decreases. For examples, with Mg^{+2}, Co^{+2} and Cd^{+2}, DMAPBO did not interact but bind with DMAPOP. This difference in behaviour can be explained using ICT. Due to ICT the charge density on the dimethylamino nitrogen decreases and that on azole nitrogen increases which enhances the metal binding at azole nitrogen. Replacing the >NH group by electron withdrawing oxygen atom decreases the charge on azole nitrogen thereby decreasing its coordinating ability. Therefore, the binding ability of DMAPBO decreases and some metal ions also bind at dimethylamino nitrogen. When pyridyl nitrogen was substituted on benzene ring again ICT increases, as a result the binding ability of DMAPOP increases compared to DMAPBO.

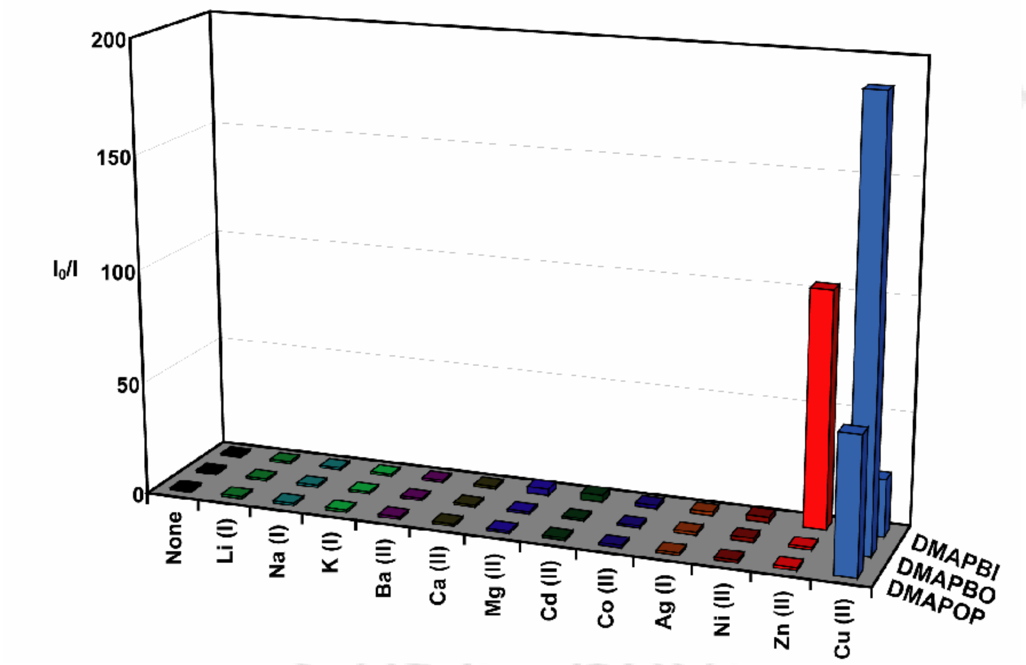

Figure 7.15. Histogram plot of the intensity ratio (I_0 / I) of the three fluorophores to different metal cations (metal ion concentrations fixed at 100 µM).

A set of experiments are carried out by considering the metal ion at 100 µM for all the three ligands with a series of metal ions studied in the present work. The histogram plot is constructed by considering the intensity ratios (I_0 / I) (**Figure 7.15**). The change in fluorescence intensity ratio of DMAPBI is highest in presence of Zn^{+2} followed by Cu^{+2}. Whereas the change in fluorescence intensity ratios of both

DMAPBO and DMAPOP are highest in presence of Cu^{+2} and are negligible in presence of other metal ions. The intensity ratio of DMAPBI in presence of Zn^{2+} is 104 and in presence of Cu^{+2} is 25. The intensity ratios of DMAPBO and DMAPOP in presence of Cu^{+2} are 193 and 60 respectively.

7.4. Conclusion

The sensing abilities of three ICT fluorophores DMAPBI, DMAPBO and DMAPOP toward a series of metal cations are investigated to understand the effect of heteroatoms. The studies revealed that benzimidazole derivative has higher binding affinity than the oxazole derivatives due to ICT from dimethylamino group to azole nitrogen. DMAPBI interacts with all the metal ions through azole nitrogen. Since, the charge of the azole nitrogen is decreased in DMAPBO, depending on the metal ion, it coordinates through azole nitrogen and/or dimethylamino nitrogen. When in benzene ring pyridyl nitrogen was substituted, the molecule interacts through azole nitrogen and/or pyridyl nitrogen. From the histogram plot it is found that the change in fluorescence intensity ratios of DMAPBI is highest in presence of Zn^{+2} followed by that of Cu^{+2}. However in both oxazole derivatives change in fluorescence intensity ratios are more with Cu^{+2}.

Chapter 8

Effect of micelles on the prototropic equilibriums of a few push-pull styryl azoles

8.0. Introduction

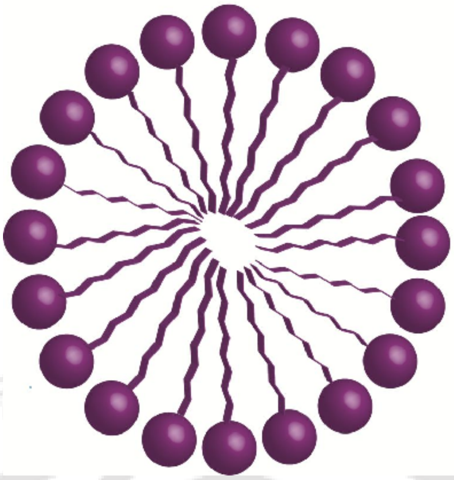

Figure 8.1. Structure of micelle.

Micelles are studied as rudimentary models for biological lipid membrane systems.[240,328] Surfactant molecules aggregate in the presence of water to form micelle. In micelle the hydrophobic long chain (tail) is projected towards the core and the polar head group projects outward and is in contact with the surrounding solvent molecule (**Figure 8.1**). Micelles are of two types i.e. ionic and nonionic. Core of the micelle is surrounded by a polar shell known as stern layer for ionic micelle and palisade layer for nonionic micelle. It is found that the thickness of the stern layer for cationic CTAB and anionic SDS is 6-9 Å and for nonionic TX-100 the palisade layer is about 20 Å.[329,330]

Variation of viscosity and polarity of different micelles render them to use in many processes including ICT process. The photoinduced electron transfer from *N*,*N*-dimethylaniline to coumarin dyes becomes much faster in CTAB micelle.[331] As the hydrophobic interaction with the micelles increases the rates of the hydrolysis of *p*-nitrophenyl esters are increased with alkyl chain length (of esters) in CTAB micelles.[332] The oxidation of ethylenediaminetetraacetic acid by chromic acid shows the higher rate in the micellar pseudo-phase due to association of the reactants with the nonionic micellar head groups via hydrogen bonding.[333]

Studying the spectral characteristics in micellar environment is also an active area of research.[85,334-336] To analyze the ion distribution between bulk aqueous phase and interface, micelles have been used extensively. In micellar medium the molecule experiences totally different environment than that of the bulk solvent in terms of polarity, viscosity etc. As ICT molecules are strongly influenced by polarity, viscosity, hydrogen bonding capacity and ionic character of the environments, thus the micellar medium will drastically affect the ICT process and are widely studied.[85,91,92,175,337-340] As protonation results charged species, the ionic character or/and the polarity of the micelle control the prototropic equilibrium. It is well known that the pK_a value of a molecule in anionic micelle is much higher than in aqueous medium, on the other hand the pK_a value in cationic micelles are lesser than that in aqueous medium and the value obtained for non-ionic micelle is little higher than cationic micelle but less than in aqueous medium.[85,175,338] In anionic micelle, the protons and the cations are concentrate in the Stern layer and suppress the release of protons, as a result the apparent pK_a increases. The decrease in pK_a in non-ionic micelle is due to decrease in dielectric constant of the medium. On the other hand, in cationic micelle positively charged species are repelled to the aqueous phase, hence the apparent pK_a decreases.[85,175,338]

On fluorophores having more than one basic center often protonation occurs at more than one basic center.[82,83,85,205-207] Several interesting observations were reported about the role of solvent on the protonation of this multi basic sites.[205,206] Owing to heterogeneity, micelles are much more interesting media to study the protonation of this multi basic sites. Nonetheless, although the effect of micelle on protropic equilibrium constantly received considerable attention, still the effect of micelle on the protonation site received less attention. Styryl based push-pull systems exhibit ICT emission. However, presence of ethylenic double bond makes the system hydrophobic in nature which increases its binding affinity with micelles. In addition, the length and the planarity of the molecule increases, which might make it to penetrate deeper inside the micelle. This leads to interesting effect on protonation. In *trans*-2-[4′-(dimethylamino)styryl]benzimidazole (*t*-DMASBI, **Scheme 8.1**) the protonation occurs only at azole nitrogen to form the monocation (assigned as MC2) in aqueous medium due to greater charge density in azole nitrogen of *t*-DMASBI.[341] In micelles, *t*-DMASBI is present in the micellar-water interface with limited exposure to water.[342] Study on prototropic equilibrium of the molecule in micelles leads to an interesting observation. Alike in aqueous medium, in micelles upon protonation only MC2 is formed. The formation of monocation is completed in SDS and TX-100 micelles. On the other hand, in cationic CTAB micelle, for initial addition of acid MC2 is formed, however at lower pH before the completion of monocation, dication formation starts to take place.

Styryl dyes *t*-DMASBT, *t*-DMASIP-b and *trans*-2-[4′-(dimethylamino) styryl]imidazo[4,5-c]pyridine (*t*-DMASIP-c) (**Scheme 8.1**) also have interesting prototropic equilibrium. In aqueous medium upon protonation of *t*-DMASBT two kinds of monocations are formed: (i) protonation at dimethylamino nitrogen (assigned as MC1, **Scheme 8.1**) and (ii) protonation at azole nitrogen (MC2, **Scheme 8.1**).[149,153] On *t*-DMASIP-c, it is found that the protonation takes place at both azole nitrogen (MC2) and pyridyl nitrogen (assigned as MC3, **Scheme 8.1**).[342] As discussed in **Section 4.7**, *t*-DMASIP-b also forms two kinds of monocations by protonation of the heterocyclic ring nitrogens. Therefore, it is interesting to find the effect of micelle on these systems. In this chapter, the effect of anionic micelle SDS, nonionic micelle TX-100 and cationic micelle CTAB on prototropic equilibriums and protonation sites of *t*-DMASBT, *t*-DMASIP-b and *t*-DMASIP-c are investigated.

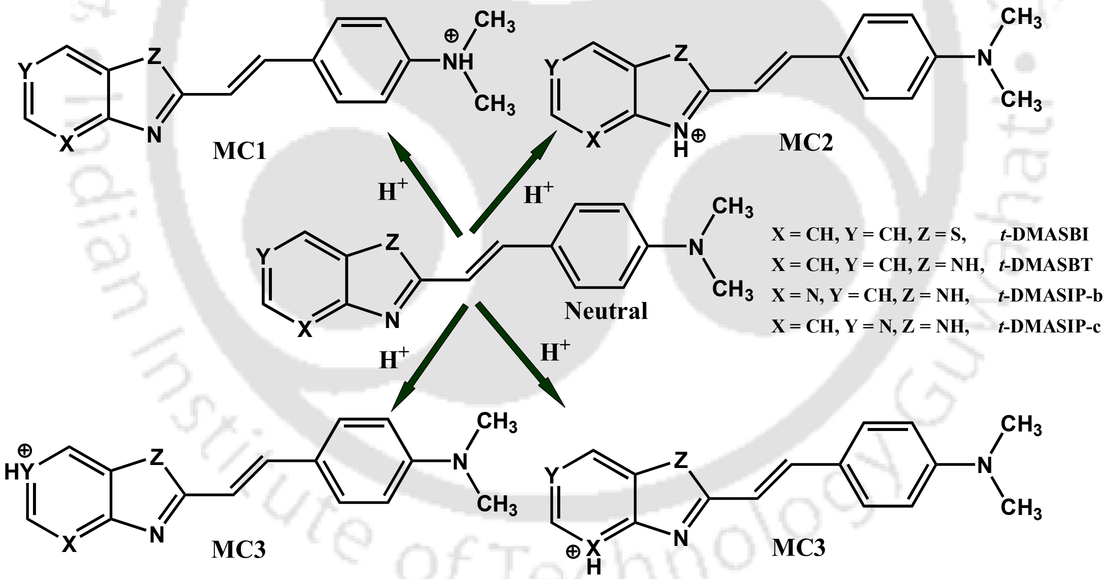

Scheme 8.1. Structures of possible monocations of benzazole and pyridazole derivatives of push-pull styryl compounds.

As mentioned in earlier chapters, it is well established in literature that the protonation of dimethylamino nitrogen causes a blue shift in the spectra with respect to the neutral band, as the lone pair of electrons on that nitrogen is no longer involved in conjugation. In contrast the protonation at electron withdrawing ring nitrogens will increase the conjugation that results in the red shift of the spectra.[82,83,85,205-207] The formation of MC1 produces a blue shift in the absorption and fluorescence spectra. On the other hand MC2 and MC3 causes a red shift in the absorption and fluorescence spectra and bathochromic shift is much more pronounced in MC3 than MC2 due to enhanced conjugation.

8.1.0. Effect of pH on *trans*-2-[4′-(dimethylamino)styryl]benzothiazole in different micelles

t-DMASBT is recommended as a good microsensor to study the biological functions and also biomimetic systems.[154] *t*-DMASBT has been reported to act as an outstanding sensor for a variety of heterogeneous systems.[155,156,343-347] It was used as a surface probe to monitor the premicellar aggregation in SDS, CTAB and TX-100[343] and brijs.[344] Purkayastha et al. used *t*-DMASBT to study the ionic surfactant created at the peripheral of confined water around silver nanoparticle.[156] The reliability of these works depends on the species present under the experimental conditions. Thus, the present study of the prototropic equilibrium of the system in micelles gains further importance.

8.1.1. Effect of sodium dodecyl sulfate (SDS)

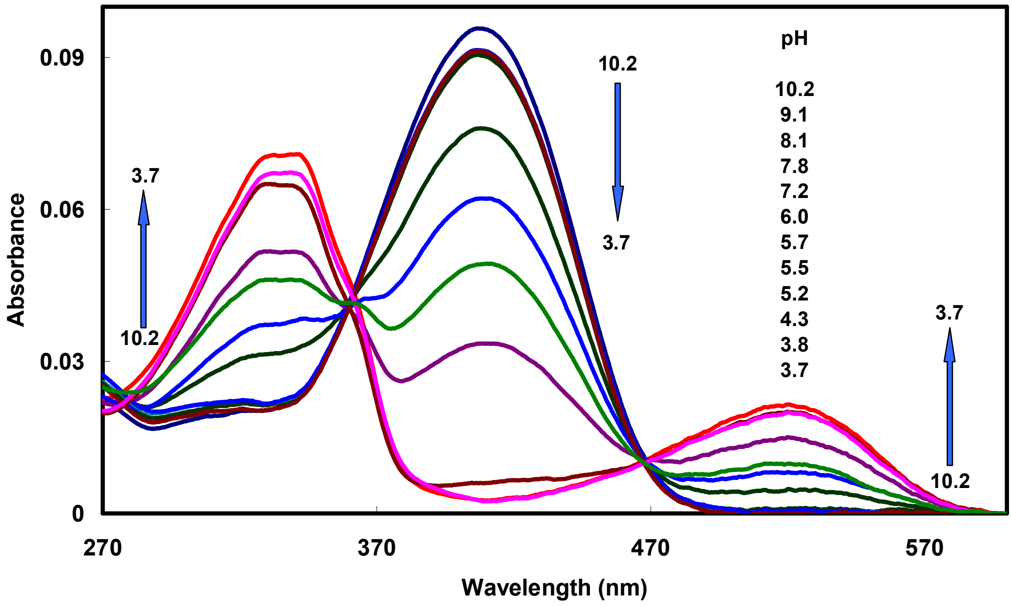

Figure 8.2. Absorption spectra of *t*-DMASBT in SDS at different pH.

In SDS micelle, with increase in acid concentration the absorbance of neutral band at 408 nm decreases and two new bands emerge on either sides of the original band with two quasi-isosbestic points at 360 nm and 467 nm (**Figure 8.2**). These spectral changes indicate that two new species are formed upon decreasing the pH and are in equilibrium with the neutral molecule. At pH ~ 3.7, the molecule completely exists in monocationic form and shows two distinct bands at 334 nm and 521 nm. The results obtained in SDS environment are quite similar with that obtained in aqueous medium.[153] However the pK_a obtained in SDS micelle is 5.5 which is higher than that obtained in aqueous medium (4.8).[153]

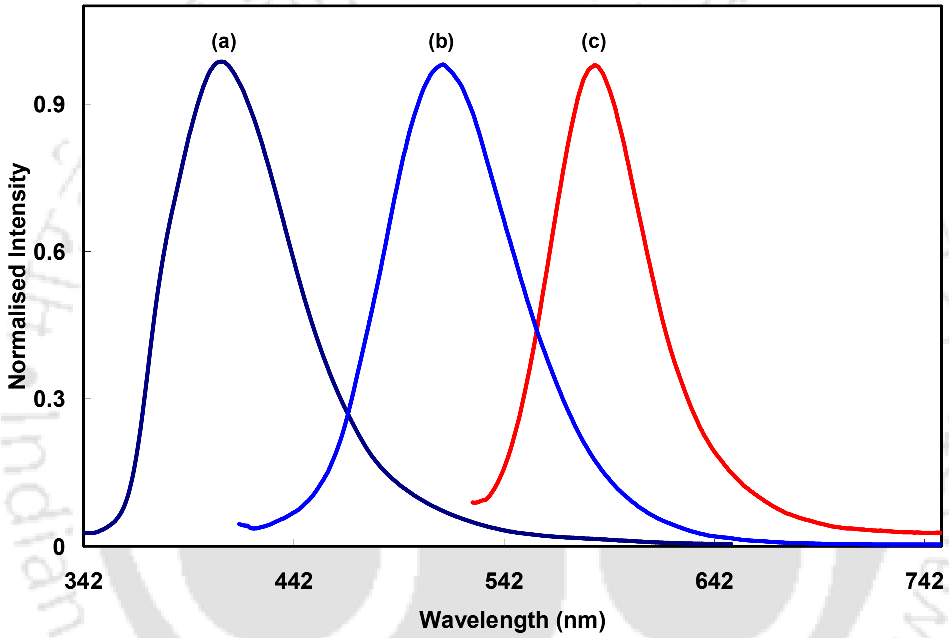

Figure 8.3. Normalised emission spectra of *t*-DMASBT in SDS: (a) MC1 (λ_{exc} = 330 nm), (b) Neutral (λ_{exc} = 408 nm) and (c) MC2 (λ_{exc} = 520 nm).

The emission and excitation spectra were recorded at different wavelengths. When excited at the shorter wavelength isosbestic point (λ_{exc} = 360 nm), at pH 10.2 only one band appears at 513 nm and upon increasing the acid concentration, the intensity of the band decreases and one new band appears at the shorter wavelength side (411 nm) (figure not shown). Similarly; when excited at the red side isosbestic point (λ_{exc} = 467 nm), upon increasing the acid concentration the intensity of the band appears at 513 nm decreases and at the expense, one new band arises at 585 nm (figure not shown). At cationic pH, different excitation and emission spectra were recorded which clearly shows that two different species one emitting at shorter wavelength and the other one at longer wavelength relative to the neutral band are present. The normalized emission spectra for both the cations along with the neutral band are shown in **Figure 8.3**. From the spectral shift, the absorption band at 334 nm and the corresponding emission band at 411 nm can be assigned to MC1 and the absorption band at 521 nm and the corresponding fluorescence band at 585 nm can be assigned to MC2. From the above results and discussions it is inferred that alike in aqueous medium in anionic SDS micelle also dimethylamino nitrogen and azole nitrogen are protonated forming MC1 and MC2, respectively. However the relative ratio of MC2:MC1 obtained from the absorption spectral data in SDS is three times higher than that obtained in aqueous medium (**Table 8.1**). This clearly indicates that SDS micelle enhances the formation of MC2 than water.

Table 8.1. Absorption band maxima (λ_{max}^{ab}, nm) and fluorescence band maxima (λ_{max}^{em}, nm) of neutral and monocationic form of *t*-DMASBT and the absorbance ratio of both the monocations (MC2:MC1).

t- DMASBT	λ_{max}^{ab}			λ_{max}^{em}			MC2:MC1
	N	MC2	MC1	N	MC2	MC1	(Absorbance ratio)
Water[a]	415	455	351	508	549	456	0.09
SDS	408	521	334	513	590	411	0.30
TX-100	410	522	334	513	587	407	0.06
CTAB	413	530	345	524	590	400	0.05

[a] from ref. 153.

8.1.2. Effect of triton X-100 (TX-100)

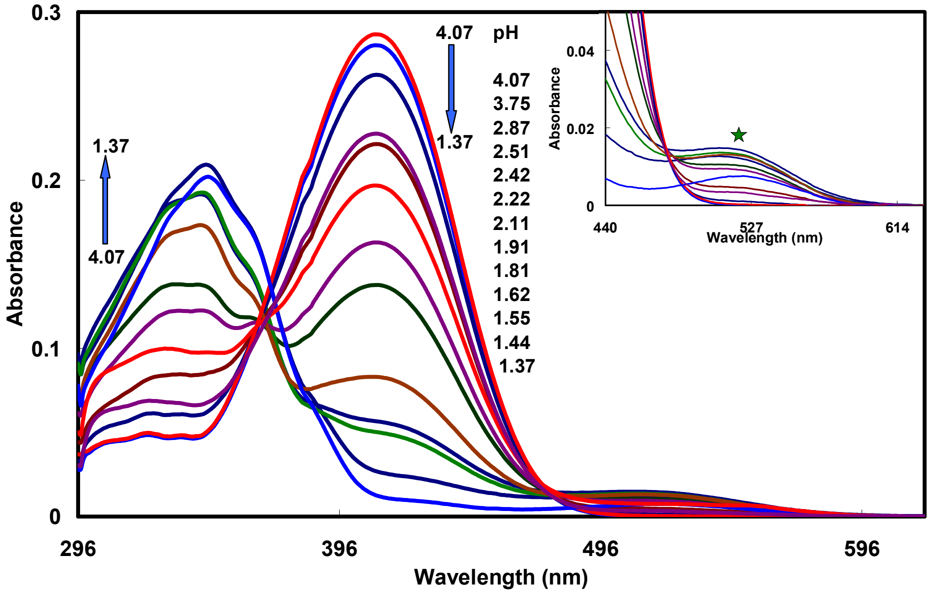

Figure 8.4. Absorption spectra of *t*-DMASBT in TX-100 at different pH (inset shows the magnified band appears at 522 nm).

The effect of pH on absorption spectra of *t*-DMASBT in TX-100 are similar to that in SDS (**Figure 8.4**). Upon increasing the acid concentration the absorbance of the neutral band decreases and bands of MC1 and MC2 starts to appear at both side of the neutral band. Two quasi-isosbestic points are obtained at 368 nm and at 476 nm. However unlike in SDS, the band of MC2 appears at 522 nm is not much prominent and hence the magnified spectra are shown in the inset of **Figure 8.4**. The absorbance ratio of MC2:MC1 obtained in TX-100 is approximately 5 times less than that obtained in SDS micelle. The results show that in TX-100 micelle, the formation of MC2 is higher than water, but less than SDS (**Table 8.1**). The pK_a value for DMASBT in TX-100 micelle is found to be 2.2 which is lesser than that obtained in aqueous medium and in SDS micelle.

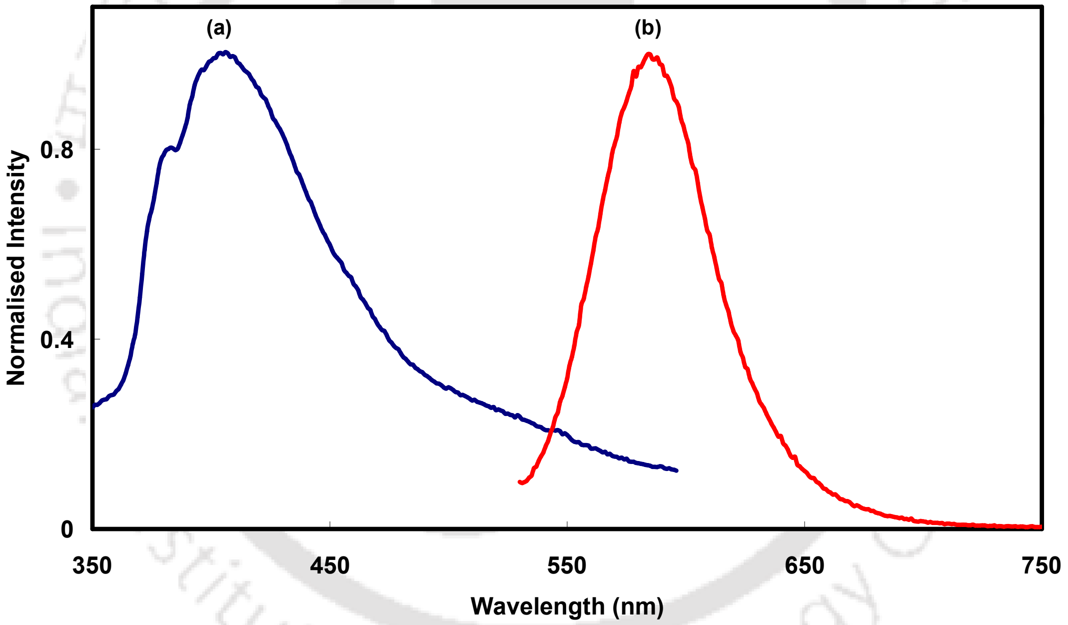

Figure 8.5. Normalised emission spectra of *t*-DMASBT in TX-100 at monocationic pH: (a) MC1 (λ_{exc} = 330 nm) and (b) MC2 (λ_{exc} = 520 nm).

The emission and excitation spectra of *t*-DMASBT at different pH in TX-100 were recorded. Upon exciting at 336 nm, it is observed that at pH 4.09 only single emission is observed at 513 nm and further decreasing the pH results in one new band at 407 nm at the expense of the original band. On the other hand exciting at 409 nm produces only the neutral species band (at 513 nm), but upon increasing the acid concentration, the intensity of the band decreases (figure not shown). However, though upon exciting at 520 nm no emission is observed at pH 4.09, a new band appears at 587 nm and the band intensity increases by increasing the acid concentration. From the above results it is concluded that the absorption band at 344 nm and the corresponding emission band at 407 nm are those of MC1, the absorption band at 410 nm and the corresponding emission band at 513 nm are those of neutral species and the absorption band at 522 nm and the corresponding emission band at 587 nm are those of MC2, respectively. The normalized emission spectra at monocatinic pH are shown in **Figure 8.5**.

8.1.3. Effect of cetyltrimethylammonium bromide (CTAB)

The effect of pH on the absorption spectral characteristics of *t*-DMASBT in CTAB micelle are quite similar to those in TX-100. Therefore, the absorption spectra are not shown. In CTAB micelles also upon increasing the acid concentration, two quasi-isosbestic points are obtained at 369 nm and at 482 nm with two new bands at both the sides of the original band which corresponds to two monocations at lower pH. The absorbance ratio of MC2/MC1 obtained in CTAB is even lesser than that obtained in TX-100 and is approximately 6.2 times less than that obtained in SDS micelle (**Table 8.1**).

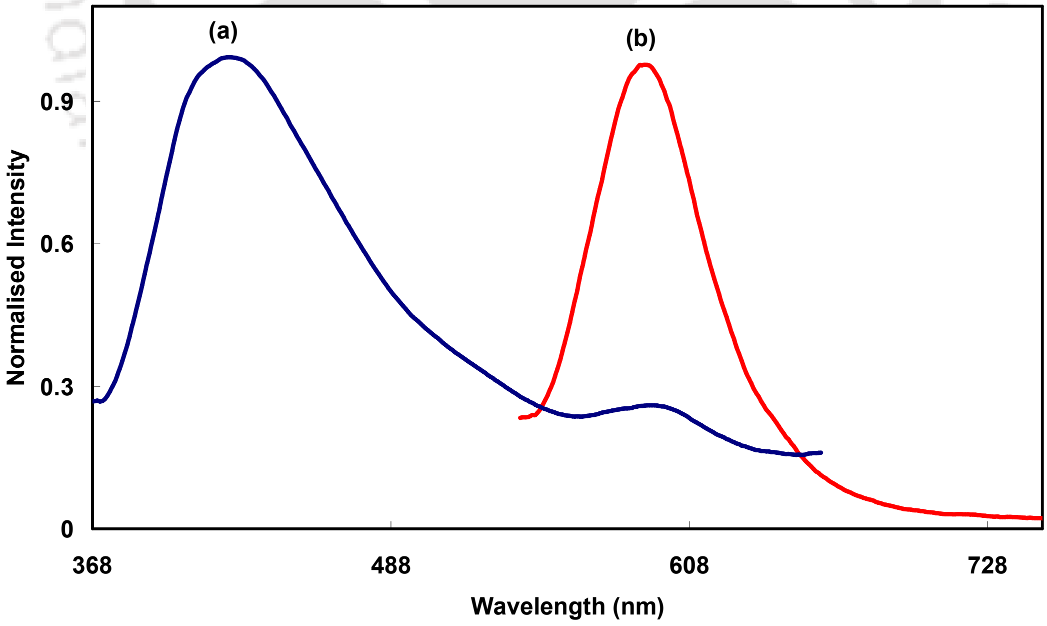

Figure 8.6. Normalised emission spectra of *t*-DMASBT in CTAB at cationic pH: (a) MC1 (λ_{exc} = 355 nm) and (b) MC2 (λ_{exc} = 535 nm).

The fluorescence spectra obtained in CTAB micelle are also quite similar to those obtained in TX-100 micelle and the normalized emission spectra at cationic pH for both the monocations are shown in **Figure 8.6**. This is consistent with the formation of MC1 and MC2.

The above results can be summarized as below: like in aqueous medium in micelles also both MC1 and MC2 are formed in the ground as well as excited states. MC1 dominates over MC2 in all the media. However compared with that in aqueous medium, the relative population of MC2 increases in SDS, but decreases in other two micelles and is least in CTAB. (see **Section 8.5**).

8.2.0. Effect of pH on *trans*-2-[4′-(dimethylamino)styryl]imidazo[4,5-c]pyridine in different micelles

As mentioned earlier, *t*-DMASIP-c also found to form two kinds of monocations in water.[342] But unlike in *t*-DMASBT dimethylamino nitrogen is not protonated on *t*-DMASIP-c to monocation in aqueous medium. The monocation formed are by protonation at azole nitrogen and at pyridyl nitrogen resulting in MC2 and MC3, respectively.

8.2.1. Effect of sodium dodecyl sulfate (SDS)

The absorption spectra of *t*-DMASIP-c in SDS at different pH are depicted in **Figure 8.7**. The band of the neutral species at 380 nm undergoes a bathochromic shift with increase in acid concentration. This suggests the formation of monocation by protonation at the ring nitrogen(s).

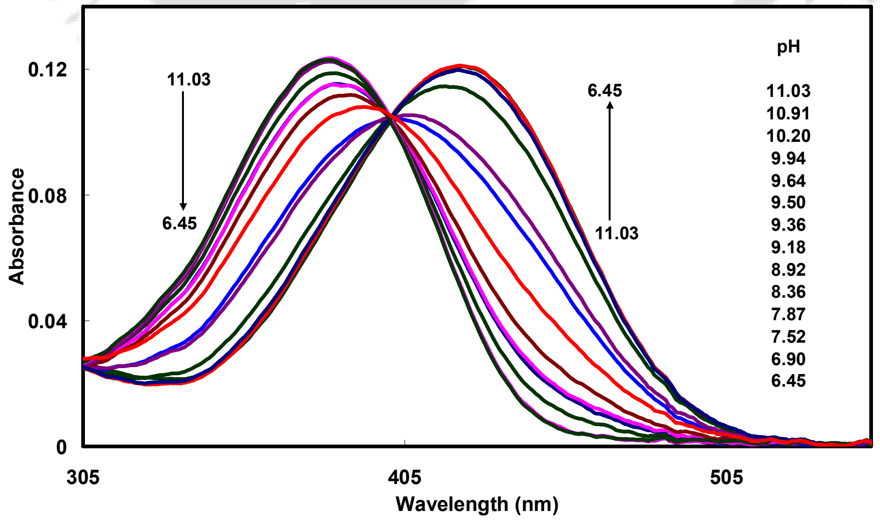

Figure 8.7. Absorption spectra of *t*-DMASIP-c in 50 mM SDS at different pH.

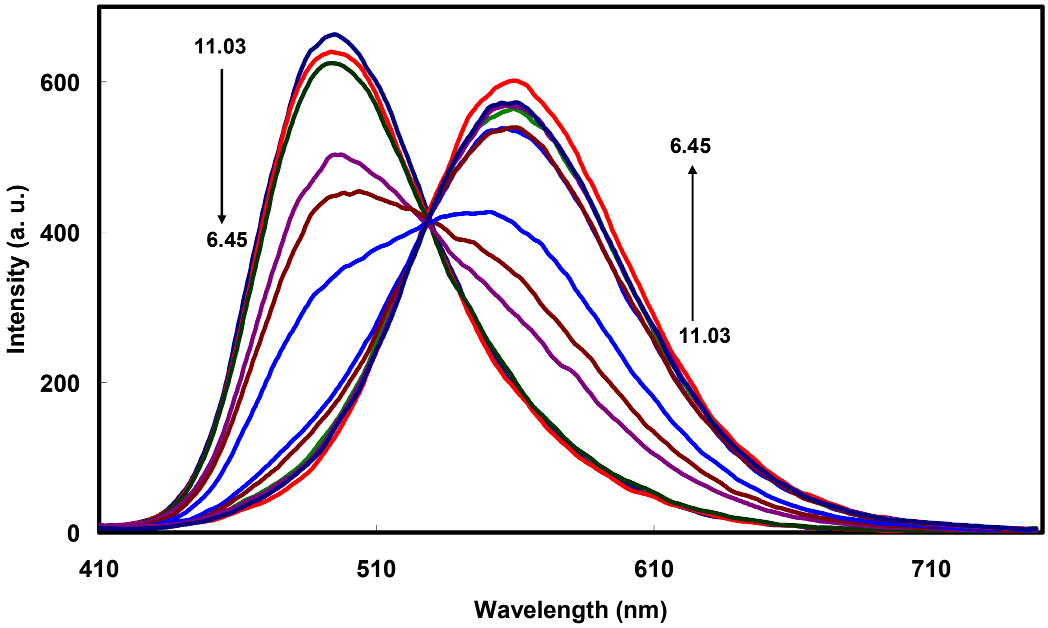

Figure 8.8. Emission spectra of *t*-DMASIP-c in 50 mM SDS at different pH (λ_{exc} = 400 nm).

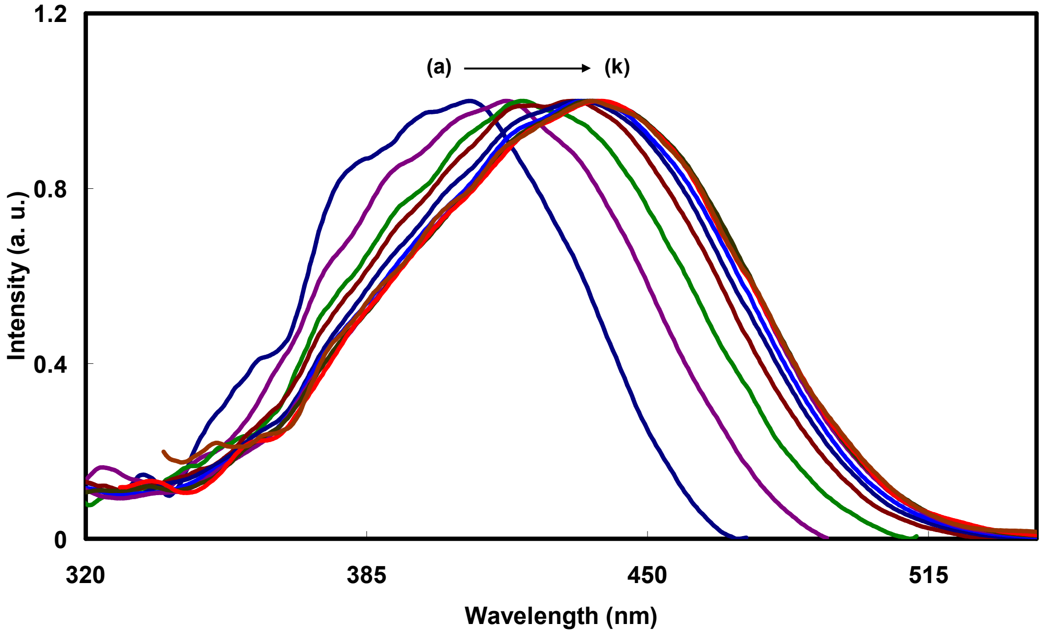

Figure 8.9. Normalised excitation spectra of *t*-DMASIP-c in SDS at cationic pH (7.54): (a) λ_{em} = 480 nm, (b) λ_{em} = 500 nm, (c) λ_{em} = 520 nm, (d) λ_{em} = 540 nm, (e) λ_{em} = 560 nm, (f) λ_{em} = 580 nm, (g) λ_{em} = 600 nm, (h) λ_{em} = 620 nm, (i) λ_{em} = 640 nm, (j) λ_{em} = 660 nm and (k) λ_{em} = 680 nm.

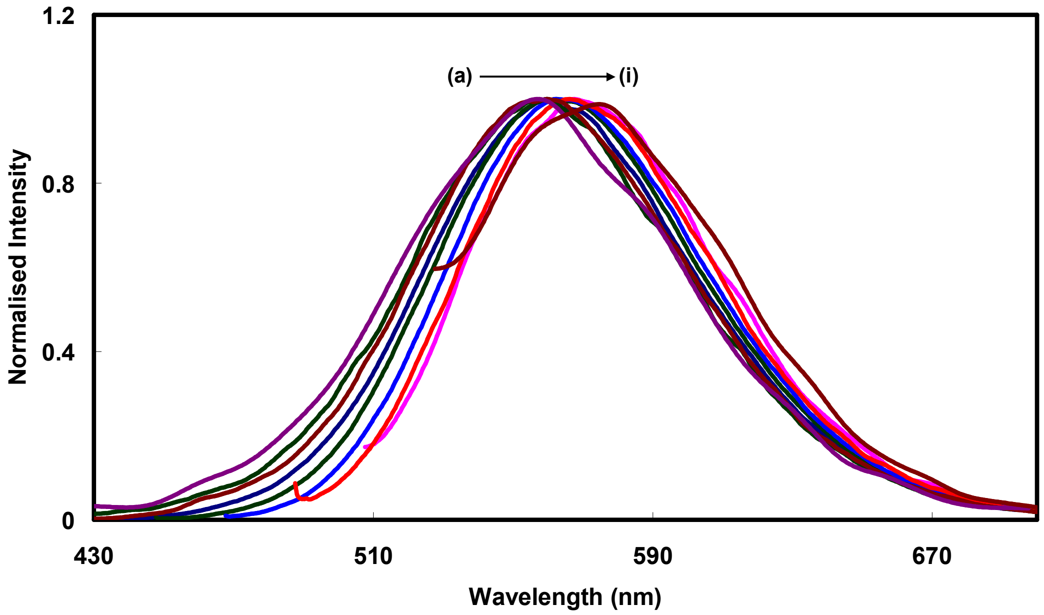

Figure 8.10. Normalised emission spectra of *t*-DMASIP-c in SDS at cationic pH (7.54). (a) λ_{exc} = 360 nm, (b) λ_{exc} = 380 nm, (c) λ_{exc} = 405 nm, (d) λ_{exc} = 422 nm, (e) λ_{exc} = 440 nm, (f) λ_{exc} = 460 nm, (g) λ_{exc} = 480 nm, (h) λ_{exc} = 500 nm and (i) λ_{exc} = 520 nm.

The fluorescence emission spectrum (λ_{exc} = 400 nm) of neutral species at 495 nm slowly diminishes with emergence of a red shifted band at 562 nm and the intensity increases with increase in acid concentration (**Figure 8.8**). At pH 7.52, the 495 nm band completely vanishes. As both absorption and emission spectra are red shifted corresponding to the neutral species, it can be concluded that in SDS micelle protonation takes place at the ring nitrogen(s). The excitation and emission spectra at monocationic pH were recorded at different emission and excitation wavelengths. The normalised excitation and emission spectra of *t*-DMASIP-c at pH 7.52 in SDS micelle are shown in **Figure 8.9** and **Figure 8.10**, respectively. The emission spectrum shifts bathochromically (35 nm) when the excitation wavelength is shifted to longer wavelengths. Similarly, the excitation spectrum also shifted towards longer wavelength when monitored at longer wavelength. This illustrates the presence of more than one kind of monocation. Since all the spectra are red shifted with respect to those of neutral species, it clearly indicates the formation of two kinds of monocations and they are formed by the protonation of azole nitrogen and pyridyl nitrogen. In other words, both MC2 and MC3 are formed in SDS micelles.

8.2.2. Effect of triton X-100 (TX-100)

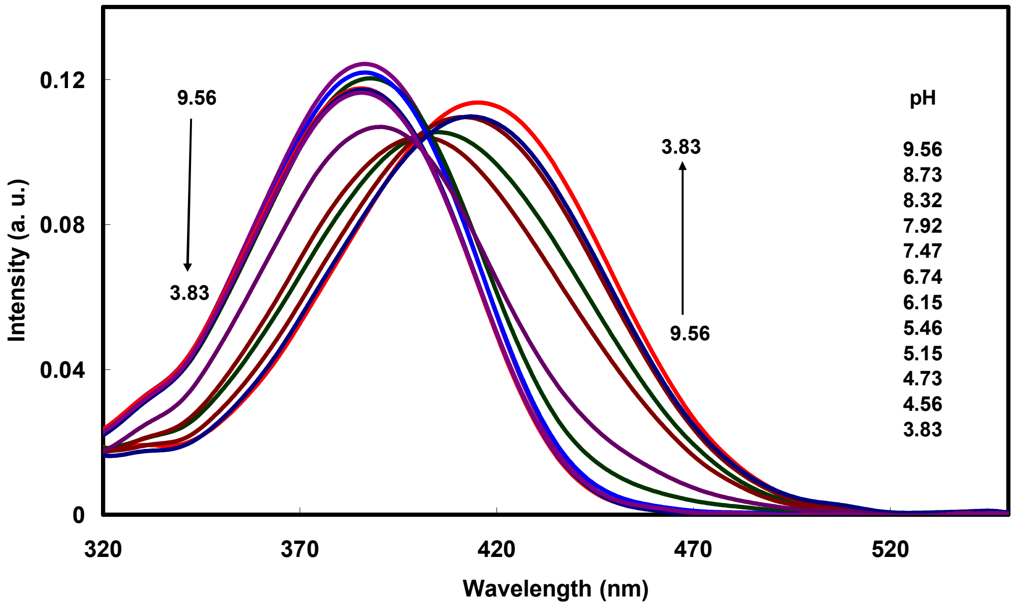

Figure 8.11. Absorption spectra of *t*-DMASIP-c in TX-100 at different pH.

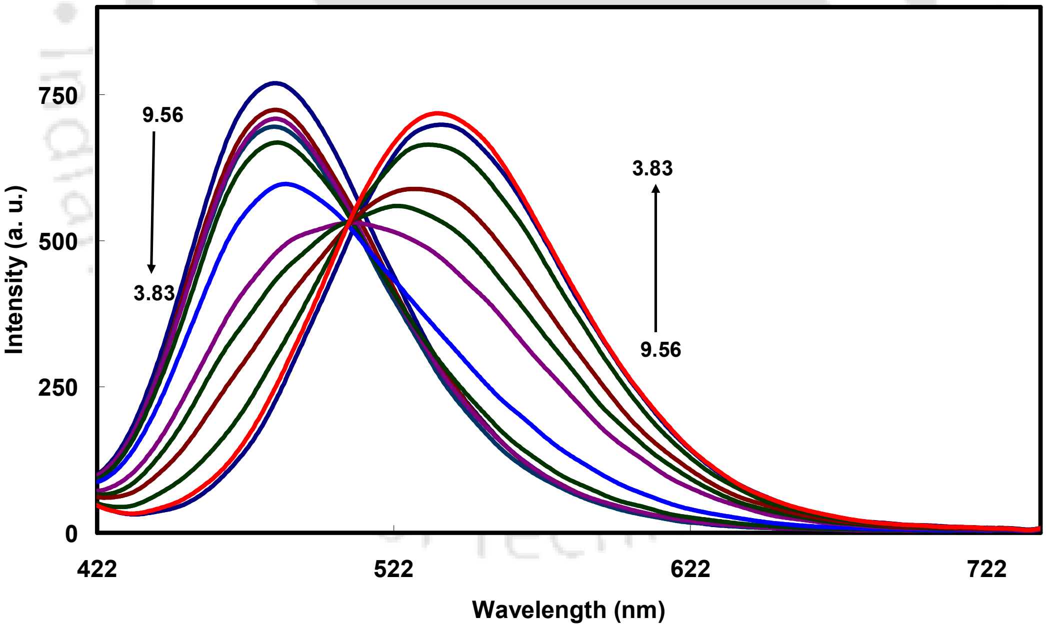

Figure 8.12. Emission spectra of *t*-DMASIP-c in TX-100 at different pH (λ_{exc} = 402 nm).

The effect of pH on the absorption spectrum of *t*-DMASIP-c in TX-100 is presented in **Figure 8.11**. Same as in SDS, in TX-100 upon increasing the acid concentration the absorbance of the neutral band decreases and a new band arises at the red side of the band of neutral species with a quasi-isosbestic point at 402 nm. The effects on the fluorescence spectra of the molecule in TX-100 are also as same as that in SDS. On exciting at the quasi isosbestic point (λ_{exc} = 402 nm), the fluorescence intensity of the neutral species decreases with the formation of a new band at longer wavelength with a quasi-isoemissive point (**Figure 8.12**). The fluorescence excitation and emission spectra of the fluorophore at cationic pH also undergo bathochromic shift when monitored and excited at longer wavelengths, respectively. From these spectral characteristics it can be inferred in TX-100 also both MC2 and MC3 formed and formation of MC1 is ruled out.

8.2.3. Effect of cetyltrimethylammonium bromide (CTAB)

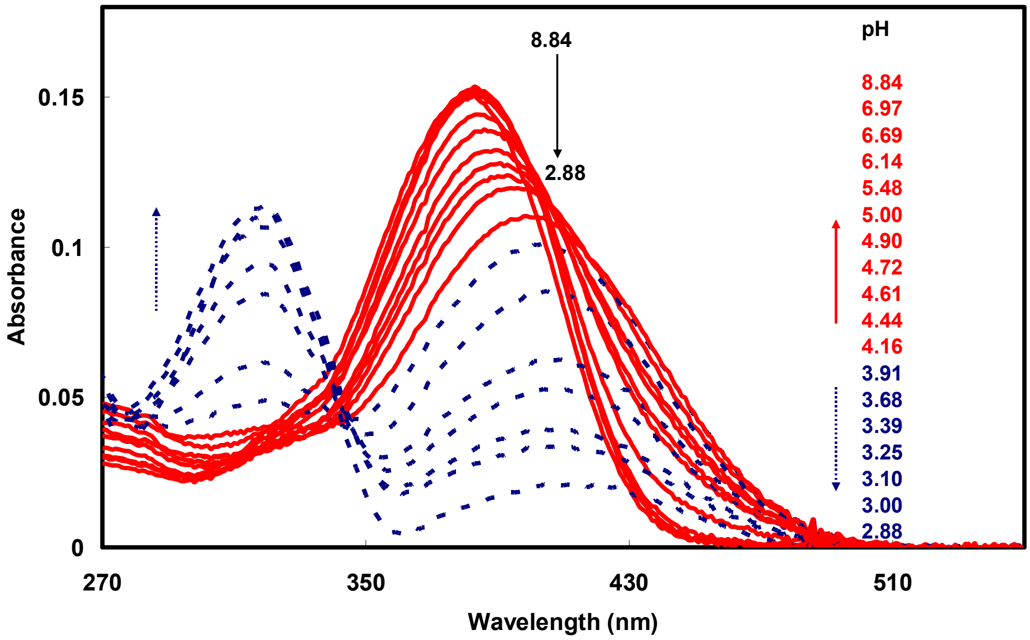

Figure 8.13. Absorption spectra of *t*-DMASIP-c in CTAB at different pH.

The prototropic equilibrium of *t*-DMASIP-c in CTAB micelle is quite different from other micelles and also different from the results obtained for *t*-DMASBT in CTAB. The effect of pH on the absorption spectra of *t*-DMASIP-c is shown in **Figure 8.13**. At pH 8.84 only one band is observed at 383 nm. Upon increasing the acid concentration the absorbance of the neutral band decrease with a bathochromic shift and a weak band appears at the red side of the neutral species band and the absorbance increases up to pH 4.16. However, upon further decrease in pH, before complete conversion of neutral species to monocation, the absorbance of the red shifted band decreases and a new band starts to appear at shorter wavelength at 319 nm. The band is also blue shifted relative to the band of neutral species. Initial red shift shows the formation of monocation due to protonation of ring nitrogen(s). The blue shift indicates the formation of dication due to the protonation of dimethylamino group of the initially formed monocation. The absorption spectral changes suggest the shifting away from neutral-monocation equilibrium towards formation of dication before the completion of monocation. The changes in the fluorescence spectra are also substantiate this premature shifting of neutral-monocation equilibrium towards monocation-dication equilibrium.

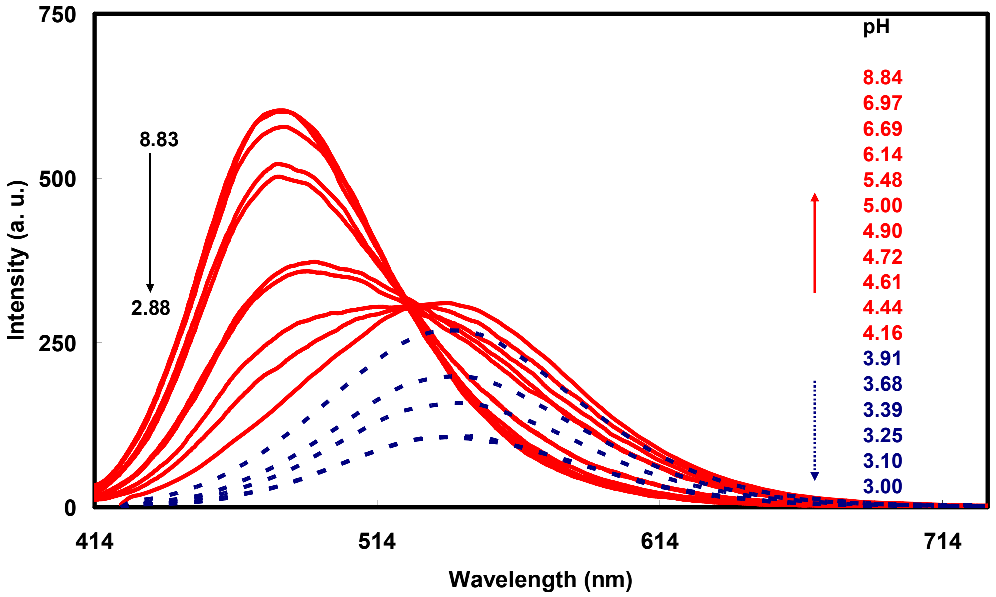

Figure 8.14. Emission spectra of *t*-DMASIP-c in CTAB at different pH by exciting at the red side isosbestic point (λ_{exc} = 405 nm).

The fluorescence spectra obtained by exciting at 405 nm are depicted in **Figure 8.14**. At pH 8.84 a single band is observed at 479 nm and upon increasing the acid concentration the intensity of the band decreases and a new band starts to appear at 542 nm and it gains intensity till pH 4.16 (solid lines in **Figure 8.14**), but decreases with further decrease in pH (dotted lines in **Figure 8.14**). The characteristics of the fluorescence spectra are also consistent with the absorption spectra that the existence of neutral-monocation equilibrium till pH 4.16 and drifting away from the equilibrium for further decrease in pH. Thus, it is clear that unlike in other micelles and in aqueous medium, in CTAB micelles dication starts to appear before the completion of monocation formation. To confirm the formation of more than one monocation, excitation and emission spectra are recorded at different wavelengths. The excitation spectral shift occurs from 412 nm to 430 nm and the emission spectral shift occurs from 533 nm to 564 nm. These results indicate that both MC3 and MC2 are formed (normalised emission spectra are shown in **Figure 8.15**).

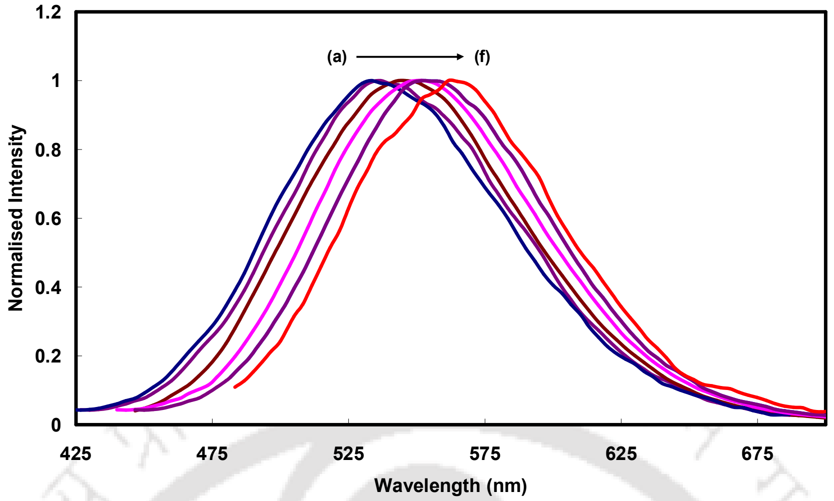

Figure 8.15. Normalised emission spectra of *t*-DMASIP-c in CTAB at cationic pH (pH 3.0). (a) λ_{exc} = 383 nm, (b) λ_{exc} = 405 nm, (c) λ_{exc} = 425 nm, (d) λ_{exc} = 444 nm, (e) λ_{exc} = 465 nm and (f) λ_{exc} = 480 nm.

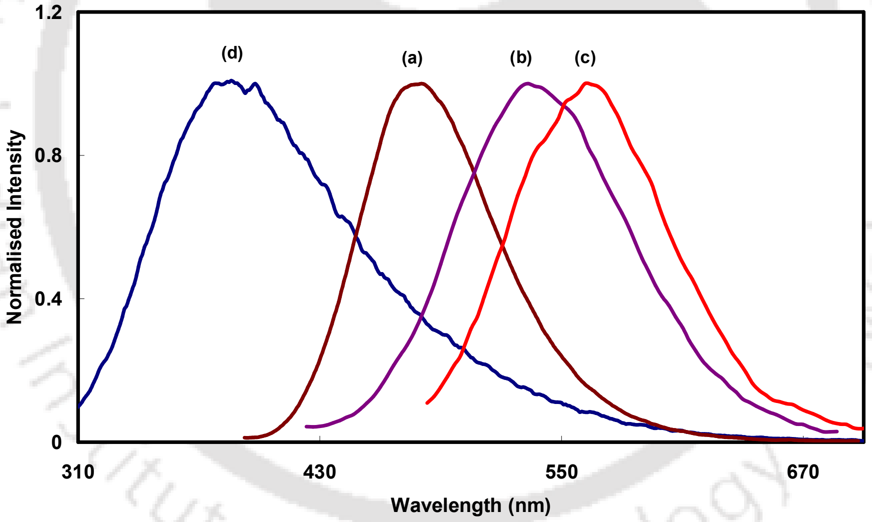

Figure 8.16. Normalised emission spectra of *t*-DMASIP-c in (a) neutral, (b) MC2, (c) MC3 and (d) dicationic form in CTAB.

Table 8.2. Absorption band maxima (λ_{max}^{ab}, nm), fluorescence band maxima (λ_{max}^{em}, nm) of neutral and monocationic form of *t*-DMASIP-c in micelles (the values in aqueous medium are given for comparison).

Medium	λ_{max}^{ab}		λ_{max}^{em}	
	N	MC	N	MC
Water[1]	368	405	512	580
SDS	380	424	495	562
TX-100	386	418	483	542
CTAB	383	438	479	542

[1] from ref 342.

The normalised fluorescence spectra of all the species are shown in **Figure 8.16** and the absorption and fluorescence maxima of all the species are compiled in **Table 8.2**. In summary, alike in aqueous medium, *t*-DMASIP-c forms two monocations by protonation of ring nitrogens (MC2 and MC3) in all the micelles. Unlike in other micelles, in CTAB, dication formation starts before the completion of monocation, whereas, in SDS and TX-100 monocation formation is completed.

8.3.0. Effect of pH on *trans*-2-[4′-(dimethylamino)styryl]imidazo[4,5-b]pyridine in different micelles

Alike *t*-DMASIP-c, *t*-DMASIP-b also has three basic centers. The prototropic equilibrium of *t*-DMASIP-b in aqueous medium is described in **Section 4.7**. It is reported that *t*-DMASIP-b forms two kinds of monocations MC2 and MC3; and MC1 is not formed in the aqueous medium.

8.3.1. Effect of sodium dodecyl sulfate (SDS)

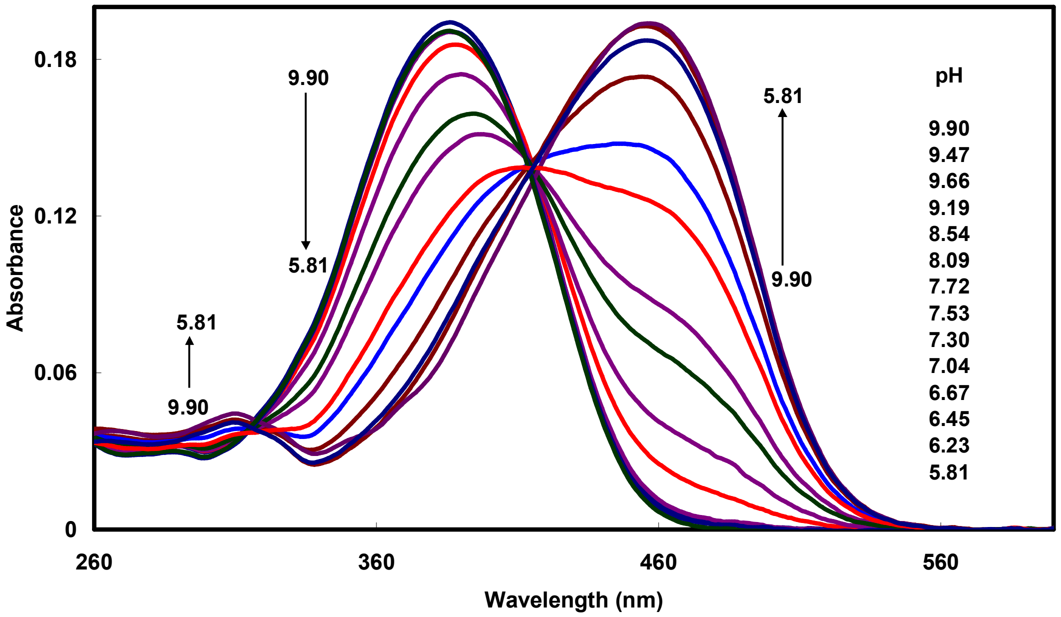

Figure 8.17. Absorption spectra of *t*-DMASIP-b in SDS at different pH.

The absorption spectra of *t*-DMASIP-b in SDS micelle at various pH are shown in **Figure 8.17**. At pH 9.90 only one band is obtained at 385 nm and upon increasing the acid concentration the absorbance of the original band decreases and two new bands appear at both sides (308 nm and 458 nm) of the neutral band with appearance of two quasi-isosbestic points at 317 nm and 415 nm. This indicates that in the ground state more than one new species are formed. However the absorbance of the shorter wavelength band is very less.

Upon exciting at 385 nm, the intensity of the neutral band at 508 nm decreases with increase in acid concentration and two new bands appear on both side of the neutral band (**Figure 8.18**). The band emerges at the shorter wavelength is weak compared to that appears at longer wavelength. The presence of blue shifted absorption and emission bands clearly indicate the dimethylamino nitrogen is protonated. Thus, unlike in aqueous medium MC1 is formed in SDS. Like in aqueous medium (**Section 4.7**), the emission spectra of *t*-DMASIP-b in SDS at cationic pH undergo bathochromic shift upon excitation at longer wavelength (figure not shown). This suggests the existence of more than one kind of red shifted monocation i.e. MC2 and MC3. However, unlike water all three monocations MC1, MC2 and MC3 are coexisting in SDS.

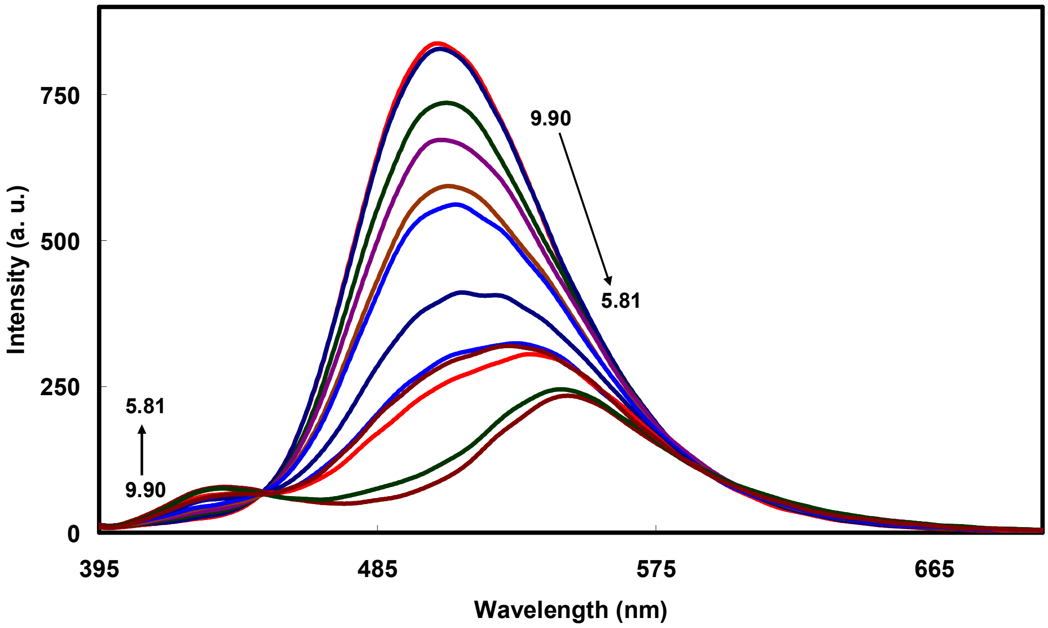

Figure 8.18. Emission spectra of *t*-DMASIP-b in SDS at different pH (λ_{exc} = 385 nm).

8.3.2. Effect of triton X-100 (TX-100)

The absorption spectra of *t*-DMASIP-b in TX-100 by varying pH are shown in **Figure 8.19**. The results obtained in TX-100 for *t*-DMASIP-b are different from that in SDS, but similar to those obtained for *t*-DMASIP-c in TX-100 micelles. i.e.

bathochromically shifted broad band is found upon addition of acid and it gains absorbance with decrease in pH with appearance of a quasi-isosbestic point.

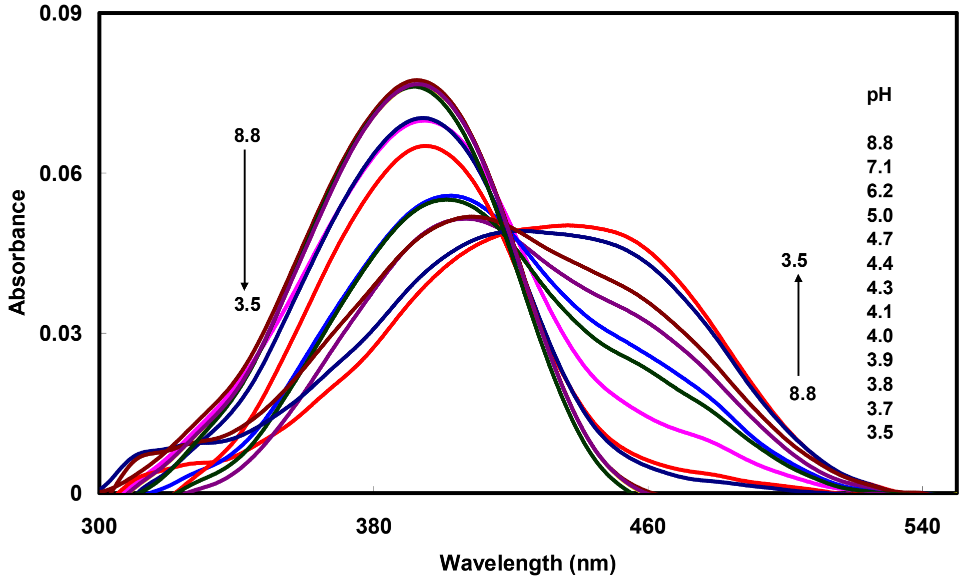

Figure 8.19. Absorption spectra of *t*-DMASIP-b in TX-100 at different pH.

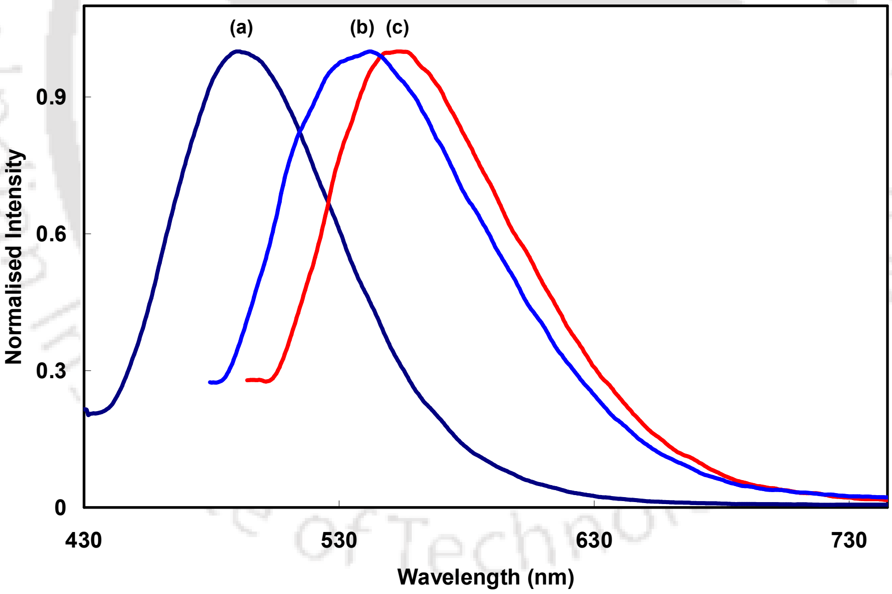

Figure 8.20. Normalised emission spectra of different species of *t*-DMASIP-b: (a) neutral, (b) MC2 and (c) MC3 in TX-100.

Upon exciting at the quasi-isosbestic point a band appears at 493 nm and by increasing the acid concentration the intensity of the band decreases with appearance of a new band at 550 nm with a quasi-isoemissive point. The emission and excitation spectra at the cationic pH suggest that both MC2 and MC3 are formed. The fluorescence spectra of different species are depicted in **Figure 8.20**.

8.3.3. Effect of cetyltrimethylammonium bromide (CTAB)

The absorption spectral changes of *t*-DMASIP-b in CTAB micelle at various pH are similar to those obtained for *t*-DMASIP-c in CTAB (**Figure 8.21**). i.e. the monocations are formed initial decrease in pH, but upon further lowering the pH, the formation of dication starts before completion of monocation formation.

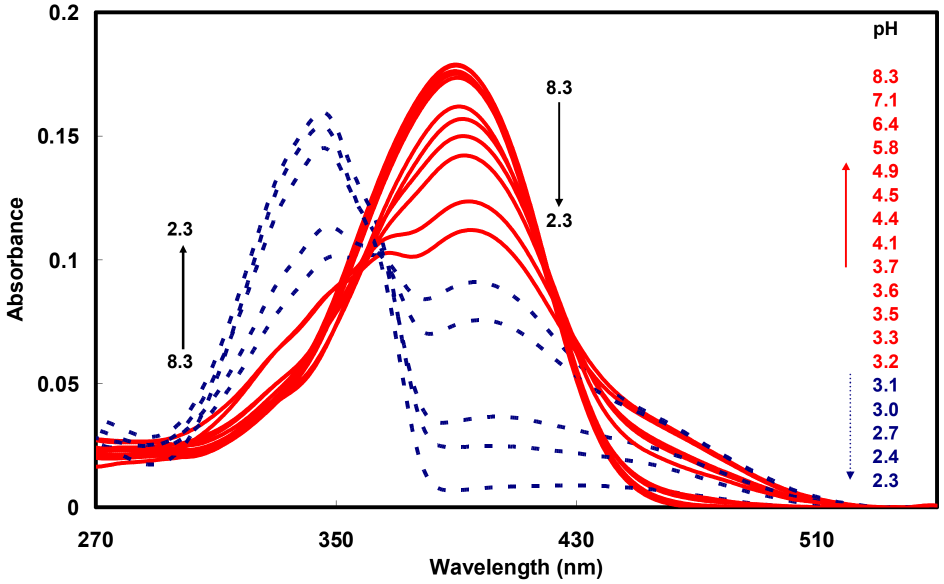

Figure 8.21. Absorption spectra of *t*-DMASIP-b in CTAB at different pH.

The emission and excitation spectral changes of *t*-DMASIP-b are in consistent with this observation. Alike *t*-DMASIP-c, *t*-DMASIP-b also forms MC2 and MC3 in CTAB. The emission spectra of different species are presented in **Figure 8.22**.

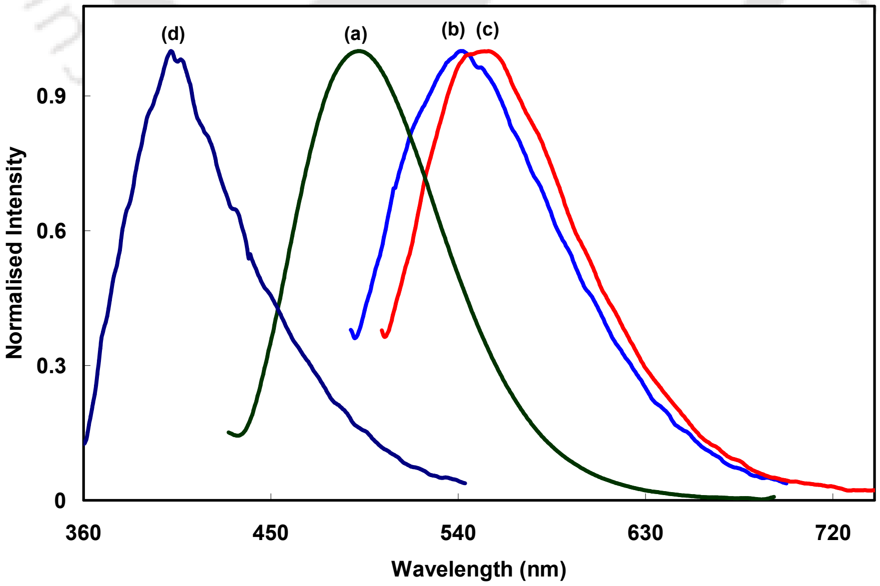

Figure 8.22. Normalised emission spectra of *t*-DMASIP-b in (a) neutral and monocationic ((b) MC2 and (c) MC3) and (d) dicationic forms in TX-100.

Table 8.3. Absorption band maxima (λ_{max}^{ab}, nm) and emission band maxima (λ_{max}^{em}, nm) of neutral and monocationic forms of *t*-DMASIP-b in the micellar media and the corresponding data of aqueous medium is given for comparison.

Medium	λ_{max}^{ab}		λ_{max}^{em}	
	N	**MC**	**N**	**MC**
Water	374	436	525	544
SDS	385	308, 458	508	430, 550
TX-100	393	455	490	550
CTAB	391	464	493	550

In summary, unlike in aqueous medium protonation takes places in all three basic center of *t*-DMASIP-b forms MC1, MC2 and MC3 in SDS. However, in TX-100 and CTAB only MC2 and MC3 are formed. Like in *t*-DMASIP-c, *t*-DMASIP-b dication starts to appear before the completion of monocations formation. The monocation formations in all three micelles are summarized in **Table 8.4**.

Table 8.4. Overview of formation of monocations in aqueous medium and in different micellar environments.

Medium	*t*-DMASBT		*t*-DMASIP-c			*t*-DMASIP-b		
	MC1	**MC2**	**MC1**	**MC2**	**MC3**	**MC1**	**MC2**	**MC3**
Water	Yes	Yes	No	Yes	Yes	No	Yes	Yes
SDS	Yes	Yes	No	Yes	Yes	Yes	Yes	Yes
TX-100	Yes	Yes	No	Yes	Yes	No	Yes	Yes
CTAB	Yes	Yes	No	Yes	Yes	No	Yes	Yes

8.4. The effect of micelles on pK_a

The pK_a values for neutral-monocation equilibrium in the ground state and the excited state of all three molecules in all the micelles are calculated and compiled in **Table 8.5** along with the pK_a value in aqueous medium. The observation of MC1 and MC2 in *t*-DMASBT and MC2 and MC3 in *t*-DMASIP-b and *t*-DMASIP-c can be explained as follows. Due to charge flow from dimethylamino group to heterocyclic ring the electron density on dimethylamino nitrogen decreases and that on heterocyclic nitrogen(s) increases. Hence, the protonation at heterocyclic ring nitrogen(s) becomes more probable than at dimethylamino nitrogen. This is supported by the fact that only azole nitrogen is protonated to form MC2 in benzimidazole analogue, *t*-DMASBI.[341] Therefore, only heterocyclic ring nitrogens are protonated on *t*-DMASIP-b and *t*-DMASIP-c to form MC2 and MC3. The difference in behavior of *t*-DMASIP-b in SDS is due to anionic micelles effect and is discussed in next section. On the other hand in *t*-DMASBT, the >NH group is replaced with sulfur which has dorbitals pull the charge towards itself, as a consequence, the charge density on the azole nitrogen decreases. Hence, both dimethylamino and azole nitrogens are protonated to form MC1 and MC2. The lower pK_a of thiazole dyes compared to that of imidazole analogues substantiates it.

Table 8.5. Ground state and excited state pK_a values of *t*-DMASBT, *t*-DMASIP-c and *t*-DMASIP-b in water and micelles.

Molecules	Water		SDS		TX-100		CTAB	
	pK_a	pK_a^*	pK_a	pK_a^*	pK_a	pK_a^*	pK_a	pK_a^*
t-DMASBT[a]	4.8	8.5 (-1.7)	5.5	13.3(-5.3)	2.2	9.8 (-9.0)	1.5	8.8 (-10.1)
t-DMASIP-c	6.9	11.1	9.2	14.6	5.7	10.3	5.0	10.9
t-DMASIP-b	5.2	8.3	7.3	12.5	4.1	9.8	3.4	9.4

[a] in parenthesis indicates the pK_a^* value for MC1

The apparent pK_a value obtained in different media are in the order SDS > water > TX-100 > CTAB and are consistent with the results obtained for other dyes.[85,175,231,338,348] This can be explained by pseudo-phase ion-exchange (PIE) model.[85,231,232] According to the model, the apparent pK_a values of the acids increase in the anionic micelles and decrease in the cationic micelles compared to those in aqueous medium. The decrease in apparent pK_a value in nonionic micelle TX-100 has been ascribed to the smaller effective dielectric constant of the micelles compared to water.[85,175,338,348] Due to cationic head group in CTAB micelles, the positively charged protons are repelled to the aqueous phase and that also contribute to the decrease in apparent pK_a.

On the basis of the PIE model, in anionic micelle the protons and the cations are likely to concentrate in the Stern layer and hence suppress the release of protons from the molecule, ensuing in an increase in apparent pK_a of the equilibrium. However, the apparent increase in pK_a value of the present dyes can not be explained merely by involving the dielectric constant and the surface potential. The distribution of the neutral and cationic species in the aqueous phase and in the micellar phase also plays a major role.[349] To understand whether the increase in apparent pK_a is because of change in dielectric constant and potential (ψ_0) at the surface or any other factor also play some role, the following equation is used.[350]

$$pK_a^{obs} = pK_a^{i} - (e\psi_0 / 2.303k_bT) \qquad \textbf{(8.1)}$$

where pK_a^{obs} and pK_a^{i} are the apparent pK_a value at the charged surface and for the interface when surface potential is zero respectively and e, k_b, and T are charge on the electron, Boltzmann constant and temperature in Kelvin, respectively. Considering the highest value of surface potential as -140 mV for SDS,[348,349] pK_a^i as the apparent pK_a obtained in TX-100, the pK_a^{obs} in SDS are calculated and compiled in **Table 8.6**. The difference in the apparent pK_a values obtained in SDS micelle and the value predicted by PIE model for all the three molecules are complied in **Table 8.6**. The different in pK_a suggests that apart from dielectric constant and electrostatic potential, some specific interactions also exist between the dye and the surfactant. Same behavior for other imidazole derivatives in SDS micelle is reported in literature.[85,175,338,348,349]

Table 8.6. Observed p*K*a values in SDS, p*K*a value calculated using PIE model and the difference in p*K*a of *t*-DMASBT, *t*-DMASIP-c and *t*-DMASIP-b.

Molecules	SDS (pK_a)	PIE model (pK_a)	Difference (pK_a)
t-DMASBT	5.5	4.6	0.9
t-DMASIP-c	9.2	8.1	1.1
t-DMASIP-b	7.3	6.5	0.8

The excited state pK_a (pK_a^*) for neutral-monocation equilibrium were calculated using Forster cycle method (**Table 8.5**).[351] Same as in the ground state the pK_a^* obtained for *t*-DMASIP-c is highest. The positive value of pK_a^* are obtained for the ring nitrogen(s) protonation in all the three molecules in all media including water. This suggests that the basicity of the ring nitrogen(s) of these molecules increases in the excited state due to more charge flow from the dimethylamino group. This is also supported by the negative value of the pK_a^* obtained for the protonation of dimethylamino nitrogen of *t*-DMASBT (**Table 8.5**). In other words, MC1 will be a stronger acid in the excited state than in the ground state.

8.5. Orientation of the fluorophore inside the micelles

The present studies revealed that the micelles not only affect the pK_a but also the site of protonation on the dyes. The location and orientation of the dye is primary responsible for this difference in behavior. Protonation occurs on all the dyes in all three micelles. This indicates that the dyes are located near water accessible stern layer but not deeper inside the hydrophobic core of the micelles. It also appears that the heterocyclic ring is present inside the micelles near the stern layer and the dimethylamino group is projected towards the aqueous phase (**Figure 8. 23**).

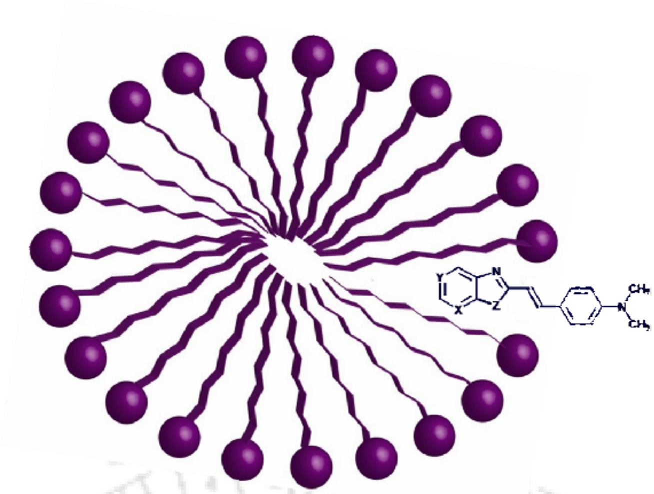

Figure 8.23. Orientation of the fluorophore inside the micelles.

The relative population of MC2 of *t*-DMASBT is less than its MC1 in all environments and this is due to presence of sulfur atom as explained earlier. Compared to those in aqueous medium, the relative population of MC2 increases in SDS and decreases in other two micelles. Since, SDS is anionic micelles it attracts the positively charged protons and it is also responsible for the increase in pK_a value of the dyes as explained in previous section. The azole nitrogen is present in the stern layer. Therefore, formation of MC2 in SDS is more favored in compared to all other micelles and water. However, in general the cation penetration is less in micelles due to hydrophobicity of the environment as a result protonation of azole nitrogen decreases in other micelles. In CTAB, protonation of the azole nitrogen becomes much more difficult owing to repulsion of proton by the positively charged trimethyl ammonium cation.

As mentioned earlier, the protonation of pyridyl nitrogen produces greater red shift than the protonation of azole nitrogen. Since, the fluorescence spectra of both MC2 and MC3 are bathochromically shifted and are not resolved; it is difficult to find the relative population of monocatonic form of *t*-DMASIP-c and *t*-DMASIP-b. Upon monocation formation, the bathochromic shift in the absorption spectra is higher in *t*-DMASIP-b (**Table 8.3**) than in *t*-DMASIP-c (**Table 8.2**). It appears that the relative protonation of pyridyl nitrogen over azole nitrogen is more for *t*-DMASIP-b than *t*-DMASIP-c. The occurrence of dication before completion of monocation in CTAB is again due to repulsion of proton by the positively charged polar head group. Since the heterocyclic ring is present inside the micelle, it is very difficult to protonate them.

Therefore, higher acid concentration is required which is sufficient to protonate the dimethylamino nitrogen of the monocation which is projected in the aqueous phase. This results in dication formation. The dimethylamino nitrogen of *t*-DMASIP-b is protonated only in SDS to form monocation, because of the anonic nature of the micelle. This makes it easy to protonate the dye. No such protonation of dimethylamino nitrogen occurs on *t*-DMASIP-c and this can be explained as follows. Due to charge flow from dimethylamino nitrogen, the charge on the dimethylamino nitrogen decreases therefore requires a higher concentration of acid to protonate the amino nitrogen. The protonation of *t*-DMASIP-c occurs at comparatively lower concentration of acid which is not sufficient to protonate the dimethylamino nitrogen. On the other hand the protonation of *t*-DMASIP-b and *t*-DMASBT occurs at relatively lower pH. This hypothesis is supported by the higher pK_a of *t*-DMASIP-c than *t*-DMASIP-b and *t*-DMASBT.

8.6. Conclusion

The effects of anionic, cationic and nonionic micelles on the prototropic equilibriums of *t*-DMASBT, *t*-DMASIP-b and *t*-DMASIP-c were studied. In *t*-DMASBT, alike in aqueous medium in micelle also the azole nitrogen and the dimethylamino nitrogen are protonated to form both MC1 and MC2. Though, same as in water the relative population of MC1 is higher than MC2 in micelles also, their relative ratio varies with nature of the micelle. The relative population of MC2 increases in anionic micelles compared to that in water. On the other hand it decreases in nonionic and cationic micelles. Same as in water, only the ring nitrogens of imidazopyridine derivatives (*t*-DMASIP-b and *t*-DMASIP-c) are protonated to form monocations in micelles except on *t*-DMASIP-b in SDS micelle which forms MC1 in addition to MC2 and MC3. The relative populations of MC2 and MC3 depend on the position of the pyridyl nitrogen and the relative population of MC3 is more in *t*-DMASIP-b than in *t*-DMASIP-c. The monocation formations of imidazopyridine derivatives are completed before further protonation in anionic and nonionic micelles, but not completed in cationic micelle due to repulsion of proton by the cationic head group. Therefore, the dimethylamino nitrogen of monocationic form of *t*-DMASIP-b and *t*-DMASIP-c are also protonated to form dications before the completion of monocation formation. This is attributed to the orientation of the fluorophores inside the micelles. All the fluorophores have same orientation inside the micelles. The heterocyclic ring projects towards the micellar core and the dimethylamino group projects towards the bulk water. The molecules are not fully entrapped by the micelle but remain at the interface region.

References

1. Z. R. Grabowski, K. Rotkiewicz and W. Rettig, *Chem. Rev.*, 2003, **103**, 3899-4031.

2. W. Rettig, *Angew. Chem. Int. Ed. Engl.*, 1986, **25**, 971-988.

3. W. Rettig, in Electron transfer I, J. Mattay (Ed.), Topics in current chemistry Springer-Verlag: Berlin, 1994, **169**, 253-299.

4. B. Valeur, Molecular fluorescence principles and applications. Wiley-VCH: Weinheim, 2002.

5. A. Mallick, P. Purkayastha and N. Chattopadhyay, *J. Photochem. Photobiol., C*, 2007, **8**, 109–127.

6. M. A. Haidekker, T. P. Brady, D. Lichlyter and E. A. Theodorakis, *Bioorg. Chem.*, 2005, **33**, 415–425.

7. M. Mac, W. Baran, T. Uchacz, B. Baran, M. Suder and S. Lesniewski, *J. Photochem. Photobiol., A*, 2007, **192**, 188–196.

8. V. Martínez-Martínez, J. Lim, J. Bañuelos, I. López-Arbeloa and O. Š. Miljanić, *Phys. Chem. Chem. Phys.*, 2013, **15**, 18023-18029.

9. E. Ishow, R. Guillot, G. Buntinx and O. Poizat, *J. Photochem. Photobiol., A*, 2012, **234**, 27-36.

10. T. Stalin and N. Rajendiran, *Chem. Phys.*, 2006, **322**, 311–322.

11. W. Schuddeboom, S. A. Jonker, J. M. Warman, U. Leinhos, W. Kuhnle and K. A. Zachariasse, *J. Phys. Chem.*, 1992, **96**, 10809-10819.

12. A. L. Sobolewski and W. Domcke, *Chem. Phys. Lett.*, 1996, **250**, 428-436.

13. N. Chattopadhyay, C. Serpa, M. M. Pereira, J. S. de Melo, L. G. Arnaut and S. J. Formosinho, *J. Phys. Chem. A*, 2001**, 105**, 10025-10030.

14. K. A. Zachariasse, *Chem. Phys. Lett.*, 2000, **320**, 8-13.

15. J. Dobkowski, J. Wojcik, W. Kozminski, R. Kołs, J. Waluk and J. Michl, *J. Am. Chem. Soc.*, 2002, **124**, 2406-2407.

16. T. Yoshihara, S. I. Druzhinin and K. A. Zachariasse, *J. Am. Chem. Soc.*, 2004, **126**, 8535-8539.

17. S. Cogan, S. Zilberg and Y. Haas, *J. Am. Chem. Soc.*, 2006, **128**, 3335-3345.

18. R. A. Marcus and N. Sutin, *Biochim. Biophys. Acta*, 1985, **811**, 265-322.

19. W. Siebrand, *J. Chem. Phys.*, 1971, **55**, 5843.

20. A. Siemerczuk, Z. R. Grabowski, M. Asher and M. Ottolenghi, *Chem. Phys. Lett.*, 1977, **51**, 315-320.

21. L. –H. Ma, Z-. B. Chen and Y. –B. Jiang, *Chem. Phys. Lett.*, 2003, **372**, 104-113.

22. K. Dahl, R. Biswas, N. Ito and M. Maroncelli, *J. Phys. Chem. B*, 2005, **109**, 1563-1585.

23. R. J. Visser, C. A. G. O. Varma, J. Konijenberg and P. C. M. Weisenborn, *J. Mol. Struct.*, 1984, **114**, 105-112.

24. A. Nag, T. Kundu and K. Bhattacharyya, *Chem. Phys. Lett.*, 1989, **160**, 257-260.

25. (a) B. K. Paul, A. Samanta, S. Kar and N. Guchhait, *J. Luminesc.*, 2010, **130**, 1258–1267. (b) S. Jana, S. Dalapati, S. Ghosh and N. Guchhait, *J. Photochem. Photobiol., A*, 2013, **261**, 31-40.

26. D. Sahoo, P. Bhattacharya and S. Chakravorti, *J. Phys. Chem. B*, 2011, **115**, 10983–10989.

27. R. V. Pereira, A. P. G. Ferreira and M. H. Gehlen, *J. Phys. Chem. A*, 2005, **109**, 5978-5983.

28. P. Dahiya, S. D. Choudhury, D. K. Maity, T. Mukherjee and H. Pal, *Spectrochim. Acta, Part A*, 2008, **69**, 134–141.

29. Y. H. Pang, S. M. Shuang, M. S. Wong, Z. H. Li and C. Dong, *J. Photochem. Photobiol. A*, 2005, **170**, 15-19.

30. S. Phukan, M. Saha, A. K. Pal and S. Mitra, *J. Mol. Struct.*, 2013, **1039**, 119–129.

31. Y. Sun, X. Liang, Y. Zhao and J. Fan, *Spectrochim. Acta, Part A*, 2013, **102**, 194-199.

32. Y. -A. Son, S. -Y. Gwon, S. -Y. Lee and S. -H. Kim, *Spectrochim. Acta, Part A*, 2010, **75**, 225–229.

33. S. -H. Kim, S. -Y. Lee, S. -Y. Gwon, Y.-A. Son and J. -S. Bae, *Dyes Pigm.*, 2010, **84**, 169–175.

34. A. K. Satpati, M. Kumbhakar, D. K. Maity and H. Pal, *Chem. Phys. Lett.*, 2005, **407**, 114–118.

35. J. M. Hicks, M. T. Vandersall, E. V. Sitzmann and K. B. Eisethal, *Chem. Phys. Lett.*, 1987, **135**, 413-420.

36. J. M. Hicks, M. Vandersall, Z. Babarogic and K. B. Eisethal, *Chem. Phys. Lett.*, 1985, **116**, 18-24.

37. S. Tazuke, R. K. Guo and T. Ikeda, *J. Phys. Chem.*, 1990, **94**, 1408-1413.

38. R. M. Yusop, A. Unciti-Broceta and M. Bradley, *Bioorg. Med. Chem. Lett.*, 2012, **22**, 5780–5783.

39. K. A. Al-Hassan, *Chem. Phys. Lett.*, 1991, **179**, 195-198.

40. P. Changenet, P. Plaza, M. M. Martin and Y. H. Meyer, *J. Phys. Chem. A*, 1997, **101**, 8186-8194.

41. K. A. Al-Hassan, M. A. Meetani and Z. F. M. Said, *J. Fluoresc.*, 1998, **8**, 93-100.

42. W. Rettig, R. Fritz and J. Springer, Fluorescence probes based on adiabatic photochemical reactions, in photochemical processes in organized molecular systems, K. Honda (Ed.), Elsevier science, Amsterdam, North-Holland, 1991, 61-81.

43. J. Paczkowski and D. C. Neckers, *Macromolecules*, 1991, **24**, 3013-3016.

44. M. A. Haidekker, D. Lichlyter, M. B. Johny and C. A. Grimes, *Sens. Lett.*, 2006, **4**, 257-261.

45. A. Mustafic, H.-M. Huang, E. A. Theodorakis and M. A. Haidekker, *J. Fluoresc.*, 2010, **20**, 1087-1098.

46. A. Rei, G. Hungerford and M. I. C. Ferreira, *J. Phys. Chem. B*, 2008, **112**, 8832-8839.

47. Z. -Y. Wu, J. -N. Cui, X. -H. Qian and T. -Y. Liu, *Chin. Chem. Lett.*, 2013, **24**, 359-361.

48. J. Sutharsan, D. Lichlyter, N. E. Wright, M. Dakanali, M. A. Haidekker and E. A. Theodorakis, *Tetrahedron*, 2010, **66**, 2582-2588.

49. K. Wang, W. Shi, J. Jia, S. Chen and H. Ma, *Talanta*, 2009, **77**, 1795–1799.

50. A. A. Maskevich, V. I. Stsiapura, V. A. Kuzmitsky, I. M. Kuznetsova, O. I. Povarova, V. N. Uversky and K. K. Turoverov, *J. Proteome Res.*, 2007, **6**, 1392–1401.

51. P. Friedhoff, A. Schneider, E. M. Mandelkow and E. Mandelkow, *Biochemistry*, 1998, **37**, 10223–10230.

52. E. S. Voropai, M. P. Samtsov, K. N. Kaplevskii, A. A. Maskevich, V. I. Stepuro, O. I. Povarova, I. M. Kuznetsova, K. K. Turoverov, A. L. Fink and V. N. Uverskii, *J. Appl. Spectrosc.*, 2003, **70**, 868–874.

53. V. I. Stsiapura, A. A. Maskevich, S. A. Tikhomirov and O. V. Buganov, *J. Phys. Chem. A*, 2010, **114**, 8345-8350.

54. V. I. Stsiapura, A. A. Maskevich, V. A. Kuzmitsky, K. K. Turoverov and I. M. Kuznetsova, *J. Phys. Chem. A*, 2007, **111**, 4829–4835.

55. V. I. Stsiapura, A. A. Maskevich, V. A. Kuzmitsky, V. N. Uversky, I. M. Kuznetsova and K. K. Turoverov, *J. Phys. Chem. B*, 2008, **112**, 15893–15902

56. C. Cazeau-Dubroca, A. Peirigua, M. B. Brahim, G. Nouchi and Ph. Cazeau, *Chem. Phys. Lett.*, 1989, **157**, 393-397.

57. C. Cazeau-Dubroca, A. Peirigua, M. B. Brahim, G. Nouchi and Ph. Cazeau, *Proc. Indian Acad. Sci. (Chem. Sci.)*, 1989, **104**, 209-217.

58. C. Cazeau-Dubroca, G. Nouchi, M. B. Brahim, M. Pesquer, D. Gorse and Ph. Cazeau, *J. Photochem. Photobiol., A*, 1994, **80**, 125-133.

59. C. Cazeau-Dubroca, A. Peirigua, S. Ait-Lyazidi, G. Nouchi, P. Cazeau and R. Lapouyade, *Chem. Phys. Lett.*, 1986, **124**, 110-115.

60. K. A. Al-Hassan and T. Azumi, *Chem. Phys. Lett.*, 1988, **146**, 121-124.

61. C. Cazeau-Dubroca, S. A. Lyazidi, P. Cambou, A. Peirigua, Ph. Cazeau and M. Pesquer, *J. Phys. Chem.*, 1989, **93**, 2347-2358.

62. T. Kobayashi, M. Futakami and O. Kajimoto, *Chem. Phys. Lett.*, 1986, **130**, 63-66.

63. R. B. Singh, S. Mahanta, S. Kar and N. Guchhait, *Chem. Phys.*, 2007, **342**, 33-42.

64. S. Mahanta, R. B. Singh, S. Kar and N. Guchhait, *J. Photochem. Photobiol., A*, 2008, **194**, 318-326.

65. D. Pilloud, P. Suppan and L. V. Haelst, *Chem. Phys. Lett.*, 1987, **137**, 130-133.

66. J. Herbich, Z. R. Grabowski, H. Wójtowicz and K. Golankiewicz, *J. Phys. Chem.*, 1989, **93**, 3439-3444.

67. J. Herbich, J. Karpiuk, Z. R. Grabowski, N. Tamai and K. Yoshihara, *J. Lumin.*, 1992, **54**, 165-175.

68. M. Zakharov, O. Krauss, Y. Nosenko, B. B. Brutschy and A. Dreuw, *J. Am. Chem. Soc.*, 2009, **131**, 461-469.

69. M. J. Kamlet, C. Dickinson and R. W. Taft, *Chem. Phys. Lett.*, 1981, **77**, 69-72.

70. K. Rechthaler and G. Köhler, *Chem. Phys.*, 1994, **189**, 99-116.

71. D. Panda and A. Datta, *J. Chem. Phys.*, 2006, **125**, 054513.

72. M. S. Alexiou, V. Tychopoulos, S. Ghorbanian, J. H. P. Tyman, R. G. Brown and P. I. Brittain, *J. Chem. Soc., Perkin Trans.***,** 1990, **2**, 837-842.

73. S. Dhar, S. S. Roy, D. K. Rana, S. Bhattacharya, S. Bhattacharya and S. C. Bhattacharya, *J. Phys. Chem. A*, 2011, **115**, 2216–2224.

74. W. -M. Kwok, M. W. George, D. C. Grills, C. -S. Ma, P. Matousek, A. W. Parker, D. Phillips, W. T. Toner and M. Towrie, *Angew. Chem. Int. Ed. Engl.*, 2003, **42**, 1826-1830.

75. G. Zhao and K. Han, *J. Comput. Chem.*, 2008, **29**, 2010–2017.

76. J. Herbich and J. Waluk, *Chem. Phys.*, 1994, **188**, 247-268.

77. E. Fasani, A. Albini, P. Savarino, G. Viscardi and E. Barni, *J. Heterocycl. Chem.*, 1993, **30**, 1041-1044.

78. Y. H. Kim, D. W. Cho, M. Yoon and D. Kim, *J. Phys. Chem.*, 1996, **100**, 15670.

79. G. Krishnamoorthy and S. K. Dogra, *Spectrochim. Acta, Part A*, 1999, **55**, 2647-2658.

80. G. Krishnamoorthy and S. K. Dogra, *J. Colloid Interface Sci.*, 2000, **228**, 335-343.

81. G. Krishnamoorthy and S. K. Dogra, *J. Phys. Chem. A*, 2000, **104**, 2542-2551.

82. N. Dash, F. A. S. Chipem, R. Swaminathan and G. Krishnamoorthy, *Chem. Phys. Lett.*, 2008, **460**, 119-124.

83. N. Dash, F. A. S. Chipem and G. Krishnamoorthy, *Photochem. Photobiol. Sci.*, 2009, **8**, 1708-1715.

84. G. Krishnamoorhy, Hydrogen-bonding effects on intramolecular charge transfer, in Hydrogen bonding and transfer in the excited state, K. –L. Han and G. J. Zhao (Eds.), John Wiley & Sons Ltd. 2011, **1**, 313-327.

85. N. Dash and G. Krishnamoorthy, *J. Fluoresc.*, 2010, **20**, 135-142.

86. N. Dash and G. Krishnamoorthy, *Photochem. Photobiol. Sci.*, 2011, **11**, 939-946.

87. Y. Hirata, T. Okada and T. Nomoto, *J. Phys. Chem. A*, 1998, **102**, 6585-6589.

88. A. Chakraborty, S. Kar and N. Guchhait, *Chem. Phys.*, 2006, **324**, 733–741.

89. R. W. Taft and M. J. Kamlet, *J. Am. Chem. Soc.*, 1976, **98**, 2886-2894.

90. E. M. Kossower, *Acc. Chem. Res.*, 1982, **15**, 259-266.

91. A. Samanta, B. K. Paul and N. Guchhait, *J. Fluoresc.*, 2012, **22**, 289–301.

92. T. S. Singh and S. Mitra, *J. Colloid. Interface Sci.*, 2007, **311**, 128–134.

93. M. Gaber, S. A. El-Daly and Y. S. El-Sayed, *Colloids Surf. B Biointerfaces*, 2008, **66**, 103-109.

94. M. Gaber, T. A. Fayed, S. A. El-Daly and Y. S. El-Sayed, *Photochem Photobiol. Sci.*, 2008, **7**, 257-262.

95. A. M. Asiri, S. A. El-Daly and S. A. Khan, *Spectrochim. Acta, Part A*, 2012, **95**, 679-684.

96. D. Sahoo and S. Chakravorti, *Photochem. Photobiol.*, 2009, **85**, 1103-1109.

97. M. Novaira, M. A. Biasutti, J. J. Silber and N. M. Correa, *J. Phys. Chem. B*, 2007, **111**, 748-759.

98. D. Mandal, S. K. Pal, A. Datta and K. Bhattacharyya, *Anal. Sci.*, 1998, **14**, 199-202.

99. R. Biswas, N. Rohman, T. Pradhan and R. Buchner, *J. Phys. Chem. B*, 2008, **112**, 9379-9388.

100. A. Datta, D. Mandal, S. K. Pal, and K. Bhattacharyya, *J. Phys. Chem. B*, 1997, **101**, 10221-10225.

101. P. Hazra and N. Sarkar, *Chem. Phys. Lett.*, 2001, **342**, 303-311.

102. P. Hazra, D. Chakraborty, A. Chakraborty and N. Sarkar, *J. Photochem. Photobiol., A*, 2004, **167**, 23-30.

103. P. Hazra, D. Chakraborty and N. Sarkar, *Chem. Phys. Lett.*, 2003, **371**, 553-562.

104. P. Hazra, D. Chakraborty and N. Sarkar, *Langmuir*, 2002, **18**, 7872-7879.

105. A. Mallick, B. Haldar, S. Maiti, S. C. Bera and N. Chattopadhyay, *J. Phys. Chem. B*, 2005, **109**, 14675-14682.

106. A. Mallick, B. Haldar and N. Chattopadhyay, *J. Phys. Chem. B*, 2005, **109**, 14683-14690.

107. Y. Suzuki and K. Yokoyama, *J. Am. Chem. Soc.*, 2005, **127**, 17799–17802.

108. V. S. Jisha, K. T. Arun, M. Hariharan and D. Ramaiah, *J. Phys. Chem. B*, 2010, **114**, 5912–5919.

109. S. Ghosh, S. Jana, D. Nath and N. Guchhait, *J Fluoresc.*, 2011, **21**, 365-374.

110. X. Zeng, X. Zhang, B. Zhu, H. Ji, Y. Li and J. Xue, *Analyst*, 2011, **136**, 4008-4012.

111. Y. Suzuki and K. Yokoyama, *Proteomics*, 2008, **8**, 2785–2790.

112. D. F. Eaton, *Tetrahedron*, 1987, **43**, 1551-1570.

113. T. S. Singh and S. Mitra, *J. Incl. Phenom. Macrocycl. Chem.*, 2009, **63**, 335-345.

114. R. B. Singh, S. Mahanta and N. Guchhait, *J. Mol. Struct.*, 2010, **963**, 92-97.

115. Y. Matshushita and T. Hikida, *Chem. Phys. Lett.*, 1998, **290**, 349-354.

116. S. Kundu, S. C. Bera and N. Chattopadhyay, *Ind. J. Chem. A*, 1998, **37**, 102-108.

117. S. Kundu and N. Chattopadhyay, *J. Photochem. Photobiol., A*, 1995, **88**, 105-108.

118. P. Hazra, D. Chakraborty, A. Chakraborty and N. Sarkar, *Chem. Phys. Lett.*, 2004, **388**, 150-157.

119. P. Das, A. Chakrabarty, B. Haldar, A. Mallick and N. Chattopadhyay, *J. Phys. Chem. B*, 2007, **111**, 7401-7408.

120. H. L. Breton, B. Bennetau, J. -F. Letard, R. Lapouyade and W. Rettig, *J. Photochem. Photobiol., A*, 1996, **95**, 7–20.

121. M. Dekhtyar and W. Rettig, *J. Phys. Chem. A*, 2007, **111**, 2035–2039.

122. A. Sczepan, W. Rettig, A. I. Tolmachev and V. V. Kurdyukov, *Phys. Chem. Chem. Phys.*, 2001, **3**, 3555–3561.

123. X. -M. Wang, Y. -F. Zhou, W. -T. Yu, C. Wang, Q. Fang, M. -H. Jiang, H. Leib and H. -Z. Wang, *J. Mater. Chem.*, 2000, **10**, 2698–2703.

124. J. -S. Yang, K. -L. Liau, C. -M. Wang and C. -Y. Hwang, *J. Am. Chem. Soc.*, 2004, **126**, 12325–12335.

125. Y. Amatatsu, *Chem. Phys.*, 2001, **274**, 87–98.

126. B. L. Feringa, *J. Org. Chem.*, 2007, **72**, 6635-6652.

127. R. A. Mathies and J. Lugtenburg, The primary photoreaction of rhodopsin, in Molecular mechanisms in visual transduction; D. G. Stavenga, W. J. DeGrip and E. N. Pugh, Jr. (Eds.), Elsevier: Amsterdam, the Netherlands, 2001, **3**, 55-90.

128. W. Qu, M. –P. Kung, C. Hou, T. E. Benedum and H. F. Kung, *J. Med. Chem.*, 2007, **50**, 2157-2165.

129. U. Abraham, An introduction to ultrathin organic films: from Langmuir-Blodgett to self-assembly, Academic press, Boston, 1991.

130. J. Messier, F. Kajzar and P. Prasad (Eds.), Organic molecules for nonlinear optics and photonics, Klumer academic publishers, Dordrecht, Boston, 1991.

131. G. G. Gurzadyan and H. Görner, *Chem. Phys. Lett.*, 2002, **359**, 146–152.

132. S. –L. Wang and J. –M. Lin, *Chem. Phys. Lett.*, 2007, **444**, 71-75.

133. B. Jędrzejewska, P. Krawczyk, M. Pietrzak, M. Gordel, K. Matczyszyn, M. Samoć and P. Cysewski, *Dyes Pigm.*, 2013, **99**, 673–685.

134. Z. Zheng, H. -p. Zhou, G. -y. Xu, Z. -p. Yu, X. -f. Yang, L. -h. Cheng, L. Kong, Y. Feng, J. –y. Wu and Y. -p. Tian, *Tetrahedron*, 2012, **68**, 6569-6574.

135. V. D. Gupta, V. S. Padalkar, K. R. Phatangare, V. S. Patil, P. G. Umape and N. Sekar, *Dyes Pigm.*, 2011, **88**, 378-384.

136. A. Gáplovský, J. Donovalová, P. Magdolen, Š. Toma and P. Zahradník, *Spectrochim. Acta, Part A*, 2002, **58**, 363–371.

137. V. D. Gupta, A. B. Tathe, V. S. Padalkar, P. G. Umape and N. Sekar, *Dyes Pigm.*, 2013, **97**, 429–439.

138. Y. V. Ipichev and K. A. Zachariasse, *Ber. Bunsen-Ges. Phys. Chem.*, 1997, **101**, 625-635.

139. W. Akemann, D. Laage, P. Plaza, M. M. Martin and M. Blanchard-Desce, *J. Phys. Chem. B*, 2008, **112**, 358-368.

140. M. Cigán, A. Gáplovsky, P. Gajdos, P. Magdolen, P. Zahradník and Z. Vetríková, *Spectrochim. Acta, Part A*, 2010, **77**, 984–993.

141. D. H. Waldeck, *Chem. Rev.*, 1991, **91**, 415-436.

142. J. Saltiel and J. T. D. Agostino, *J. Am. Chem. Soc.*, 1972, **94**, 6445-6456.

143. E. –J. Shin and S. -H. Lee, *Bull. Korean Chem. Soc.*, 2002, **23**, 1309-1314.

144. (a) H. Gruen and H. Gorner, *Z. Naturforsch.*, 1983, **38a**, 928-936, (b) H. Gruen and H. Gorner, *J. Phys. Chem.*, 1989, **93**, 7144-7152.

145. R. Lapouyade, K. Czeschka, W. Majenz, W. Rettig, E. Gilabert and C. Rulliere, *J. Phys. Chem.*, 1992, **96**, 9643-9650.

146. S. -L. Wang and T. -I. Ho, *J. Photochem. Photobiol., A*, 2000, **135**, 119–126.

147. M. Shaikh, J. Mohanty, P. K. Singh, A. C. Bhasikuttan, R. N. Rajule, V. S. Satam, S. R. Bendre, V. R. Kanetkar and H. Pal, *J. Phys. Chem. A*, 2010, **114**, 4507–4519.

148. T. A. Fayed, *J. Photochem. Photobiol., A*, 1999, **121**, 17–25.

149. T. A. Fayed and S. S. Ali, *Spectrosc. Lett.*, 2003, **36**, 375–386.

150. S. E. -D. H. Etaiw, T. A. Fayed and N. Z. Saleh, *J. Photochem. Photobiol., A*, 2006, **177**, 238–247.

151. M. Sowmiya, A. K. Tiwari, Sonu and S. K. Saha, *J. Photochem. Photobiol., A*, 2011, **218**, 76–86.

152. T. A. Fayed, S. E. -D. H. Etaiw and N. Z. Saleh, *J. Luminesc.*, 2006, **121**, 431–440.

153. S. K. Saha, P. Purkayastha and A. B. Das, *J. Photochem. Photobiol., A*, 2008, **195**, 368–377.

154. S. K. Saha, P. Purkayastha, A. B. Das and S. Dhara, *J. Photochem. Photobiol., A*, 2008, **199**, 179–187.

155. S. S. Jaffer, S. K. Saha, G. Eranna, A. K. Sharma and P. Purkayastha, *J. Phys. Chem., C*, 2008, **112**, 11199–11204.

156. A. Maity, S. S. Jaffer, T. Das, P. Ghosh and P. Purkayastha, *Langmuir*, 2011, **27**, 4068–4075.

157. A. Mishra, A. Thangamni, S. Chatterjee, F. A. S. Chipem and G. Krishnamoorthy, *Photochem. Photobiol.*, 2013, **39**, 247–252.

158. F. A. S. Chipem, S. Chatterjee and G. Krishnamoorthy, *J. Photochem. Photobiol., A*, 2010, **214**, 121–127.

159. V. Bavetsias, C. Sun, N. Bouloc, J. Reynisson, P. Workman, S. Linardopoulos and M. Edward, *Bioorg. Med. Chem. Lett.*, 2007, **17**, 6567–6571.

160. N. Dash, A. Mishra and G. Krishnamoorthy, *J. Pharm. Biomed. Anal.*, 2013, **77**, 55-62.

161. J. -S. Yang, C. -K. Lin, A. M. Lahoti, C. -K. Tseng, Y. -H. Liu, G. -H. Lee and S. -M. Peng, *J. Phys. Chem. A*, 2009, **113**, 4868–4877.

162. I. Grabchev and T. Philipova, *Dyes Pigm.*, 2000, **44**, 175–180.

163. A. Mokdad, J. L. Belof, S. W. Yi, S. E. Shuler, M. L. McLaughlin, B. Space and R. W. Larsen, *J. Phys. Chem. A*, 2008, **112**, 8310–8315.

164. W. Akemann, D. Laage, P. Plaza, M. M. Martin and M. Blanchard-Desce, *J. Phys. Chem. B*, 2008, **112**, 358–368.

165. J. -S. Yang, K. -L. Liau, C. -Y. Hwang and C. -M. Wang, *J. Phys. Chem. A*, 2006, **110**, 8003–8010.

166. F. L. Cui, J. Fan, W. Li, Y. C. Fan and Z. D. Hu, *J. Pharm. Biomed. Anal.*, 2004, **34**, 189–197.

167. E. L. Gelamo, C. H. Silva, H. Imasato and M. Tabak, *Biochim. Biophys. Acta*, 2002, **1594**, 84–99.

168. X. M. He and D. C. Carter, *Nature*, 1992, **358**, 209–215.

169. I. Sjoholm, B. Ekman, A. Kober, I. Ljungstedt-Pahlman, B. Seiving and T. Sjodin, *Mol. Pharmacol.*, 1979, **16**, 767–777.

170. K. Yamasaki, T. Maruyama, U. Kragh-Hansen and M. Otagiri, *Biochim. Biophys. Acta*, 1996, **1295**, 147–157.

171. K. Eiichi and T. Koike, *Chem. Soc. Rev.*, 1998, **27**, 179–184.

172. P. Chowdhury and S. Chakravorti, *J. Photochem. Photobiol., A*, 2006, **179**, 95-104.

173. N. Sharma, S. K. Jain and R. C. Rastogi, *Spectrochim. Acta, Part A*, 2007, **68**, 927–941.

174. P. V. Jaiswal, V. S. Ijeri and A. K. Srivastava, *Colloids. Surf. B Biointerfaces*, 2005, **46**, 45-51.

175. G. Krishnamoorthy and S. K. Dogra, *J. Colloid Interface Sci.*, 1999, **213**, 53-61.

176. D. W. Hein, R. J. Alheim and J. J. Leavitt, *J. Am. Chem. Soc.*, 1957, **79**, 427-429.

177. R. W. Middleton and D. G. Wibberely, *J. Heterocycl. Chem.*, 1980, **17**, 1757-1760.

178. H. Yu, H. Kawanishi and H. Koshima, *J. Photochem. Photobiol. A.*, 2006, **178**, 62–69.

179. F. Wu, C. M. Chamchoumis and R. P. Thummel, *Inorg. Chem.*, 2000, **39**, 584-590.

180. Y. -P. Tong, S. -L. Zheng and X. -M. Chen, *J. Mol. Struct.*, 2007, **826**, 104–112.

181. G. A. Crosby and J. N. Demas, *J. Phys. Chem.*, 1971, **75**, 991-1024.

182. A. D. Becke, *J. Chem. Phys.*, 1993, **98**, 5648–5652.

183. C. T. Lee, W. Yang and R. G. Parr, *Phys. Rev. B*, 1988, **37**, 785–789.

184. P. Hohenberg and W. Kohn, *Phys. Rev. B*, 1964, **136**, 864-871.

185. W. Kohn and L. J. Sham, *Phys. Rev. A*, 1965, **140**, 1133-1138.

186. J. F. Stanton, J. Gauss, N. Ishikawa and M. Head-Gordon, *J. Chem. Phys.*, 1995, **103**, 4160–4174.

187. K. B. Wiberg, Y. -G. Wang, A. E. de Oliveira, S. A. Perera and P. H. Vaccaro, *J. Phys. Chem. A*, 2005, **109**, 466–477.

188. M. J. Frisch, G. W. Trucks, H. B. Schlegel, G. E. Scuseria, M. A. Robb, J. R. Cheeseman, J. A. Montgomery, Jr., T. Vreven; K. N. Kudin, J. C. Burant, J. M. Millam, S. S. Iyengar, J. Tomasi, V. Barone, B. Mennucci, M. Cossi, G. Scalmani, N. Rega, G. A. Petersson, H. Nakatsuji, M. Hada, M. Ehara, K. Toyota, R. Fukuda, J. Hasegawa, M. Ishida, T. Nakajima, Y. Honda, O. Kitao, H. Nakai, M. Klene, X. Li, J. E. Knox, H. P. Hratchian, J. B. Cross, V. Bakken, C. Adamo, J. Jaramillo, R. Gomperts, R. E. Stratmann, O. Yazyev, A. J. Austin, R. Cammi, C. Pomelli, J. W. Ochterski, P. Y. Ayala, K. Morokuma, G. A. Voth, P. Salvador, J. J. Dannenberg, V. G. Zakrzewski, S. Dapprich, A. D. Daniels, M. C. Strain, O. Farkas, D. K. Malick, A. D. Rabuck, K. Raghavachari, J. B. Foresman, J. V. Ortiz, Q. Cui, A. G. Baboul, S. Clifford, J. Cioslowski, B. B. Stefanov, G. Liu, A. Liashenko, P. Piskorz, I. Komaromi, R. L. Martin, D. J. Fox, T. Keith, M. A. Al-Laham, C. Y. Peng, A. Nanayakkara, M. Challacombe, P. M. W. Gill, B. Johnson, W. Chen, M. W. Wong, C. Gonzalez and J. A. Pople, *Gaussian 03*, Revision E.01, Gaussian, Inc., Wallingford CT, 2004.

189. http://www.ncbi.nlm.nih.gov/protein/CAA76847.1.

190. G. M. Morris, D. S. Goodsell, R. S. Halliday, R. Huey, W. E. Hart, R. K. Belew and A. J. Olson, *J. Comput. Chem.*, 1998, **19**, 1639-1662.

191. W. L. Delano, The PyMOL molecular graphics system. DeLano scientific, San Carlos, USA, 2004.

192. R. Lakowicz, Principles of fluorescence spectroscopy, 3rd ed.; Springer: New York, 2006.

193. B. Valeur, and J. -C. Brochon, New trends in fluorescence spectroscopy: applications to chemical and life science, Springer: New York, 2001.

194. J. A. Ross, and D. M. Jameson, *Photochem. Photobiol. Sci.*, 2008, **7**, 1301-1312.

195. M. Y. Berezin, and S. Achilefu, *Chem. Rev.*, 2010, **110**, 2641-2684.

196. W. Becker, Advanced time-correlated single photon counting techniques; Springer: Berlin, 2005.

197. W. Becker, The bh TCSPC handbook, 3rd Ed.; Becker & Hickl Gmbh: Berlin, Germany, 2008.

198. F. A. S. Chipem, A. Mishra and G. Krishnamoorthy, *Phys. Chem. Chem. Phys*., 2012, **14**, 8775-8790.

199. M. H. Abraham, P. L. Greillier, J. L. M. Abboud, R . M. Doherty and R. W. Taft, *Can. J. Chem.*, 1988, **66**, 2673–2686.

200. M. J. Kamlet, J. L. M. Abboud, M. H. Abraham and R. W. Taft, *J. Org. Chem.*, 1983, **48**, 2877–2887.

201. C. Reichardt, *Angew. Chem. Int. Ed. Engl.*, 1979, **18**, 98–110.

202. E. Lippert, Z. *Electrochem*. 1957, **61**, 962–975.

203. S. Dhar, D. K. Rana, S. S. Roy, S. Roy, S. Bhattacharya and S. C. Bhattacharya, *J. Lumin.*, 2012, **132**. 957–964.

204. Y. Kim, M. Yoon and D. Kim, *J. Photochem. Photobiol., A*, 2001, **138**, 167–175.

205. G. Krishnamoorthy and S. K. Dogra, *J. Org. Chem.*, 1999, **64**, 6566–6574.

206. J. K. Dey and S. K. Dogra, *J. Phys. Chem.*, 1994, **98**, 3638–3644.

207. G. Krishnamoorthy and S. K. Dogra, *Chem. Phys.*, 1999, **243**, 45–59.

208. G. Krishnamoorthy and S. K. Dogra, *J. Photochem. Photobiol., A*, 1999, **123**, 109–119.

209. V. Vetokhina, K. Dobek, M. Kijak, I. I. Kaminska, K. Muller, W. R. Thiel, J. Waluk and J. Herbich, *ChemPhysChem*, 2012, **13**, 3661–3671.

210. X. -F. Yu, S. Yamazaki and T. Taketsugu, *J. Phys. Chem. A*, 2012, **116**, 10566–10573.

211. N. Basaric, N. Doslic, J. Ivkovic, Y.–H. Wang, J. Veljkovic, K. Mlinaric-Majerski and P. Wan, *J. Org. Chem.*, 2013, **78**, 1811-1823.

212. N. Dash and G. Krishnamoorthy, *Spectrochim. Acta, Part A*, 2012, **95**, 540-546.

213. S. R. Vázquez, C. R. Rodríguez, M. Mosquera and F. R. Prieto, *J. Phys. Chem. A*, 2007, **111**, 1814–1826.

214. F. A. S. Chipem and G. Krishnamoorthy, *J. Phys. Chem. A*, 2009**, 113***,* 12063–12070.

215. H. Konoshima, S. Nagao, I. Kiyota, K. Amimoto, N. Yamamoto, M. Sekine, M. Nakata, K. Furukawa and H. Sekiya, *Phys. Chem. Chem. Phys.*, 2012, **14**, 16448-16457.

216. A. Douhal, T. Fiebig, M. Chachisvilis and A. H. Zewail, *J. Phys. Chem. A*, 1998, **102**, 1657-1660.

217. Y. Kim and M. Yoon, *Bull. Korean Chem. Soc.*, 1998, **19**, 980–985.

218. S. Jana, S. Dalapati and N. Guchhait, *J. Phys. Chem. A*, 2012, **116**, 10948−10958.

219. S. K. Dogra, *Proc. Indian Acad. Sci.*, 1992, **104**, 635-647.

220. K. Rotkiewicz, K. H. Grellmann and Z. R. Grabowski, *Chem. Phys. Lett.*, 1973, **19**, 315-318.

221. S. I. Druzhinin, S. A. Kovalenko, T. A. Senyushkina, A. Demeter, R. Januskevicius, P. Mayer, D. Stalke, R. Machinek and K. A. Zachariasse, *J. Phys. Chem. A*, 2009, **113**, 9304-9320.

222. J. Saltiel and Y.-P. Sun, *J. Phys. Chem.*, 1989, **93**, 6246-6250.

223. S. Malkin, and E. Fischer, *J. Phys. Chem.*, 1964, **68**, 1153-1163.

224. J. Saltiel, A. S. Waller, D. F. Sears, Jr., E. A. Hoburg, D. M. Zeglinski and D. H. Waldeck, *J. Phys. Chem.*, 1994, **98**, 10689-10698.

225. J. Saltiel, A. Waller, Y.-P. Sun and D. F. Sears, Jr., *J. Am. Chem. Soc.*, 1990, **112**, 4580-4581.

226. J. Saltiel, A. S. Waller and D. F. Sears, Jr., *J. Photochem. Photobiol., A*, 1992, **65**, 29-40.

227. J. Saltiel, A. S. Waller and D. F. Sears, Jr., *J. Am. Chem. Soc.*, 1993, **115**, 2453-2465.

228. S. Sharafy and K. A. Muszka, *J. Am. Chem. Soc.*, 1971, **93**, 4119-4125.

229. C. Dugave and L. Demange, *Chem. Rev.*, 2003, **103**, 2475-2532.

230. I. Gryczyński and A. Kawski, *Z. Naturforsch.*, 1975, **30a**, 287-293.

231. C. J. Drummond, F. Grieser and T.W. Healy, *J. Phys. Chem.*, 1988, **92**, 2604-2613.

232. C. J. Drummond, F. Grieser and T.W. Healy, *J. Chem. Soc. Faraday, Trans. I* 1988, **85**, 521, 537, 551, 561.

233. A. K. Mishra, S. K. Dogra, *Spectrochim. Acta, Part A*, 1983, **39**, 609-611.

234. M. Gelbart, A. Ben-Shaul and D. Roux, Micelles, membranes, microemulsions and monolayers; Springer-Verlag: New York, 1994.

235. K. L. Mittal and B. Landman (Eds.); Surfactants in solutions, Plenum press, New York, 1984.

236. D. Langevin, *Acc. Chem. Res.*, 1988, **21**, 255-260.

237. J. Eastoe, W. K. Young, B. H. Robinson and D. C. Steytler, *J. Chem. Soc. Faraday Trans.*, 1990, **86**, 2883-2889.

238. T. K. Jain, M. Varshney and A. J. Maitra, *J. Phys. Chem.*, 1989, **93**, 7409-7416.

239. N. Nandi, K. Bhattacharyya and B. Bagchi, *Chem. Rev.*, 2000, **100**, 2013-2045.

240. J. H. Fendler, in Membrane mimetic chemistry, Wiley, New York, 1982.

241. D. L. Sacket, J. R. Knutson and J. Wolff, *J. Biol. Chem.*, 1990, **265**, 14899-14906.

242. P. L. Luisi, M. Giomini, M. P. Pileni, and B. H. Robinson, *Biochim. Biophys. Acta*, 1988, **947**, 209-246.

243. A. S. Klymchenko and A. P. Demchenko, *Langmuir*, 2002, **18**, 5637-5639.

244. A. Douhal, G. Angulo, M. Gil, J. A. Organero, M. Sanz and L. Tormo, *J. Phys. Chem. B*, 2007, **111**, 5487-5493.

245. E. Levinger, *Science*, 2002, **298**, 1722-1723.

246. I. A. Heisler, M. Kondo and S. R. Meech, *J. Phys. Chem. B*, 2009, **113**, 1623-1631.

247. K. Bhattacharyya, *Acc. Chem. Res.*, 2003, **36**, 95-101.

248. R. K. Mitra, S. S. Sinha and S. K. Pal, *Langmuir*, 2008, **24**, 49-56.

249. D. S. Venables, K. Huang and C. A. Schmuttenmaer, *J. Phys. Chem. B*, 2001, **105**, 9132-9138.

250. N. M. Correa and N. E. Levinger, *J. Phys. Chem. B*, 2006, **110**, 13050-13061.

251. K. Bhattacharyya and B. Bagchi, *J. Phys. Chem. A*, 2000, **104**, 10603-10613.

252. S. Nave, J. Eastoe, R. K. Heenan, D. Steytlar and I. Grillo, *Langmuir*, 2000, **16**, 8741-8748.

253. A. K. Shaw and S. K. Pal, *J. Phys. Chem. B*, 2007, **111**, 4189-4199.

254. G. Palazzo, L. Carbone, G. Colafemmina, R. Angelico, A. Ceglieb and M. Giustini., *Phys. Chem. Chem. Phys.*, 2004, **6**, 1423-1429.

255. M. A. Sedgwick, D. C. Crans and N. E. Levinger, *Langmuir*, 2009, **25**, 5496-5503.

256. L. Yang and K. H. Zhao, *Langmuir*, 2007, **23**, 8732-8739.

257. S. Rafiq, R. Yadav and P. Sen, *J. Phys. Chem. B*, 2010, **114**, 13988-13994.

258. G. Krishnamoorthy and S. K. Dogra, *Spectochim. Acta A*, 2001, **57**, 2617-2628.

259. D. Sahoo and S. Chakravorti, *J. Photochem. Photobiol., A*, 2009, **205**, 129-138.

260. Y.-B. Jiang and L. Lin, *Appl. Spectrosc.*, 1995, **49**, 1017-1021.

261. Y.-B. Jiang and M.-G. Jin, *Spectrochim. Acta, Part A*, 2000, **56**, 623– 627.

262. C. H. Cho, M. Chung, J. Lee, T. Nguyen, S. Singh, M. Vedamuthu, S. Yao, S. -B. Zhu and G. W. Robinson, *J. Phys. Chem.*, 1995, **99**, 7806-7812.

263. G. Angulo, J. A. Organero, M. A. Carranza and A. Douhal, *J. Phys. Chem. B*, 2006, **110**, 24231-24237.

264. S. M. Andrade, S. M. B. Costa and R. Pansu, *Photochem. Photobiol.*, 2000, **71**, 405-412.

265. D. E. Moilanen, N. E. Levinger, D. B. Spry and M. D. Fayer, *J. Am. Chem. Soc.*, 2007, **129**, 14311-14318.

266. I. R. Piletic, D. E. Moilanen, D. B. Spry, N. E. Levinger and M. D. Fayer, *J. Phys. Chem. A*, 2006, **110**, 4985-4999.

267. C. Banerjee, C. Ghatak, S. Mandal, S. Ghosh, J. Kuchlyan and N. Sarkar, *J Phys Chem B*, 2013, **117**, 6906-6916.

268. S. Basu, S. Mondal and D. Mandal, *J. Chem. Phys.*, 2010, **132**, 034701.

269. K. J. Tielrooij, M. J. Cox and H. J. Bakker, *ChemPhysChem*, 2009, **10**, 245–251.

270. C. Kumar and D. Balasubramanian, *J. Colloid Interface Sci.*, 1980, **74**, 64-70.

271. H. F. Eicke and H. Christen, *Helv. Chim. Acta*, 1978, **61**, 2258-2263.

272. B. Djermouni and H. J. Ache, *J. Phys. Chem.*, 1979, **83**, 2476-2479.

273. U. Hermann and Z. A. Schely, *J. Am. Chem. Soc.*, 1979, **101**, 2665-2669.

274. J. Rouviere, J. M. Couret, M. Lindhermer, J. L. Dejardin and R. Marrony, *J. Chim. Phys.*, 1979, **76**, 289-296.

275. M. A. J. Rodgers and P. C. Lee, *J. Phys. Chem.*, 1984, **88**, 3480-3484.

276. M. Goffredi, V. Turco Liveri and G. Vassallo, *J. Solution Chem.*, 1993, **22**, 941-949.

277. G. B. Dutt, *J. Phys. Chem. B*, 2004, **108**, 7944-7949.

278. S. D. Choudhury, M. Kumbhakar, S. Nath, S. K. Sarkar, T. Mukherjee and H. Pal, *J. Phys. Chem. B*, 2007, **111**, 8842-8853.

279. D. A. Kelkar and A. Chattopadhyay, *J. Phys. Chem. B*, 2004, **108**, 12151-12158.

280. P. K. Singh, M. Kumbhakar, H. Pal and S. Nath, *J. Phys. Chem. B*, 2009, **113**, 1353-1359.

281. A. Chattopadhyay and S. Mukherjee, *J. Phys. Chem. B*, 1999, **103**, 8180-8185.

282. Jr. T. Peters, *Adv. Protein Chem.*, 1985, **37**, 161–245.

283. M. K. Helms, V. Paterson, N. V. Bhagavan and D. M. Jameson, *FEBS Lett.*, 1997, **408** ,67–70.

284. J. S. Mandeville and H. A. Tajmir-Riahi, *Biomacromolecules*, 2010, **11**, 465-472.

285. (a) D. C. Carter and X. M. He, *Science*, 1990, **249**, 302-303. (b) D. C. Carter, J. X. Ho, Adv. Protein Chem., 1994, **45**, 153-203. (c) M. Dockal, D. C. Carter and F. Ruker, *J. Biol. Chem.*, 1999, **274**, 29303-29310.

286. (a) V. Lhiaubet-Vallet, Z. Sarabia, F. Bosca and M. A. Miranda, J. *Am. Chem. Soc.*, 2004, **126**, 9538-9539. (b) M. C. Jimenez, M. A. Miranda and I. Vaya, *J. Am. Chem. Soc.*, 2005, **127**, 10134-10135.

287. P. C. A. Barreleiro and B. Lindman, *J. Phys. Chem. B*, 2003, **107**, 6208–6213.

288. A. P. Demchenko, Fluorescence and dynamics in proteins; in Topics in fluorescence spectroscopy: biochemical applications, L. R. Lakowicz (Ed.); Plenum: New York, 1992, **3**, 65-111.

289. B. Haldar, A. Chakrabarty, A. Mallick, M. C. Mandal, P. Das and N. Chattopadhyay, *Langmuir*, 2006, **22**, 3514–3520.

290. A. Mallick, B. Haldar and N. Chattopadhyay, *J. Phys. Chem. B*, 2005, **109**, 14683 –14690.

291. A. Chakraborty, S. Ghosh, S. Kar, D. N. Nath and N. Guchhait, *J. Mol. Struct.*, 2009, **917**, 148 –157.

292. S. Ghosh and N. Guchhait, *Chem. Phys. Chem.*, 2009, **10**, 1664 –1671.

293. S. Mahanta, R. B. Singh and N. Guchhait, *J. Fluoresc.*, 2009, **19**, 291–303.

294. S. Deepa and A. K Mishra, *J. Pharma. Biomed. Anal.*, 2005, **38**, 556-563.

295. B. Bhattacharya, S. Nakka, L. Guruprasad and A. Samanta, *J. Phys. Chem. B*, 2009, **113**, 2143-2150.

296. M. S. Baptista and G. L. Indig, *J. Phys. Chem. B*, 1998, **102**, 4678-4688.

297. D. M. Togashi, A. G. Ryder and D. O'Shaughnessy, *J. Fluoresc*, 2010, **20**, 441-452.

298. J. Mallicka, I. Gryczynski and J. R. Lakowicz, Anal. Biochem., 2003, 315, 57-66.

299. A. Granzhan, H. Ihmels and G. Viola, *J. Am. Chem. Soc.*, 2007, **129**, 1254-1267.

300. B. K Paul, A. Samanta and N. Guchhait, *J. Phys. Chem. B*, 2010, **114**, 6183-6196.

301. A. Chakraborty, D. Seth, P. Setua and N. Sarkar, *J. Phys. Chem. B*, 2006, **110**, 16607-16617.

302. J. Zhang, D. Xiong, L. Chen, Q. Kang and B. Zeng, *Spectrochim. Acta, Part A*, 2012, **96**, 132-138.

303. M. Tonelli, G. Paglietti, V. Boido, F. Sparatore, F. Marongiu, E. Marongiu, P. L. Colla and R. Loddo, *Chem. Biodivers.*, 2008, **5**, 2386-2401.

304. G. Vitale, P. Corona, M. Loriga, A. Carta, G. Paglietti, P. L. Colla, B Busonera, E. Marongiu, D. Collu, R. Loddo, *Med. Chem.*, 2009, **5**, 507-516.

305. G. Vitale, P. Corona, M. Loriga, A. Carta, G. Paglietti, G. Giliberti, G. Sanna, P. Farci, M. E. Marongiu, P. L. Colla, *Eur J. Med. Chem.*, 2012, **53**, 83-97.

306. M. Tonelli, M. Simone, B. Tasso, F. Novelli, V. Boido, F. Sparatore, G. Paglietti, S. Pricl, G. Giliberti, S. Blois, C. Ibba, G. Sanna, R. Loddo and P. L. Colla., *Bioorg. Med. Chem.*, 2010, **18**, 2937-2953.

307. M. M. Karpińska, J. Matysiak and A. Niewiadomy, *Arch. Pharm. Res.*, 2011, **34**, 1639-1647.

308. A. O. H. El-Nezhawy, S. T. Gaballah, M. A. A. Radwan, A. R. Baiuomy and O. M. E. Abdel-Salam, *Med. Chem.*, 2009, **5**, 558-569.

309. J. -I. Kuroyanagi, K. Kanai, Y. Sugimoto, T. Horiuchi, I. Achiwa, H. Takeshita and K. Kawakami, *Bioorg. Med. Chem.*, 2010, **18**, 7593-7606.

310. R. Paramashivappa, P. P. Kumar, P. V. S. Rao and A. S. Rao, *Bioorg. Med. Chem. Lett.*, 2003, **3**, 657-660.

311. W. M. Abdou, R. F. Barghash and A. A. Sediek, *Eur. J. Med. Chem.*, 2012, **57**, 362-372.

312. R. L. Clark, A. A. Pessolano, B. Witzel, T. Lanza, T. Y. Shen, C. G. VanArman and E. A. Risley, *J. Med. Chem.*, 1978, **21**, 1158–1162.

313. E. Barni, S. Pasquino, P. Savarino, G. D. Modica and G. Giraudo, *Dyes Pigm.*, 1985, **6**, 1 –12.

314. S. P. G. Costa, E. Oliveira, C. Lodeiro and M. M. M. Raposo, *Sensors*, 2007, **7**, 2096–2114.

315. S. -I. Um, *Dyes Pigm.*, 2007, **75**, 185–188.

316. H. A. Benesi and J. H. Hildebrand, *J. Am. Chem. Soc.*, 1949, **71**, 2703–2707.

317. G. Pagona, S. P. Economopoulos, G. K. Tsikalas, H. E. Katerinopoulos and N. Tagmatarchis, *Chem. Euro. J.*, 2010, **16**, 11969-11976.

318. S. S. Tan, Y. N. Teo and E. T. Kool, *Org. Lett.*, 2010, **12**, 4820-4823.

319. H. Wang, J. Lin, W. Huang, Wei and W. Wei, *Sens. Actuators B: Chem.*, 2010, **150**, 798-805.

320. X. F. Wu, B. W. Xu, H. Tong and L. X. Wang, *Macromolecules*, 2010, **43**, 8917-8923.

321. E. L. Que, D. W. Domaille and C. J. Chang, *Chem. Rev.*, 2008, **108**, 1517-1549.

322. J. N. Wilson and U. H. Bunz, *J. Am. Chem. Soc.*, 2005, **127**, 4124-4125.

323. V. Tharmaraj, S. Devia and K. Pitchumani, *Analyst*, 2012,**137**, 5320-5324.

324. X. Wang, W. Zheng, H. Lin, G. Liu, Y. Chen and J. Fang, *Tetrahedron Lett.*, 2009, **50**, 1536-1538.

325. Z. Xu, Y. Xiao, X. Qian, J. Cui and D. Cui, *Org. Lett.*, 2005, **7**, 889-892.

326. B. Wang, T. Fu, S. Yang, J. Lia and Y. Chen, *Anal. Methods*, 2013, **5**, 3639-3641.

327. N. Dash, Dual fluorescence of 2-(4′-*N,N*-dimethylaminophenyl)imidazo[4,5-b]pyridine: effect of homogeneous and microheterogeneous environments, Indian Institute of Technology Guwahati, India, Chapter 3, Section 3.3, page 78-95.

328. V. Ramamurthy, Photochemistry in organized and constrained media, VCH, New York, 1991.

329. H. H. Paradies, *J. Phys. Chem.*, 1980, **84**, 599-607.

330. S. S. Berr, *J. Phys. Chem.*, 1987, **91**, 4760-4765.

331. S. Ghosh, K. Sahu, S. K. Mondal, P. Sen and K. Bhattacharyya, *J. Chem. Phys.*, 2006, **125**, 054509.

332. Y. Taniguchi, S. Makimoto and K. Suzuki, *J. Phys. Chem.*, 1981, **85**, 2218-2222.

333. Kabir-ud-Din, M. Akrama and Z. Khan, *Inorg. React. Mech.*, 2010, **4**, 187-196.

334. W. Rettig and R. Lapouyade, Fluorescence probes based on twisted intramolecular charge transfer (TICT) states and other adiabatic photoreactions, in Topics in fluorescence spectroscopy, probe design and chemical sensing, J. R. Lakowicz (Ed.), Plenum press, New York, 1994, **4**, 109-149.

335. F. Lopez, F. Cuomo, A. Ceglie, L. Ambrosone and G. Palazzo, *J. Phys. Chem.B*, 2008, **112**, 7338-7344.

336. K. Singh and M. Darshi, *Biochim. Biophys. Acta*, 2002, **1563**, 35-44.

337. M. Yoon, D. W. Cho, S. G. Kang and M. Lee, *Bull. Korean Chem. Soc.*, 1993, **14**, 704-708.

338. G. Krishnamoorthy and S. K. Dogra, *Phys. Chem. Chem. Phys.*, 2000, **2**, 2521-2528.

339. S. Santra and S. K. Dogra, *Spectochim. Acta A*, 2000, **56**, 915-925.

340. Y. -B. Jiang, X. -J. Wang, M. -G. Jin and L. -R. Lin, *J. Photochem. Photobiol., A*, 1999, **126**, 125-133.

341. A. Mishra, S. Chatterjee and G. Krishnamoorthy, *J. Photochem. Photobiol., A*, 2013, **260**, 50-58.

342. S. Chatterjee, Photophysical and photochemical properties of some push-pull aromatic olefins and photochemistry of a few *ortho*-substituted stilbenes, Indian Institute of Technology Guwahati, India.

343. S. S. Jaffer, M. Sowmiya, S. K. Saha and P. Purkayastha, *J. Colloid Interface Sci.*, 2008, **325**, 236–242.

344. M. Sowmiya, A. K. Tiwari and S. K. Saha, *J. Colloid Interface Sci.*, 2010, **344**, 97-104.

345. M. Sowmiya, P. Purkayastha, S. K. Saha and S. S. Jaffer, *J. Photochem. Photobiol. A*, 2009, **205**, 186–196.

346. S. S. Jaffer, S. K. Saha and P. Purkayastha, *J. Colloid Interface Sci.*, 2009, **337**, 294–299.

347. T. Das, A. Kumar, P. Ghosh, A. Maity, S. S. Jaffer and P. Purkayastha, *J. Phys. Chem. C*, 2010, **114**, 19635–19640.

348. S. K. Saha, P. Tiwari and S. K. Dogra, *J. Phys. Chem.*, 1994, **98**, 5953-5955.

349. L. S. Romsted and D. Zanethe, *J. Phys. Chem.*, 1988, **92**, 4690-4698.

350. A. Dreuw, J. L. Weisman and M. J. Head-Gordon, *Chem. Phys.*, 2003, **119**, 2943–2946.

351. T. Forster, *Z. Elektrochem.*, 1950, **54**, 531-535.

List of publications

1. N. Dash, **A. Mishra** and G. Krishnamoorthy, Comment on “The interaction of 5-(Alkoxy)naphthalen-1-amine with bovine serum albumin and its effect on the conformation of protein”, *J. Phys. Chem. B*, 2011, **115**, 6806–6807.[#]

2. F. A. S. Chipem, **A. Mishra** and G Krishnamoorthy, The role of hydrogen bonding in excited state intramolecular charge transfer, *Phys. Chem. Chem. Phys.*, 2012, **14**, 8775–8790.[#]

3. **A. Mishra** and G. Krishnamoothy, Photophysical study of 2-(4′-*N*,*N*-dimethylaminophenyl)oxazolo[4,5-b]pyridine in different solvents and at various pH, *Photochem. Photobiol. Sci.*, 2012, **11**, 1356−1367.

4. **A. Mishra**, A. Thangamani, S. Chatterjee, F. A. S. Chipem and G. Krishnamoorthy, Photoisomerization of *trans*-2-[4′-(dimethylamino) styryl]benzothiazole, *Photochem. Photobiol.*, 2013, **89**, 247−252.[#]

5. N. Dash, **A. Mishra** and G. Krishnamoorthy, Alkyl chain dependent interactions of ligands with bovine serum albumin, *J. Pharm. Biomed. Anal.*, 2013, **77**, 55−62.[*]

6. **A. Mishra**, S. Chatterjee and G. Krishnamoorthy, Intramolecular charge transfer emission of *trans*-2-[4′-(dimethylamino)styryl]benzimidazole: Effect of solvent and pH, *J. Photochem. Photobiol. A*, 2013, **260**, 50−58.[#]

7. S. Sahu, **A. Mishra** and G. Krishnamoorthy, Specific site binding of metal ions on the intramolecular charge transfer fluorophore in micelles, *Analyst*, 2013, **138**, 5942−5948.[*]

8. **A. Mishra**, S. Sahu, N. Dash, S. K. Behera and G. Krishnamoorthy, Double proton transfer induced twisted intramolecular charge transfer emission in 2-(4′-*N*,*N*-dimethylaminophenyl)imidazo[4,5-b]pyridine, *J. Phys. Chem. B*, 2013, **117**, 9469−9477.

9. **A. Mishra**, S. Sahu and G. Krishnamoorthy, Photoinduced intramolecular charge transfer in *trans*-2-[4′-(dimethylamino)styryl]imidazo[4,5-b]pyridine. (manuscript submitted)

10. **A. Mishra**, A. Malakar, M. K. Barman and G. Krishnamoorthy, Interactions of a few dimethylaminophenyl substituted azoles with bovine serum albumin: role of heteroatoms. (manuscript submitted)

11. **A. Mishra** and G. Krishnamoorthy, Effect of micelles on the prototropic equilibriums of some push pull styryl azoles. (manuscript to be submitted)

12. **A. Mishra**, A. Srivastava and G. Krishnamoorthy, Metal sensing ability of a few dimethylaminophenyl substituted azoles toward metal ions: role of heteroatoms. (manuscript to be submitted)

13. **A. Mishra** and G. Krishnamoorthy, Spectral characteristics of 2-(4′-*N*,*N*-dimethylaminophenyl)imidazo[4,5-b]pyridine in aerosol OT reverse micelle. (manuscript to be submitted)


भारतीय प्रौद्योगिकी संस्थान गुवाहाटी
Indian Institute of Technology Guwahati

List of conference proceedings

1. **A. Mishra**, F. A. S. Chipem, A. Thangamani, S. Chatterjee and G. Krishnamoorthy, Spectral characteristics and photochemistry of *trans*-2-[4′-(dimethylamino)styryl]benzothiazole: A combined theoretical and experimental study.#
International Conference on Recent Frontiers in Applied Spectroscopy (ICORFAS-2010)

2. **A. Mishra** and G. Krishnamoorthy, Spectral characteristic of *trans*-2-(4′-*N*,*N*-dimethylaminostyryl)imidazo[4,5-b]pyridine.
Chemical Research Society of India - Royal Society of Chemistry (CRSI-RSC-2011).

3. **A. Mishra,** S. Sahu, S. K. Behera and G. Krishnamoorthy, Spectral characteristics of methyl derivatives of 2-(4′-*N*,*N*-dimethylaminophenyl)imidazo[4,5-b]pyridine.
Conference on Photochemistry & Luminescence (CPL 2012).

4. **A. Mishra,** S. Maity and G. Krishnamoorthy, Effect of polar protic solvents on the TICT emission of 2-(4′-*N*,*N*-dimethylaminophenyl)oxazo[4,5-b]pyridine and effect of pH on the prototropic equilibria.
Conference on Photochemistry & Luminescence (CPL 2012).

5. **A. Mishra**, A. Srivastava and G. Krishnamoorthy, Effect of solvents and pH on the Spectral characteristics of *trans*-2-[4′-(dimethylamino)styryl]benzimidazole.
Conference on Photochemistry & Luminescence (CPL 2012).

6. S. Chatterjee, M. K. Barman, **A. Mishra** and G. Krishnamoorthy, Solvatochromism and prototropic equilibria of *trans*-2-(4′-*N*,*N*-dimethylaminostyryl)imidazo[4,5-c]pyridine.#
Conference on Photochemistry & Luminescence (CPL 2012).

#not part of the present thesis

***partial part is included in the present thesis**